Investigation and Characterization of In-Vehicle EMC Coupling Mechanisms of Multi-Gigabit Ethernet Communication Systems

PhD Thesis Sanaz Mortazavi

Berlin 2021

Investigation and Characterization of In-Vehicle EMC Coupling Mechanisms of Multi-Gigabit Ethernet Communication Systems

vorgelegt von
Sanaz Mortazavi, M.Sc.

von der Fakultät IV - Elektrotechnik und Informatik
der Technischen Universität Berlin

zur Erlangung des akademischen Grades

Doktor der Ingenieurwissenschaften
- Dr.-Ing. -

genehmigte Dissertation

Promotionsausschuss:

Vorsitzender: Prof. Dr.-Ing. Slawomir Stanczak
Gutachter: Prof. Dr. Ing. Friedel Gerfers
Gutachter: Prof. Dr. Ir. Ing. Frank Leferink
Gutachter: Prof. Dr. Ing. Joachim Meißner

Tag der wissenschaftlichen Aussprache: 25.03.2021

Berlin 2021

For my mother, Parvaneh

Abstract

The future car might well have just an electric engine and be driven by artificial intelligence. To enable the implementation of fully autonomous driving, a large number of sensors, radar nodes, and cameras must provide the required information for the central decision-making unit(s), which control(s) the actuators. For this purpose, tens of gigabits of data must be transferred between different nodes through an appropriate communication network. The traditional automotive communication networks cannot satisfy the requirements of the future car. Ethernet technology is the choice of the automotive industry for the mentioned reasons. The automotive Ethernet for the implementation of two different data rates, i.e., 100 Mbit/s and 1000 Mbit/s, have been standardized. The next outstanding standard deals with data rates of 2.5 Gbit/s, 5 Gbit/s, and 10 Gbit/s; the so-called Multi-Gigabit or Multi-Gig Ethernet. The IEEE P802.3cy taskforce will standardize the implementation of the data rates greater than 10 Gbit/s (25 Gbit/s, 50 Gbit/s, and 100 Gbit/s).

As the vehicles move steadily, their electromagnetic environment continuously changes. Such changes may affect the functionality of the system and jeopardize the safety and reliability of the automotive Ethernet technology. One of the main problems for the development of automotive Multi-Gig Ethernet systems is the corresponding EMC issues. In this work, some of the essential EMC investigations into the automotive Multi-Gig Ethernet are performed and studied for the first time (to the author's knowledge). The prepared results of this work can help the semiconductor and automotive industry consider the possible EMC issues of these high-speed networks during the early design stages.

The implementation of gigabit data rates assumes signal bandwidths in the gigahertz range. In such frequency domains the design of electronic components is challenging when considering the EMC issues. Accurate simulation models of the system components can help to reduce the costs and development times. Such simulation models should contain the corresponding high-frequency (HF) and EMC issues. One objective of this work is the development and verification of the components simulation models of the analog front-end of the automotive Ethernet for data rates of

100 Mbit/s, 1000 Mbit/s, and 2.5 Gbit/s. The simulation models of the common-mode termination, common-mode choke, low-pass filter, and the transceiver are presented. To verify the mentioned models, corresponding printed circuit boards have been developed and measured. Measurement results verify the simulation models.

Furthermore, the channel of the Multi-Gig Ethernet is studied. Different possible cable types, i.e., unshielded twisted pair, shielded twisted pair and shielded parallel pairs are studied in regards to their signal integrity and EMC suitability for their use in automotive Multi-Gig Ethernet. The EMC investigations include laboratory and in-vehicle measurements, consider HF-properties, noise immunity, and radiation. For the immunity and radiation of the channel, corresponding limits are suggested.

Due to the radiation of the channel, the functionality and robustness of the other vehicle's components may be affected by the interferences. A 3D-field simulation method for the radiation of the automotive Multi-Gig channel up to 10 GHz is proposed in the latter part of this work. This simulation method is used for the calculation of the coupled voltages to different vehicle's antennas as the result of the channel radiation. The proposed simulation method can serve to aid the automotive industry in the choice of the proper cable routing.

Zusammenfassung

Das zukünftige Auto könnte durchaus nur einen Elektromotor haben und von künstlicher Intelligenz gesteuert werden. Um ein vollständig autonomes Fahren zu ermöglichen, muss eine große Anzahl von Sensoren, Radaren und Kameras die erforderlichen Informationen für die zentrale(n) Entscheidungseinheit(en) liefern, die die Aktoren steuern. Zu diesem Zweck müssen mehrere Gigabits an Daten zwischen verschiedenen Knoten über ein geeignetes Kommunikationsnetz übertragen werden. Die traditionellen Kfz-Kommunikationsnetzwerke können die Anforderungen des zukünftigen Autos nicht erfüllen. Deswegen hat sich die Automobilindustrie für die Ethernet-Technologie entschieden. Das Automotive-Ethernet für die Implementierung von zwei verschiedenen Datenraten, 100 Mbit/s und 1000 Mbit/s, ist bereits standardisiert worden. Der nächste noch ausstehende Standard befasst sich mit Datenraten von 2,5 Gbit/s, 5 Gbit/s und 10 Gbit/s (Multi-Gigabit-Ethernet). Die IEEE P802.3cy-Taskforce wird die Implementierung der Datenraten von mehr als 10 Gbit/s (25 Gbit/s, 50 Gbit/s und 100 Gbit/s) standardisieren.

Da sich die Fahrzeuge ständig bewegen, ändert sich ihre elektromagnetische Umgebung. Solche Veränderungen können die Funktionalität des Systems beeinträchtigen und die Sicherheit und Zuverlässigkeit der automobilen Ethernet-Technologie gefährden. Eines der Hauptprobleme bei der Entwicklung von automobilen Multi-Gigabit-Ethernet-Systemen sind die entsprechenden elektromagnetische verträglichkeit (EMV)-Aspekte. In dieser Arbeit wurden einige der wesentlichen EMV-Untersuchungen bzgl. automobilen Multi-Gig-Ethernet zum ersten Mal (nach Kenntnis des Autors) durchgeführt. Die Ergebnisse dieser Arbeit können der Halbleiter- und Automobilindustrie helfen, die möglichen EMV-Probleme der Automotive-Ethernet-Netzwerke bereits in den frühen Entwicklungsphasen zu berücksichtigen.

Die Implementierung von Gigabit-Datenraten setzt Signalbandbreiten im Gigahertz-Bereich voraus. In solchen Frequenzbereichen ist das Design von elektronischen Komponenten unter Berücksichtigung der EMV-Aspekte eine Herausforderung. Genaue Simulationsmodelle der Systemkomponenten können helfen, die Kosten

und Entwicklungszeiten zu reduzieren. Solche Simulationsmodelle sollten die entsprechenden Hochfrequenz- (HF) und EMV-Probleme enthalten. Ein Ziel dieser Arbeit ist die Entwicklung und Verifikation der Komponenten-Simulationsmodelle des analogen Front-Ends vom Automotive Ethernet für Datenraten von 100 Mbit/s, 1000 Mbit/s und 2,5 Gbit/s. Die Simulationsmodelle der Gleichtaktterminierung, der Gleichtaktdrossel, des Tiefpassfilters und des Transceivers werden vorgestellt. Um die genannten Modelle zu verifizieren, wurden entsprechende Leiterplatten entwickelt und gemessen. Die Messergebnisse validieren die Simulationsmodelle.

Außerdem wurde der Übertragungskanal des Multi-Gig-Ethernet untersucht. Verschiedene mögliche Kabeltypen, UTP (unshielded twisted pair), STP (shielded twisted pair) und SPP (shielded parallel pair), wurden hinsichtlich ihrer Signalintegrität und EMV-Eignung für den Einsatz im Automotive Multi-Gig-Ethernet untersucht. Die Labor- und Fahrzeug-interne EMV-Untersuchungen berücksichtigen HF-Eigenschaften, Störfestigkeit und Abstrahlung der Kabel. Für die Störfestigkeit und Abstrahlung des Kanals werden entsprechende Grenzwerte vorgeschlagen.

Aufgrund der Abstrahlung des Übertragungskanals kann die Funktionalität der anderen Fahrzeugkomponenten beeinträchtigt werden. Eine 3D-Feldsimulationsmethode für die Abstrahlung des automobilen Multi-Gig-Kanals bis zu 10 GHz wird in dieser Arbeit vorgeschlagen. Diese Simulationsmethode wird für die Berechnung der eingekoppelten Spannung an verschiedenen Fahrzeugantennen als Ergebnis der Kanalstrahlung verwendet. Die vorgeschlagene Simulationsmethode kann dazu dienen, die Automobilindustrie bei der Wahl der richtigen Kabelführung zu unterstützen.

Acknowledgements

My special thanks go to my supervisor, professor Friedel Gerfers, who always encouraged and helped me improve the quality of my research.

Dr. -Ing. Detlef Schleicher, as my industry supervisor, has always been by my side and has helped me through every encountered difficulty. I thank him for his invaluable contribution during my time in the Volkswagen EMC department. He has supported me throughout the years in so many ways.

Professor Joachim Meißner has always helped me to improve my knowledge. He aroused my interest in EMC when I first attended his undergraduate lecture course on electromagnetic compatibility.

I would like to thank professor Frank Leferink for his kind support, reviewing this work, and giving valuable feedback.

I am also most thankful to Mr. Frank Golisch, and Dr. -Ing. Lorena Diaz Ortega, who afforded me the opportunity to begin and fulfill my Ph.D. I also thank Dr. -Ing. Ralf Borngräber, Dr. -Ing. Olaf Krieger, and Mr. Lothar Claus, who supported me with their knowledge and expertise during the past two years.

Finally, my deep and sincere gratitude to Ali and my family for their affection, encouragement, and support. I am aware that I could not achieve this milestone without them.

List of Own Publications

This thesis is based on the following peer-reviewed publications.

1. S. Mortazavi, D. Schleicher and F. Gerfers, "Characterization of common-mode choke for automotive ethernet networks enabling 100 Mbit/s," 2017 International Symposium on Electromagnetic Compatibility - EMC EUROPE, Angers, 2017, pp. 1-6. doi: 10.1109/EMCEurope.2017.8094720

2. S. Mortazavi, D. Schleicher, F. Schade, F. Gerfers, "Charakterisierung der Gleichtaktdrossel für Multi-Gig-Kommunikation in Automotive-Ethernet Netzwerken." Internationale Fachmesse und Kongress für Elektromagnetische Verträglichkeit, Düsseldorf, 2018, S. 340-347. https://doi.org/10.15488/4362
   This paper was selected as one of the finalists for the best student paper award.

3. S. Mortazavi, D. Schleicher and F. Gerfers, "Characterization and verification of Gigabit ethernet-based bus systems in vehicles," 2018 IEEE International Symposium on Electromagnetic Compatibility and 2018 IEEE Asia-Pacific Symposium on Electromagnetic Compatibility (EMC/APEMC), Singapore, 2018, pp. 428-433. doi: 10.1109/ISEMC.2018.8393814

4. S. Mortazavi, D. Schleicher and F. Gerfers, "Modeling and Verification of Automotive Multi-Gig Ethernet Communication up to 2.5 Gbps and the Corresponding EMC Analysis," 2018 IEEE Symposium on Electromagnetic Compatibility, Signal Integrity and Power Integrity (EMC, SIPI), Long Beach, CA, pp. 329-334. doi: 10.1109/EMCSI.2018.8495375

5. S. Mortazavi, D. Schleicher, F. Schade, C. Gremzow and F. Gerfers, "Toward Investigation of the Multi-Gig Data Transmission up to 5 Gbps in Vehicle and Corresponding EMC Interferences," 2018 International Symposium on Electromagnetic Compatibility (EMC EUROPE), Amsterdam, pp. 60-65. doi: 10.1109/EMCEurope. 2018.8485142.
   This paper was selected as one of the finalists for the best student paper award.

6. S. Mortazavi, D. Schleicher, A. Stieler, A. Sinai, F. Gerfers, M. Hampe, "EMC Analysis of Shielded Twisted Pair and Shielded Parallel Pair Transmission Lines for Automotive Multi-Gig Ethernet," 2019 IEEE International Symposium on Electromagnetic Compatibility, Signal & Power Integrity (EMC+SIPI), New Orleans, LA, USA, 2019, pp.193-198. doi: 10.1109/ISEMC.2019.8825261
This paper won the best student paper award.

7. S. Mortazavi, D. Schleicher, A. Sinai and F. Gerfers, "RF Ingress Automotive Immunity Measurement on STP Cable in the Vehicle up to 6 GHz," 2019 IEEE International Symposium on Electromagnetic Compatibility, Signal & Power Integrity (EMC+SIPI), New Orleans, LA, USA, 2019, pp. 298-303. doi: 10.1109/ISEMC.2019.8825296

8. S. Mortazavi, D. Schleicher, D. Eremyan, A. Gheonjian, I. Badzagua, I. Danelyan, R. Jobava, A. Sinai, F. Gerfers, "Investigation of Possible EM Interference of Automotive Multi-Gig Communication Link in the FM and DAB Ranges Using 3D Field Simulation," 2019 Joint International Symposium on Electromagnetic Compatibility and Asia-Pacific International Symposium on Electromagnetic Compatibility, Sapporo (EMC Sapporo & APEMC). doi: 10.23919/EMCTokyo.2019.8893840

9. S. Mortazavi, D. Schleicher, D. Eremyan, A. Gheonjian, R. Jobava, A. Sinai, F. Gerfers, "Investigation of Possible EMC Interferences between Multi-Gig Communication link and RF Applications in Vehicle," 2019 International Symposium on Electromagnetic Compatibility (EMC EUROPE), Barcelona. doi: 10.1109/EMCEurope.2019.8872099

The contents of the following publications are not included in this dissertation.

10. S. Mortazavi, A. Sinai, A. Hamidian, A. Malignaggi, H. Abdullah, G. Böck, “Broadband cavity-backed antenna arrays on glass substrate for 60 GHz application”, 2014 IEEE 44th European Microwave Conference, Rom Italy, doi: 10.1109/EuMC.2014.6986766

11. M. Hampe, S. Mortazavi, A. Stieler, K :D. Tieste, L. Claus, “Analysis and Assessment of the Common Mode Termination for Automotive Ethernet 1000BASE-T1“, 2020 International Symposium on Electromagnetic Compatibility (EMC EUROPE), Rom. doi: 10.1109/EMCEUROPE48519.2020.9245722

12. H. Ghafarian, S. Shivapakash, S. Mortazavi, P. Scholz, N. Lotfi, F. Gerfers, “A 9-bit, 45 mW, 0.05 mm2 Source-Series-Terminated DAC Driver With Echo Canceller in 22-nm CMOS for In-Vehicle Communication”, 2020 IEEE Solid-State Circuits Letters, doi: 10.1109/LSSC.2020.3048752

Disclaimer:

The results, opinions and conclusions expressed in this thesis are not necessarily those of Volkswagen Aktiengesellschaft.

Ergebnisse, Meinungen und Schlüsse dieser Dissertation sind nicht notwendigerweise die der Volkswagen Aktiengesellschaft.

Acronyms

ABS	Anti-lock brake system
ACC	Automatic cruise control
ADAS	Advanced driver assistance systems
ADC	Analog digital converter
AFE	Analog front-end
ALSE	Absorber lined shielded enclosure
AN	Auto-negotiation
APIX	Automotive pixel link
AWG	American wire gauge
AXT	Alien crosstalk
Balun	Balanced to unbalanced transformer
BAN	Broadband artificial network
BB	Broadband
BCI	Bulk current injection
BER	Bit error rate
BERT	Bit error rate tester
BIN	Bus interface network
BR	BroadR-Reach
BW	Bandwidth
CAN	Controller area network
CAN FD	CAN with flexible data rate
CDMR	Common to differential mode rejection
CFI	Call for interest
CM	Common-mode
CMC	Common-mode choke
CMT	Common-mode termination
CPW	Coplanar waveguide
CSMA/CA	Carrier sense multiple access / collision avoidance
DAC	Digital analog converter
DCMR	Differential to common mode rejection
DPI	Direct power injection
DUT	Device under test
E/E	Electric / electronic

ECUs	Electronic control units
EEE	Energy-efficient Ethernet
EMC	Electromagnetic compatibility
ESD	Electrostatic discharge
ESP	Electronic stability program
FEC	Forward error correction
FEXT	Far-end crosstalk
FPGA	Field programmable gate array
GMII	Gigabit media independent interface
GPS	Global positioning system
H-MTD	High-speed modular twisted-pair data
HD	High definition
HF	High-frequency
HMI	Human machine interface
HSD	High-speed data
IL	Insertion loss
IMU	Inertial measurement unit
IP	Internet protocol
ISI	Intersymbol interference
IVN	In-vehicle network
LCL	Longitudinal conversion loss
LCTL	Longitudinal conversion transmission loss
LiDAR	Light detection and ranging
LIN	Local interconnect network
LISN	Line impedance stabilization network
LTE-Advanced	Long term evolution-Advanced
LVDS	Low-voltage differential signaling
MAC	Media access control
MDI	Medium dependent interface
MDIO	Management data input/output
MII	Media independent interface
MLT-3	Multilevel transmission encoding – 3 levels
MoM	Method of moments
MOST	Media oriented systems transport

MTL	Multi-conductor transmission lines
NB	Narrowband
NEXT	Near-end crosstalk
NRZ	Non-return-to-zero
OCU	Online communication unit
OEM	Original equipment manufacturers
Opt-BIN	Optimized MDI interface test network
OSI	Open systems interconnection
OTS	Outdoor test site
PCB	Printed circuit board
PCS	Physical coding sublayer
PHY	Physical layer
PLL	Phase-locked loop
PMA	Physical medium attachment
PoDL	Power over data lines
PoE	Power over Ethernet
POF	Polymer optical fiber
PP	Polypropylene
PRBS	Pseudo random binary sequence
PSAACRF	Power sum alien attenuation to cross talk ratio-far end
PSANEXT	Power sum alien near-end crosstalk
RF	Radio frequency
RFI	Radio frequency interference
RL	Return loss
RZ	Return-to-zero
S-parameter	Scattering parameter
SMD	Surface-mounted device
SNR	Signal-to-noise ratio
SPP	Shielded parallel pair
STP	Shielded twisted pair
STQ	Shielded twisted quad
SYNC	Synchronization
TCL	Transverse conversion loss

TCTL	Transverse conversion transmission loss
TDR	Time domain reflectometry
TEM	Transverse electromagnetic
TLS	Transmission line system
TP	Twisted pair
TWC	Tubular wave coupler
UTP	Unshielded twisted pair
V2I	Vehicle-to-infrastructure
V2V	Vehicle-to-vehicle
VNA	Vector network analyzer
WLAN	Wireless local area network

List of Symbols

C	Capacitance
a_c	Coupling attenuation
K	Coupling coefficient
D	Diameter
tanδ	Dissipation factor
ε_r	Relative permittivity
f	Frequency
L	Inductance
λ	Wavelength
l	Length
T	Time period
R	Resistance
a_s	Screening attenuation
a_u	Unbalanced attenuation

Contents

Chapter 1
Introduction

Over the past decades enormous developments in the semiconductor industry have enabled the automotive industry to open up new avenues in regards to the implementation of novel electric / electronic (E/E) ideas. The traditional hydraulic or mechanical components, which are limited regarding achievable cost reductions and technological improvements, have since been replaced by electronic systems (X-by-Wire)[1, 2].

The use of tens of meters of copper cables for the connection of car components such as the power light, horn, and radio in the 1950s [3] is no longer a conceivable solution. At that time, the communication between the components was fulfilled with point-to-point connections [1].

The increasing number of electronic components in vehicles has led to the creation of modern cabling systems. To connect electric units, and avoid the point-to-point connection of all elements, a bus system takes the role of communication service. According to IEC 60050-351:2006, entry 351-32-10, a bus is a *"functional unit for the transfer of data between several participants, these being functional units for data processing, via a common transmission path, wherein participants are not involved in the transfer of data between other participants."*

The idea of using bus systems in the vehicle has gained considerable importance for the realization of various electronic concepts in the automotive industry. Using a bus system in the car has many advantages in comparison to point-to-point connections [2, 4, 5]. As the number of cables can be decreased, the cost and complexity are reduced. The installation of the cabling systems is comfortable, and the vehicle's weight could be reduced. The latter of the two mentioned factors, i.e., cost and weight of the cable harness, are most important for the original equipment manufacturers (OEM) [6]. In [7], it is noted that the overall length of the vehicle's cable harness is more than 2 km and weighs more than 30 kg. A communication network has the advantage that the data of a sensor can be shared with other network participants [4]. Furthermore, depending on the customer's wishes, various options could be installed

during the production by plugging new sensors or electronic control units (ECUs) to the bus systems.

Depending on the component's function and the required data rate, different bus systems have been developed in the past decades. Such bus systems differ according to parameters, e.g., jitter, bandwidth, transmission error tolerances, and response time, etc. The bus systems can be implemented in different domains, defined in the following [1].

Powertrain and chassis domains assume safe and real-time communication. The powertrain domain includes functionalities for engine control and transmission, such as engine speed and fuel injection. Chassis domain contains steering and braking functions, electronic stability program (ESP), and anti-lock brake system (ABS). The comfort functions and multimedia communications are in the field of the body and human-machine interface (HMI) domains, respectively. The latter subsystems are not safety-critical and rely mostly on the driver's interaction. The monitoring and wireless communication systems count on the telematics domain. As the last defined domain in [1], the emerging domain is responsible for driver assistance systems that deal with passenger's safety, like airbag systems.

The proposed domains can be classified into two major categories, i.e., event-triggered and time-triggered. In the case of event-triggered systems, the signals are transmitted to the bus if an event happens (e.g., if the seat belt is unfastened). In such an event, the data protocols receive the highest priority for communicating over the bus [1]. Event-triggered buses do not require high bandwidth. In the time-triggered systems, the frames are transmitted on predefined scheduled time intervals. The advantage of time-triggered systems is the recognition ability of malfunctioning components. The drawback of the time-triggered buses is the lack of flexibility, as all the communication nodes must be synchronized, and each change affects the system as a whole [1].

There are different bus systems, which are implemented in the mentioned in-vehicle domains. The first standardized bus system, widely used amongst automotive vendors, is the controller area network (CAN) [2]. Local interconnect network (LIN), FlexRay, media oriented systems transport (MOST), and Ethernet are the other well-known bus systems in the vehicle. The communication between various bus systems is realized over a gateway in the car [3]. Multiple bus systems can be used for various applications simultaneously.

The goal of automating most of the vehicle-components resulted in the increased number of digital components. Consequently, the corresponding bus systems had to support higher data rates. For instance, in modern vehicles, up to eight cameras are installed, each one with its own function, i.e., surround view, virtual exterior mirror, front view, night vision, driver observation camera, etc. Each of the mentioned camera links requires a considerable data transmission rate. The needed data rate for

uncompressed data is in Gbit/s range, which depends on camera resolution and frame rate etc. [8]. In order to increase the data rate, a higher operating frequency is needed.

The increase of frequency makes the analog components of the bus systems susceptible to noise. In higher frequency ranges, problems such as crosstalk, inter-symbol interference (ISI), larger insertion loss, etc. lead to the degradation of system performance.

The automotive high-speed bus systems should be able to operate in their harsh electromagnetic environment. Their emissions should not affect the other (on-board, and off-board) devices, and the functionality of high-speed components themselves should not be susceptible to interference from external noise. Hence, the investigation of electromagnetic compatibility (EMC) of bus systems plays an essential role in system security and reliability.

Furthermore, the use of power-electronic components, e.g., DC-DC-converters, for hybrid or electric cars can lead to EMC problems [9]. The implementation of wireless technologies, e.g., wireless local area network (WLAN), increases the electromagnetic interference (EMI) problems [7]. WLAN can be used for the implementation of car-2-car technology, which requires a high-speed automotive bus system. The frequency range of WLAN is around 2.4 GHz or 5.9 GHz.

The EMC investigations of the high-speed bus systems should also consider the disturbances originating from high-pulsed currents of injection units, Bluetooth devices, civil or military radars, etc. The emission of bus components can lead to disturbances with mobile phones, TV/radio, etc. These should also be taken into account [9].

Ethernet is the choice of the automotive industry for the implementation of different technologies, such as autonomous driving, car-to-car, car-to-x, and the use of 5G in vehicles. The investigation of EMC issues of automotive Ethernet plays a significant role, as the upcoming technologies have a high demand for safety and reliability.

The focus of this work is on two parts. First, the components of the analog front-end (AFE) of the automotive Ethernet are to be investigated. In this regard, the EMC issues of the AFE components for different standards are studied in Chapters 3 and 4. The second part of this work includes the EMC analysis, i.e., radiation and immunity, of the corresponding channels. The channel investigations are presented in Chapters 5 to 7. In both parts, the established standards (100Base-T1, and 1000Base-T1), as well as the up-coming standard (NGBase-T1), are considered. The block diagram of the automotive Ethernet AFE and the channel is presented in Figure 1.1.

The second chapter focuses on a general overview of the automotive EMC tests, based on existing standards. The described test methods are used for the measurements, as laid out in the following chapters. The most used communication networks,

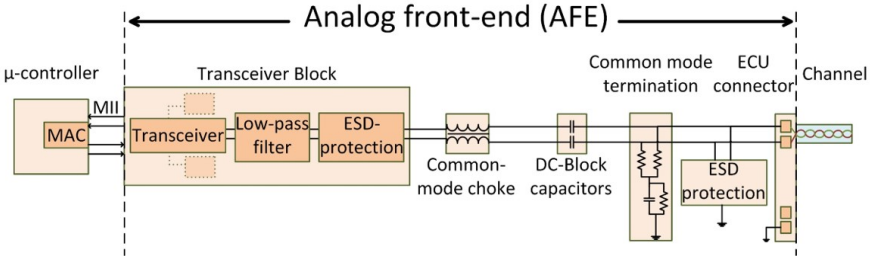

Fig. 1.1: Block diagram of the automotive Ethernet analog front-end and channel [10]

with the focus on the physical layer, are discussed briefly. Automotive Ethernet networks are explained at the end of the second chapter, where the state of the knowledge in automotive Ethernet is presented.

One of the main EMC issues in higher frequencies is the common-mode (CM) disturbance, which affects the functionality of the transceiver. The AFE of existing Ethernet standards contains the common-mode choke (CMC) (Figure 1.1), which suppresses the CM noise the channel and of the ECU. Hence, the detailed study of the CMC is an important issue of the AFE. A new high-frequency equivalent circuit model of CMC is presented in Chapter 3. The circuit model is validated using corresponding measurements. The measurements of 100BASE-T1 CMC are presented in the same chapter. Further, the comparison of 100BASE-T1 CMC with 1000BASE-T1 common-mode choke is discussed.

In Chapter 4, the AFE of 100BASE-T1, 1000BASE-T1, and 2.5 Gbit/s are modeled and verified using simulation and measurements. The AFE includes the physical layer (PHY) transceiver, CMC, low-pass filter, and common-mode termination. However, the measurements do not contain the corresponding transceivers.

The use of STP, or shielded parallel pair (SPP), cables for the Gigabit automotive Ethernet regarding their EMC issues is studied in Chapter 5. Using mixed-mode scattering parameter (S-parameter) measurements up to 8 GHz, the frequency domain properties of the mentioned cables are studied. The coupling attenuation and the time domain characteristics of these cables are presented in this chapter.

In Chapter 6, the in-vehicle immunity tests of the Multi-Gig links are presented. For this purpose, the immunity of STP cables for a frequency range of 150 kHz – 6 GHz is measured in an absorber lined shielded enclosure (ALSE). The results of these measurements are compared with the state of the knowledge, as based on laboratory measurements. The optimization of the immunity limits is suggested. In addition, the in-vehicle emission of the 5 Gbit/s communication link over a wide frequency band is presented in Chapter 6. As explained above, the Gigabit PHYs are

still in the early development stages. Hence, the function of the PHY is substituted by a field programmable gate array (FPGA). The FPGA feeds an STP cable, and the corresponding emissions are measured in a vehicle. In the same chapter and based on the measurements, the EMC study of unshielded twisted pair (UTP) and shielded twisted pair (STP) cables is presented.

Chapter 7 deals with the radiation of STP cables using a 3D field simulator. Using the presented simulation methods of these chapters, the OEMs can evaluate the emission issues of the Multi-Gig Ethernet cables already in the early design phase.

In the final chapter, the summary and conclusion of this work are presented.

Chapter 2
Automotive EMC Tests and Communication Networks

In this chapter, a brief overview of the established automotive EMC standards is presented. The reliability and stability of the gigabit automotive networks, and their corresponding EMC issues, should be verified using appropriate EMC test methods. Hence, the EMC test methods for immunity, emission, and electrostatic discharge (ESD) immunity are reviewed.

The second part of this chapter describes the existing automotive networks with the focus on the automotive Ethernet technology. In this regard, the two existing automotive Ethernet standards are discussed. The state of the knowledge of the automotive Gigabit Ethernet technology is presented at the end of this chapter.

2.1 Automotive EMC tests

The automotive EMC standards are primarily published by three organizations, i.e., IEC/CISPR, ISO, and SAE. The ISO and IEC/CISPR standards are generally used worldwide, while the SAE is in the focus of attention in North America [11]. In this section, the international automotive standards for the emission tests (CISPR 12, CISPR 25), immunity tests (ISO 11451, ISO 11452), and the ESD test standard ISO 10605 are briefly presented. Based on the test methods of this subsection, the EMC measurements described in the next chapters are performed.

2.1.1 Automotive emission tests

2.1.1.1 CISPR 12

Standard title: *"vehicles, boats and devices with internal combustion engines or traction batteries – radio disturbance characteristics – limits and methods of measurement for the protection of off-board receivers"*

The electromagnetic emission of the vehicle's electric / electronic (E/E) components may disturb the functionality of off-board devices (receivers). The corresponding measurement test methods for the protection of off-board receivers in a residential

environment are provided in CISPR 12 [12]. According to this international standard, the mentioned off-board receivers may have a minimum distance of 10 m to the vehicle. The covered frequency range of CISPR 12 is between 30 MHz and 1 GHz.

CISPR 12 deals with the emission of the vehicle in two different states, i.e., "key-on, engine-off" and running engine. For each state, a corresponding electromagnetic emission limit is defined. In both states, the receiver antenna is at a 10 m or 3 m distance from the car.

In the "key-on, engine-off" state, the emission is measured using the average detector mode of a spectrum analyzer or scanning receiver. The peak or quasi-peak mode should be used only when the engine is running. The latter measurement mode is also applicable to when an electric/hybrid car is tested in charging mode. For reasons of simplicity, the mathematical equations of the mentioned limit lines are not mentioned here. They can be obtained from [12].

The receiver antenna could be a balanced dipole or any broadband linearly polarized antenna placed 10 m away from the vehicle. The antenna should have a distance of 3 m from the ground. The measurement should be performed in vertical and horizontal polarization for all frequencies. The measurements should be done in an outdoor test site (OTS) or in an absorber room. On OTS, no electromagnetic reflecting surfaces should be placed within a minimum radius of 30 m from the antenna position. For 3 m emission measurement, the minimum radius is 20 m. As an alternative, an ALSE may be used if the obtained results can be correlated to the results obtained using the OTS. The emission is recorded from the left and right sides of the vehicle. For the electric/hybrid car during conducted or wireless charging, further normative recommendations regarding the position of antenna, car, etc. are proposed in CISPR 12 [12].

2.1.1.2 CISPR 25

Standard title: *"Vehicles, boats and internal combustion engines - Radio disturbance characteristics - Limits and methods of measurement for the protection of on-board receivers"*

The functionality of the onboard receivers could be affected by interferences caused by conducted and radiated in-vehicle noise. The safe operation of the receivers in a frequency range between 150 kHz and 2.5 GHz, despite the presence of the mentioned noise, is the subject of the CISPR 25 standard. This standard introduces the measurement methods and the corresponding limits for allowable emitted electromagnetic noise caused by the vehicle's electrical systems. Furthermore, the emissions test procedure for electrical components and modules, regardless of the type of vehicle, is introduced. Examples for appropriate limits are given to prevent the disturbing effects of the component's electromagnetic emission [13].

There are two types of noise defined in CISPR 25, i.e., broadband (BB) and narrowband (NB). BB noise usually has a continuous spectrum distribution, while NB noise is concentrated in one specific frequency. The vehicle components, which generate BB are, e.g., spark ignition, electrical motors, and rectifiers. Devices like power switching transistors introduce NB noise [14].

The structure of the absorber room is depended on certain factors, i.e., room size, objects in the room, characteristics of absorber materials for component or vehicle measurements, measurement device requirements, and power supply specification.

Furthermore, the emission measurement test method with an antenna in the same vehicle is outlined. The pre-installed antennas in the vehicle should be used for the measurements in their frequency bands. External antennas should be used for the other frequency bands, which are not supported by the antennas of the vehicle. The external antenna types, and their recommended measurement frequency range, are noted. Moreover, CISPR 25 characterizes and describes the required properties of measurement devices, the corresponding cables, amplifiers, etc. The position of the vehicle in the absorber room is marked by specifying the distances to the outer walls.

The measurement methods for the emission of the components and modules in absorber-lined shielded enclosure (ALSE) are explained in the further course of this standard. To measure the emission of components/modules, five measurement methods are depicted as follows [13]:

- Measurement of conducted emissions using:
  - Voltage method
  - Current probe method
- Measurement of radiated emissions using:
  - ALSE method
  - Transverse electromagnetic (TEM) cell method
  - Stripline method

Conducted emissions - voltage method

The E/E components or modules generate electrical noise over their power supply lines. CISPR 25 discusses the measurement methods for characterizing the conducted noise over power lines. The device under test (DUT) should be driven using a load simulator that leads to the maximum emission of the DUT. A line impedance stabilization network (LISN) device is placed between the power supply and DUT. The LISN suppresses the noise of the power supply. In the same way, the conducted noise of the DUT is filtered and cannot reach the power supply. The LISN allows the measurement of the conducted noise of the DUT over a separate radio frequency (RF) output port, utilizing, e.g., a spectrum analyzer or scanning receiver.

The DUT vendor and the vehicle manufacturer should define the corresponding limit lines for the measurement of the conducted emissions using the voltage method. However, CISPR 25 suggests the limit lines in different frequency ranges that can be obtained from [13].

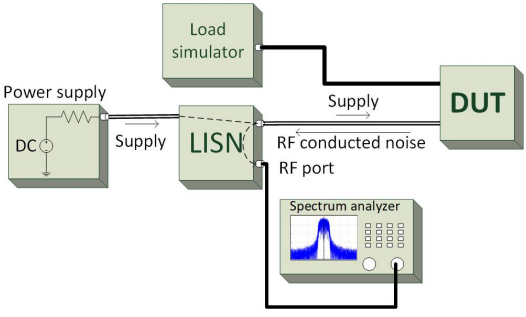

Fig. 2.1: The block diagram of conducted emissions (voltage method) measurement setup [15]

Conducted emissions - Current probe method

The conducted emissions on the DUT's cable harness are measured using the current probe method. For this purpose, a current probe, first at a distance of 50 mm and then at a distance of 750 mm from the DUT, is positioned over the cable harness, including signal and control cables. The cable harness is connected to the load simulator. The power source is connected with two LISN. Compared to the voltage method, the LISN is not connected to the DUT directly, and the power is supplied through the load simulator. The current probe is then connected with the measurement device, e.g., spectrum analyzer. CISPR 25 suggests the corresponding limit lines in different frequency ranges for the conducted emissions using the current probe method. However, the DUT vendor and vehicle manufacturer should define the required limits.

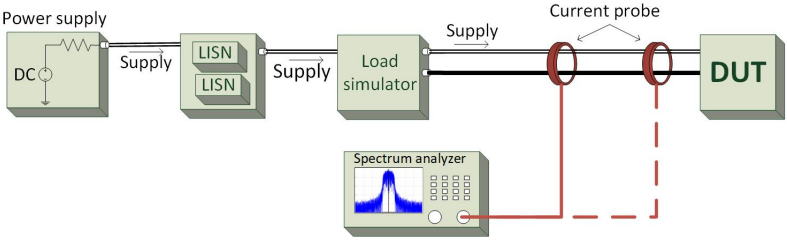

Fig. 2.2: The block diagram of conducted emissions (current probe method) measurement setup [15]

Radiated emissions – ALSE method

The radiated emissions measurements of automotive components in an anechoic chamber using antennas are described in the ALSE method. In CISPR 25, the complete measurement setup, including the anechoic chamber properties, measurement devices, and the arrangement of test components and cable harness, are defined (Figure 2.3). The DUT should be so loaded to ensure the maximum possible emission is generated. Using different antennas, suitable for various frequency bands, the radiation of E/E components can be measured. The specified frequency bands are 150 kHz – 30 MHz (using monopole antenna), 30 MHz – 300 MHz (using Biconical antenna), 200 MHz – 1 GHz (using log-periodic antenna), 1 GHz – 2.5 GHz (using horn or log-periodic antenna) [14]. In all frequency ranges, the vertical and horizontal polarization should be measured. An exception is the 150 kHz – 30 MHz frequency band, where the vertical polarization should be measured. The corresponding limits for the allowed emission of components and modules in various frequency bands are represented in CISPR 25. The emission measurements of the UTP cables in 100BASE-T1 are presented and discussed in [16].

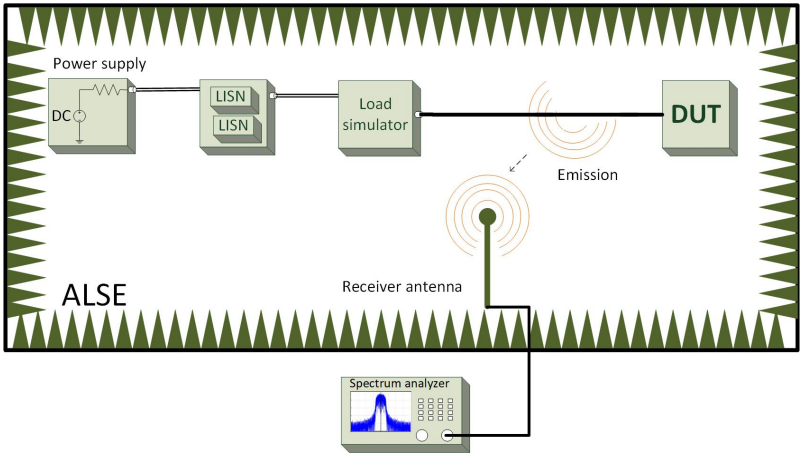

Fig. 2.3: The block diagram of the measurement setup related to radiated emissions – ALSE method

Radiated emission – TEM cell method

The measurement of radiated emission in a TEM cell is also explained in CISPR 25. This method supports the frequency range of 150 kHz – 200 MHz. The connection of DUT's cable harness with the connector panel of the TEM cell and the high-frequency (HF) properties of measurement cables are depicted in CISPR 25. The electromagnetic emission of cable harness has to be minimized using appropriate shield topologies and the perpendicular position of the cable harness, which lies on the ground plane of the TEM cell, to the DUT. If the DUT is connected with coaxial cables, each cable should be equipped with a filter.

Radiated emissions – Stripline method

If the cable harness is the main radiating/coupling element, the stripline method in the frequency range of 150 kHz – 400 MHz is applicable. However, the upper frequency limit can be expanded to 1 GHz, if certain conditions are fulfilled, as described in CISPR 25.

In this test method (Figure 2.4), the DUT is placed between the ground plane and the conductor (septum). Septum and ground plane construct an open waveguide. This waveguide does not have any sidewalls and has a constant characteristic impedance (50 Ohm or 90 Ohm) over the whole frequency range. Due to the open structure of the stripline measurement setup, the tests should be performed in an absorber room. The septum is connected on one side with an impedance matching element. The other side of the septum is connected to the second impedance matching element and the measurement device.

The DUT is placed over a non-conductive base with low permittivity. A load simulator is connected with the DUT, which generates the maximum possible emission. The power supply is connected to the LISN, which has a connection to the load simulator. The required DC voltage of the DUT is supplied through the load simulator. The cable harness of the DUT has a typical length of 1.7 m and does not exceed 2 m. The cable harness should be parallel to the septum length. CISPR 25 introduces limits for the radiated emission measured by the stripline method.

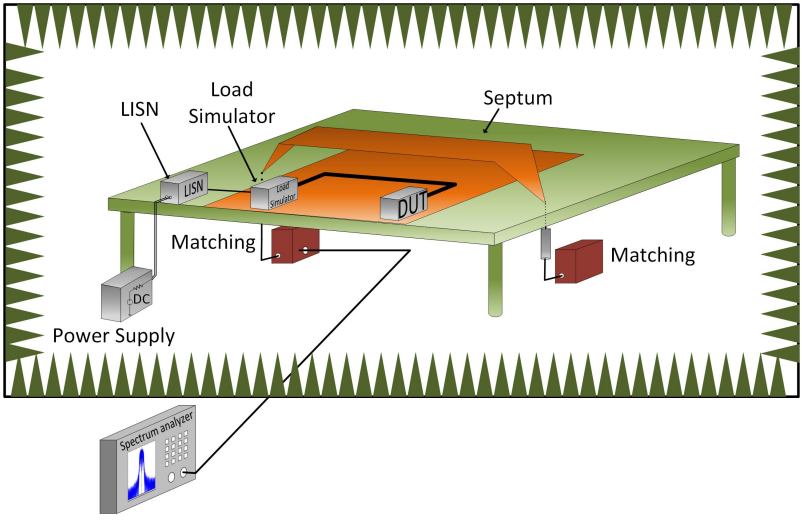

Fig. 2.4: The measurement setup related to radiated emission – Stripline method

2.1.2 Automotive immunity tests

2.1.2.1 ISO 11451

Standard title: *"Road vehicles – Vehicle test methods for electrical disturbances from narrowband radiated electromagnetic energy"*

The functionality of the automotive E/E components and devices should not be affected by external disturbances. Narrowband electromagnetic noise can originate from on-board or off-board sources. ISO 11451 [17–20] introduces the corresponding test methods for the in-vehicle immunity test in a frequency range from 100 kHz to 18 GHz. This standard covers the immunity tests for the combustion engine and electric/hybrid vehicles. Three different situations for electrically driven cars are considered: not charging, conducted charging, and wireless charging. This standard contains four parts. After describing the general principles and terminology in part 1 [17], the off-vehicle radiation sources are explained in the second part. Part 3 and part 4 of this standard deal with the onboard transmitter simulation and the bulk current injection (BCI) test, respectively.

Off-board radiation source (ISO 11451-2)

The dimensions of the absorber-lined shielded enclosure are proposed in the second part of the standard. Depending on the size of the test object, the enclosure dimensions can be varied. The external electromagnetic field, which plays the role of external noise for the vehicle's components, is radiated by an antenna or a transmission line system (TLS). Field probes, RF signal generator, power amplifier, and power meter are the main instruments required for the tests.

A minimum distance of 0.5 m is needed between antenna / TLS and the vehicle. In the further course of the standard, the antenna's position and the corresponding orientation angle are defined [18]. By defining a vehicle reference point/line, the proper distances can be adjusted. Furthermore, for battery-powered cars, the position of the power charging cable during the tests is standardized. Depending on AC or DC power charging with or without communication cable, the distances should be set correspondingly. Additional arrangements should be made if wireless charging is implemented.

Before the measurement starts, a field calibration using the field probe(s) and without the car has to be performed (substitution method). The field probe(s) should be placed at the vehicle's reference point/line. For the frequency range 10 kHz – 30 MHz / 2 GHz – 18 GHz, one field probe can be placed on the reference point. For the other frequency band (30 MHz – 2 GHz) four field probes are placed over the

reference line. During calibration, the transmitted and the sensor-detected power are recorded for each frequency range. The calibration should be done for both vertical and horizontal polarization.

On-board radiation source (ISO 11451-3)

The source of disturbance, which can degrade the functionality of automotive E/E devices, could originate from an on-board device. The third part of the ISO 11451 standard covers the immunity to electromagnetic disturbances from on-board transmitters. The frequency range of 1.8 MHz – 18 GHz is supported for the proposed test methods of this part.

An absorber-lined shielded enclosure should be used for the specified measurements. The signal generator, power amplifier, and the antenna can be placed inside or outside of the car. For the outside test setup, external antennas with specific properties can be chosen. The position of external antennas is defined in this standard. For the inside test setup, specific antennas are suggested.

Bulk current injection (ISO 11451-4)

The BCI test method is an important measurement for checking the immunity by inducing disturbances into the cable harness. The advantage of this method is that there is no need for any changes in cabling, as the current injection probe can be clamped onto the harness. The current probe is a transformer, which contains a magnetic core and the fixed primary windings. The secondary windings of the transformer are the cables of the harness. The RF interference is injected into the primary windings and is transformed to the secondary windings, i.e., the harness. The injected interference current flows to the DUT by common-mode and can degrade the performance of the device. The covered frequency range of the BCI test method in the fourth part of the ISO 11451 is between 1 MHz and 400 MHz [20].

2.1.2.2 ISO 11452

Standard title: *"Road vehicles — Component test methods for electrical disturbances from narrowband radiated electromagnetic energy"*

The test methods for the immunity of the automotive components against narrowband disturbances is discussed in ISO 11452. The presented laboratory test methods in this standard facilitate the test of the components during development and implementation. This standard contains ten parts, described briefly in the following paragraphs.

General principles and terminology (ISO 11452-1)

The first part deals with parameters such as test temperature, supply voltage (low voltage, high voltage DC, and charger power supply). Furthermore, the modulation type of generated electromagnetic wave for the immunity test and the corresponding frequency ranges are described. The properties of grounding and shielding, load simulator, and the test signal quality are explained in this part [21].

Absorber-lined shielded enclosure (ISO 11452-2)

In this part [22], the test method for the immunity against radiation of E/E components within an ALSE is described. The radiation measurement is performed using different antennas over various frequency bands. The supported measurement frequency range for the test methods presented in this part is from 80 MHz to 18 GHz. The characteristics of the required devices, i.e., antennas, power amplifier, signal generator, field probes, artificial network (AN), and power amplifier are discussed.

The measurement setup and the corresponding position of the DUT, test harness, and the required instruments for low voltage and high voltage applications are explained later. The last section describes the test procedure. The test usually begins with the calibration. During calibration, the DUT, harness, etc. are not present in the ALSE. After the calibration, the intended immunity test can be performed [23].

Transverse electromagnetic (TEM) cell (ISO 11452-3)

Using a TEM cell, the immunity test can also be performed. The DUT is exposed to a TEM wave. TEM cells usually have a characteristic impedance of 50 ohms. This part covers measurements in a frequency range between 10 kHz and 200 MHz. Like the previous parts, the positioning of the DUT and harness are addressed. This part [24] includes additional information for the dimensioning of the TEM cell, calculation of the frequency range of TEM cell, and measurement with and without low-pass filters.

Harness excitation methods (ISO 11452-4)

The fourth part of the standard discusses the immunity test of the cable harness with the BCI test. To measure and validate the immunity of the DUT, RF noise should be induced to the cables. The current probe, which includes the transformer's core and the primary windings, induces the high-frequency current to the cable or cable harness that acts as the second transformer winding. It is possible to measure the coupled current using a second current probe [25].

Depending on the frequency band, two tests are standardized. The BCI test is standardized for frequencies up to 400 MHz, while the tubular wave coupler (TWC) test method has a frequency band from 400 MHz to 3 GHz [26].

Stripline (ISO 11452-5)

This part of the standard deals with the immunity test of the automotive DUTs and cable harness in a stripline enclosure [27]. This test setup includes two parallel plates, i.e., septum and ground plane. A homogenous TEM wave can be created between the two plates, where the DUT is placed. One side of the stripline structure is connected with the signal generator, power amplifier, matching elements, etc. The other side is matched to, e.g., 50 Ohm. The characteristic impedance of the structure over the frequency band is constant. In the standard, a frequency range of 10 kHz – 400 MHz is suggested for this test. The test should be performed in an anechoic chamber to avoid any unwanted disturbances during the test setup.

Direct radio frequency (RF) power injection (ISO 11452-7)

Here the focus is the direct power injection (DPI) of RF signals into the DUT [28]. The DPI test verifies the immunity of the electronic components of the vehicle to the external narrowband disturbances. The applicable frequency range of the DPI test is 250 kHz to 500 MHz.

Figure 2.5 shows the block diagram of the DPI test setup. The RF signal is injected, through a coupling capacitor, to the DUT. The injected RF power level and signal frequency are changed, and the functionality of the DUT and its' external components will be examined [29]. As illustrated in Figure 2.5, a 10 dB attenuator is used on the injection point to minimize reflection. A coupling capacitor on the injection point isolates the DC voltage between DUT and the injection device. After the capacitor, the 3-port broadband artificial network (BAN) is placed [30]. The BAN is an LC low-pass filter with series inductors (L_{BAN}) and a capacitor (C_{BAN}). The low-pass filter provides good isolation between the supply and the DUT [31].

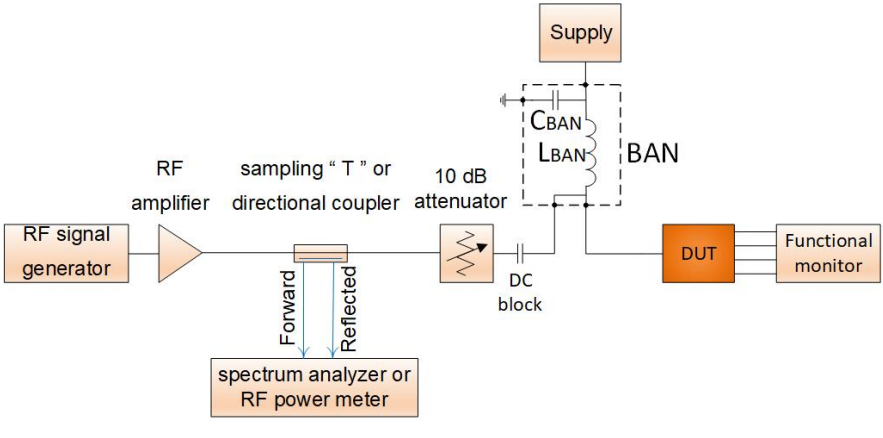

Fig. 2.5: Block diagram of the DPI test method [28, 29, 31]

Immunity to magnetic fields (ISO 11452-8)

This section of the standard explains the test methods for the immunity of electronic components to the magnetic field. The source of magnetic disturbance can be inside the vehicle or outside of it. According to the standard, the internal source can be from various sources, such as vehicle electric motors, actuators, etc. The power transmission lines, generating stations, etc. are the external magnetic sources, as mentioned in this part of the standard [32]. To generate a magnetic field and check the performance of the automotive systems, two methods are suggested - the radiating loop and the Helmholtz coil. Both methods have their restrictions due to the size of the DUT and coil. However, for the larger DUTs, the change of the position of the radiating loop is suggested in this standard.

Portable transmitter (ISO 11452-9)

To measure the electromagnetic immunity of the electronic components to external disturbances, the method of the portable transmitter can be applied. The measurements of this standard should be performed in an ALSE. The DUT and cable harness are radiated with electromagnetic disturbances generated by a portable transmitter. The corresponding peripheral devices can be placed either inside or outside the ALSE. The frequency range of continuous narrowband electromagnetic fields can be from 26 MHz to 5.85 GHz [33].

Either a commercial portable transmitter with integral antennas or a simulated portable transmitter can be used for the measurements. The simulated portable transmitter includes an RF signal generator, RF amplifier, directional coupler for the measurements of the forward and reflected power, coaxial cable, and transmit antenna. The antenna can be a broadband dipole antenna, a broadband sleeve antenna, or a folded dipole antenna. The different positions of the antenna are illustrated and described in this standard [33].

The power supply of DUT is provided through an artificial network. The functionality of DUT and cable harness is monitored using fiber-optic coupler. The operation of DUT is tested in the most significant conditions like; stand-by mode and a mode with which the maximum possible load can be reached [33].

Immunity to conducted disturbances in the extended audio frequency range (ISO 11452-10)

In this part of the standard, the immunity of DUTs to narrowband conducted disturbances in the low-frequency range (15 Hz to 250 kHz) is explained. Devices with acoustic or visible display functions can be tested using this measurement method.

In the presence of the conducted disturbances, the operation of DUT is examined. In contrast to the other parts of ISO 11452, no specific shielding or grounding requirements are suggested for the measurements. [34]

The disturbances are provided by an audio oscillator or signal generator. The generated signals are amplified and coupled to the DUT by an isolation transformer. The conducted voltage and the current of DUT are measured by a voltage measuring device – oscilloscope, voltmeter, etc. – and current probe, respectively [34].

Reverberation chamber (ISO 11452-11)

The test of immunity to the external disturbances in a reverberation chamber is outlined in part 11 of this standard [35]. The anechoic chamber has absorber materials so that the reflection of the electromagnetic waves is avoided. In contrast, a reverberation chamber has no absorber, and the walls of the chamber are made of highly conductive materials. Hence, the transmitted wave of the antenna is reflected within the enclosure. A mechanical stirrer, controlled by an external motor, provides the formation of a uniform wave in a specific volume of the chamber. The DUT is placed within the uniform wave region. The minimum applicable frequency of this test is a function of the room and the stirrer size [36].

There are two antennas within the reverberation chamber - the transmit and receive antenna. On the transmit path, the signal generator is connected to a power amplifier that feeds the antenna. Using a directional coupler and a power meter, the transmit power is measured. The resulting uniform field wave in which the DUT is placed is measured with a field probe. The receiver antenna is connected to an attenuator and a spectrum analyzer [36].

2.1.3 ESD immunity ISO 10605

The ISO 10605 standard deals with the test methods and the requirements of vehicle components and systems regarding their immunity to electrostatic discharges. This standard considers two discharge types - direct contact and air discharge. In the direct contact test, the generated ESD pulse is directly applied to the DUT. However, for the air discharge measurement, the arc discharge is initiated between the metal tip and DUT. The DUT is placed on an insulating material [37]. The positioning of the DUT, corresponding connections, related measurement devices, etc. are explained in this standard [38].

The implementation of the tests considers an ESD gun, which can generate a specific and standardized pulse shape. The ESD pulse shape has two parts. The first part introduces a high amount of current within ca. 1 ns followed by the second part that has a duration of around 60 ns, but with a smaller amount of current [37].

The equivalent circuit of the ESD gun consists of a voltage source with a resistor in series. The resistor is connected to a grounded capacitor (storage capacitance) and a discharge resistor (or storage resistor). The discharge resistor is connected to a switch that conducts the ESD current to the metal tip of the ESD gun [37].

In ISO 10605, the contact discharge mode is performed from 2 kV to 15 kV, and the air discharge test is implemented from 2 kV to 25 kV. The mentioned voltage levels require 150 pF/330 pF storage capacitance and 330 Ohm/2000 Ohm storage resistance [36]. Ten pulses per second should be generated for the tests. Further information can be found on page 164 of [37].

2.2 Automotive communication networks

The physical structure of the communication network includes ECUs and cables. To reduce the number of wires, various bus systems have been developed and implemented over the past few years. The reason for further investigations and developments regarding communication networks is due to the need for higher data rates and more reliable structures. Ethernet technology is a promising approach for the future of the automotive network, which requires data rates up to 100 Gbit/s or beyond. Such data rates enable, for instance, the implementation of autonomous driving in the future.

The communication cables are essential parts of the networks, as they enable data transfer between network nodes. Generally, two different channel types can come into question, i.e., copper wire and fiber-optic channels. These two cable types are briefly discussed in the following paragraphs.

The copper cables can be divided into two categories - unshielded and shielded wires. The traditional low-speed communication networks use unshielded wires, while high-speed networks (in Multi-Gigabit range) require shielded twisted cables. Additionally, using twisted pair cables and differential signaling can improve the immunity of the physical layer to noise, as the signals of both differential lines will be subtracted in the ECU, so the coupled noise can be suppressed.

In addition to the signal attenuation, the copper cables are susceptible to (common-mode) noise. The emission from the harness, generated from the common-mode currents [14], can produce interferences with other network participants. The mentioned drawbacks of the copper cables can have negative impacts on the performance of the system as a whole.

There are several copper cable types that come into question for high-speed data transmission. Three important cables that are of interest in the automotive industry are UTP, STP, and SPP cables.

The UTP cables are the choice of the automotive industry for Fast-Ethernet (100 Mbit/s). Unshielded twisted pairs are more susceptible to environmental noise, compared to the STP cables. In [39], the measurement setup and analytical method for calculating the transmission line parameters, i.e., complex line impedance, complex propagation constant of the UTP cables, is presented.

The STP cables possess better EMC characteristics in regards to emission and immunity to the external noise. The use of shielded cables can improve network

performance by introducing lower insertion loss, emission, cross-talk, and more robustness. The drawbacks of the shielded wires are higher weight, costs, and size [40]. Grounding the shield of STP cables is an important issue, which should also be considered.

Using optical fiber link for data communication has steadily been gaining more importance as the MOST network was introduced in 2001. However, the use of fiber optic cables in the vehicle was first introduced in 1998, with the domestic digital bus (D^2B) [41].

The implementation of Ethernet over fiber in harsh environments, e.g., in vehicles, can reduce EMC issues better, when compared to the use of copper twisted pairs. The use of fiber optic cables can also reduce harness complexity and weight, while the bandwidth can be increased [42]. In non-automotive applications, data rates of up to 400 Gbit/s with fiber are feasible. By using wavelength multiplexing, the transmission of different signals over a single fiber is possible. Furthermore, there is no need for the termination of fiber cables, considering the reflected waves at the end of the channel. This is the case in copper links [42].

The drawback of this method is that the voltage supply of ECUs should be realized over separate copper lines [43]. Compared to the copper links, optical fiber communication is still expensive. The use of plastic optical fiber for a full-duplex 1000 Mbit/s automotive data communication was discussed in IEEE 802.3bv-2017 (1000BASE-RHC) [44]. The application area of 1000BASE-RHC was infotainment and advanced driver assistance systems (ADAS).

The optical fiber and the corresponding in-line connectors should aim to fulfill various requirements for in-vehicle installation. The mentioned components have to be protected against dust and should be robust to vibrations. Safety, tensile strength, etc. are further specifications of the channel components, which have to also be considered [45].

The fiber optic channel of 1000BASE-RHC should support data communication over 15 m or 40 m. If the channel has a length of 15 m, up to four in-line connectors are allowed to be used. For the 40 m case, the introduced insertion loss through the channel should be less than 8 dB, without in-line connectors [41, 45].

As previously mentioned , the need for higher data rates has led to developments in the automotive communication networks. Later in this section, the most important automotive networking solutions are briefly discussed. Table 2.1 provides an overview of the discussed networks.

Table 2.1: Different automotive communication networks and the corresponding properties [1, 3, 4, 46]

Network Technology	Data rate	Topology	Channel	Protocol	Application	Standards
LIN	20 Kbit/s	Bus	Single wire	Master-Slave and scheduling	Seat control, door lock, lighting, trunk release, rain sensor, etc.	ISO 9141
Low-speed CAN	10 Kbit/s - 125 Kbit/s	Bus	Twisted pair	Message-based protocol	Air-condition control, seat control, power window unit, mirror adjuster, etc.	ISO 11898-3 (distance up to 500 m)
High-Speed CAN	125 Kbit/s - 1 Mbit/s	Bus	Twisted pair	Message-based protocol	Engine-management system, electronic transmission control, stabilization systems, etc.	ISO 11898-2 (distance up to 40 m)
CAN-FD	10 MBit/s	Bus	Twisted pair	Message-based protocol	Same as high-speed CAN	ISO 11898-1
FlexRay	10 Mbit/s	Star, bus	Twisted pair/ Optical Fiber	TDMA**	Safety-critical functions in power train and chassis	ISO 17458
LVDS*	655 Mbit/s	Point-to-point	Twisted pair	SerDes (Serializer / De-Serializer)	Infotainment and automotive camera	IEEE 1596.3
MOST	150 Mbit/s	Ring	Polymer Optical Fiber (POF)	TDMA	Infotainment / Multimedia, e.g., radio, GPS navigation, video displays and entertainment systems	MOST150
Ethernet	100 Mbit/s	Star (switch-based)	UTP / STP	Point-to-point link	Collision avoidance, lane departure detection, traffic sign classification, blind spot detection, driver intent detection, pedestrian detection, automatic cruise control	IEEE 802.3bw
	1000 Mbit/s					IEEE 802.3bp

*LVDS is not a communication technology. It is a communication principle [47]

**TDMA: Time Division Multiple Access

2.2.1 LIN

For applications that do not need large bandwidth and real-time response, the LIN bus system has been designed. The LIN network is implemented for the control of lights, seats, mirrors, climate control, etc. One of the main advantages of LIN is its cost-effectiveness. Due to the simple structure, the (micro-) controllers need less power consumption, less memory usage, etc. [1, 2].

Figure 2.6 shows the concept of LIN-Cluster. In this cluster, there is one master node and several slave nodes. The master node manages the data that is transmitted over the bus. The master node, which also includes a slave node, controls the other slave nodes in the network. Up to 16 slave nodes can be integrated into a LIN fieldbus [46].

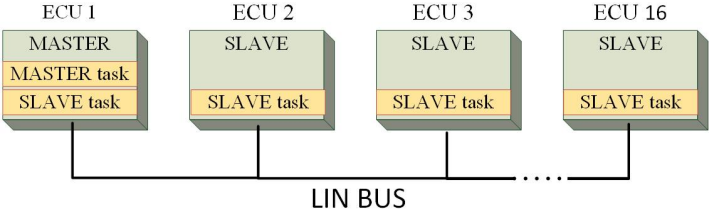

Fig. 2.6: LIN bus topology [46]

As the application area of the LIN does not contain critical functionalities, the data rate can be limited to 20 kbit/s. The channel (cable) is a single wire. The LIN bus is commonly used in conjunction with CAN. Both networks are connected over a CAN/LIN Gateway. The master node is responsible for the communication with other buses, e.g., CAN bus. Should the master node be damaged, the whole LIN bus no longer functions. The mentioned bus combination makes the communication system cost-effective and simpler.

The corresponding data coding of the LIN bus is the return-to-zero (RZ). In RZ coding, the “zero” and “one” state of digital communication is relative to the supply voltage of the bus system. If the signal has an amplitude between 60% and 100% of the supply voltage, a logical “one” is interpreted as. An amplitude of less than 40% of the supply voltage is recognized as a “zero” [46].

2.2.2 CAN

The corresponding standard of the CAN defines the specifications of the physical and data link layer of the OSI network model [5]. Using the CAN bus system, the different network participants (ECUs and devices) are enabled to communicate with each other without a host computer. Event-triggered traffic can be handled by CAN conveniently [2, 4]. There is no trigger signal, which synchronizes all the components of the CAN bus system. Therefore, CAN is an asynchronous serial bus network. The transmitted data from one ECU can be received from all the bus participants. To avoid the collision of data, especially if the bus traffic is high, the carrier sense multiple access/collision avoidance (CSMA/CA) method is applied [42].

Low-speed CAN has an operation data rate between 10 kbit/s and 125 kbit/s. For data rates higher than 125 kbit/s to 1 Mbit/s, the high-speed CAN is used [1]. However, there have been some studies to increase the CAN data rate, even up to 100 Mbit/s [48].

The use of differential signaling and twisted-pair cables improve the EMC safety of the CAN bus system. Using two wires, two different signal amplitude levels, i.e., “High” and “Low”, are transmitted. Over both wires, the same data sequence is used, while the signals have opposite amplitudes. The CAN bus uses non-return to zero (NRZ) signaling [1]. The high signal has an amplitude of 3.75 V, while the low signal is transmitted with 1.25 V. In the receiving mode, based on the voltage difference between the high and low level, the data can be processed. The interfered noise on the channel can be canceled in the receiver [4, 48]. Besides differential signaling, the use of priority based protocols makes the CAN bus suitable for safety-critical applications, like powertrain and engine control [48].

As shown in Figure 2.7, a CAN ECU consists of three components - the transceiver, controller, and microcontroller [4]. The CAN transceiver has the function of transmitting and receiving the analog signals. The controller checks whether the received information is expected or is addressed to other ECUs. The controller arranges the data timing. At the same time, the controller prepares the digital data for transmitting to the bus system. The microcontroller processes the digital data. The two terminations on both ends of the bus prevent the signal reflection [48].

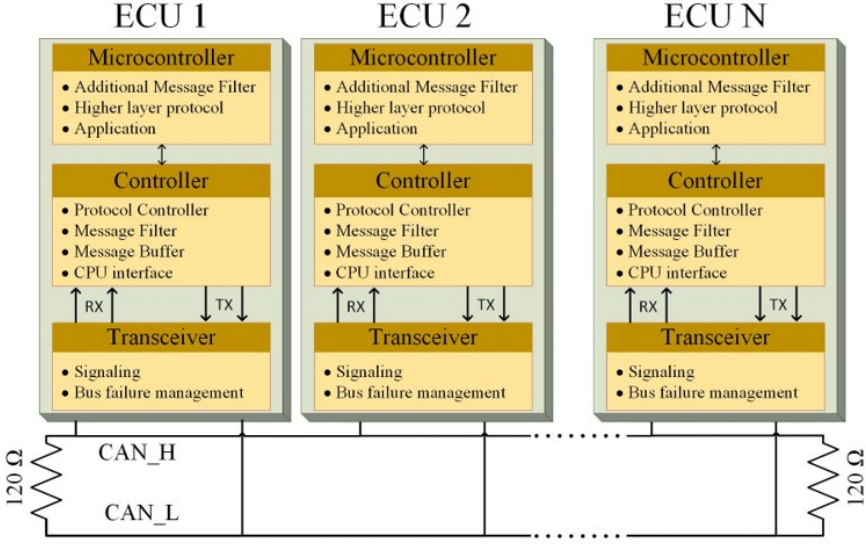

Fig. 2.7: CAN bus architecture [4, 48]

As the number of ECUs is increasing, the available bandwidth cannot support data communication. This problem can be solved using parallel CAN networks, which are connected over a gateway. However, utilizing multiple subnetworks leads to problems like fault-handling, timing response, wake-up, and sleep synchronization [1].

As described previously, the maximum reachable data rate with the CAN is 1 Mbit/s. This data rate cannot support the automotive industry for its planned broadband projects. The short message length of CAN protocols, i.e., 130 bits, are not practical for high-speed applications. The defined time delay of CAN messages (1 ms to 10 ms) is not suitable for real-time use. The priorities of data protocols are defined using the identifier. The lower the priority of a message, the higher the corresponding identifier. Therefore, the message of ECUs with higher identifiers will be delayed. The delivery of a message protocol in a specific time interval cannot be assured [42].

2.2.3 CAN FD

Utilizing CAN with flexible data rate (CAN FD) network, higher data rates - which can be chosen freely - are realizable. Depending on the network topology and the efficiency of the PHY's transceiver, the bitrate is configurable [1].

As the data rate of CAN FD is much higher than the CAN, the software download for initialization of the system or maintenance needs less time. Higher data rate gives the ability to use long messages in big frames at once and not segment them. Besides the higher data rate, the other advantage of CAN FD compliant ECUs is the ability to support CAN protocol [1, 49]. The physical layer of CAN FD, compared to the CAN PHY, is unchanged. The enhancement just happens in the CAN protocol controllers [50].

2.2.4 FlexRay

To increase the data rate over the bus system compared to CAN, in 2009 seven companies decided to develop the FlexRay communication protocol. The core members of FlexRay consortium are Volkswagen AG, Daimler AG, BMW AG, General Motors, NXP Semiconductors, Robert Bosch GmbH, and Freescale Semiconductor [51].

With FlexRay, the data rate of up to 10 Mbit/s is feasible. For critical applications, where constant latency and jitter is needed, FlexRay can be used. One of the application areas of FlexRay is the x-by-wire systems [2, 4]. The FlexRay uses a time-triggered protocol, which is based on the use of cycles and times slots. Each ECU has a predefined time slot, in which the corresponding data can be transmitted

to the bus. In time-triggered protocols, the ECUs can access the bus in the case of any event. The probability of data packets collision in event-triggered systems is much higher than time-triggered fieldbuses. In time-triggered systems, error-free communication is possible [51].

As it is shown in Figure 2.8, FlexRay can be installed in bus, star, or multi-star configuration [1, 51]. The bus topology can be implemented using a single bus or dual bus. The dual bus is a redundant approach, which increases the system reliability in case of error. To further enhance the robustness of the FlexRay, the star topology can be used. In the case of failure, the whole network is not affected, provided the nodes are connected in a star configuration.

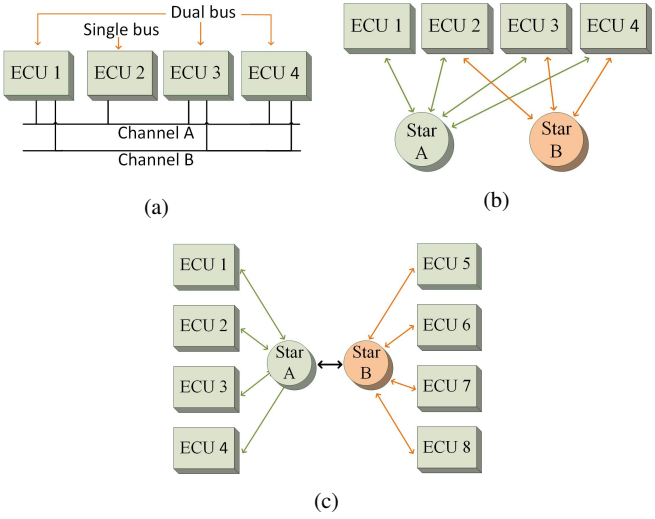

Fig. 2.8: FlexRay network configuration possibilities (a) dual bus (b) two star (c) cascading of stars [51]

2.2.5 MOST

For applications, e.g., multimedia, infotainment, and GPS navigation, higher data rates are needed [1, 2]. The goal of this network is the transport of audio and video data in digital format. Three data rate levels are reached with MOST networks. MOST25 supports a data rate of 25 Mbit/s. With MOST50 and MOST150 higher data rates of 50 Mbit/s and 150 Mbit/s are applicable, respectively.

According to the MOST150 standard, a maximal data rate of 150 Mbit/s is realizable with this technology. This network has a point-to-point communication between nodes.

To ensure an EMC secure data transmission, a polymer optical fiber (POF) material is used for the channel. MOST bus system uses a ring topology, where up to 64 nodes could be included [48].

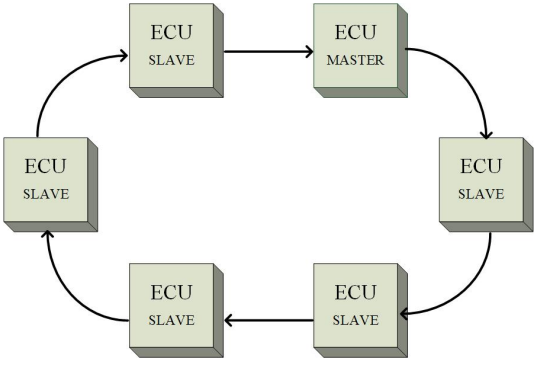

Fig. 2.9: The ring topology of the MOST network

2.2.6 LVDS

Low voltage differential signaling (LVDS) is a communication principle that enables differential signaling over a serial link. With LVDS, a high-speed communication with data rate around 655 Mbit/s is realizable. The communication is over a twisted pair cable [1]. The use of this principle is mostly for the implementation of the video data transmission in the vehicle and is used, e.g., in automotive pixel link (APIX) [47].

The uni-directional point-to-point connection and the use of costly shielded cables make this technology impractical for the implementation in the car [47, 52].

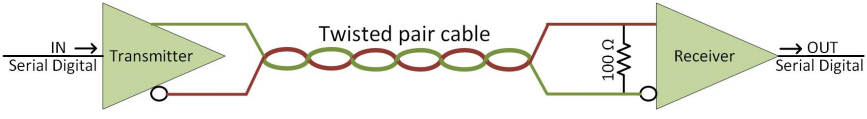

Fig. 2.10: The principle of low voltage differential signaling (LVDS) [8]

2.2.7 Ethernet

Ethernet is a technology in which the IP-based communication between multiple computers and devices is realizable. This technology defines the specification of the required software and hardware. In 1983 the IEEE 802.3 standard, as the first Ethernet standard, was released. With the introduction of 10BASE-T, a data rate of 10 Mbit/s over two twisted-pair cables is possible. With this standard, full-duplex communication is possible. One of the twisted pairs is used for transmitting and the other one for data receiving [53]. The implementation of 10BASE-T happened using the Manchester encoding scheme, where the bit representation is encoded in the middle of the bit frame. If the first half of the frame has a high level, then followed by a low level in the second half, the logical "0" is transmitted. In contrast, if the first half has a low amplitude, and the second half is high, the binary "1" is transferred (Figure 2.11).

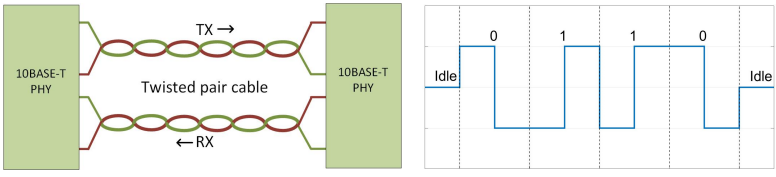

Fig. 2.11: (a) 10BASE-T structure and (b) the corresponding Manchester coding scheme [53]

The next generation of Ethernet was the 100BASE-T over two twisted-pair cables enabling 100 Mbit/s. The used coding scheme for this standard is multilevel transmission encoding – 3 levels (MLT-3). In MLT-3 signaling three voltage levels (-V, 0, +V) are used. If the amplitude of the signal does not change and is continuous over the bit frames, a logical "0" is transmitted. The change of amplitude is considered as a logical "1" (Figure 2.12).

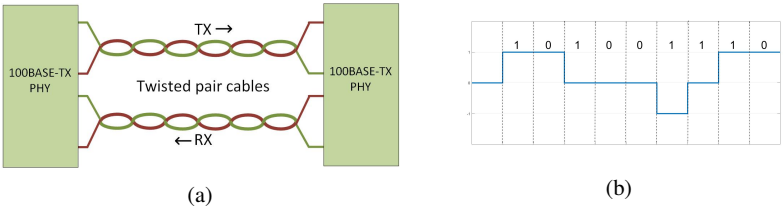

Fig. 2.12: (a) 100BASE-T structure and (b) the corresponding MLT-3 coding scheme [53]

By increasing the number of twisted-pair cables to four and using 4-dimensional, 5-level pulse amplitude modulation (4D-PAM-5), a new standard (1000BASE-T) with an effective data rate of 1000 Mbit/s was introduced in 1999. As shown in Figure 2.13, four twisted-pair cables carry four signals, each with five states (-2, -1, 0, 1, 2). With the 4D-PAM-5 signaling, the simultaneous transmission of 8 bit at a rate of 125 MHz is possible [54, 55]. The corresponding voltage levels over each twisted pair cable are (-1 V, -0.5 V, 0 V, +0.5 V, +1 V). "0 V" is used for error correction [56].

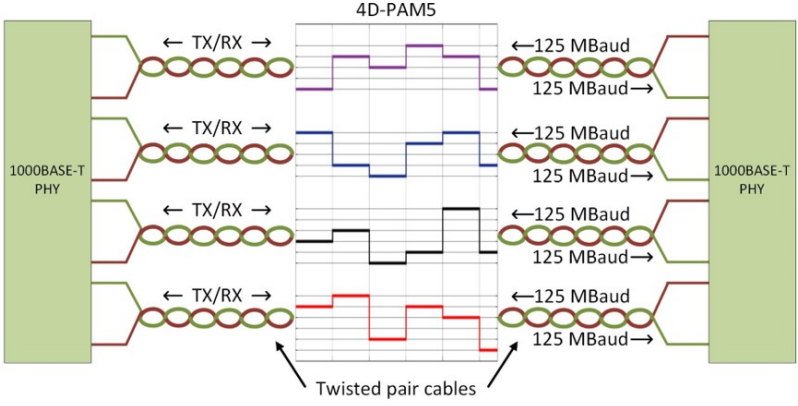

(a)

Fig. 2.13: (a) 1000BASE-T structure and (b) the corresponding 4D-PAM-5 coding scheme [53, 55, 56]

The 10GBASE-T standard supports a data rate of 10 Gbit/s. The channel has the same configuration as 1000BASE-T and consists of four twisted-pair cables. Each twisted pair delivers 2.5 Gbit/s at a baudrate of 800 Mbaud in full-duplex mode. To increase the data rate, PAM-16 signaling is implemented [57].

The Ethernet technology has found great importance over the past years in the transportation industry. The use of Ethernet in aircraft was introduced in the 90s by Airbus [58]. For infotainment and multimedia application in the cabin, higher data rates are required. However, the use of Ethernet in airplanes is confronted with important EMC issues, such as lightning strikes effects; high intensive radiated fields originated from, e.g., radars, ESD from occupants, and the electromagnetic issues from various onboard electrical devices [53].

Ethernet bus system is the choice of the automotive industry for the realization of broadband communication systems. The cost reduction, higher bandwidth - even in gigabit/s range - and the flexibility of this technology make it attractive for the

OEMs [4]. The past Ethernet improvements in non-automotive sectors can help the OEMs adapt this bus system more easily to their needs. To integrate the Ethernet in the vehicle, some changes like power over Ethernet, partial networking, and improvement of EMC susceptibility have to be implemented [1].

The use of Ethernet enables the OEMs improve the driver assistance technologies, which require various sensors and robust algorithms for data analysis and decision making. The used sensor systems for distance measurement applications include short-range 24 GHz sensors, long-range 77 GHz RADAR, ultrasonic sensor, and light detection and ranging (LiDAR). The infrared camera and RGB optical video cameras are for recognition and tracking applications. Global positioning system (GPS), together with the inertial measurement unit (IMU), act for the localization of the vehicle [59].

The mentioned sensors provide information for various algorithms, like automatic cruise control (ACC), surround-view parking, pedestrian detection, collision avoidance, classification of traffic signs, blind spot recognition, lane departure detection, night vision assistance, and driver intent detection [1, 4, 5]. The Ethernet bus system can support the required bandwidth and data rate. The implementation of car-to-car, car-to-x, and autonomous driving can also be implemented using Multi-Gig Ethernet communication systems.

Artificial intelligence and autonomous driving

The implementation of self-driving cars is the target of the automotive industry over the next few years. The fully autonomous car should be secure and reliable regardless of weather conditions and traffic situation etc. In [59], detailed information for implementation of autonomous driving regarding the hardware and software requirements is discussed.

The central core of a self-driving vehicle is the neural network algorithm, which controls the motion of the car. The inputs of the algorithm are the information, provided by different sensors and cameras, as explained above. According to [60], a forward-facing radar produces 1.26 TB of data in one hour. Hence, just the radar generates 2800 MBits of data in a second. A two-megapixel camera with 30 frames/s produces 1440 MBit in a second. So, an autonomous vehicle with just four radars and four cameras needs to process 7160 Mbit/s. As the mentioned example is an elementary assumption, one can imagine that an autonomous car, fully connected with other vehicles and infrastructures and in possession of a large number of sensors and actuator, has to process tens of gigabits of data in a second. This is why the automotive industry has decided to implement Multi-Gig Ethernet technology in vehicles. In the next subsection an overview of the automotive Ethernet standards is provided.

2.3 Automotive Ethernet standards

IEEE 802.3 working group is responsible for the standardization of PHYs and media access control (MAC) layers of wireline IP-based Ethernet communication. There are several automotive Ethernet standards and categories, which differ in their data rates. The designations of these categories contain three parts. The first part describes the data rate. The second part, "BASE," means that the signals are baseband signals. The third part, "T1," reveals the use of a single twisted pair as the communication channel.

Depending on the required data rate, the automotive Ethernet can be subdivided into the following categories:

2.3.1 10BASE-T1S / IEEE 802.3cg

As described in the previous subsection, the cost and complexity reduction is a major key factor in automotive electronic systems. For some applications, where there is less bandwidth and data rate demand, a simple 10 Mbit/s Ethernet-based bus system can be implemented [40]. The IEEE P802.3cg 10 Mb/s single pair Ethernet task force is currently working on the publication of the first draft standard for this low-speed fieldbus. The call for interest of this Ethernet standard was published in July 2016.

Figure 2.14 shows the overview of a 10BASE-T1S network structure. There is no need for a switch to manage the data transfer between ECUs of this network. Using one bus has the advantage of less cabling and less power assumption. The whole 10BASE-T1S network can be connected through a switch with other network categories, e.g., 100BASE-T1.

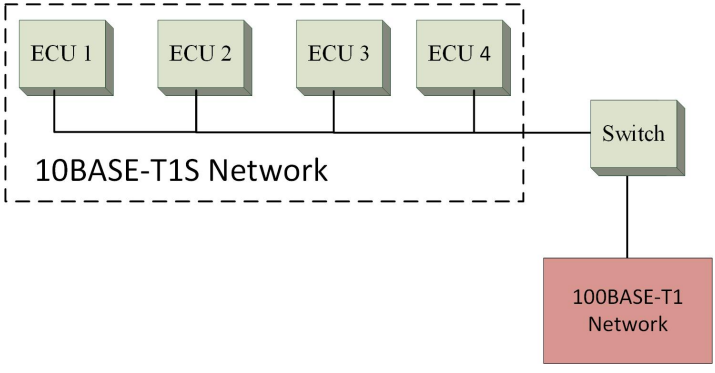

Fig. 2.14: Overview of the 10BASE-T1 network [61]

2.3.2 100BASE-T1 / IEEE 802.3bw

The consortium OPEN Alliance has developed a 100 Mbit/s physical layer standard, a so-called BroadR-Reach (BR). The main advantage of this automotive 100 Mbit/s network is the use of a single twisted pair instead of two pairs, compared to 100BASE-Tx, and realizing a bit error rate (BER) of less than or equal to 10^{-10}. The call for interest (CFI) of this standard was announced in March 2014, which led to the standard in October 2015.

In this subsection a brief explanation of 100BASE-T1 regarding the structure of the bus interface network (BIN), related test method, and EMC issues is given.

Bus interface network

The BR-PHY consists of a physical coding sublayer (PCS) and physical medium attachment (PMA). As illustrated in Figure 2.15, the PCS sublayer undertakes the task of signal transmitting/receiving between the media independent interface (MII) interface and PMA sublayer. The received 4-bit serialized data stream from MII is encoded into 3 bits code-groups (+1, 0, -1), which will be transmitted to PMA for the electrical signaling. In the opposite direction, the code-groups of PMA will be decoded and sent to MII.

The PMA sublayer, between PCS and medium dependent interface (MDI), has two main functionalities, that is, link management and PHY control. In the slave mode of the PHY, the clock recovery, signal equalization, and echo cancellation are performed in PMA sublayer [62].

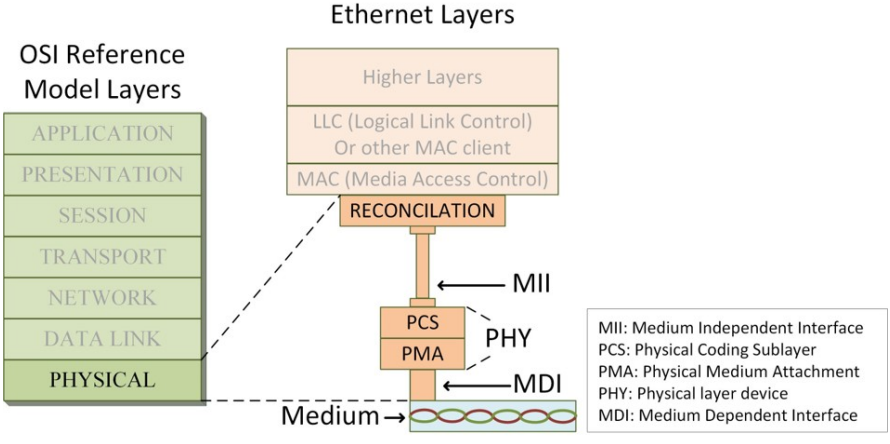

Fig. 2.15: The block diagram and structure of the 100BASE-T1 physical layer

A detailed overview of the 100BASE-T1 analog front-end is given in Figure 2.16. As illustrated, the digital 4-bit data is transferred to/from a microcontroller from/to the transceiver. The PHY has an on-chip clock generator, low-pass filter, and ESD protection. The PHY is connected to a CMC for suppressing the common-mode noise. The common-mode termination reduces EMI and susceptibility to CM noise. An ESD protection in front of the ECU connector suppresses the discharges. The connection to the UTP cable is realized through the ECU connector.

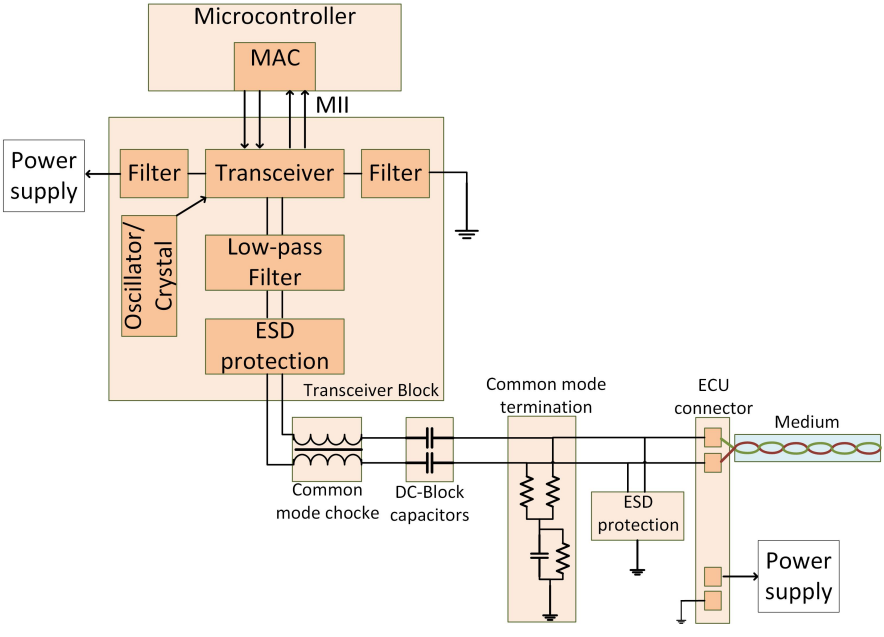

Fig. 2.16: The AFE of 100BASE-T1 [10]

Master-Slave configuration

The BR-PHY can operate in two modes, i.e., master or slave. This setting is performed using a FORCE mode [62]. In master mode (transmit function), the clock signal (66.6 MHz) is generated using a local crystal or oscillator. By contrast, in slave mode (receive function), the clock is recovered from the received signal. The default configuration of all BR-PHYs after power-up or reset is the slave mode. The FORCE mode generated from the management system, a processor or microcontroller, changes the operation mode of the PHY.

Pulse amplitude modulation

BroadR-Reach adopted the PAM-3 modulation format. In this modulation, the signal can have voltage levels of [-1, 0, +1]. With PAM-3 signaling, each data symbol contains 1.5 bits and has a time length of 15 ns. The resulting symbol rate for 100 Mbit/s is 66.6 Mbaud. The use of PAM-3 signaling reduces the required bandwidth, EMI, and the cost of corresponding cables [62].

Data scrambling

A consecutive sequence of zeros or ones in the data stream may lead to bit synchronization problems. Such periodic patterns create discrete spectral lines in the signal spectrum and lead to cross-talk issues on the adjacent channels. To avoid the mentioned problems, 100BASE-T1 uses a scrambling technique by which the data sequences are randomized and transmitted. Further information can be found on page 35 of [62].

Switch

As previously described, the CAN protocols use identifiers in data protocol for defining the priority of messages. In BroadR-Reach the data communication is a point-to-point connection with which full-duplex data transfer between two network nodes is possible. The problem of data collision is solved using the corresponding switches [26].

PoE

Power over Ethernet (PoE) is also possible with this standard. The use of PoE decreases the number of cables and reduces cost. Hence, there is no need for separate power supply cables, which feed the ECUs. PoE is standardized in IEEE802.3af. In this standard, the implementation of this technology over Ethernet cables is discussed.

Echo cancellation

The objective of the BR PHY is the implementation of a full-duplex communication link over a twisted pair cable. Hence, the transmitted and received signals should be separated using an echo cancellation circuit. 100BASE-T1 PHY utilizes the hybrid subtraction method, enabling usage of the full channel bandwidth in each direction simultaneously [40]. In this technique, the known transmitted signal of the PHY is subtracted from the unknown channel signal, which includes both Tx and Rx signals (Figure 2.17). With this method, the Rx signal can be extracted.

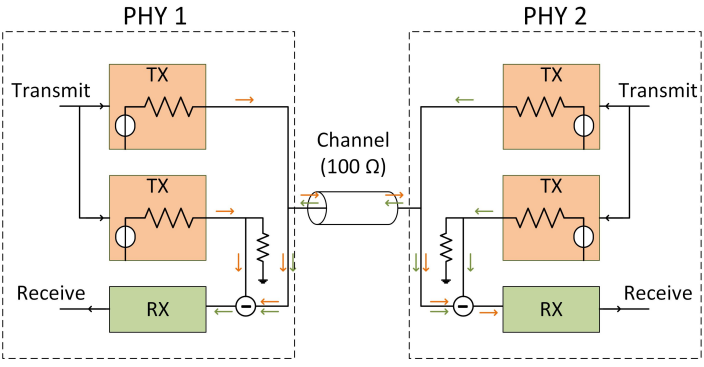

Fig. 2.17: Hybrid subtraction block diagram for 100BASE-T1 echo-cancellation [40]

PHY tests

To measure the transmit droop[1], jitter, transmitter distortion, and PSD mask, five test modes are defined in OPEN Alliance BroadR-Reach®. By just setting three bits of the control register, the mentioned parameters are tested. No changes to the transceiver circuit, compared to the regular operation, should be performed. The related measurement setups of the PHY test can be found in [62] pages 59 and 60.

- The transmitter droop is measured by sending N "+1" symbols followed by N "-1" symbols. As described before, each symbol has a time length of 15 ns. The parameter N should be so chosen that $N \times 15ns > 500ns$. The maximum voltage droop after 500 ns should be 45% of the initial peak after the zero-crossing.

- Transmitter jitter test in master mode is the second PHY test mode. A data sequence symbol +1, -1 is transmitted continuously. The applied symbol clock for this test corresponds to the normal master mode clock frequency, i.e., 66.6 MHz.

- The third test mode, i.e., transmitter jitter in slave mode, is optional. The same scenario as in test mode two is implemented while the PHY is in slave mode.

- The measurement of the transmitter distortion is implemented in the fourth test mode. In this mode, a sequence of PAM-3 symbols is transmitted. Further details can be found in [62] pages 59 and 61.

- In order to measure the PSD mask of the transmitter, a sequence of random PAM-3 symbols must be transmitted. The corresponding scrambling function is explained in [62] section 3.2.4. The applicable PSD limits of the 100BASE-T1 are presented in Figure 2.18.

[1] Droop is the pulse amplitude reduction between its beginning and end points.

Frequency	PSD Upper Limit (dBm)	PSD Lower Limit (dBm)
1 MHz	-23.3	-30.9
20 MHz	-24.8	-35.8
40 MHz	-28.5	-49.2
57 MHz - 200 MHz	-36.5	-

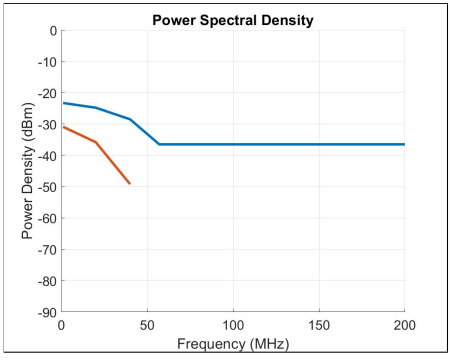

Fig. 2.18: PSD mask limits of 100BASE-T1 [62]

EMC requirements

Due to the high operating frequency of the 100BASE-T1 and the utilization of UTP cables, the EMC issues play a significant role in the network [63]. The PHY should be tested with the test method defined in CISPR 25. In [63], following EMC tests are prescribed:

- **Immunity - DPI test / IEC 62132-4**

  The functionality of the PHY can be disturbed due to the CM and DM noise. The coupled CM noise over UTP cable, in-line connector, MDI, etc. can affect the performance of the PHY. Further, the conversion of CM to DM noise leads to malfunctioning of the PHY. With the DPI test, according to IEC62132-4, the sensitivity of PHY to the CM noise can be measured [62]. The measurement method of the DPI test is explained in section 2.1.2.2. Further details regarding the measurement of DPI test for 100BASE-T1 are noted in [63] on page 21.

- **RF emission - 150 Ohm test / IEC 61967-4**

  A PHY with a high-frequency functionality emits RF signals, which can cause interferences with its surrounding components. With the 150 Ohm test, according to IEC61967-4, the emission of the PHY can be measured. The required test setup for this test is explained in [63] on page 17.

- **Transient immunity / ISO 7637-2**

  The occurrence of the electrical transients can lead to malfunctioning or damage to the PHYs. On page 26 of [63], the corresponding direct capacitive coupling test method for the measurement of transient immunity is explained.

- **ESD immunity / IEC 61000-4-2**

  The immunity of 100BASE-T1 PHY against ESD is tested using a direct galvanic contact, utilizing a contact discharge module according to IEC 61000-4-2. Further information regarding measurement setup can be found in [63] on page 31.

100BASE-T1 CMC

The use of a common-mode choke is the preliminary step to suppress the CM noise. Figure 2.19 shows an SMD CMC suitable for 100BASE-T1 standard. However, the CMC can introduce DM-to-CM noise due to possible asymmetries in the structure of the choke [64, 65]. The characterization and working principle of the 100BASE-T1 suitable CMC are investigated in chapter 3.

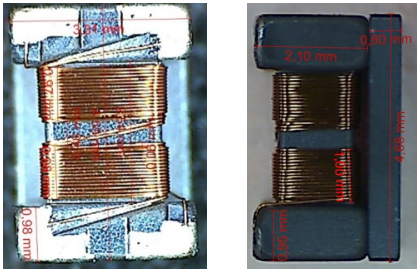

Fig. 2.19: SMD CMC suitable for 100BASE-T1

Noise environment and alien crosstalk

As explained, the separation of the Tx and Rx signals is performed using a hybrid subtraction method. This circuit can introduce signal echo on the channel. Impedance discontinuities of the channel components also lead to signal echo. The second noise source is thermal noise. According to [62], this noise type has a signal level of -140 dBm/Hz, which does not have any remarkable impact on the system performance as a whole.

The use of one twisted pair cable for data communication in 100BASE-T1 has a dominant advantage regarding cross talk. The use of one pair eliminates the problem of near-end crosstalk (NEXT) or far-end crosstalk (FEXT) on the channel. However, the use of several cables in harness introduces the alien crosstalk (AXT). The AXT cannot be canceled out, as the signal of the disturbing cable is unknown to the victim channel. According to the 100BASE-T1 standard, the BR-PHY should be tested regarding AXT. For this purpose, the measurement setup shown in Figure 2.20 is suggested.

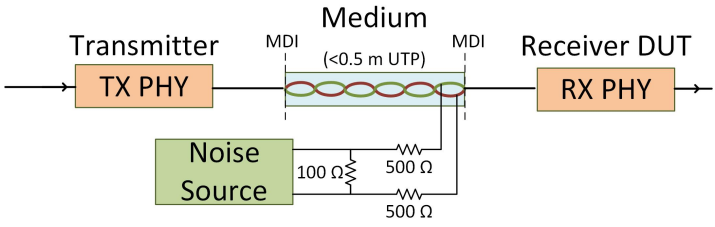

Fig. 2.20: Alien crosstalk noise rejection measurement setup for 100BASE-T1 [62]

The use of in-line connectors in the communication link increases the AXT problem. In the in-line connector, the implementation of twisted configuration is not possible. This untwisted region is a weak point, regarding AXT [66]. In [66], the study of AXT for the 100BASE-T1 link and the influence of the untwisted pair region on the coupling between cables is introduced. To characterize the AXT issue of the 100BASE-T1 channel, two parameters for a 5-around-1 cable bundle are suggested in BroadR-reach. The mentioned parameters are power sum alien near-end crosstalk (PSANEXT) and power sum alien attenuation to crosstalk ratio-far end (PSAACRF). On page 73 of [62], the corresponding bounds of these parameters are presented.

Manufactured PHYs

In [43], the AFE of Broadcom for the 100BASE-T1 is introduced. In the first stage, an off-chip CMC suppresses the CM noise picked up by the channel. On-chip CM clamping is the second part of the AFE, which deals with the reduction of the residual CM amplitudes. The asymmetries of the CMC, power over data line (PoDL) inductors and the UTP channel lead to CM to DM noise conversion. The produced DM noise is suppressed by a 3^{rd} – order Bessel filter, which is implemented in the Rx path. In the Tx circuit and to minimize the emission caused by DM-to-CM noise, digital FIR and RC filters have been designed. The transmitted voltage has a peak-to-peak amplitude of 2.2 V. Due to the full-duplex operation mode, the overall voltage swing over the channel is 4.4 V.

Marvel has introduced 88Q2110/88Q2112 PHYs, which are suited for 100BASE-T1 and 1000BASE-T1 standard. According to [67], the PHYs can be used for infotainment and driver assist systems, body electronics, and automotive diagnostics. The required voltage supply is 3.3 V. The PHYs have the ability for error correction, signal equalization, data recovery, echo cancellation, and crosstalk suppression.

100BASE-T1 channel

As described before, the communication channel of 100BASE-T1 is an unshielded twisted-pair copper cable. The channel can have a maximum length of 15 m, where

up to two in-line connectors and two end connectors are foreseen. The following four transmission parameters of the channel are defined in BroadR-Reach.

- The differential impedance of the twisted pairs should have a nominal value of 100 Ohm (±10 Ohm). The impedance measurement is performed with time domain reflectometry (TDR) using a rise-time larger than 700 ps.

- The attenuation of the channel, including the cable and connectors, is characterized with the insertion loss (IL) parameter. According to [62], the IL of the channel should be less than the values presented in Table 2.2.

Table 2.2: The channel IL limits for 100BASE-T1 channel [62]

Frequency	Insertion loss (dB)
1 MHz	< 1.0
10 MHz	< 2.6
33 MHz	< 4.9
66 MHz	< 7.2

- Over the frequency range between 1 MHz and 66 MHz, the return loss (RL) should be equal to, or better than, the limits noted in Table 2.3.

Table 2.3: The channel RL limits for 100BASE-T1 Channel [62]

Frequency	Return loss (dB)
1 MHz - 20 MHz	≥ 18
20 MHz - 60 MHz	$\geq 18 - 10 \cdot log_{10}(\frac{frequency}{20})$

- The asymmetries in cable and in-line connectors introduce DM to CM conversion. This conversion is measured using mixed-mode S-parameters S_{dc11}, S_{dc22}, S_{dc21}, and S_{dc12} [62]. The study of mode conversion caused by in-line connectors of 100BASE-T1 is presented in [65]. As a result of mode conversion, the CM emission increases. The specified frequency range for the mode conversion is from 1 MHz to 200 MHz. The limits presented in Table 2.4 are defined for the mode conversion of 100BASE-T1.

Table 2.4: The channel mode conversion limits for 100BASE-T1 Channel [62]

Frequency	Mode Conversion (dB)
1 MHz - 33 MHz	≥ 43
20 MHz - 60 MHz	$\geq 43 - 20 \cdot log_{10}(\frac{frequency}{33})$

100BASE-T1 MDI

The MDI connectors (with two or multiple pins) are the interface between the AFE and channel. The connectors should not degrade the signal quality regarding RL or IL. The explained electrical requirements for the channel are valid for the MDI connector. The only change is the RL limit, as defined in Table 2.5.

Table 2.5: The channel RL limits for 100BASE-T1 MDI [62]

Frequency	Return loss (dB)
1 MHz - 30 MHz	≥ 20
30 MHz - 66 MHz	$\geq 20 - 20 \cdot log_{10}(\frac{frequency}{30})$

Delay constraints

In BroadR-reach, the signal delay measurement is divided into two parts. The first part is the introduced delay between MII and twisted pair in transmit mode, which should be less than 240 ns. In receive mode, the signal delay between channel and MII should be less than 780 ns.

2.3.3 1000BaseT1 / IEEE 802.3bp

To further increase the applicable data rate to 1000 Mbit/s, the IEEE 802.3bp working group was founded in 2012. The CFI of this standard was published in March 2012, and the standard was released in June 2016. The main objective of the working group was the realization of 1 Gbit/s data transmission over a single twisted pair cable.

The corresponding PHY of the 1000BASE-T1 standard is capable of operating at 1000 Mbit/s in a full-duplex operation mode. This means that an effective data rate of 1 Gbit/s in each direction and simultaneously should be applicable. Using PAM-3 modulation, a baud rate of 750 Mbaud is used [68].

Bus interface network

According to IEEE 802.3bp, the PHY sublayers are PCS, PMA, and auto-negotiation (AN) as an optional sublayer (Figure 2.21). The MDI undertakes the responsibility of communication between PHY and the channel. The PCS is responsible for encoding and decoding the data from the gigabit medium independent interface (GMII) and PMA, respectively. The PMA serializes the code group coming from PCS and converts the incoming serialized data from MDI to code groups for use in PCS. The analog-to-digital and digital-to-analog conversion happens in PMA [68].

Auto-negotiation, as an optional sublayer, controls the functional mode of the PHY. It determines either the PHY is in master or slave mode. This sublayer can advertise the ability of the PHY for supporting 1000BASE-T1 in the network, as well.

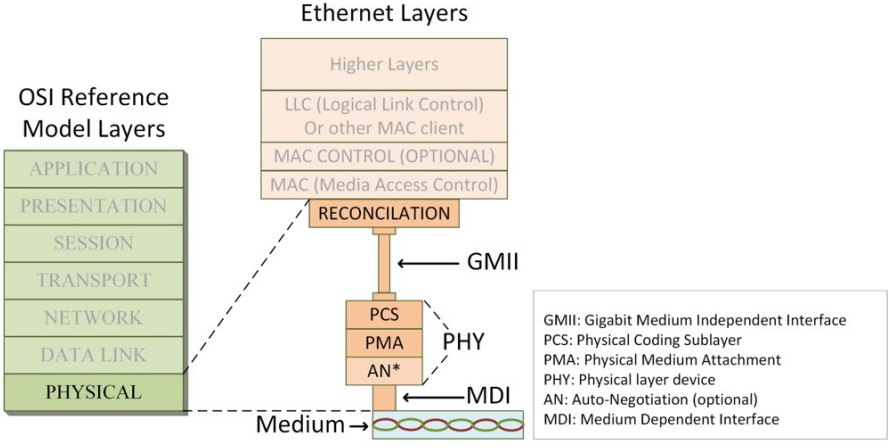

Fig. 2.21: The block diagram and structure of the 1000BASE-T1 physical layer [68]

Master-Slave configuration

Using runtime configuration, a master or slave mode operation can be applied with a 1000BASE-T1 PHY. The mentioned configuration controls the runtime behavior of the PHY. In master mode, the PHY determines the timing of the transmitter operation using a local clock. A PHY in slave mode receives the signals and recovers the transmitted clock [68].

Pulse amplitude modulation

The 1000BASE-T1 utilizes PAM-3 modulation. The symbol rate of this standard is 750 Mbaud, in which around 12% overhead for error correction is considered. Each symbol has a duration of 1.3 ns. The PAM-3 mapping is implemented in the PCS sublayer of Figure 2.21. The analog modulated signal can have voltage levels of [-1, 0, +1].

Data scrambling

To avoid long sequences of zeros or ones, which lead to the presence of discrete amplitudes in the signal spectrum, a 15-bit data scrambler is implemented in 1000BASE-T1 [68]. The data scrambling is performed in the PCS sublayer.

Energy-Efficient Ethernet

The optional use of energy-efficient Ethernet (EEE) for reducing the power consumption of the network is forecasted in [68]. The implementation of EEE is the subject of IEEE802.3az.

Echo cancellation

The echo cancellation technique is also foreseen in IEEE 802.3bp. However, the author was unable to find further information on the implementation of the echo cancellation for this standard. As of now (mid-2020), no publication from the semiconductor industry - which explains the details about the circuitry implementation of the 1000 Gbit/s PHYs - could be found.

PHY tests

There are seven test modes with which the transmitter's jitter, distortion, PSD, droop, and BER could be tested. These tests are performed by setting three bits of the management data input/output (MDIO) registers. The seven test modes are as follows [68]:

- Test of the transmitter timing jitter on master and slave transmitter using a 125 MHz clock (one-sixth of the standard operating frequency, i.e., 750 MHz).
- If the transmitter is in master mode, the transmitter jitter on MDI is tested using a clock frequency of 750 MHz. Tx transmits a continuous pattern of three "+1" symbols followed by three "-1" symbols.
- The third test mode is not defined and is reserved for future use.
- The fourth test mode is the linearity test of the transmitter. In this mode, a sequence of symbols using a polynomial equation is generated and transmitted. Detailed information can be found in [68] page 129.
- Evaluating the transmitter power level and checking the compliance with the transmitter PSD mask is the subject of the fifth test mode. In Figure 2.22, the corresponding PSD limits of 1000BASE-T1 are illustrated.
- Generating a 25 MHz transmitter output frequency is the next test mode. For this purpose, a continuous symbol pattern, including fifteen "+1" followed by fifteen "-1" symbols are transmitted using the regular clock operation frequency of 750 MHz.
- The final test mode is for calculating the BER of the link. Using the local clock, a symbol sequence of zeros is transmitted over the channel. Any non-zero received symbol in Rx is counted as an error.

Frequency	PSD Upper Limit (dBm/Hz)	PSD Lower Limit (dBm/Hz)
0 - 40 MHz	-80	-
40 - 100 MHz	-80	-86
200 MHz	-84	-90
300 MHz	-88	-94
400 MHz	-92	-98
500 MHz	- 93.6	-
600 MHz	- 95.2	-

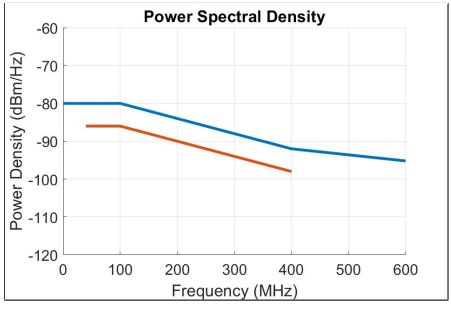

Fig. 2.22: PSD mask limits of 1000BASE-T1 [68]

EMC requirements

The RF immunity and RF emission test of 1000BASE-T1 PHY should be performed according to ISO 11452 and CISPR 25, respectively [68]. In [69], the required EMC test setups and methods are explained, which are the same as the EMC test methods for 100BASE-T1 (Section 2.3.2). The following tests should be performed:

- Immunity - DPI Test / IEC 62132-4
- RF emission - 150Ohm Test / IEC 61967-4
- Transient immunity / ISO 7637-2
- ESD immunity / IEC 61000-4-2

CMC

The evaluation of the 1000BASE-T1 CMC is performed using mixed-mode S-parameter measurements, immunity to ESD, and the saturation effect test [70]. An optional TDR measurement is also suggested.

As illustrated in Figure 2.23a, the measurements should be performed with a four-port vector network analyzer (VNA). The tests are carried out in a frequency range between 1 MHz and 1 GHz. The S_{dd11}, S_{dd22}, S_{dd21}, and S_{cc21} parameters should be measured. Figure 2.23b and 2.23c show the test setup for differential to common-mode (S_{sd21} and S_{sd12}) and common-mode to differential-mode conversion (S_{ds21} and S_{ds12}), respectively.

The ESD immunity of the 1000BASE-T1 CMC should be tested through the direct galvanic coupling of the ESD generator and the CMC test board [70].

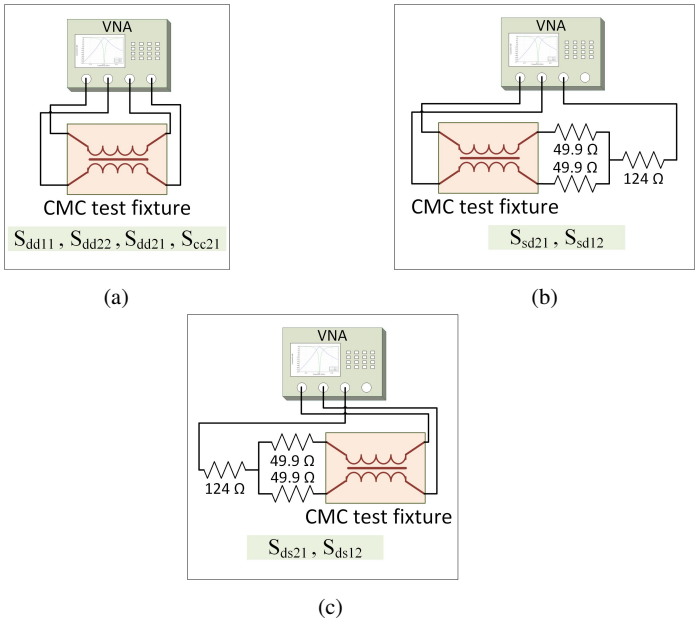

Fig. 2.23: Block diagram of the CMC test setup for (a) 4-port measurement of S_{dd11}, S_{dd22}, S_{dd21}, and S_{cc21} (b) 3-port measurement of S_{sd21} and S_{sd12} (c) 3-port measurement of S_{ds21} and S_{ds12} [70]

The RF saturation measurement of the CMC should be performed with VNA, RF amplifier, and RF attenuator (Figure 2.24). For this measurement, each side of the CMC is short-circuited. The injected common-mode, which is amplified with 40 dB, should be suppressed by the choke. However, the CMC loses its CM suppression ability if it is saturated. The amount of the CM signal that passes through the choke can be measured on the second port of the VNA.

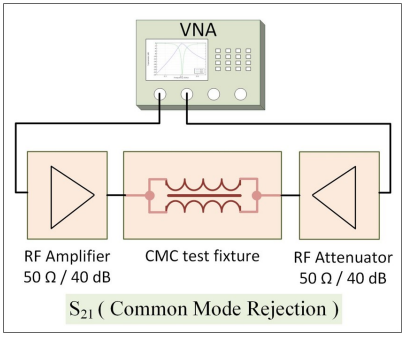

Fig. 2.24: Block diagram of the CMC test setup for the RF saturation test (common-mode rejection) [70]

Noise environment and alien crosstalk

The measurement setup for receiver tolerance to alien cross talk is shown in Figure 2.20. A Gaussian signal generator with a bandwidth of 550 MHz acts as the noise source and is connected to the MDI of the Rx side. Depending on the link segment type, the magnitude of the noise signal will be set. For the type A link, the noise magnitude is -100 dBm/Hz, while -110 dBm/Hz is the defined magnitude for the type B link segment. Using this measurement setup, the BER of the transmission should be less than 10^{-10} [68].

Besides the described receiver tolerance to alien cross talk, the alien cross talk between two adjacent cables should be measured. The corresponding limits for the AXT between channels of the 1000BASE-T1 standard are described on page 142 of [68].

Manufactured PHYs

One of the leading semiconductor companies for presenting the suitable 1000BASE-T1 PHY is Marvel, who introduced the 88Q2112A2 PHY. The PHY can be utilized for infotainment and driver assist systems, body electronics, and automotive diagnostics [67].

1000BASE-T1 channel

The full-duplex operation mode of 1000BASE-T1 should be realized over a twisted-pair copper cable. An effective data rate of 1 Gbit/s in the Tx and Rx path should be simultaneously applicable. In [68], two link segments are defined:

- Link segment type A is for automotive applications and contains a twisted-pair copper cable with a maximum length of 15 m. Up to four inline connectors can be used in type A.

- For non-automotive applications, i.e., transportation, automation controls, and industrial usage, a single copper twisted pair cable with four in-line connectors and a total length of 40 m is forecasted: a so-called link segment type B.

For the link segment type A, which is in the focus of this work, the corresponding limits are predefined in [68]. The electrical parameters, which should satisfy the presented bounds of the standard, are insertion loss of the cable, 100 Ohm differential impedance, return loss, and the differential to common-mode conversion.

Due to asymmetries in the cable or the structure of in-line connectors, mode conversion can occur. The mode conversion can be measured using mixed-mode S-parameter measurements. In Table 2.6, the related parameters are presented.

Table 2.6: Corresponding mixed-mode S-parameters for the measurement of the mode conversion in the channel of 1000BASE-T1

Parameter name	Mixed-mode S-parameter	Description
Longitudinal conversion loss (LCL)	S_{dc11} / S_{dc22}	Common-mode to differential-mode return loss
Transverse conversion loss (TCL)	S_{cd11} / S_{cd22}	Differential-mode to common-mode return loss
Longitudinal conversion transmission loss (LCTL)	S_{dc12} / S_{dc21}	Common-mode to differential-mode insertion loss
Transverse conversion transmission loss (TCTL)	S_{cd12} / S_{cd21}	Differential-mode to common-mode insertion loss

One of the other essential parameters of the channel is the maximum link delay. According to the standard, the channel of 1000BASE-T1 should not introduce a signal delay of more than 94 ns for its operating frequency range (2 MHz - 600 MHz).

The test setup and the arrangement of the cable bundles are also defined in 1000BASE-T1. The harness should be located over an isolation material with low permittivity (ε_r<1.4), which is placed over the ground plane. The cables of the bundle should be fixed together at 30 cm intervals using cable straps or adhesive tape. The related measurement setup for the AXT test is explained in [68].

2.3.4 NGBaseT1 / IEEE 802.3ch

This subsection concerns the state of the knowledge of the automotive Multi-Gig Ethernet. The presented information is based on the meeting's presentations of the IEEE 802.3ch working group, which are available (as of mid-2020) via the following web address: (http://www.ieee802.org/3/ch/).

The CFI of the gigabit Ethernet was published in November 2016, and the release of the standard is expected in 2020. The goal of this project is the implementation of automotive Ethernet with data rates of more than 1 Gbit/s, which are required for the ADAS systems.

The objectives of this task force state that the Ethernet frame format and frame size of IEEE 802.3 should be preserved. A full-duplex operation should be within 100 ms, from power-off state, realizable. A BER better than 10^{-12} should be applicable for the data rates of 2.5 Gbit/s, 5 Gbit/s, and 10 Gbit/s. Auto-negotiation and EEE are the optional parameters of the BIN, while the BIN and the channel should support the harsh automotive EMC conditions and be compatible with federal communications commission (FCC) and CISPR requirements [71].

Bus interface network

In [72], the possible OSI model of the NGBase-T1 is presented (Figure 2.25).

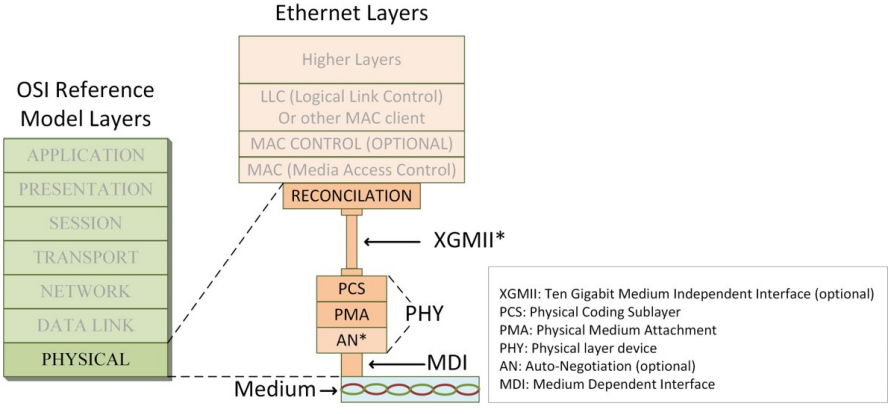

Fig. 2.25: The possible block diagram and structure of the NGBASE-T1 physical layer [72]

Asymmetrical data transmission is of interest in this standard. The sensors, cameras, etc. produce a large amount of data, which should be transferred to the corresponding ECUs. In the opposite direction, the transferred data volume from ECUs to sensors or cameras is considerably smaller. Hence, full-duplex communication with the same data rate in both directions (symmetrical) is not the best approach. The implementation of asymmetrical transmission could be supported by the corresponding modifications in PCS (Figure 2.25) [72]. In [72], the use of 100 Mbit/s for low data rate direction is suggested.

The forward error correction (FEC) method enables the receiver to correct data transmission errors. Otherwise, the receiver has to generate a request for resending the data. Using FEC, the BER can be improved. The use of Reed-Solomon code for the implementation of FEC is suggested for NGBase-T1 [73–75].

Pulse amplitude modulation

For the implementation of the gigabit data rates of IEEE 802.3ch multiple possibilities for the signal coding are discussed during the task force meetings. Approximately, the required bandwidth for the implementation of 10 Gbit/s with NRZ coding can be calculated using equation 2.1 [76].

$$0.75 \cdot bit\ rate = bandwidth \tag{2.1}$$

If the NRZ coding is applied, a bandwidth of 7.5 GHz is required for 10 Gbit/s link. However, the required bandwidth encounters the PHY and the channel with RF EMC issues (emission and susceptibility). This is why other possibilities for decreasing the bandwidth should be pursued [76].

The emission of the UTP cables, as a possible channel candidate for 1000Base-T1, limits the choice of baud rate and the PAM level selection. This is why the use of shielded cables is intended for NGBase-T1. The channel characteristics, signal-to-noise ratio (SNR), and the required excess bandwidth beyond Nyquist are the essential points for the choice of modulation [77]. Further, the need for FEC- and Ethernet coding-overhead increases the needed data rate (about 11.5% - 12.5%) and the corresponding bandwidth.

Lower bandwidth (e.g., < 3 GHz using PAM-4) can simplify the PHY complexity regarding equalization, echo-cancellation, and linearity. A decrease in signal frequency leads to less clock jitter error and power consumption in the digital part of the ECU [78]. However, the use of higher modulation levels leads to multi-level eye diagrams, which needs a higher SNR and the corresponding higher Tx signal level. Furthermore, higher PAM levels require complicated digital signal processing [79].

As described earlier, the bandwidth of the channel has an essential influence on the complexity of the PHY. In order to define the required bandwidth, several companies have presented their measurements regarding the channel characteristics. Considering the various measurements, a maximum required bandwidth of 3 GHz for 2.5 Gbit/s, 5 Gbit/s, and 10 Gbit/s is suggested in [80] and [81].

The proposed peak-to-peak transmit voltage (Tx-Vpp) for the implementation of this standard could be around 1 V [82]. The choice of Tx-Vpp has a significant impact on system power consumption. According to [83, 84], the modulation level should be optimized for 10 Gbit/s because the 2.5 Gbit/s and 5 Gbit/s are the scaled-down modes of the highest data rate. As an example, if the 10 Gbit/s is implemented at 5.6 Gbaud with PAM-4 and around 12% overhead for FEC, the 2.5 Gbit/s data rate is realizable with 2.8 Gbaud and PAM-2 with the same FEC method. Consequently, 5 Gbit/s data rate operates with 5.6 Gbaud / 2.8 Gbaud with PAM-2 / PAM-4 [84]. The mentioned up or down-conversion of PHY‘s data rate is also preferred to OEMs [85].

The mentioned 3 GHz bandwidth could be applied if PAM-4 or higher modulation levels are used. In addition, the optimum SNR, relative power, and noise tolerance are further criteria that should be considered. Using PAM-4 or PAM-5 for 10 Gbit/s can satisfy the latter mentioned parameters [86].

Considering further issues, e.g., the required PHY area [87], the use of PAM-4 for 10 Gbit/s is suggested by many participants of the working group [83, 88].

Data scrambling

As explained in the last two subsections, the use of data scrambling methods helps to prevent peaks in the discrete spectrum. The presence of the spectral peaks leads to emissions of the data line. The comparison of the various scrambler methods for NGBase-T1 is presented in [89].

PoE / EEE

The implementation of EEE is included in IEEE 802.3ch. The EEE technique is intended to work in a network with bursty [2] traffic. In such a network, the data traffic is not predictable. It could be the case that in any given period of the time, there is no data flow and, after a while, a considerable amount of data should be transmitted in the network within, e.g., 1 ms or less [90]. The system power saving is out of the scope of the NGBASE-T1 task force. Therefore, this task force intends to concentrate on PHY power-saving [90].

The wake-up procedure of the ECU is a critical factor for the implementation of EEE. Three possible wake-up types - wake on traffic, partial network, and pseudo partial network - are discussed in [91]. The first possibility for wake up is that all the ECUs are awake if there is any traffic at all in the network. The second wake-up type is the partial network, in which the wake-up signal and the data are embedded in one message. In the pseudo partial network method, a separate signal is used for the wake-up process of the ECU.

As described earlier, the symmetric or asymmetric operation mode has a significant impact on the power consumption of the network. The asymmetric data transfer using LVDS for high-speed transmission and the very low power I^2C bus for low-speed receive link is reported [92]. Hence, the implementation of asymmetric operation mode in automotive Multi-gig Ethernet is desired. The application area of the asymmetric data transmission is, for example, camera, display, and sensor links. Furthermore, the symmetrical or asymmetrical operation mode of the PHY should preferably be configurable [93].

The implementation of the PoDL is foreseen for NGBase-T1, as well. According to [94], the required power for automotive Gigabit Ethernet PHYs should be about 0.5 W or less for combustion engine vehicles, and 1.0 W or less for electric cars.

PHY test / Tx-PSD mask

The definition of the Tx-PSD mask for NGBase-T1 depends on the peak emission requirements, which are defined by the OEMs. According to [95], the defined limit for radiated emissions field strength by the OEMs over the frequency band of 70 MHz

[2] bursty "is used to describe computer data that is sent in short, sudden periods of activity" [Cambridge dictionary]

– 1 GHz is 15 dBµV. The emission is the addition of the Tx-PSD mask limit and the coupling attenuation. Also, to calculate the related Tx-PSD mask, the measurement of the coupling attenuation is necessary. The corresponding measurements of the coupling attenuation are described later in this subsection.

Further, the transmit peak-to-peak amplitude is important for the PSD mask. Using PAM-4 signaling and 1 Vpp, a power range between +0.25 dBm and +1.5 dBm is required. However, in [96], a power range between -0.5 dBm and +2.5 dBm for a symmetrical window around the nominal value was suggested. Further investigations considering system variation and loss effects and required safety margin have led to the suggestion of -0.5 dBm to +2.0 dBm Tx power range [97].

As explained, the Tx-PSD mask depends on multiple factors such as signal amplitude, channel emission and so on. Because the corresponding investigations are still in process (as of mid-2020), several suggestions have been made [95, 98]. Figure 2.26 illustrates the current status of the working group concerning the PSD-mask limits [99].

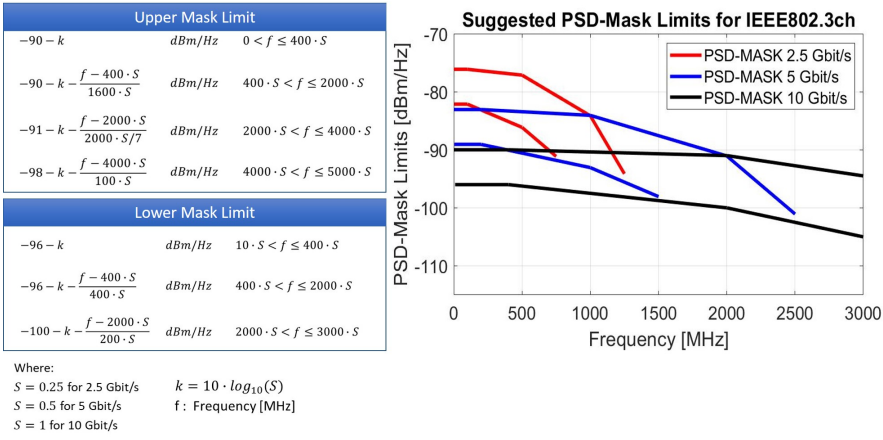

Fig. 2.26: The proposed Tx-PSD mask for NGBase-T1 in [99]

EMC requirements / DPI test

According to ISO 11452-7 (section 2.1.2.2), the DPI test is performed using a resistive coupling network. Such resistive networks are suitable for DUTs with lower frequency operation ranges. The use of directional coupler for the DPI test is suggested for NGBase-T1 PHYs in [100]. Furthermore, the use of an NGBase-T1 PHY as the noise source is proposed, opposed to a noise generator device.

NGBASE-T1 channel

According to the objective of the IEEE 802.3ch, one of the following cable types can be chosen for the implementation of NGBASE-T1: UTP, shielded twisted quad (STQ) , STP, SPP, Coax, or Twinax. The channel should have a maximum length of 15 m, in which the use of up to four in-line connectors is considered. The cable has a differential impedance of 100 Ohm.

The channel bandwidth is of significant importance for the physical layer of the NGBase-T1, as the complexity of the PHY depends on the bandwidth. The minimum possible bandwidth is half of the signal baud rate or Nyquist frequency (f_{Nyq}) [80]. In practice, signal power above f_{Nyq} cannot easily be avoided . To suppress the high-frequency parts of the signal, supplementary filtering methods are needed. To facilitate the complexity of PHY, additional bandwidth to Nyquist frequency can be considered, a so-called excess bandwidth. According to [80], using pulse shaping and filtering, the complexity of the PHY can be reduced, and the required excess bandwidth can be just 10%.

Several presenters have studied the cables mentioned above and made their suggestions regarding the appropriate channel for IEEE 802.3ch. Overall, the use of STP cable is more likely to be chosen as the channel of the Multi-Gig automotive Ethernet [101].

Differential vs. single-ended

The use of a single-ended cable, e.g. coax, requires a proper grounding concept for the return current. The presence of non-metal parts in the chassis leads to problems for the grounding of single-ended cables. If the ground (return current) of coax cable is unbalanced with the signal current, the cable produces undesired CM emissions. As both sides of the coax return path should be grounded, the ground loop is unavoidable. However, if the differential signaling is implemented, the CMC can cancel out the CM noise. The remaining CM noise, not filtered by the CMC, can be suppressed at the differential input stage of the transceiver. The ground loop can be avoided if the shield of the cable is grounded on just one side [102]. Hence, the use of twisted-pair cable is suggested in [102].

Link segment configuration

For the characterization of the link segments, the OEMs have prepared their required configurations (Figure 2.27). Although four in-line connectors are proposed in the objectives of the standard, the OEMs present a need for a maximum of two in-line connectors [103–105].

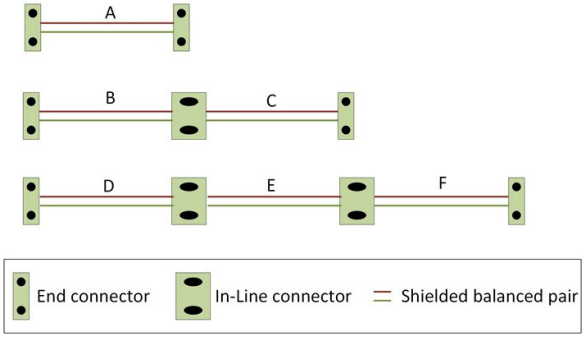

OEM \ Segment	A	B	C	D	E	F
VW / Porsche / Audi	0.5 to 8 m	0.5 to 4.5 m	0.5 to 8 m	0.3 to 2 m	0.5 to 2 m	0.5 to 7 m
Ford	0.2 to 7 m	0.5 to 2.5 m	0.5 to 7 m	0.5 to 2.5 m	0.5 to 7 m	0.5 to 7 m
GM	0.5 to 7 m	0.5 to 2.5 m	0.5 to 7 m	0.5 to 2.5 m	0.5 to 7 m	0.5 to 7 m

Fig. 2.27: The proposed link segment configuration by OEMs [103–105].

RF immunity – BCI

Using the BCI test method, the RF immunity of UTP is compared to coax in [106]. Two coax cable types, i.e., single-shielded (RG174) and double-shielded (PE-C100), are used for this measurement. It is shown that the RF injected current to the single-ended coax and UTP have similar amplitudes over the measured frequency range (1 MHz – 400 MHz). Double-shielded coax possesses a better immunity (about 20 dB) compared to the other two cables. In [106], it is underlined that the existing EMC standards should be improved to cover the required frequency bands (e.g., up to 3 GHz) of the Multi-Gig automotive networks.

The RF immunity of the STP and STQ cables using the BCI test method is studied in [107]. On the whole, it is shown that the induced voltage on STQ is of similar value as STP. The latter two cables have better performance regarding RF immunity than the double-shielded coax.

The BCI ingress noise comparison between STP and SPP cable is performed in [108]. During the measurement, each cable is terminated (ground or float) on one side and is connected through a balun to a spectrum analyzer on the other side. It is shown that the ingressed differential noise varies from 1 mV up to 8 mV, depending on the termination.

RF immunity – radiation

The radiated immunity test of the STP cables in ALSE is performed and presented in [109]. Over the frequency bands 80 MHz – 1 GHz and 1 GHz – 3 GHz, the immunity of a 2 m long STP cable with high-speed modular twisted-pair data (H-MTD) and high-speed data (HSD) connectors, is tested. The corresponding measurement results

for H-MTD and HSD connectors are illustrated in Figure 2.28 and Figure 2.29, respectively. As shown, the measurement setup with the H-MTD adapter is much more immune to the radiated disturbances. An RF ingress peak limit of around 3 mV rms is introduced for STP cables with H-MTD connectors over the measured frequency range. However, Figure 2.29 shows that the corresponding coupled voltage in STP cables with HSD connector is around 10 mV.

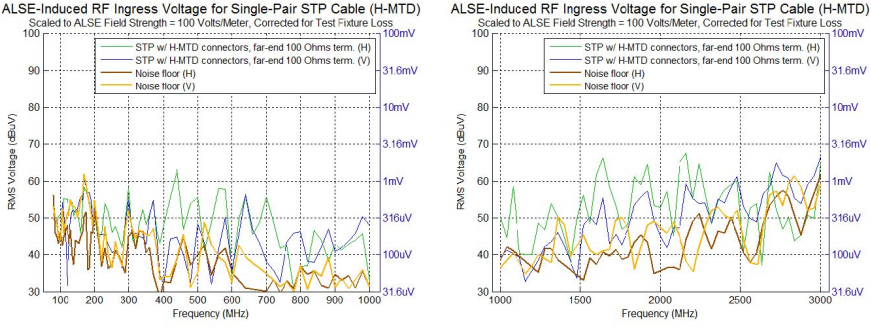

(a) (b)

Fig. 2.28: The RF ingress immunity test of the STP cables with H-MTD connector in ALSE up to a) 1 GHz b) 3 GHz [109] (Copyright © 2017 by L. Cohen and R. Shirani[3])

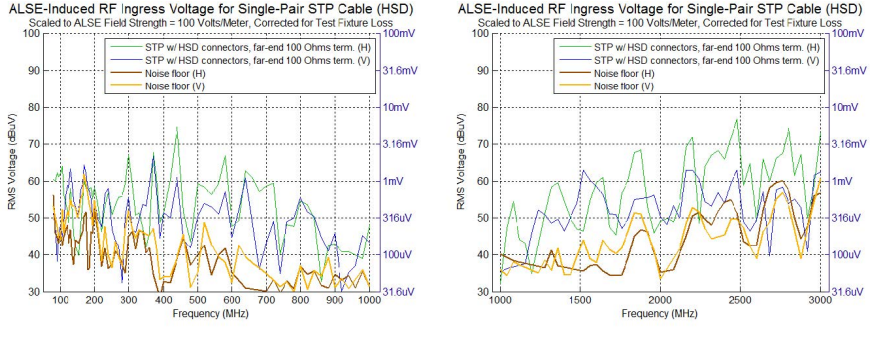

(a) (b)

Fig. 2.29: The RF ingress immunity test of the STP cables with HSD connector in ALSE up to a) 1 GHz b) 3 GHz [109] (Copyright © 2017 by L. Cohen and R. Shirani[3])

Further ALSE immunity tests on the STP cables with the corresponding connectors are presented in [110]. The STP cables under test have a length of 1.7 m and 2 m. To consider the manufacturing tolerances, three samples of H-MTD connectors are used for the tests. The measurements are carried out up to 3 GHz. It is shown that the differential coupled noise to the STP link is lower than 5 mV. Shield termination and the grounding concept play a key role in the coupled voltage.

[3] Authors allowed the reuse of figures in this work

As illustrated in Figure 2.30, improving the shield termination, and using ferrite clamps over the measuring cables have improved the quality of the test setup results in [111]. The ALSE immunity test of the 2 m STP cable up to 5 GHz has led to a maximum measured coupled voltage of 4.5 mV [111].

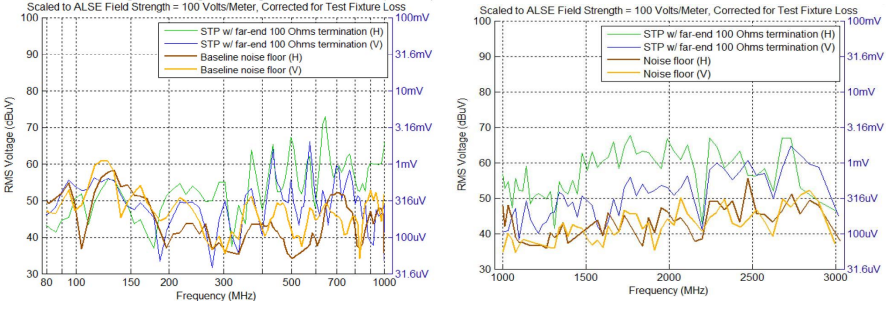

(a) (b)

Fig. 2.30: The improved RF ingress immunity test of the STP cables with H-MTD connector in ALSE up to a) 1 GHz b) 3 GHz [111] (Copyright © 2018 by R. Farjadrad and L. Cohen[4])

Insertion loss

The focus of the IEEE 802.3ch is to define the limits for the insertion loss and return loss of the channel. The mentioned limit lines represent the required bandwidth of the physical layer and have an essential influence on the complexity of the PHY. A comparison between STP and coax, considering insertion loss, is performed in [101]. The measurements are done in a frequency range from DC to 6 GHz. It is shown that the insertion loss of the coax is lower than that of the STP cable. Generally, the use of cables with a smaller diameter ($D < 3.8$ mm) is proposed.

The SPP and STP cable have a similar IL up to around 3 GHz. However, for higher frequencies, the SPP cable has less IL. STQ, and UTP cables show worse IL results, respectively [76]. The increase of coax diameter leads to better IL. According to [76], the cable diameter should be smaller than 4.6 mm and 3.6 mm for differential and coaxial links, respectively.

Due to the harsh vehicle environment, other important factors, such as temperature, should be considered in the physical layer of the network. In [112] and [113], the influence of the temperature on the insertion loss of the STP cable is investigated. It is shown that an 80°C increase in the temperature leads to a 24% degradation of IL at 3.2 GHz.

The defined IL limit in IEEE 802.3bp (1000Base-T1) follows the inequality 2.2, where l is the cable length, f is frequency, n is the number of the connectors, and the C_x are constants [114].

[4] Authors allowed the reuse of figures in this work

$$IL(f) < l \cdot (C_1 \cdot \sqrt{f} + C_2 \cdot f + \frac{C_3}{\sqrt{f}}) + n \cdot C_4 \cdot \sqrt{f} + C_5 \cdot \sqrt{f} \tag{2.2}$$

The right side of inequality 2.2 consists of three parts, which are added. The first part describes the cable parameter, i.e., conductive- and dielectric loss. The connector and return loss can be calculated using the second and third parts, respectively. The coefficients C_x should be calculated by the analysis of the cable and the connectors [114].

Finding an inequality, similar to inequality 2.2, is pursued in the NGBase-T1 working group. Several investigations, based on various link segment configurations under different temperatures, are performed. The number of in-line connectors, cable segment lengths, cable diameter or american wire gauge (AWG), temperature, and operation frequency are the decisive factors for the IL limit lines. Generally, 24AWG and 26AWG cables are studied in the working group. The influence of the temperature, in a range of between -40°C and +105°C, is examined in a climatic chamber from multiple working group participants. The proposed inequality for the IL limit of the Multi-Gig channel follows the inequality 2.3, where f is the frequency and C_x, and n are the corresponding constants.

$$IL(f) < C_1 \cdot f + C_2 \cdot \sqrt[n]{f} + \frac{C_3}{\sqrt{f}} + C_4 \tag{2.3}$$

As mentioned, IL depends on multiple factors. Different companies have investigated the mentioned factors and presented their suggestion regarding the IL limit. The summary of the suggestions can be obtained from Table 2.7.

Table 2.7: Corresponding coefficients for the IL inequality 2.3, presented from various companies and depending on different issues

Company	Cable	Link length [m]	Number of cable segments	Number of In-line Connectors	Temperature effects	C1	C2	C3	C4	n
TE Connectivity [115]	SPP	15	5	4	No	0.0036	0.44	0	0	0.5
General Motors [116, 117]	STP (24AWG)	15	5	4	No	0.0030	0.40	0	0	0.5
TE Connectivity [118]	STP (24AWG)	15	3	2	Yes	0.0031	0.30	0	1.5	0.5
TE Connectivity [119]	STP (26AWG)	15	3	2	Yes	0.0020	0.45	1	0	0.5
Leoni Kabel GmbH [120]	STP (24AWG)	10	1	0	Yes	0.0025	0.35	1	0	0.5
NXP [121]	STP (26AWG)	15	5	4	Yes	0.0020	0.68	0	0	0.45

Return loss

The choice of cable, cable length, and impedance mismatch are important factors that affect the definition of the RL limits. According to [122], the effect of the temperature changes on RL of the channel is negligible. For the return loss of the STP segment link, the illustrated limits in Figure 2.31 are suggested in [117]. As it is illustrated, the definition of the RL limits depends on the corresponding IL value at 3 GHz. Since the IL values are not defined yet, the illustrated RL limits are foreseen for the three possible cases.

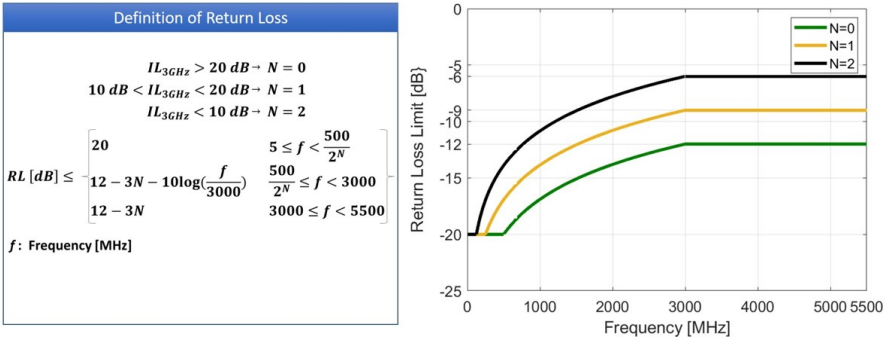

Fig. 2.31: The suggested limit line for the RL of the STP link segment [80, 117]

Coupling and screening attenuation

The screening attenuation (a_s) describes the effectiveness of the cable's screen. Using the mixed-mode S-parameter S_{sc21}, the screening attenuation can be measured. S_{sc21} is the measurement of the common-mode to single-ended conversion amplitudes. The differential to common-mode conversion, as the results of cable asymmetries, is shown using unbalanced attenuation (a_u). The mixed-mode S-parameter S_{cd21} describes the unbalanced attenuation. The coupling attenuation (a_c) of a cable is a measurement parameter for describing the performance of the cable in the presence of EMI effects. The parameter a_c is the sum of a_s and a_u. Hence, the measurement results of the coupling attenuation include the screen and asymmetry parameter [123].

As illustrated in Figure 2.32, the asymmetries of the channel lead to common-mode signals over the channel. This common-mode couples to the screen of the cable. The screening attenuation is the ability of the screen to prevent the mentioned common-mode voltage coupling. The present common-mode current over the shield of the cable is the source of the emission.

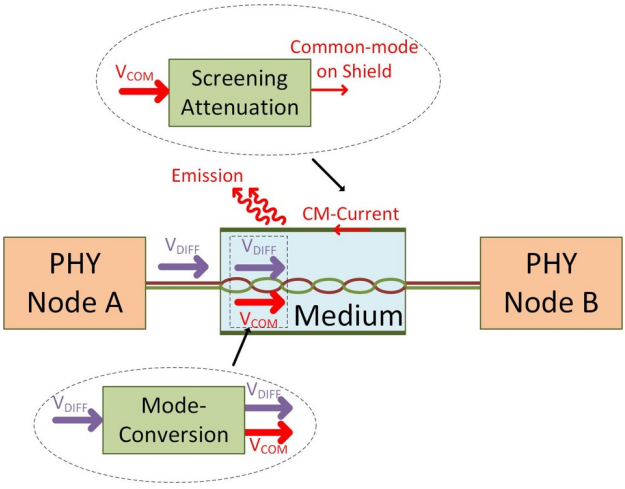

Fig. 2.32: Mode-conversion, screening attenuation and emission of the shielded channel [124]

In [101], the coupling and screening attenuation of SPP and coax are examined for frequencies up to 6 GHz. It is shown that the common-mode emission of SPP is lower than the coax. In a further step, the influence of the in-line connectors is studied in [125]. A 1 m test setup with one in-line connector is compared to a 3 m cable segment with two in-line connectors. The maximum coupling attenuation amplitude for both measurement setups shows no significant change.

The screening and coupling attenuation of STP and SPP cables up to 3.5 GHz using a triaxial tube are compared in [76] and [108]. A 1 m STP/SPP cable has a screening attenuation of less than around -55 dB/-45dB over the tested frequency band. The measured coupling attenuation of the STP/SPP cable is less than -62 dB/-68 dB.

As previously described , the coupling attenuation of the channel is necessary for the definition of the Tx-PSD mask. The measurement of the coupling attenuation can be performed by a triaxial tube test, or using a stripline test setup. The comparison between these two mentioned test methods for STQ cable with HSD in-line connectors is made in [95]. The performed measurements show that the coupling attenuation of the STQ link using stripline- and triaxial tube test setup are less than -75 dB and -71 dB, respectively. The presented results do not show any critical difference between the test methods.

In [126], the use of the shown topology in Figure 2.33 for the measurement of the coupling attenuation is suggested. In this topology, the test of 1 m cable with one in-line and one printed circuit board (PCB) connector is proposed. Using a VNA, the mixed-mode S-parameter S_{sd21} should be measured. The calculation of the coupling measurement is performed using equation 2.4 [127].

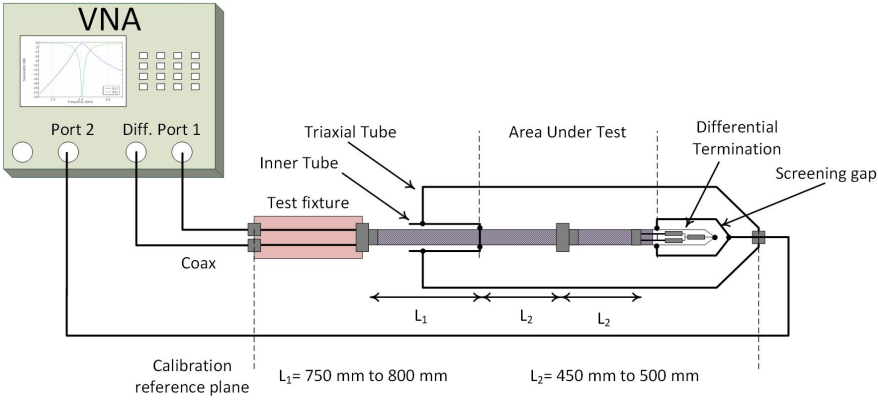

Fig. 2.33: The suggested topology for the coupling attenuation measurement of NGBase-T1 channel [126, 128]

$$A_c = S_{sd21} - 10 \cdot log_{10}(\frac{2 \cdot Z_S}{Z_{diff}}) \tag{2.4}$$

Where $Z_S = 150\ \Omega$ and Z_{diff} is the differential wave impedance of the cable under test.

Considering various measurements, the illustrated coupling attenuation limit in Figure 31 is proposed for the channel of IEEE802.3ch [126].

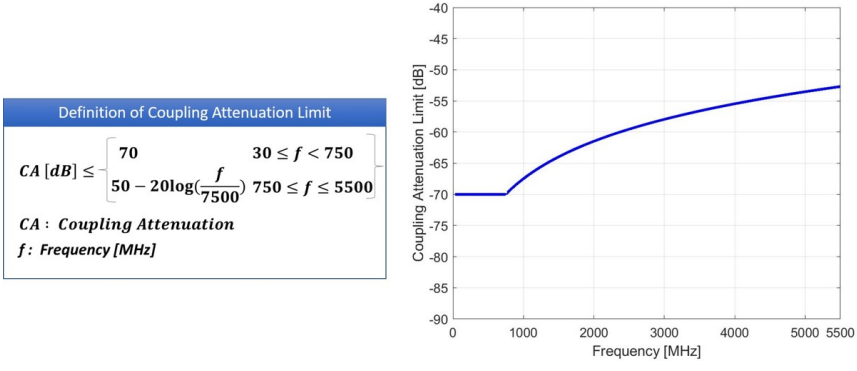

Fig. 2.34: Proposed coupling attenuation limit for the channel of IEEE802.3ch [126]

The measurements of the screening attenuations have led to a proposed limit of $a_s > 45$ dB, provided by multiples presenters [124, 129].

In-line connectors

The impact of the in-line connectors on the channel performance utilizing shielded parallel pair cables is studied in [130] and [131]. It is shown that the in-line connectors increase the insertion loss from frequencies beyond 1.1 GHz. The mode conversion worsens from around 900 MHz, as the result of four in-line connectors.

The choice of proper channel

Based on the measurements presented in this subsection, the use of STP cables with a bandwidth of 3 GHz is suggested in [132]. It is addressed that discontinuities or mismatches larger than $\lambda/10$ have significant impact on the performance of the channel. The use of higher bandwidths (e.g., 5.5 GHz) lead to higher costs and a decrease in the size of the components. Smaller components are harder to handle during fabrication and less robust [132]. In addition, SPP cables that support 5.5 GHz bandwidth have a higher cost, and there is a lack of experience in the vehicle with this cable type.

MDI

Based on the simulations, the EMI tolerance at MDI for different PAM levels is calculated in [79]. It is illustrated that the EMI immunity tolerance is decreasing with the increase of PAM-levels. The solution for increasing EMI tolerance would be higher signal voltage levels, which is not desirable due to power consumption issues.

One of the main parameters for defining the performance of the MDI of NGBase-T1 is the corresponding return loss limit. Several suggestions for the mentioned RL are made [133, 134]. Due to the deviations between the proposals, the RL limits are not noted in this work.

Delay constraints

The response of the ECU in “real-time” is an essential factor for the high-speed network. One can talk about real-time behavior if the ECU can perform its tasks within 300 ms [135]. Generally, the needed wake-up time of the ECU is about 30 ms. For the initialization of the microprocessor, a time of around 70 to 100 ms should be considered [135]. Configuring the Master/Slave state requires more time, which can postpone the data communication. In [135], it is suggested that a Master/Slave pre-configuration should be implemented to minimize the delay issues.

2.3.5 Beyond 10 Gbit/s / IEEE 802.3cy

The implementation of fully autonomous driving requires a large number of sensors and cameras, which permanently sense and record information about the short and long-range environment of the car . The data of the mentioned assistance systems has to be processed in one or more central unit(s), which fuse(s) the data and make(s) the decisions regarding the motion and reaction of the vehicle. Such a complex system requires reliable and high-speed sensors, actuators, and the central unit(s) that are connected through a powerful data network. As explained earlier, the automotive Ethernet networks can implement the mentioned requirements. However, data rates, even up to 10 Gbit/s, cannot support the required transmission data rate. The uncompressed data of the cameras and the communication between central units require data rates higher than 10 Gbit/s.

To overcome the required high-computational power, the use of more than one central unit is needed. This means that a central unit processes the gathered information from the corresponding sensors or cameras and makes related decisions. This information will be shared with the other central units, which make the decisions in other fields. One of the other essential components is the high-speed data switch, which should redirect the data from various sensors and cameras to the central units and vice versa. The communication between switches and the corresponding central units also requires data rates beyond 10 Gbit/s.

The need for the mentioned requirements on data rate led to the introduction of a CFI for “10G+ Automotive Ethernet Electrical PHYS” in March 2019 [136]. The need for multiple central units, which process the data from the corresponding sensors and cameras within their zones, has introduced the “zonal architecture” (Figure 2.35).

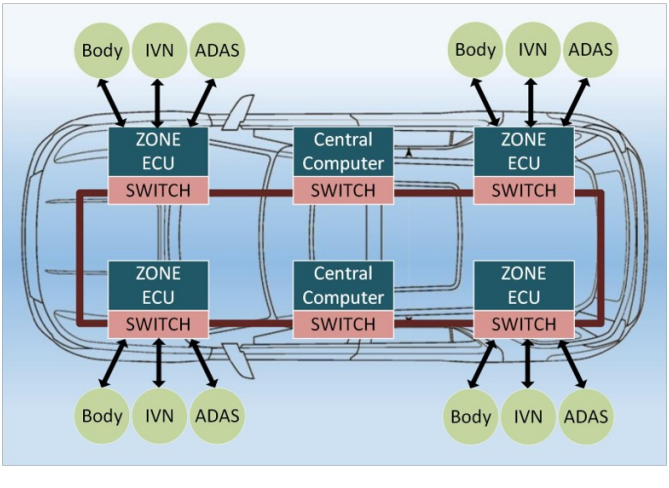

Fig. 2.35: Zonal architecture of 10G+ automotive Ethernet network [136]

The 10G+ Ethernet network should have an asymmetric data transmission method. The communication from sensors and cameras etc. toward switch requires high bandwidth and data rate. In the opposite direction, the data rate could be in Mbit/s range, with which the controlling and initialization of the devices could be handled.

According to [136], data rates of 25 Gbit/s, 50 Gbit/s, and 100 Gbit/s should be implemented in the proposed project.

Chapter 3
Characterization of Common-Mode Choke for Automotive (Multi-Gig) Ethernet Applications

Abstract

One of the important components of the automotive Ethernet AFE is the CMC. Common-mode noise is a critical noise type, which is transferred over MDI to the AFE, or vice versa. The CMC suppresses the existing common-mode noise, which is a result of mode-conversion due to the system asymmetries or external disturbances on the channel.

The simulation of the AFE components helps the industry to forecast the ECU behavior during the design stage. There is also a need for the simulation model of the CMC that is verified by the measurements.

In this chapter, three common-mode chokes in surface-mounted device (SMD) packages required for automotive communication systems (such as 100BASE-T1 and 1000BASE-T1) are characterized. The characterization considers the high-frequency properties of the CMCs.

In this study, a high-frequency simulation model of the CMC is developed and described. Firstly, a CMC suitable for 100BASE-T1 is characterized using mixed-mode S-parameters. The mixed-mode S-parameters of the simulation model are compared with the measurements, and the developed model is verified. In the next step, the simulation model is extended to the 1000BASE-T1 CMCs. The 1000BASE-T1 Ethernet standard enables data communication with an effective data rate of 1 Gbit/s over a single twisted pair cable. The increase in data rate requires a higher bandwidth (BW). Using the PAM-3 modulation type, the 1000BASE-T1 standard has a bandwidth of 375 MHz, while the required bandwidth for 100 Mbit/s data transmission is 33.3 MHz. There is a trade-off between BW and PAM levels. With lower PAM levels, more robustness against interference will be achieved, but a larger BW is required. On the other hand, the large bandwidth makes the communication network susceptible to RF-noise.

The novel idea of this part of work is the presented SPICE equivalent circuit model of CMC. The components values are extracted from impedance measurements of the common-mode choke, both in CM and DM. Thus, the proposed model incorporates parasitic effects (like packaging, mounting, and soldering). The simulation model is verified through comparisons with the measurement results. To characterize and measure the CMCs, a set of PCB boards (test fixtures) with 3-port and 4-port configurations have been designed and fabricated. To remove the test fixture effects, the de-embedding method is applied.

The presented simulation model in the current chapter is completed in the next chapter by the modeling of the PHY, the low-pass filter and the common-mode termination. Hence, the simulation model of the entire AFE related to 100BASE-T1, 1000BASE-T1 and 2.5GBASE-T1 will be presented.

The contents of this chapter have been published in the following two articles:

1. International Symposium on Electromagnetic Compatibility - EMC EUROPE, Angers (2017) under the following title:

   S. Mortazavi, D. Schleicher and F. Gerfers, "Characterization of common-mode choke for automotive Ethernet networks enabling 100 Mbit/s," 2017 International Symposium on Electromagnetic Compatibility - EMC EUROPE, Angers, 2017, pp. 1-6. doi: 10.1109/EMCEurope.2017.8094720

2. International Trade Fair and Congress for Electromagnetic Compatibility, Düsseldorf (2018) under the following title:

   Mortazavi, Sanaz; Schleicher, Detlef; Schade, Frank; Gerfers, Friedel: "Charakterisierung der Gleichtaktdrossel für Multi-Gig-Kommunikation in Automotive-Ethernet-Netzwerken." 2018 Internationale Fachmesse und Kongress für Elektromagnetische Verträglichkeit, Düsseldorf, 2018, S. 340-347. doi: 10.15488/4362. Unter Mitarbeit der Leibniz Universität Hannover.

   The original publication is in the German language. The contents of the second article are the translated version of the paper mentioned above.

Contribution

The first author designed the test boards, performed the modeling and the simulations, post-processed the data, and wrote the publications. The measurements were carried out together with the second author. The other authors gave constructional advice and reviewed the publication.

3.1 Introduction

With the ongoing trend of growth in the number of applications within communication devices, the number of differential interfaces is also increasing [137]. Future automotive broadband requirements pose new challenges for automobile manufacturers worldwide. The automotive industry is preparing for the complete implementation of autonomous driving (artificial intelligence), new 5G communication standards, and car-2-car or car-2-x technology. The increasing demand for video data transmission in motor vehicles, in particular, requires very fast data communication. The currently established Ethernet standard has a data rate of 100 Mbit/s. In the next generation of Ethernet communication, the goal is to increase data rates to 1 Gbit/s. However, data rates of up to 50 Gbit/s, with higher PAM levels, are already under discussion. High-speed data transmission requires a wide bandwidth, resulting in interference of electromagnetic emissions and the degradation of immunity [138].

In most high-speed communications systems, twisted pair (TP) data lines are used as the medium to enable differential-mode signaling to profit from its advantages over common-mode transmission [139]. Compared to CM, DM signaling is relatively well protected against environmental noise.

With increasing frequencies, the data lines become more susceptible to interference. The established 100 Mbit/s Ethernet via UTP data lines cannot fully meet the requirements of Multi-Gig communication. STP, SPP, and coaxial cables seem to be suitable alternatives, as these cables have better high-frequency characteristics.

During the transmission of the DM signal over the mentioned data lines, they will be accompanied by some undesired CM noise, which is the result of mode conversion due to the asymmetry of the cable cores, adapter lines [140] and externally coupled interference on the channel. Mode conversion leads directly to emissions of the data line [140]. This CM noise should be suppressed at both ends of the data line so that no excessive emission levels occur and only the desired signals are received and decoded.

To suppress the CM noise, a coupling-inductive filter, known as the CMC, is inserted between the channel and the physical layer, so that the unwanted CM signals are significantly attenuated. The function of CMCs can have a strong effect on the overall system performance. For example, the DM and CM impedance behavior of CMC regarding the BW and signal frequency have to be considered. Therefore, the characteristic of the CMC should be optimized for the desired application.

S-parameters help measure the reflection and transmission, while mixed-mode S-parameters are used to determine the mode conversion. These parameters are useful to evaluate the noise suppression effect and the CMC general characteristics; most importantly the differential characteristics such as insertion loss, return loss, and mode conversion rejection ratio. Moreover, the manufacturers of CMCs often

characterize choke performance by specifying CM and DM impedance. The higher the common-mode impedance, the smaller the common-mode noise that can get through the CMC [141].

The following sections present the characterization of common-mode chokes, which are used in vehicles for fast communication technologies with a high data rate of 100 Mbit/s or 1000 Mbit/s. The S-parameters and the impedance of the mentioned CMCs are measured in terms of common-mode and differential-mode signaling. To check the ability of the CMCs to suppress the common-mode noise and avoid the mode conversion, mixed-mode S-parameters are measured, as well. The presented results are de-embedded to remove the test fixture effects and to improve the accuracy of the CMC measurements.

The design and optimization of the CMC using simulations require a high-frequency model, which includes parasitic elements [142]. An equivalent circuit model is designed and its characterization process, based on the impedance measurements, is described. The common-mode suppression effect of the CMC is simulated using the proposed equivalent model. The simulation results are compared with the measurement results, and the accuracy of the proposed model of the CMC are verified.

Section 3.2 explains the theory of differential-mode, common-mode signaling, and the function of the common-mode choke. In Section 3.3, the designed equivalent circuit model is described. Section 3.5 shows the measured S-parameters and mixed-mode S-parameters. The results of the impedance measurement in comparison to the simulation results are also presented. Section 3.6 summarizes and concludes this chapter.

3.2 Theoretical background

The circuit simulation depends on the validity of the device model as well as on the accuracy of the values used as model parameters [141]. To successfully design a model for CMCs, the differential signaling as a normal operating mode at high frequencies and the behavior of the CMC as a filter against common-mode noise will be discussed.

3.2.1 Theory and concept of differential signaling

Figure 3.1 illustrates the ideal current and voltage behavior of a single-ended vs. differential signaling. The single-ended signal will usually be measured with reference to the ground. If the measured signal is transmitted between two nodes with equal amplitudes and opposite direction, and around a fixed potential, the signaling will be differential. An important advantage of this method is the high level of immunity to

"environmental" noise [143]. The return signal of the differential method, compared to the single-ended mode through the ground, is almost zero [144]. However, if there is a CM noise over the data lines, the return path of CM current can be through the ground. This CM current leads to non-zero current over the ground path.

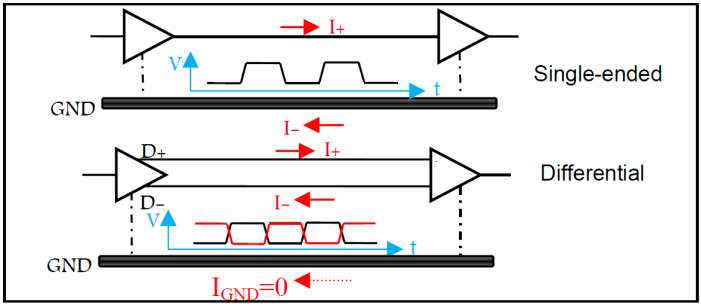

Fig. 3.1: Single-ended and differential signaling - © 2017 IEEE

The single-ended configuration is used for systems with low frequencies, while the differential signaling is preferred for higher data rates and frequencies. The ideal differential configuration consists of two transmission lines with the same impedance, equal length, and perfect symmetry. The radiation from a low to high transition on a channel is canceled by the radiation from the high to the low transition on the other channel. Therefore, the ideal differential compound does not radiate [144]. But in reality, the design of the high-performance balanced components is difficult and all devices will have some non-ideal behavior.

The unbalances in a differential system lead to mode conversion. This means that the device/component converts part of its incoming differential signal into a common-mode signal. Because of this conversion, the common-mode gain is not zero and EMI radiation will be generated. Conversely, when the system converts common-mode noise to a differential-mode, the immunity of the system against the noise will be reduced.

For example, asymmetry in a twisted-pair cable and the corresponding different propagation delays on the two lines of a differential pair leads to signal skew in the receiver. Such asymmetry increases the CM energy and decreases DM energy. It can also convert the used signals to undesired signals.

The most efficient way to cancel out this noise is to insert a filter to suppress it. This can be achieved by using a common-mode choke, which is inserted into the transmission channel.

3.2.2 Noise suppression by common-mode choke

The common-mode choke is based on two coupled inductors. In other words, it incorporates two coils with several windings. Sometimes, to remove the self-inductance of the coil, a solenoid with multiple windings on ferrite cores, such as a bifilar wound coil, is used. The windings are connected so that common-mode currents tend to cancel, while differential-mode currents are relatively and ideally unaffected [145].

Figure 3.2 shows a symbol of the CMC, where R_1 and R_2 are the DC resistance of the coils. The coupling coefficient is labeled K. If L_1, L_2 are two inductance values and M the mutual inductance, the equation 3.1 applies [144].

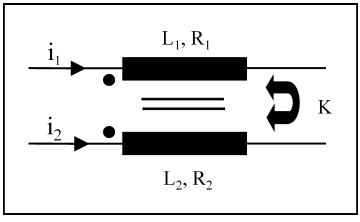

Fig. 3.2: The equivalent symbol for the common-mode choke - © 2017 IEEE

$$K = \frac{M}{\sqrt{L_1 \cdot L_2}} \tag{3.1}$$

Common-mode chokes show low impedance for differential-mode currents (signals). This happens because the magnetic fluxes of the two coils cancel each other out. For CM signals, the magnetic fluxes flow in the same direction inside the ferrite core. As a result, a high impedance is generated within the ferrite core of the CMC. Thus, the choke acts as a filter against the common-mode current (noise). This argumentation will be used, and in the following, it will be explained how the equivalent circuit of the CMC is modeled.

3.3 Design of a general simulation model for the common-mode choke

To develop a general equivalent circuit model of the CMC, only the CMC suitable for 100BASE-T1 is examined and described in this section. The same procedure will be used for CMC suitable for 1000BASE-T1. The associated parameters for both mentioned CMCs are summarized in Table 3.3.

In the first step, the equivalent circuit model of the ferrite core inductor is considered, Figure 3.3 [146]. The circuit model contains inductance (L) and a resistance in series (R_s) defining the copper losses with low value (3.5 Ω for the investigated CMC). The parasitic capacitance (C_p) between the windings is parallel to inductance (L). The ferrite core resistance (R_p) is placed parallel to the inductor, and it has a high value (22 kΩ for the investigated CMC).

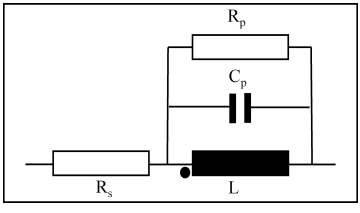

Fig. 3.3: The equivalent circuit for the ferrite core inductor - © 2017 IEEE

In further steps, and based on the circuit model of Figure 3.3, the common-mode and differential-mode equivalent circuits will be designed separately. Using the manufacturer's datasheet and impedance measurements, the parameters of each circuit are calculated. In the end, the proposed models are validated by the simulations.

3.3.1 Common-mode equivalent circuit model of the CMC

The common-mode current flows in the same direction over the two CMC inductors. The corresponding produced magnetic fluxes in the core have the same direction and will be added together. The generated flux introduces an opposing impedance and attenuates the CM current. In this case, the leakage inductances of the choke can be neglected [147]. The two inductors of the choke are connected in parallel in the equivalent circuit of the CM part, illustrated in Figure 3.4.

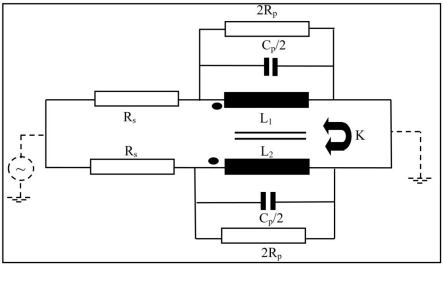

Fig. 3.4: Simple CM equivalent circuit of the CMC - © 2017 IEEE

To estimate the parameters of the CMC equivalent circuit, the inductance value, which is usually indicated in the manufacturer's datasheet, had to first be obtained. To determine the remaining parameter values, CMCs suitable for 100BASE-T1 and 1000BASE-T1 are soldered on PCBs and these test fixtures are measured using an impedance analyzer. The corresponding equivalent measurement setup for CM impedance measurement is shown in Figure 3.5. Further details regarding common-mode impedance measurement are described in section 3.5.

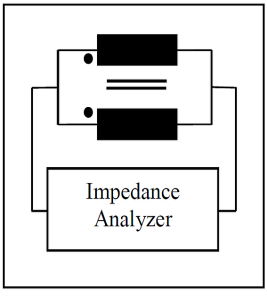

Fig. 3.5: Equivalent measurement setup for CM impedance measurement - © 2017 IEEE

The resonance frequency (f_r) of the CM impedance of the 100BASE-T1 CMC was read at 30 MHz. At the resonance frequency, the imaginary part of the complex impedance is equal to zero. Hence, the magnitude of the real part, namely the impedance of the ferrite core, can be obtained. The value of the inductance and also of the DC resistance (R_s) is taken from the datasheet of 100BASE-T1 CMC. Using these values and the given equation 3.2, the value of the parasitic parallel capacitance C_p was calculated.

$$f_r = \frac{1}{2\pi \cdot \sqrt{L \cdot C_P}} \qquad (3.2)$$
$$if: K = 1 \rightarrow L_1 = L_2 = L$$

As mentioned, the two coils of the CMC are parallel in the case of CM. Therefore, it is important to consider which value each capacitance and resistance has in the parallel equivalent circuit. The associated values of the CM equivalent circuit of the 100BASE-T1 CMC are noted in Table 3.1.

Table 3.1: Equivalent circuit parameter of the 100BASE-T1 CMC for CM impedance - © 2017 IEEE

Parameter	**Value**	**Parameter**	**Value**
L_1	200 µH	R_p	22 kΩ
L_2	200 µH	R_s	3.5 Ω
K	1	C_p	140 fF

3.3.2 Differential-mode equivalent circuit model of the CMC

The differential-mode currents flowing through both inductors of the CMC produce two magnetic fluxes in the core, which are in opposite directions. The magnetic fluxes tend to cancel each other out. Hence, a small impedance is introduced to the differential signal. Because of this compensation, only the leakage flux remains [147]. This leakage inductance follows the high-frequency equivalent circuit model of an inductor, which had already bin introduced. The high-frequency parasitic effects are represented by the parallel resistance (R_{par}) and capacitance (C_{par}). The simple equivalent circuit diagram of DM impedance is illustrated in Figure 3.6.

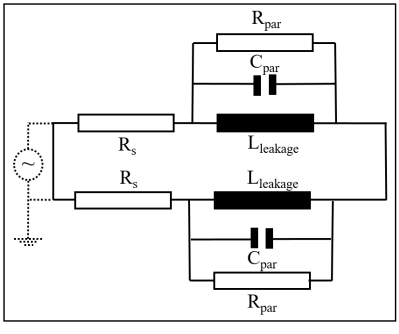

Fig. 3.6: Simple DM equivalent circuit of the CMC - © 2017 IEEE

The corresponding equivalent measurement setup of DM impedance measurement is shown in Figure 3.7. To simulate and measure the DM configuration, the two far ports of the CMC should be shorted.

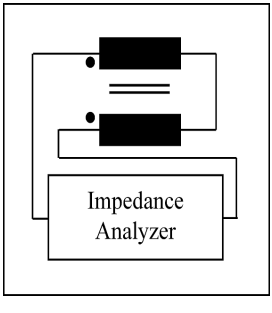

Fig. 3.7: Equivalent measurement setup of DM impedance measurement - © 2017 IEEE

In a similar way, as described in the previous section, the parasitic values of the equivalent circuit are calculated from the measured differential impedance diagram. The achieved values for the DM equivalent circuit of the 100BASE-T1 CMC are noted in Table 3.2.

Table 3.2: Equivalent circuit parameter of the 100BASE-T1 CMC for DM impedance - © 2017 IEEE

Parameter	Value	Parameter	Value
R_{par}	250 Ω	$L_{leakage}$	0.1 µH
C_{par}	10 pF		

3.3.3 General equivalent circuit model of the CMC

The complete SPICE equivalent circuit model of the CMC is shown in Figure 3.8. The middle part of the model is based on the CM model, which contains the self-inductance, the windings capacitance and the resistance of the coil. The left and right parts of the circuit represent the parasitic parameters of the CMC contributed by the DM signaling. To ensure isolation between the two coupled inductances, R_{Ins} and C_{Ins}, are inserted as insulation parameters. The insulation resistance value, 10 MΩ, is taken from the datasheet and the value of C_{Ins} is optimized and has a value of 4.7 fF. The remaining parameters of the simulation model have been extracted from the measurement results. The corresponding values of both 100BASE-T1 and 1000BASE-T1 CMCs are shown in Table 3.3.

The presented equivalent circuit can be used for simulation of both cases, i.e., DM and CM. Of course, with the consideration that the component compound is parallel in case of common-mode and is serial in differential-mode. The impedance and S-parameter simulations of the next section are based on the introduced equivalent circuit model.

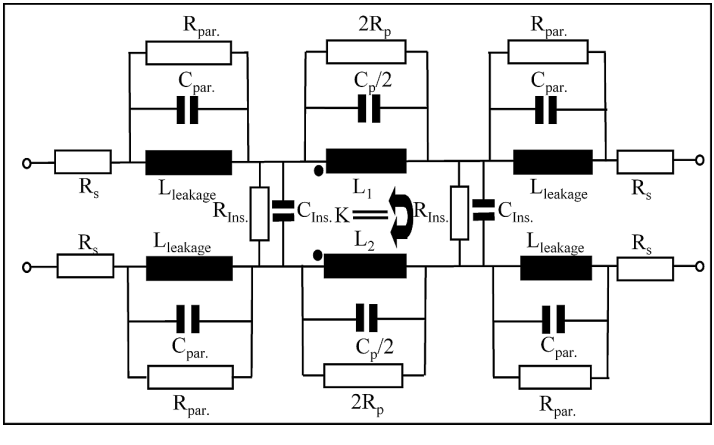

Fig. 3.8: Equivalent circuit of the CMC - © 2017 IEEE

Table 3.3: The equivalent circuit model values of 100BASE-T1 and 1000BASE-T1 CMCs - © 2017 IEEE

Parameter	100BASE-T1	1000BASE-T1
R_{ins} [MΩ]	10	10
C_{ins} [fF]	4.7	4.7
C_{par} [pF]	10	10
K	1	1
$L_{leakage}$ [µH]	0.1	0.001
R_s [Ω]	3.5	3
C_p [fF]	140	156
R_p [KΩ]	22	13.5
L_2 [µH]	200	100
R_{par} [Ω]	250	150
L_1 [µH]	200	100

The coupled interference and asymmetries in the communication system lead to DM to CM conversion. The asymmetries are, for example, imbalances in the data lines as a result of wire length differences. The unwanted common-mode signals will flow back through the ground and create radiation and EMI. However, the common-mode choke acts as a filter against the unwanted CM signals and prevents the consequential interferences.

The symmetry of the CMC is another important factor. In the presented general simulation model, a symmetric CMC was assumed, which consists of two inductors with the same size and inductance values. In this case, the coupling coefficient (K) parameter is equal to one. However, the asymmetries in the CMC package can also introduce differential-mode noise. As a result, the CM noise is converted to the DM noise, which disturbs the useful signal. The low-pass filter of the AFE circuit, located between CMC and PHY, limits the bandwidth. However, the LPF cannot suppress the DM and CM noise signals with frequencies lower than the cutoff frequency of the filter. The remaining noise is distinguished from the useful signal in the receiver and during the decoding process. The asymmetries of the CMC are not considered in the simulation model. Nevertheless, using 3-port boards, the CMC imbalance is examined and measured.

3.4 PCB design for CMC measurement

To characterize the overall properties of the CMC, 4-port and 3-port boards were manufactured as the test fixtures. The best measurement method for determining the mode conversion between CM and DM is the 3-port measurement method [64].

The CMCs are soldered between the differential signal lines. To measure the suitable CMC for 100BASE-T1, corresponding layouts on an FR4 substrate with

tanδ 0.01 and a thickness of 1.5 mm are designed and manufactured. Since the 1000BASE-T1 standard operates in higher frequency ranges, a substrate with high-frequency characteristics has been selected. For this purpose, RO4350B with tanδ 0.0037 and a permittivity ε_r = 3.48 (up to 10 GHz) was used. S-parameter measurements up to 1 GHz validated the required RF-performance of the PCBs. The characteristic impedance of the differential signal lines is 25 Ω for CM and 100 Ω for DM.

Coplanar waveguides (CPW) are used as transmission lines. The width of the signal lines and the distance to the ground plane were calculated for a single-ended impedance of 50 Ω. The following steps explain the impedance and S-parameter measurements of the CMC with the described test fixtures.

To remove the parasitic effects of the test boards and improve the accuracy of the CMC measurements, the measurement results were extracted from the DUT results using the de-embedding boards. Figure 3.9 shows the top view of the fabricated PCBs.

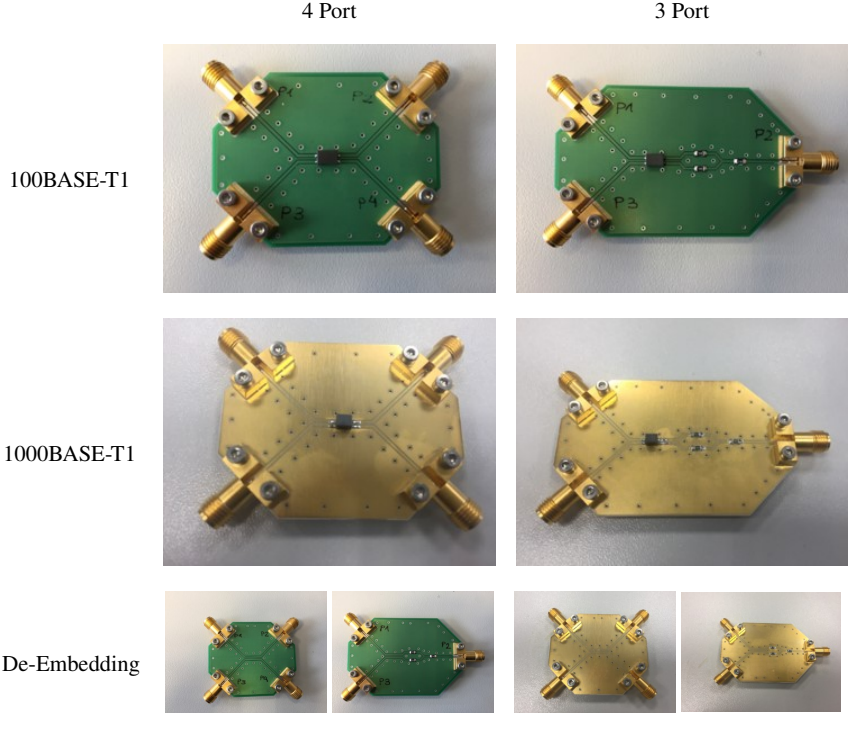

Fig. 3.9: Test fixtures with mounted CMCs and the corresponding de-embedding boards - © 2017 IEEE

3.5 Simulation and measurement results of CMCs

This section discusses the simulation and measurement results of three SMD common-mode chokes. The CMCs are suitable for 100BASE-T1 and 1000BASE-T1 Ethernet Standards. The measurements are performed using the pre-described PCBs. The mixed-mode S-parameters (up to 1 GHz) and CM and DM impedance (up to 120 MHz) of the CMCs are measured. The developed general equivalent circuit model of the choke (Section 3.3) is used for the simulations. The impedance and the S-parameters of the CMC are simulated up to 1 GHz utilizing the PSPICE simulation tools and advanced design system (ADS).

3.5.1 Impedance measurement

Often, manufacturers describe their CMC characteristics by specifying the CM and DM impedances. The higher the common-mode impedance at the desired frequency range, the smaller the common-mode signal that can pass through the CMC [141]. However, the DM impedance should match the transmission line impedance of the system, e.g., 100 Ω differential. In the following sections, the impedance measurements of the CMCs are explained.

Measurement setup for impedance measurement

To measure the impedance of the CMC, two CMCs suitable for 100BASE-T1 and 1000BASE-T1 are soldered on the mentioned test fixtures of Figure 3.9. The impedance is measured using an impedance analyzer from Agilent with a frequency range from 1 MHz to 120 MHz. As explained in Section 3.3, the two inductors of the CMC in the case of CM impedance measurement should be connected in parallel to each other. However, the inductors should be connected in series for the measurement of DM impedance. The measurement setups for the CM and DM impedance are shown in Figure 3.10.

Impedance simulation and measurement results

Using the mentioned PCBs and under consideration of the different measurement setups for the DM and CM impedance, three CMCs were measured. The first CMC is applicable in 100BASE-T1 networks. The other two CMCs are suitable for 1000BASE-T1, and they are from different manufacturers. The developed equivalent circuit model of the CMC is used for the simulations of the different CMCs. The simulation and measurement results are shown in Figure 3.11. In the mentioned figure, the measurements are shown in green, with blue illustrating the simulation results.

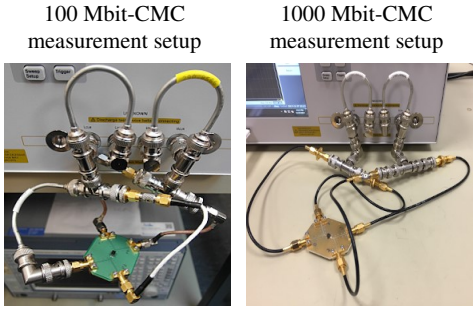

Fig. 3.10: Measurement setup for (a) differential (b) common-mode impedance - © 2017 IEEE

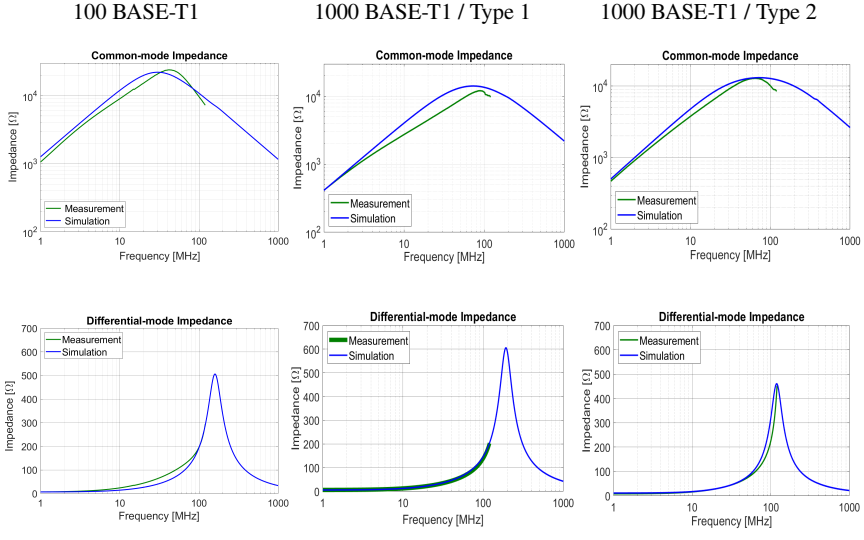

Fig. 3.11: Differential and common-mode impedance, measurement and simulation - © 2017 IEEE

As mentioned, the 100BASE-T1 standard has a signal frequency of 33.3 MHz, while the signal frequency required for the 1000BASE-T1 standard is around 375 MHz. The mentioned frequencies should be considered for the evaluation of the presented results in Figure 3.11.

The used impedance analyzer supports measurements up to 120 MHz. The good agreement between simulation and measurement results up to 120 MHz verifies the validity of the simulation model in higher frequency ranges (Figure 3.11). Hence, with a verified equivalent circuit model, the performance of the CMC in higher frequencies can be estimated.

The 100BASE-T1 CMC has a measured differential-mode impedance of around 70 Ω at 33.3 MHz and 22 kΩ for the common-mode impedance. The 1000BASE-T1 Type 1 CMC shows a DM impedance of around 120 Ω at 375 MHz and 5.5 kΩ for the CM impedance. The 1000BASE-T1 Type 2 CMC has a DM impedance of 70 Ω and a CM impedance of 6 kΩ. As expected, the tested chokes in the differential-mode have a low impedance and high resistance against common-mode signals on the associated frequencies.

3.5.2 Mixed-mode S-parameter measurement

S-parameters are suitable parameters for determining the general DUT properties, such as reflection and transmission. Mixed-mode S-parameters are used to evaluate differential transmission characteristics such as insertion loss, return loss, common to differential mode rejection (CDMR), and differential to common mode rejection (DCMR).

Common-mode chokes are used to attenuate the common-mode noise without influencing the differential-mode signal. Therefore, a high common-mode forward insertion loss and low differential-mode forward insertion loss would be expected for a good common-mode choke [141].

In [140], it is shown that the emission of the data lines results from the mode conversion between DM and CM, which originates from the connection of the coil windings to the package of the CMC. The smallest asymmetries in measurement arrangement can manipulate the measurement results and increase the mode conversion [64].

As is stated in [70], the evaluation of the tests using S-parameter measurements should be performed on at least ten samples. Unfortunately, for the measurements of this chapter, only one sample from each CMC type was available. However, the discussed measurements and simulations of this chapter introduce only the applicable methods.

Setup for mixed-mode S-parameter measurement

To evaluate the CMC characteristics, 4-port and 3-port PCB boards, shown in Figure 3.9, are used and measured with a VNA up to 1 GHz. There are two possibilities for the calibration of the test setup. First, the test fixtures (PCB boards) should be included in the test setup during the calibration of the VNA. This means that the measurement setup is calibrated right down to DUT (CMC). Second, to extract the parasitic effects of the PCBs on the measurements, the de-embedding method can be applied. The de-embedding boards have the same structure as the DUT-boards, but the DUT is not included. With this method, the effects of transmission lines and the substrate can be extracted from the DUT-boards in post-processing. The calibration of the VNA, including the corresponding coaxial cables, extracts the effects of the measurement cables from the results. In this study, the second approach is used.

The choke mounted on the 4-port PCB is fed on one side by two ports of a VNA. The opposite side of the PCB is connected to the other ports of VNA. In this configuration, the insertion loss and other mixed-mode S-parameters of the DUT were measured. IL indicates the attenuation of a signal by a component that is inserted into a signal path. Furthermore, the return loss was also measured. RL is defined as the ratio of the power supplied to the reflected power. This four-port measurement method, with 50 Ω impedance at each measurement port, is also used for characterization of S_{dd11}, S_{dd22}, S_{dd21}, and S_{cc21} parameters.

The best approach for determining the mode conversion between CM and DM is the three-port-measurement method [64]. The mode conversion of the CMCs is measured using the 3-port boards, shown in Figure 3.9. The mode conversion can be measured by S_{sd21} (DM to CM) and S_{ds12} (CM to DM) parameters, which are explained in the following paragraph.

The differential signal is fed into two ports of the choke on one side. Due to asymmetries of the choke, some part of the DM signal will be converted to CM. These signals (DM and CM) leave the choke through the other two remaining ports, located on the other side of the choke. The mentioned ports are each connected with a 50 Ω resistor. The differential data lines are connected together after the resistors. At this connection point, the DM signals will add up to zero, as they have the same amplitude but opposite polarity. Only the remaining CM signal flows toward a third resistor (75 Ω), which is connected to the single-ended port of the VNA. The described measurement method is expressed with the S_{sd21} parameter [148].

To examine the CM to DM conversion of the CMC, the S_{ds12} parameter is used. In this case, the generated CM signal, which comes from the single-ended port of the VNA, flows toward the 75 Ω resistor. After the mentioned resistor, the CM signal splits into two parts. The CM signals flow toward the two 50 Ω resistors and the connection terminals of the CMC. The asymmetries of the common-mode choke can convert a part of the CM signals to DM. While the choke suppresses the CM parts,

the DM signals can pass the CMC and reach the differential ports of VNA. This DM noise signal will be added to the useful signal during the real system operation. The measured mixed-mode parameters and their definitions are listed in Table 3.4.

Table 3.4: Definition of related mixed-mode S-parameters for 100BASE-T1 and 1000BASE-T1 CMCs

Parameter	Description
S_{dd21}	Differential bandwidth of the CMC. It shows the ability of the choke to pass the used signal without distortion.
S_{cc21}	CM attenuation, the ability of the CMC to suppress the CM in a specific frequency range.
S_{dd11}	The differential return loss of the CMC.
S_{sd21}	DM to CM rejection. Differential input, single-ended output.
S_{ds12}	CM to DM rejection. Single-ended input, differential-mode output.

Simulation and measurement results of mixed-mode S-parameters

Figure 3.12 illustrates the measurement and simulation result of the mixed-mode S-parameters for 100BASE-T1 and 1000BASE-T1 chokes. The related limit lines, defined in the corresponding specifications [70, 149], are illustrated as well. The corresponding mixed-mode S-parameter limit lines are noted in Table 3.5 [70, 149].

The simulation results of the proposed equivalent circuit model in the previous sections are illustrated with blue lines in Figure 3.12. The green and red lines represent the measurements and limits, respectively. The simulation model is validated by comparing the measurement and simulation results.

The differential input insertion loss of the 100BASE-T1 CMC is illustrated in Figure 3.12a. At the corresponding operation frequency, i.e., 33 MHz, the related limit is 0.8 dB. The IL should not exceed the 1.1 dB value at 66 MHz. The examined CMC shows an acceptable performance in the mentioned frequency range. The measurement results lie below the defined limit line in the entire frequency range and have a maximum attenuation of 0.5 dB at 66.6 MHz.

The next two diagrams, 3.12b and 3.12c, illustrate the differential input insertion loss results of both 1000BASE-T1 CMCs. The corresponding limit lines are 0.5 dB, 0.8 dB, and 1.5 dB at 20 MHz, 100 MHz, and 400 MHz, respectively. It must be considered that the signal frequency of 1000BASE-T1 is 375 MHz. The obtained results are below the limit lines. The comparison between the two diagrams shows the better performance of the CMC Type 1. The CMC Type 2 has a larger attenuation for the differential signals in higher frequencies and cannot meet the limits between 8 MHz and 33 MHz. Furthermore, the CMC Type 2 also has a larger differential input insertion loss at 375 MHz.

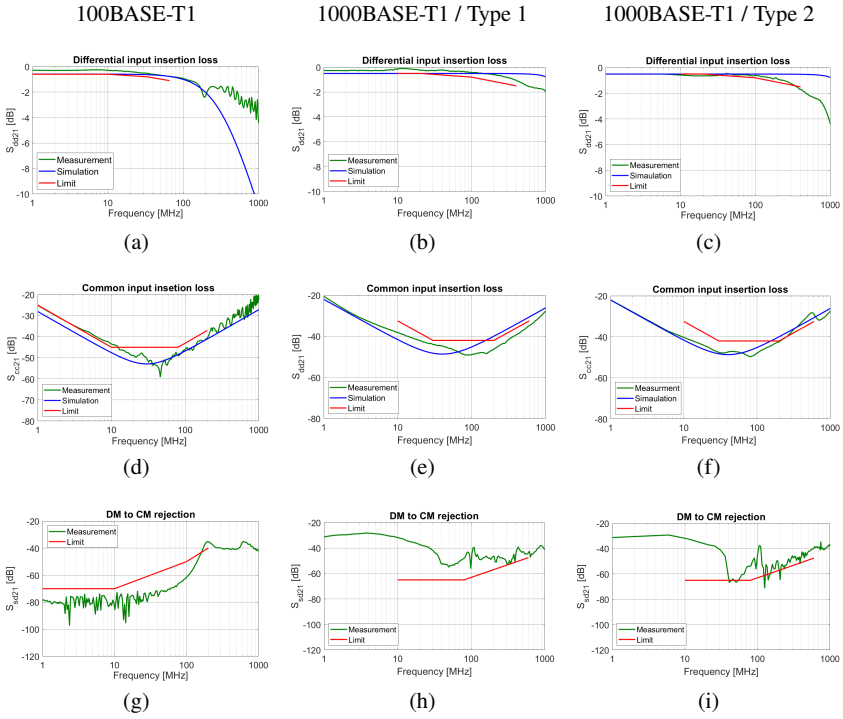

Fig. 3.12: Measurement and simulation results, differential-mode insertion loss (a,b,c), common-mode insertion loss (d,e,f), mode conversion attenuation (g,h,i)- © 2017 IEEE

Diagrams 3.12d to 3.12f deal with the ability of CMC for CM noise suppression. The first diagram (Figure 3.12d) shows the result of CMC suitable for 100 BASE-T1 standard. The corresponding illustrated limit lines have a common-mode rejection value of 25 dB (at 1 MHz), 45 dB (at 10 MHz and 80 MHz), and 37 dB (at 200 MHz). The 100BASE-T1 CMC exceeds the limit line slightly in the frequency range from 4 MHz to 11 MHz. In the higher frequencies (up to 200 MHz) the measurement and simulation results of common input insertion loss comply with the limit lines.

The limit lines for the S_{cc21} of 1000BASE-T1 are based on the common-mode rejection at 10 MHz, 30 MHz, 200 MHz, and 600 MHz with the corresponding values of 32.5 dB, 42 dB, 42 dB, and 32.5 dB. The comparison of the 1000BASE-T1 CMC regarding the S_{cc21} parameter shows the better performance of Type 1. The presented measurement results of 3.12e are less than the limit values over the entire frequency range. On the contrary, the CMC Type 2 can not show acceptable results, especially at the operation frequency of 375 MHz (3.12).

Figures 3.12g to 3.12i illustrate the measurement results of the DM to CM rejection (mode conversion). The 100BASE-T1 complies with the predefined limit up to around 190 MHz. None of the measured 1000BASE-T1 CMCs can satisfy the proposed limits.

As explained, the equivalent circuit model used for the simulations doesn't include the asymmetries of the choke. Hence, the simulation of mode conversion with the equivalent circuit model provides ideal results, which are not presented in Figure 3.12.

Table 3.5: Recommended limits for mixed-mode S-parameters of 100BASE-T1 and 1000BASE-T1 CMCs [70, 149]

Standard	Parameter	Requirement / recommended limits
100BASE-T1	S_{dd11}	$RL \geq \begin{pmatrix} 27 & 1 \leq f \leq 10 \\ 27-9.75log(\frac{f}{10}) & 10 \leq f \leq 66 \end{pmatrix} dB, frequency\ f\ in\ MHz$
	S_{dd21}	$IL \leq \begin{pmatrix} 0.5 & 1 \leq f \leq 10 \\ 0.5+0.39log(\frac{f}{10}) & 10 \leq f \leq 33 \\ 0.8+1.00log(\frac{f}{33}) & 33 \leq f \leq 66 \end{pmatrix} dB, frequency\ f\ in\ MHz$
	S_{cc21}	$CMR \geq \begin{pmatrix} 25+20log(\frac{f}{1}) & 1 \leq f \leq 10 \\ 45 & 10 \leq f \leq 80 \\ 45-20log(\frac{f}{80}) & 80 \leq f \leq 200 \end{pmatrix} dB, frequency\ f\ in\ MHz$
	S_{sd21}	$\begin{matrix} DCMR \\ CDMR \end{matrix} \geq \begin{pmatrix} 70 & 1 \leq f \leq 10 \\ 70-20log(\frac{f}{10}) & 10 \leq f \leq 100 \\ 50-33log(\frac{f}{100}) & 100 \leq f \leq 200 \end{pmatrix} dB, frequency\ f\ in\ MHz$
1000BASE-T1	S_{dd21}	$IL \leq \begin{pmatrix} 0.5 & 10 \leq f \leq 20 \\ 0.5+0.43log(\frac{f}{20}) & 20 \leq f \leq 100 \\ 0.8+1.163log(\frac{f}{100}) & 100 \leq f \leq 400 \end{pmatrix} dB, frequency\ f\ in\ MHz$
	S_{cc21}	$CMR \geq \begin{pmatrix} 32.5+20log(\frac{f}{10}) & 1 \leq f \leq 30 \\ 42 & 30 \leq f \leq 200 \\ 42-20log(\frac{f}{200}) & 200 \leq f \leq 600 \end{pmatrix} dB, frequency\ f\ in\ MHz$
	S_{sd21}	$\begin{matrix} DCMR \\ CDMR \end{matrix} \geq \begin{pmatrix} 65 & 10 \leq f \leq 80 \\ 65-20log(\frac{f}{80}) & 80 \leq f \leq 600 \end{pmatrix} dB, frequency\ f\ in\ MHz$

3.6 Conclusion

To suppress the common-mode interference, common-mode chokes are widely-used. In this chapter, an equivalent circuit SPICE model of the CMC is developed and proposed. The investigated common-mode chokes are suitable for automotive Ethernet standards 100BASE-T1 and 1000BASE-T1.

The development of the equivalent circuit model was performed in four steps. The starting point for circuit development was the equivalent circuit model of a ferrite core inductor, which includes the inductance, copper resistance, parasitic capacitance, and the core resistance. As the CMC possesses two inductors, the mentioned basic circuit model is used twice. The calculation of the circuit values is based on the common- and differential-mode impedance measurements and provided inductance value from the corresponding datasheet. To measure and characterize the impedance of CMCs, 4-port PCBs as test fixtures were designed and manufactured. The impedance of the mentioned CMCs was measured using an impedance analyzer.

The second step of the circuit development was the calculation of the parameter values for CM impedance. In this regard, the equivalent circuits models of both conductors are connected in parallel. The CMC is measured similarly, i.e., the inductors are connected in parallel to each other. Considering the CM value at the resonance frequency, the parasitic parallel capacitance is calculated. The DC resistance and the inductance values are obtained from the provided datasheet. Using the described method, the CM part of the general equivalent circuit is defined.

The next step of the circuit development was the definition of the DM part of the equivalent circuit. It was discussed that in DM, only the leakage flux should be considered. Besides, the high-frequency parasitic effects of DM are regarded with parallel resistors and capacitances. The calculation of DM component values is realized using the related DM impedance measurements with 4-port test fixtures. It was discussed that the two inductors of the CMC should be connected in series for DM impedance measurement. Again, considering the DM impedance value at the resonance frequency, the corresponding values were calculated.

The last step of the development of the circuit model was the combination of the provided CM and DM circuit parts. Furthermore, the isolation of two coupled inductors of the CMC was represented by corresponding resistors and capacitors. The latter mentioned parameter values were obtained from the datasheet and the optimization of simulation results. Finally, the parameter values of the general equivalent circuit model were presented for a 100BASE-T1 and a 1000BASE-T1 CMC.

In the further course of this chapter, the performed measurements were discussed in detail. The development of the used 4-port test boards and the corresponding impedance measurements of the CMC were explained. Using the developed equivalent circuit model the impedance simulation results were compared with the mea-

surements. Moreover, the 3-port test fixtures, which provide a method for the mode conversion measurements of the CMC, were introduced.

The mixed-mode S-parameters are appropriate tools for the investigation of differential- and common-mode behavior of 4-port components. These parameters were deployed for studying the differential and common input insertion loss (S_{dd21} and S_{cc21}) of 100BASE-T1 and 1000BASE-T1 CMCs. The latter mentioned mixed-mode S-parameters are measured and simulated using the 4-port test fixtures and the equivalent circuit model. The simulation results were compared with the measurement results, and the suitability of the proposed CMC model was verified. The DM to CM conversion of the common-mode chokes is measured using the 3-port boards. The presented results were de-embedded to remove the test fixture effects and improve the accuracy of the CMC measurements. The provided results were compared with the defined limit lines of the corresponding standards.

Chapter 4
Modeling and Verification of the Analog Front-End of Automotive Multi-Gig Ethernet Communication up to 2.5 Gbit/s

Abstract

In this chapter the complete analog front-end of the high-speed automotive Ethernet transmission systems (100BASE-T1, 1000BASE-T1, and 2.5GBASE-T1) is characterized. The AFE consists of a transceiver chip, low-pass filter, common-mode choke, DC block capacitor, and common-mode termination (CMT). For the design and the characterization of the high-speed bus systems, the development of equivalent simulation models of the mentioned components, considering the high-frequency behavior, is essential. Modeling and verifying the functionality of the physical component models of the transmission system helps to characterize the EMC issues of the physical layer in the earliest stages of development and to identify any possible problems. For this purpose, new simulation models of the mentioned system components are proposed.

The presented simple SPICE equivalent circuit model of the transceiver enables the simulation of the Ethernet full-duplex communication, including echo cancellation. The simulation of the corresponding PSD verifies the developed circuit model of the PHY. As the 2.5GBase-T1 standard is not yet finalized (at the time of writing), the presented PHY equivalent circuit model can be used for defining the corresponding PSD masks. In a further step, an appropriate low-pass filter, which can also cover the 2.5GBase-T1, is simulated, fabricated, and measured. The filter attenuation is measured considering the signal frequency. The measurements verify the simulation model.

The next component of the AFE is CMC. Although the CM noise suppression of NGBase-T1 will be most likely implemented on-chip, the applicability of the existing CMCs for 2.5GBaste-T1 is shown in this chapter. The proposed equivalent circuit model of CMC (Chapter 3) is modified for a data rate of 2.5 Gbit/s.

The CMT is the last component of the AFE, which is also modeled in this study. To investigate the effect of the CMT on the noise suppression, the corresponding boards, which also include the CMC, are manufactured and measured.

As a final step, the entire AFE of the automotive Ethernet transmission systems is modeled. The behavior of the whole model is verified by measuring the soldered circuit boards, excluding the PHY.

To the author's knowledge, this is the first time the SPICE model of the whole analog front end of automotive Multi-Gig Ethernet communication (up to 2.5 Gbit/s) has been investigated in detail and verified by measurements.

The agreement between measurement and simulation results confirms the validity of the proposed models. On this basis, the suggested models could be adapted and used for further research in the field of automotive Multi-Gig data transmission.

The contents of this chapter are published in the following three articles:

1. International Trade Fair and Congress for Electromagnetic Compatibility, Düsseldorf (2018) under the following title:

   Mortazavi, Sanaz; Schleicher, Detlef; Schade, Frank; Gerfers, Friedel: "Charakterisierung der Gleichtaktdrossel für Multi-Gig-Kommunikation in Automotive-Ethernet-Netzwerken." 2018 Internationale Fachmesse und Kongress für Elektromagnetische Verträglichkeit, Düsseldorf, 2018, S. 340-347. doi: 10.15488/4362. Unter Mitarbeit der Leibniz Universität Hannover.

2. IEEE International Symposium on Electromagnetic Compatibility and IEEE Asia-Pacific Symposium on Electromagnetic Compatibility (EMC/APEMC), Singapore (2018) under the following title:

   S. Mortazavi, D. Schleicher and F. Gerfers, "Characterization and verification of Gigabit ethernet-based bus systems in vehicles," 2018 IEEE International Symposium on Electromagnetic Compatibility and 2018 IEEE Asia-Pacific Symposium on Electromagnetic Compatibility (EMC/APEMC), Singapore, 2018, pp. 428-433. doi: 10.1109/ISEMC.2018.8393814.

3. IEEE Symposium on Electromagnetic Compatibility, Signal Integrity and Power Integrity (EMC, SI & PI), Long Beach, (2018) under the following title:

   S. Mortazavi, D. Schleicher and F. Gerfers, "Modeling and Verification of Automotive Multi-Gig Ethernet Communication up to 2.5 Gbps and the Corresponding EMC Analysis," 2018 IEEE Symposium on Electromagnetic Compatibility, Signal Integrity and Power Integrity (EMC, SI & PI), Long Beach, CA, 2018, pp. 329-334. doi: 10.1109/EMCSI.2018.8495375.

Contribution

The first author has designed the test boards, performed the modeling and the simulations, post-processed the data, and written the publication. The measurements were carried out together with the second author. The other authors gave constructional advice and reviewed the publication.

4.1 Introduction

Future automotive broadband requirements pose new challenges for automobile manufacturers worldwide. The automotive industry is preparing for the next generation of advanced driver assistance systems such as autonomous driving (including machine learning and artificial intelligence), vehicle-to-vehicle and vehicle-to-everything communications. The latest 5G communication standards, with data rates up to 10 Gbit/s, as well as the increasing demand for high definition (HD) video transfer in vehicles, require huge computing power and very fast data communication systems.

For the implementation of future self-driving vehicles, there is a high demand for interaction and data fusion between a large number of sensors like multi-mode radar, multi-purpose high-resolution cameras, long-range radars, ultrasonic sensors, etc. Such sensors produce a huge amount of data per second, which must be processed immediately. This real-time communication allows the vehicle, equipped with artificial intelligence, to make critical decisions and ensures driving safety. To enable a fast and low latency data transfer between the sensors and the computing nodes within the in-vehicle network, a secure, reliable, and cost-effective bus system is required. IP-based Ethernet communication over single-pair copper lines is a promising approach.

The bandwidth requirements for the realization of the mentioned objectives pose new challenges for the vehicle industry [7]. Pulse amplitude modulation is an effective approach for limiting the bandwidth. The increase in data rate and the use of higher modulation formats, e.g., PAM-5 to PAM-16, is associated with higher electrical interference sensitivity. The possible consequences are the reduction of signal-to-noise ratio, the increase of crosstalk, etc. Therefore, a tradeoff between bandwidth and SNR is required. Pulse amplitude modulation, with three signal levels (PAM-3), is implemented in 100BASE-T1 and 1000BASE-T1. There is no fixed definition of the PAM level for 2.5 Gbit/s data transmission (at the time of writing). As an example, for 2.5 Gbit/s with PAM-3 signaling, the required bandwidth is approx. 900 MHz – 1 GHz in the frequency domain.

In the next generation of Ethernet communication, the aim is to increase data rates to 10 Gbit/s. However, data rates of up to 50 Gbit/s, with higher PAM levels, are already under discussion.

For the investigation, analysis, and performance prediction in early-stage phases of network design, the behavior of system components, including EMC issues, should be known and characterized [150]. Based on the proposed model of the complete AFE of the automotive Multi-Gig Ethernet bus system, the transmission path simulation is possible. Using component measurements, the equivalent circuit of the AFE for three different data rate values, i.e., 100 Mbit/s, 1 Gbit/s, and 2.5 Gbit/s, is presented.

This chapter is structured as follows: Section 4.2 briefly explains the two established automotive Ethernet standards (IEEE 802.3bw and IEEE 802.3bp) and the next generation of the automotive Multi-Gig data communication (IEEE 802.3ch). The applications of each standard are described as well. Section 4.3 describes the open systems interconnection (OSI) model and the Ethernet protocol structure. In order to design and simulate the automotive Ethernet bus systems with data rate values of 100 Mbit/s, 1 Gbit/s and 2.5 Gbit/s, the individual components of the transmission path are modeled and presented in Section 4.4. In the same section, the model of the transceiver (Tx-Rx), low-pass filter, common-mode choke, and common-mode termination are presented and verified by measurements. In Section 4.5 the entire AFE model is presented. The S-parameter simulation and measurement results are compared. Finally, Section 4.6 summarizes and concludes this chapter.

4.2 Definition of the automotive Ethernet standards

The mechanical control of the individual systems in the vehicle has been almost completely replaced by electronic systems, which are connected by data networks. The modern production of the vehicles, on the one side, and the intelligent and networked vehicle systems, on the other side, require new data communication standards.

Depending on, for instance, transmission speed, error tolerance, cost, and system robustness, various communication systems and network structures can be used for data transmission [151]. The well-known implemented automotive communication systems are CAN-FD, LVDS, MOST, FlexRay, and automotive Ethernet.

The IP-based Ethernet technology standardized in IEEE 802.3 defines the requirements of the first and second layers of the OSI layer model. The stated standard is to be adapted and optimized for use in the vehicle [152]. Figure 4.1 shows the reference model (OSI model) for network protocols as a layered architecture.

4.2.1 IEEE 802.3bw standard / 100BASE-T1

The 100 Mbit/s data communication in the automotive sector is defined and standardized in IEEE 802.3bw. It allows for the integration of different applications in a compact Ethernet network via a single unshielded twisted-pair cable.

100 Mbit/s data transmission, in a full-duplex operation mode over a UTP cable using PAM-3 modulation type, is achieved with 100BASE-T1 standard. The mentioned properties distinguish this technology from non-automotive standards. The 100BASE-TX standard is not implemented in the vehicle due to the unidirectional operation mode and the need for two separate cable pairs to transmit and receive. In the 100BASE-T1 standard, the required bandwidth for 100 Mbit/s signaling is limited to 33.3 MHz, about half of the bandwidth of 100BASE-TX [153, 154].

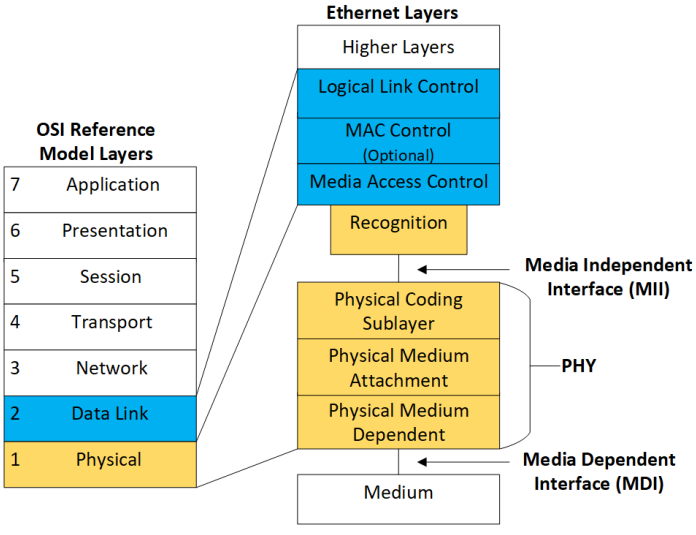

Fig. 4.1: Reference model (OSI model) for Ethernet architecture [153] - ©2018 IEEE

The reduction of bandwidth leads to reduced electrical interference sensitivity, such as crosstalk, and return loss. Thus, the EMC requirements for automotive communication systems can be met more efficiently.

4.2.2 IEEE 802.3bp standard / 1000BASE-T1

In order to increase the data rate in the vehicle up to 1 Gbit/s, the 1000BASE-T1 standard was introduced. The IEEE P802.3bp task force has developed this standard and has defined the physical layer specifications. This communication technology is based on a point-to-point full-duplex data transmission over a UTP/STP line [153, 155].

A Significant improvement, by using 1000BASE-T1 versus 1000BASE-T, is the reduction of four parallel transmission channels to a single channel. The established PAM-3 modulation is used because of better interference immunity and EMC robustness [156]. This provides a better SNR but requires a baud rate of 750 Mbaud.

To maintain the SNR-Level without increasing the signal voltage, a less sensitive channel with lower EMC interference is required. As an example, jacketed UTP cable for short distances or STP cables for longer routes with in-line connectors could be used [155, 157]. One important application of this standard is implementing the long term evolution-advanced (LTE-Advanced) technology in the vehicle. This is the fourth-generation (4G) wireless standard, which enables higher data transfer rates.

4.2.3 IEEE 802.3ch standard / NGBASE-T1

As explained, the rapid technological progress encounters automotive manufactures with the need for more bandwidth and higher data rates. The established 100 Mbit/s and 1000 Mbit/s Ethernet technologies (IEEE 100Base-T1 and 1000BASE-T1) over twisted pairs (TP) can no longer fully meet the aforementioned requirements. Therefore, the industry has identified Multi-Gig Ethernet to deliver connectivity for future in-vehicle networks.

IEEE 802.3 has initiated the next task force for specifying the requirements of data rates greater than 1 Gbit/s (up to 10 Gbit/s). The IEEE 802.3ch task force is discussing the implementation methods of this technology (at the time of writing).

In the next generation of Multi-Gig automotive Ethernet communication standard, the transmission of 2.5 Gbit/s, 5 Gbit/s, and 10 Gbit/s over a single cable has to be considered. Data lines with up to four inline connectors for at least 15 m on one type of automotive cabling (e.g., UTP, STQ, STP, SPP, Coax, etc.) could be used [158].

The applications of NGAUTO include the next-generation of ADAS, autonomous driving, 5G communication standard, etc. Table 4.1 summarizes the mentioned standards in detail.

Table 4.1: Automotive Ethernet standards - ©2018 IEEE

Ethernet Tech.	100BASE-T1	1000BASE-T1	NGBASE-T1
Standard	IEEE-802.3bw	IEEE-802.3bp	IEEE-802.3ch
Data-Rate	100 Mbps	1 Gbps	2.5/5/10 Gbps
Modulation	PAM-3	PAM-3	PAM-N
Bandwidth	33.33 MHz	375 MHz	*TBD
Operation	Full Duplex	Full Duplex	Full Duplex
Medium	1-pair UTP	1-pair STP	1-pair *TBD
Baud-Rate	66.6 MBd	750 MBd	*TBD
Medium length	15 m	15 m / 40 m	*TBD

* TBD: To Be Defined

4.3 Ethernet communication

4.3.1 Ethernet layer architecture – OSI model

The OSI model is a reference for network protocols in a layered architecture. This seven-layered model facilitates the communication between a wide range of electrical systems and further development (Figure 4.2).

The IEEE 802.3 standard defines the requirements of the first two OSI layers. The PHY as the first layer and the MAC as the second layer have to be adopted for automotive applications [152]. The ECUs contain the PHYs and communicate with each other over the Ethernet channel. The AFE of PHY is visualized in Figure 4.2.

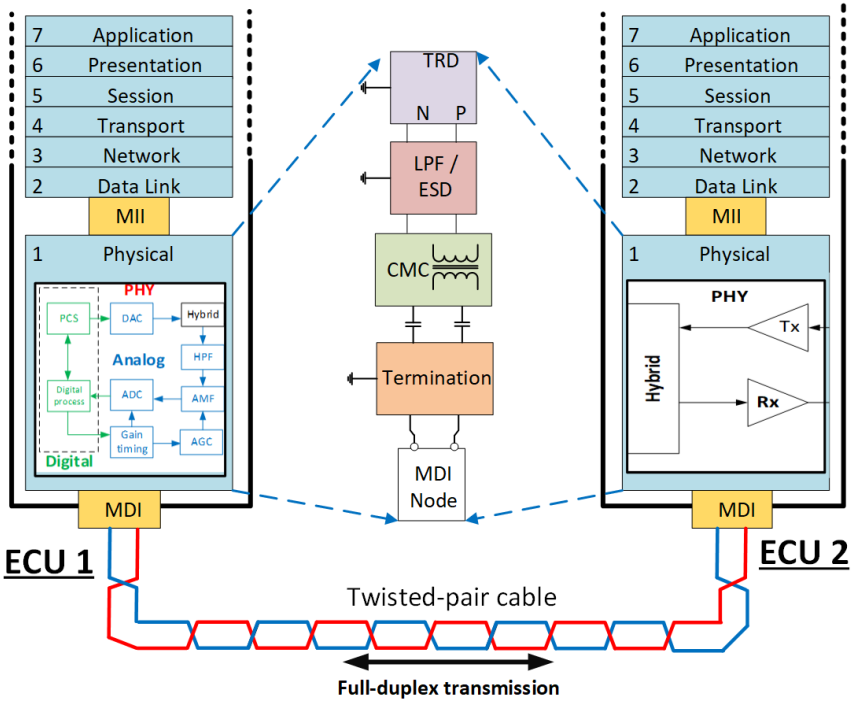

Fig. 4.2: OSI model [153] containing the Ethernet transmission path and details of the PHY - ©2018 IEEE

Media-independent interface realizes the data transfer from the Ethernet transceiver to the MAC. The interface between the channel and the PHY is MDI. In Figure 4.2, the full-duplex operation mode over a twisted pair cable employing a transmitter and a receiver on both sides of the medium is illustrated. The choice of the channel depends on EMC interferences, which are a function of bandwidth and data rate [139].

4.3.2 Ethernet transmission link

To increase transmission reliability, reduce costs, and susceptibility to interference, the fast Ethernet system has been defined. A PHY chip for automotive Ethernet assumes the role of full-duplex communication between two nodes, while simultaneously preparing the data for digital signal processing. 100BASE-T1, 1000BASE-T1

and 2.5GBASE-T1 Ethernet PHYs enable the implementation of electronic architectures such as ADAS. According to specifications and definitions of Ethernet bus systems, an optimized MDI interface test network (Opt-BIN) consists of transceiver circuits, low-pass filters, common-mode choke, DC block capacitors and common-mode termination. Figure 4.3 provides an overview of the Ethernet transmission link, MDI and MII of the Ethernet communication system. The channel is a single twisted-pair cable (UTP or STP). The data is transferred from the channel to the PHY. The PHY consists of the analog front-end, the digital blocks and the MII interface, where the data transfer from the Ethernet transceiver to the microcontroller with the MAC interface is realized.

As mentioned, high-speed data transmission over Ethernet - as a prerequisite for the implementation of Big-Data in the vehicle - requires a wide bandwidth in the frequency spectrum, which can lead to interference due to electromagnetic emissions and to a deterioration of immunity. Therefore, all individual components of the Ethernet transmission link must meet certain EMC-relevant requirements. Hence, the mentioned components should be examined from the EMC perspective [153].

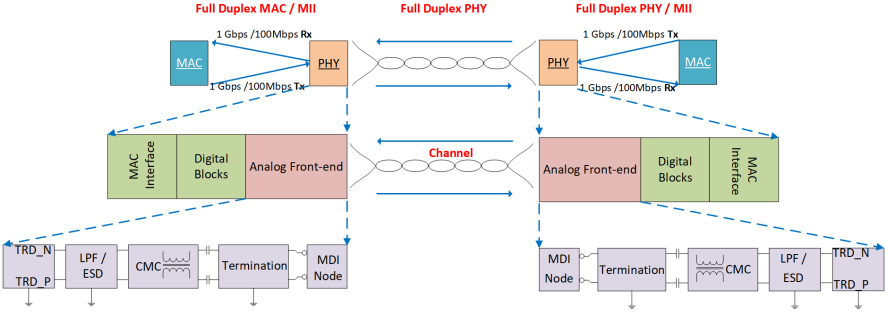

Fig. 4.3: Ethernet transmission path - ©2018 IEEE

4.4 Modeling and characterization of AFE components

The focus of this section is the functionality of the analog front-end. For this purpose, the equivalent circuits of AFE's components are introduced. The analog front-end includes the transceiver block, low-pass filter, which defines the passband, ESD protection, CMC for common-mode rejection, DC blocking capacitors, common-mode termination, which reduces the common-mode energy of the channel and MDI connectors in the last stage (Figure 4.3). The proposed equivalent circuit models include the high-frequency behavior of each component, which is verified by measurements. To characterize the AFE, the EMC issues of the above-mentioned components must meet specific EMC relevant requirements [152]. Each component is to be verified and optimized individually and, as a part of the system as a whole, on the vehicle

level. For system developments and investigations, the equivalent circuit diagrams of the individual components are to be designed. The modeling of such equivalent circuit diagrams becomes more difficult with increasing frequency. Therefore, the RF behavior of all components must be considered.

Figure 4.4 shows the simple SPICE equivalent circuit diagram for an OPT-BIN. In the following sections, the high-frequency SPICE model of the AFE for the mentioned automotive Ethernet standards and their individual circuit parameters are proposed and discussed.

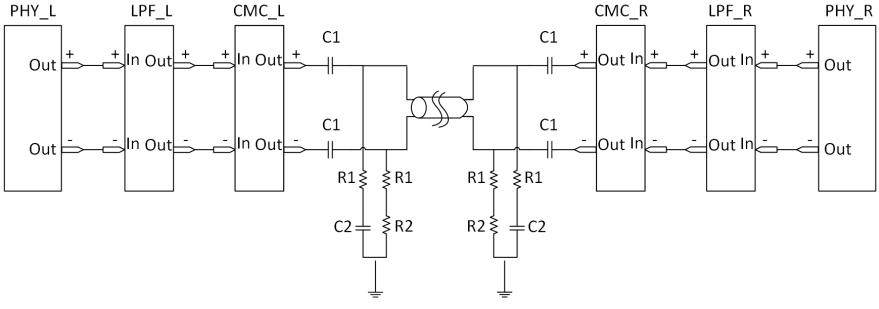

Fig. 4.4: Simulation model of complete front-end circuit - ©2018 IEEE

4.4.1 Modeling and characterization of the transceiver circuit

As described, the first layer of the OSI model is the physical layer. A PHY consists of digital and analog blocks. An automotive Ethernet connection is always a point-to-point connection with a full-duplex communication. Therefore, there is a transmitter and a receiver on both sides of the medium. A real transceiver PHY includes components like digital-analog converter (DAC), analog-digital converter (ADC), phase-locked loop (PLL) circuits, etc. (Figure 4.5).

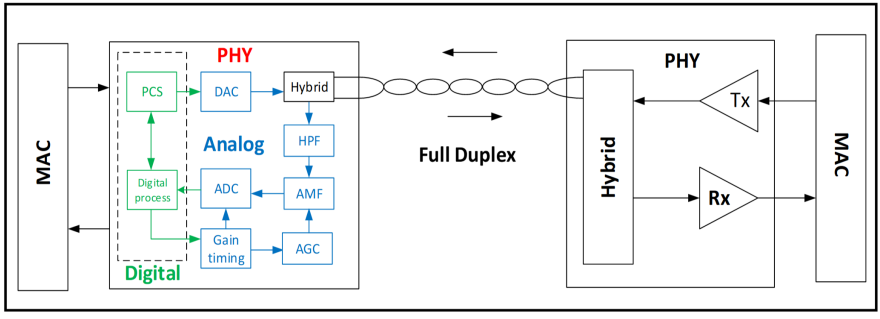

Fig. 4.5: Ethernet Physical layer – PHY - ©2018 IEEE

The simple equivalent circuit model of the complicated PHY chip is proposed in Figure 4.6. As shown in Figure 4.6, the equivalent circuit model includes Tx, Rx and echo-cancellation circuit. The differential input signal is generated by two PAM-3 voltage sources with a phase difference of 180°. Because of a full-duplex operation mode, the transmitting and receiving signals are added together on the channel side. The receiver should distinguish between these signals. For this purpose, the transmitting signal has to be subtracted internally from the whole signal. The associated circuit parameter of the transceiver for the three discussed standards is noted in Table 4.2.

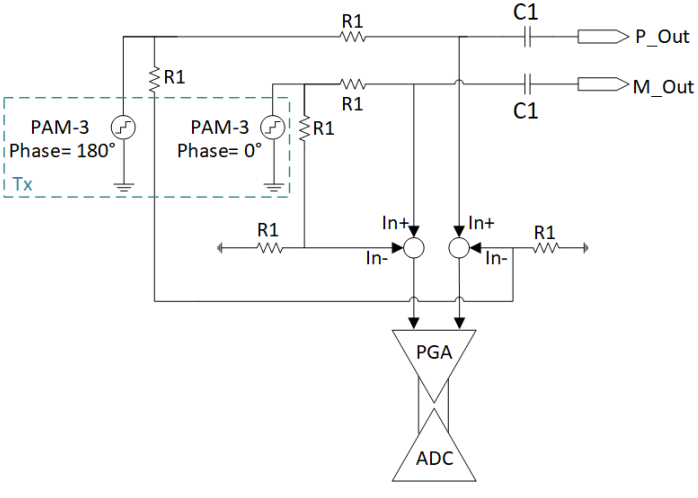

Fig. 4.6: Equivalent model of the transceiver with echo cancellation - ©2018 IEEE

Table 4.2: Associated values to the transceiver model - ©2018 IEEE

	100BASE-T1	1000BASE-T1	2.5GBASE-T1
R1	50 Ω	50 Ω	50 Ω
C1	1 pF	1 pF	1 pF

For the series production of transceiver PHY in motor vehicles, certain EMC requirements and standards must be met. The PHY chips have to pass the following tests and fulfill the corresponding requirements: a) DPI test, which has to be performed for the immunity of the system. b) 150-ohm test method measures the interference emission of the PHY. c) The PSD of the chip, which should be within predefined limits.

For the simulation of the PSD diagram, the PHY has to be fed in by a pseudo random binary sequence (PRBS) data stream. The two established automotive Ethernet standards (100BASE-T1 and 1000BASE-T1) use PAM-3 signaling. Therefore, differential PAM-3 PRBS data sequences are generated by MATLAB and imported

into the SPICE model. The modulation type of the 2.5GBASE-T1 standard had not been specified at the time of this study. Therefore, the same differential input PAM-3 signal was used for the simulation of the third standard.

The PSD diagram of the circuit model is examined in three different stages (Figure 4.7). First, the PSD is simulated after the Tx circuit. The second step shows the effect of LPF on the PSD. Finally, in the third stage, the PSD at the end of the AFE circuit is simulated.

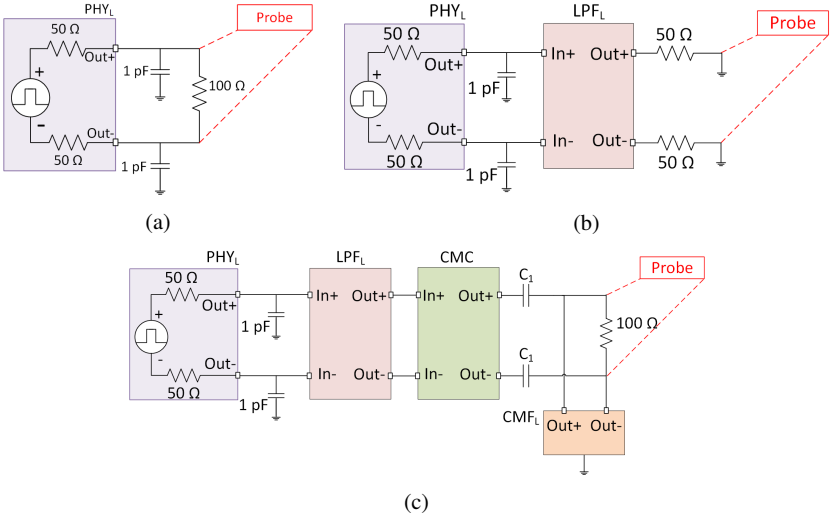

Fig. 4.7: (a) PSD after transceiver, b) PSD after LPF and c) PSD after front-end circuit - ©2018 IEEE

Figure 4.8 shows the results of the PSD diagram for the three mentioned stages of AFE. In this figure, the PSD of 100BASE-T1, 1000BASE-T1, and 2.5 Gbit/s AFE are illustrated. For the first two standards, the predefined limits are shown in Figure 4.8a and Figure 4.8b in blue. The mentioned figures illustrate the simulation results of the ideal transceiver circuit concerning the PSD masks and confirm the proposed equivalent circuit model. There is still no definition of PSD limits for automotive Ethernet communication with a data rate of 2.5 Gbit/s in Figure 4.8c.

4.4.2 Modeling and characterization of the low-pass filter

As noted in Table 4.1, the required bandwidth of 1000BASE-T1 (375 - 400 MHz) is ten times the bandwidth of 100BASE-T1 (33.3 MHz). The bandwidth of Ethernet communication with a data rate of 2.5 Gbit/s and PAM-3 signaling is around 900 - 1000 MHz. Consequently, the operation of the LPF (the 3-dB cutoff frequency)

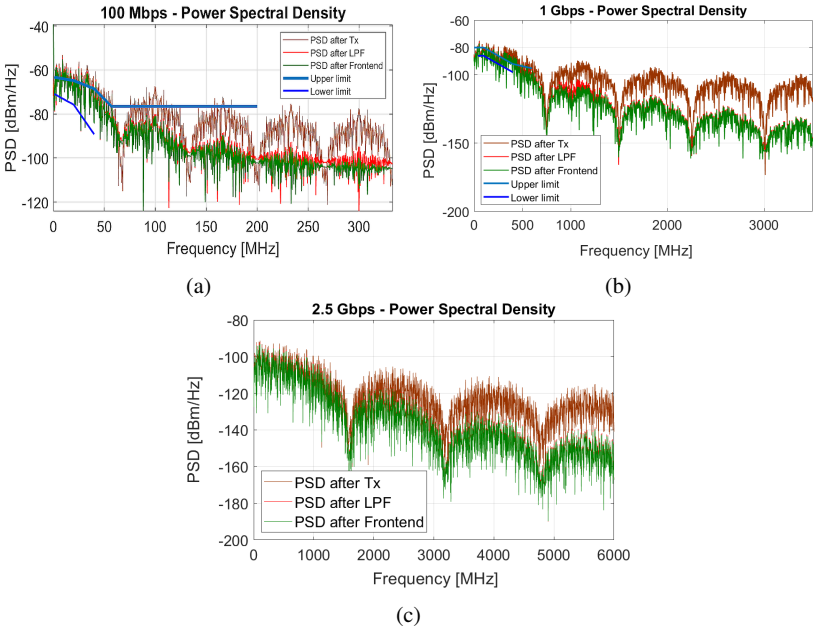

Fig. 4.8: Simulation result of the PSD mask a) 100BASE-T1, b) 1000BASE-T1, c) 2.5GBASE-T1 - ©2018 IEEE

should be adjusted so that the pass-band of the filter covers the mentioned frequencies. The LPF is an optional circuit, which is implemented for the 100BASE-T1. For 1000BASE-T1 each vendor can decide on the necessity of usage.

Figure 4.9 shows the equivalent high-frequency circuit model of the LPF. The values of the individual components were calculated separately for all mentioned Ethernet standards. In Table 4.3, the corresponding circuit parameters of the LPF are noted.

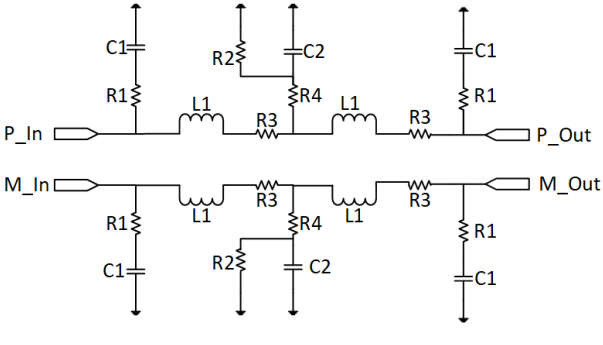

Fig. 4.9: Equivalent model of the low-pass filter - ©2018 IEEE

Table 4.3: Associated values to the LPF model - ©2018 IEEE

	100BASE-T1	1000BASE-T1	2.5GBASE-T1
R2	45.3 Ω	45.3 Ω	45.3 Ω
R3	499 Ω	499 Ω	499 Ω
R4	4.02 Ω	4.02 Ω	3.9 Ω
R5	120 Ω	120 Ω	120 Ω
C2	47 pF	4.7 pF	1.5 pF
C3	4.7 pF	4.7 pF	4.7 pF
L1	100 nH	10 nH	5.6 nH
L2	100 nH	10 nH	2.7 nH

To verify the proposed circuit model, the LPF-PCBs of the three discussed standards are manufactured and measured (Figure 4.10). The characterization of LPF is performed using mixed-mode S-parameters. Figure 4.11 shows the S_{dd21} (differential insertion loss) measurement and simulation results of the LPFs.

The good agreement between measurement and simulation results verify the proposed equivalent model of the LPF. As shown in Figure 4.11, the LPF suppresses all unwanted signals, including DM and CM, above the cut-off frequency.

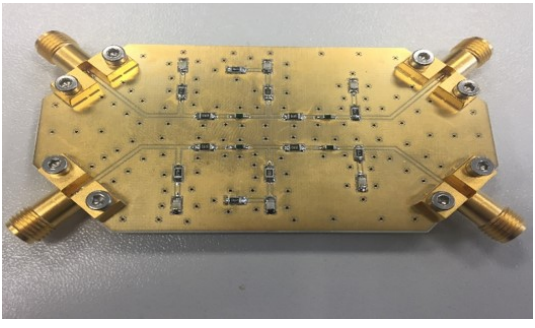

Fig. 4.10: Manufactured PCB of the low-pass filter - ©2018 IEEE

4.4.3 Modeling and characterization of the common-mode choke

Asymmetry of the cable wires or adapters [140], injected interferences and non-idealities of channels in differential systems - like automotive Ethernet - could lead to common-mode as well as differential-mode noise [157]. CM noise appears on each node pair with the same voltage level and phase [159]. Such noise signals can affect the function of components like PHY and lead to malfunctioning. The CM cancellation is an important part of Ethernet AFE circuits. CM suppression could be realized off-chip, by use of common-mode choke, or even on-chip in gigahertz frequency ranges.

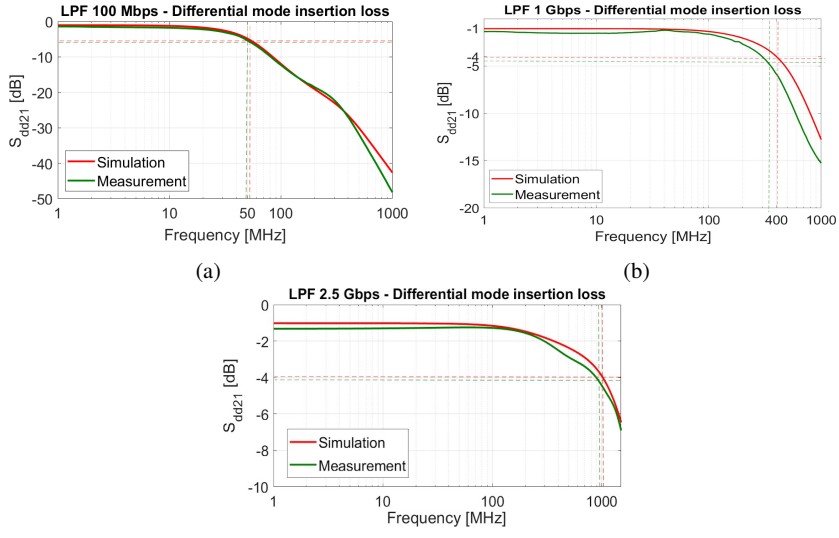

Fig. 4.11: S_{dd21} simulation and measurement results of LPFs for a) 100 Mbit/s b) 1 Gbit/s c) 2.5 Gbit/s networks - ©2018 IEEE

Automotive common-mode chokes applicable for 100BASE-T1 and 1000BASE-T1 have been investigated in the previous chapter and in [160]. In this chapter, the suitability of a CMC, as the third component of AFE, for 2.5 Gbit/s data communication is examined.

The equivalent circuit model of CMC (Figure 3.8) is used for the simulation of CMC, which is applicable for a data rate of 2.5 Gbit/s. Based on the calculation method described in Chapter 3, the corresponding circuit parameters have been calculated. The associated circuit values of CMC for 2.5GBASE-T1 standard are noted in Table 4.4.

The differential input insertion loss of the discussed CMC is examined using the S_{dd21} parameter. The corresponding measurement result is shown in Figure 4.12. In the same figure, the simulation results of the CMC equivalent circuit, which is presented in Chapter 3, is illustrated. The comparison between simulation and measurement results verifies the equivalent circuit. As described before, the required bandwidth for 2.5 Gbit/s data link using PAM-3 is approx. 900 MHz – 1 GHz.

At the time of writing, there is no defined limit for the 2.5GBASE-T1 standard. Therefore, the limit line of 1000BASE-T1 as a guideline is illustrated in Figure 4.12. The PAM level of the mentioned standard is not yet fixed. The required BW for 2.5 GBASE-T1 will be approximately 600 to 700 MHz if PAM-4 is applied.

Table 4.4: Associated values to the CMC model - ©2018 IEEE

	100BASE-T1	1000BASE-T1	2.5GBASE-T1
Rs	3.5 Ω	3 Ω	3 Ω
R_{par}	250 Ω	49 Ω	102 Ω
R_p	22 kΩ	16.6 kΩ	25 kΩ
R_{In}	10 MΩ	10 MΩ	10 MΩ
C_{par}	10 pF	24 pF	70 pF
C_p	140 fF	37.5 pF	13 fF
C_{In}	4.7 fF	4.7 fF	4.7 fF
$L_{leakage}$	0.1 µH	0.001 µH	1 pH
L_1=L_2	200 µH	100 µH	80 µH
K	1	1	1

Figure 4.12 shows the ability of the used CMC to pass the used differential signal without considerable attenuation. This means that the CMC can support 2.5GBASE-T1 with PAM-3 (BW of 900 MHz - 1 GHz) or PAM-4 (BW of 600 MHz - 700 MHz) signaling. The differential insertion loss would be around -1.8 dB and -2 dB in the required frequency range.

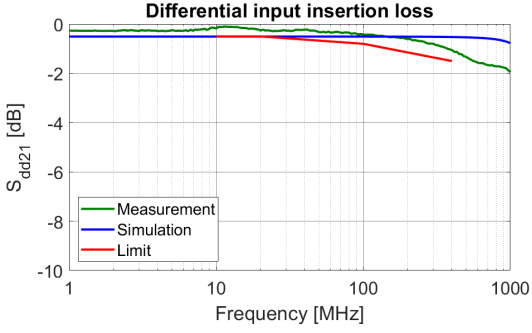

Fig. 4.12: S_{dd21} measurement and simulation results of CMC suitable for 2.5GBASE-T1 - ©2018 IEEE

4.4.4 Modeling and characterization of the common-mode termination

The common-mode termination is the last component of the AFE. To reduce EMI and sensitivity to common-mode noise in predefined frequency ranges, CM termination should be provided. Common-mode noise, which may be present in a twisted pair data line, is reduced by appropriate CM termination. Two 100 nF DC coupling capacitors are inserted into the differential signal lines. They ensure that no DC current from PHY enters the channel. In addition, two parallel resistors between plus and minus path will be included. They have a value of 1 kΩ and are high-impedance

termination. In the end, the high-impedance termination is provided by a resistor with a value of 100 kΩ and a capacitor with a value of 4.7 nF, which effectively blocks out the unwanted frequencies. Figure 4.13 shows the circuit model of the termination circuit. The associated values are shown in Table 4.5.

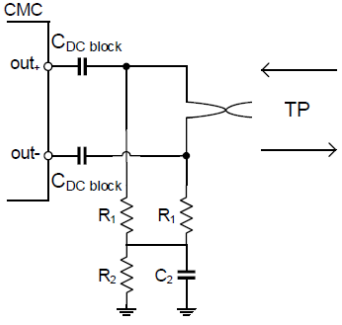

Fig. 4.13: Circuit model of common-mode termination - ©2018 IEEE

Table 4.5: Associated values to the CMT model - ©2018 IEEE

	100BASE-T1	1000BASE-T1	2.5GBASE-T1
R_1	1 KΩ	1 KΩ	1 KΩ
R_2	100 KΩ	100 KΩ	100 KΩ
$C_{DC\ block}$	100 nF	100 nF	100 nF
C_2	4.7 nF	4.7 nF	4.7 nF

Figure 4.14 shows the manufactured PCBs with soldered CMC and CMT components. To examine the combination of CMT with CMC, the measurement results are compared with the results of the PCB, including just the CMC. The CMT helps to reduce the CM energy and prevents the creation of standing CM waves in the channel [161]. The S_{cc21} and S_{dd21} measurement results of the 100BASE-T1 are illustrated in Figure 4.15. As shown in Figure 4.15a, the CMT leads to a better common input insertion loss, compared to the results of CMC. However, the presence of CMT has a negative impact on the differential input insertion loss (Figure 4.15b).

Similar observations are made by the measurement results of the 1000BASE-T1 CMC and CMT. The presence of the CMT improves the CM insertion loss (Figure 4.16a). The CMT increases the DM insertion loss by around 0.4 dB over the measured frequency range (Figure 4.16b).

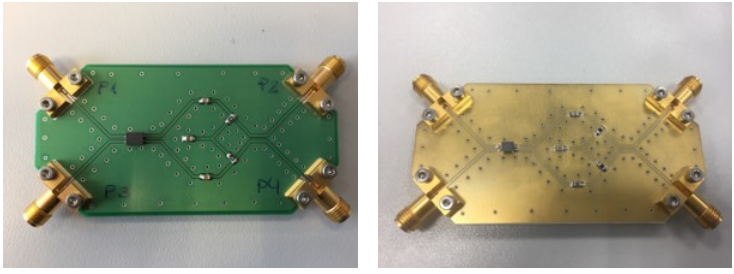

(a) (b)

Fig. 4.14: Test fixtures with CMC and CMT for (a) 100BASE-T1 (b) 1000BASE-T1 / 2.5GBASE-T1 - ©2018 IEEE

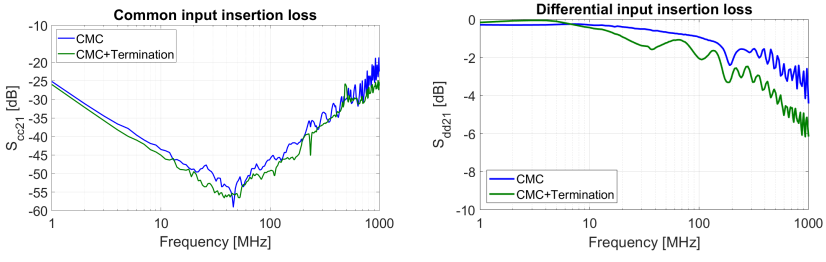

(a) (b)

Fig. 4.15: 100BASE-T1 - Measurement result 4-port CMC, 4-port CMC with termination (a) S_{cc21} (b) S_{dd21} - ©2018 IEEE

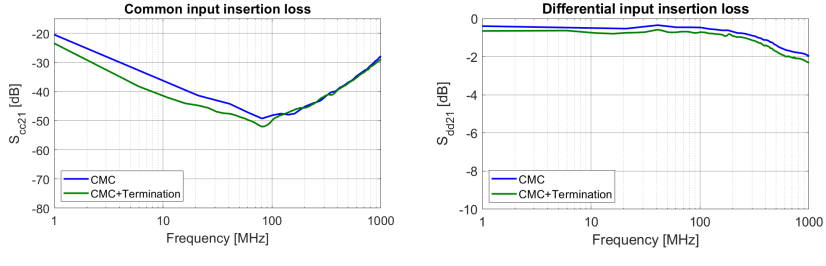

(a) (b)

Fig. 4.16: 1000BASE-T1 - Measurement result 4-port CMC, 4-port CMC with termination (a) S_{cc21} (b) S_{dd21} - ©2018 IEEE

4.5 Modeling of the entire analog front-end circuit

In the previous sections, individual components of the analog front-end and their functionality, considering the three discussed standards, were examined in detail. The related equivalent circuit models have been developed and simulated. The associated values of the circuit parameters have been noted in Tables 4.2 – 4.5.

In this section, all components are linked together and build the complete analog front-end system. Figures 4.17a and 4.17b show the fully developed AFE circuit. On the left side, the transceiver model is proposed. The LPF in the next stage defines the passband and the common-mode choke filters the undesired common-mode signals. In the last stage CMT is placed, which reduces the common-mode energy of the channel.

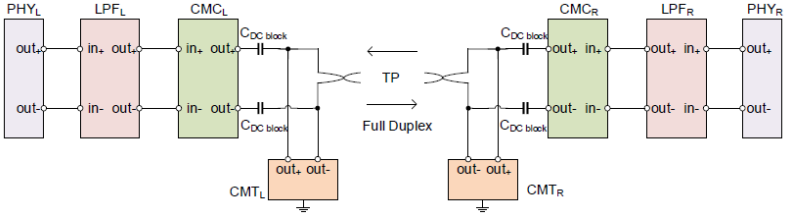

(a)

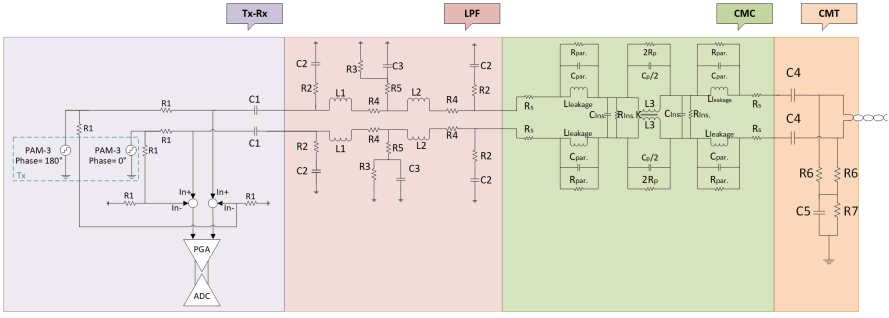

(b)

Fig. 4.17: (a) block diagram of Ethernet PHY (b) SPICE equivalent model of AFE - ©2018 IEEE

The model was simulated with the program PSPICE. Based on the calculated values, the circuits of AFEs, related to the three discussed standards, are designed and fabricated (Figure 4.18). The mixed-mode S-parameter simulation and measurement results are shown in Figure 4.19.

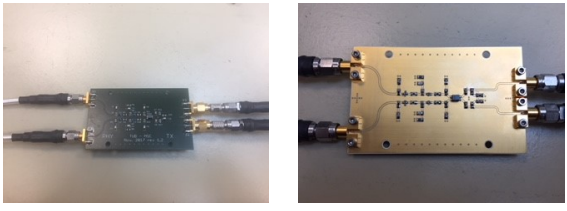

Fig. 4.18: Manufactured front-end PCB connected to STP adapter - ©2018 IEEE

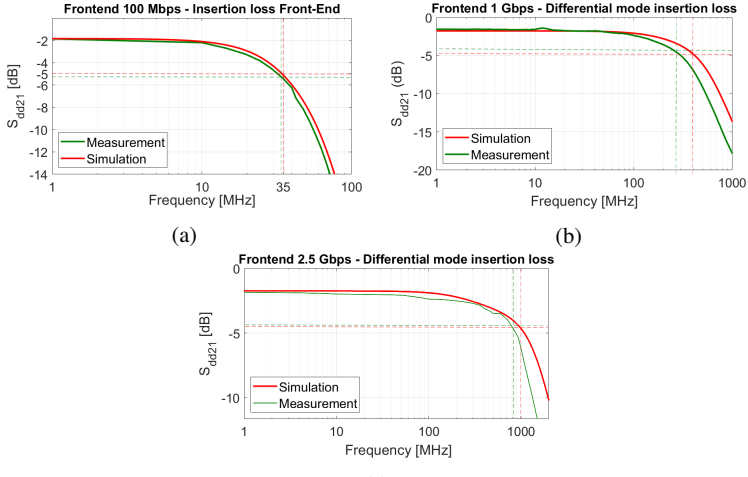

Fig. 4.19: Simulation and measurement results of complete front-end circuit a) 100 Mbit/s b) 1 Gbit/s c) 2.5 Gbit/s Ethernet communication - ©2018 IEEE

Figure 4.19a shows the differential input insertion loss of the 100BASE-T1 AFE board. The 3-dB bandwidth of this circuit is around 35 MHz, which is proved by measurement and simulation. The measured bandwidth of 1000BASE-T1 AFE board is about 290 MHz while the simulation provides a larger bandwidth around 370 MHz (Figure 4.19b). The S_{dd21} measurement of 2.5GBASE-T1 AFE board (Figure 4.19c) provides a good agreement with simulation results. In this case, the measurement bandwidth is 890 MHz and the simulation bandwidth is around 1 GHz.

4.6 Conclusions

The bandwidth requirements of future automotive network technologies pose new challenges to vehicle manufacturers worldwide. The increase in the data rate is to be realized by increasing the baud rate. In this chapter, the next generation of automotive high-speed Ethernet networks with data rates of 2.5 Gbit/s was discussed and compared with the existing standards for 100 Mbit/s and 1000 Mbit/s data rate.

The existing standards (100BASE-T1 and 1000BASE-T1) use PAM-3 signaling. The modulation type of 2.5GBASE-T1 standard is not yet defined . In this chapter, the use of PAM-3 was assumed. However, the implementation of modulation formats - such as PAM-4 to PAM-16 - are possible. The higher modulation formats increase sensitivity to electrical interferences. Therefore, the investigation of the robustness of the latest Ethernet bus systems and their components regarding electromagnetic compatibility plays an important role.

In this chapter, the characteristics of the mentioned standards were summarized and explained. Based on the OSI layer model, the Ethernet architecture and the requirements of the physical layer were discussed.

The main focus of this chapter was the function of the physical layer and the belonging components. For the development of the Multi-Gig Ethernet architectures, the simulation of the AFE is necessary. The SPICE model of the transceiver, low-pass filter, common-mode choke, and common-mode termination were presented. The models were adopted for the discussed standards. Power spectral density simulation of the transceiver model verified the proposed circuit. The circuit models for the components of the AFEs were fabricated and measured by mixed-mode S-parameters. Good agreement between simulation and measurement results was shown.

Chapter 5
EMC Analysis of UTP, STP, and SPP Transmission Lines for Automotive Multi-Gig Ethernet

To ensure a secure and reliable performance of the Multi-Gig Ethernet networks, the corresponding EMC investigations are of primary importance. The physical layer and channel of this communication network should undergo different EMC tests. The AFE of the physical layer should enable a primary "denoising" of the data. As discussed in the previous chapter, to characterize the EMC issues of the physical layer of the automotive Ethernet in the earliest stages of the development, a reliable simulation model of the AFE helps to detect the possible problems. For this purpose, the equivalent circuit models of the AFE components were presented in the previous chapter. Measurements validated the functionality of each equivalent circuit model individually and also as a part of the entire AFE.

The next important component of the Ethernet transmission path is the corresponding channel, which acts as the medium between the communication nodes. The channel of the Ethernet network plays a significant role in the overall system performance and is very critical regarding EMC issues. It is susceptible to noise and can disturb the neighboring in-vehicle components through its emission. Hence, the EMC characterization of the NGBase-T1 channel is of primary importance in the IEEE 802.3ch task force meetings.

Twisted-pair (TP) data lines are used as a medium in most high-speed telecommunications systems, such as those intended for use in vehicles. With increasing frequencies, the data lines become more susceptible to interference. The UTP cable is the choice of OEMs for the implementation of 100BASE-T1. For the 1000BASE-T1 standard, UTP or STP could be considered. However, the UTP data lines, which are implemented for 100 Mbit/s Ethernet, cannot fully meet the specifications of Multi-Gig networks. The channel of the automotive Multi-Gig Ethernet should support a large bandwidth (in gigahertz range) and be adequately immune to external noise and disturbances. The published presentations of the IEEE 802.3ch task force confirm that the shielded cables (i.e., STP or SPP) can meet the mentioned requirements of the automotive Multi-Gig Ethernet.

In this chapter, the functionality of different automotive Ethernet cables, considering their EMC behavior, is investigated and compared. Furthermore, the signal integrity of STP cable, with different lengths and carrying gigabit date rates on the lab bench, is measured and presented. The channel EMC investigations of this chapter, together with the previously presented simulation models and results, can help the engineers to evaluate the system performance in the early stages of the system design.

To the author's knowledge, the presented EMC investigations, and characterization of the gigabit data links and the performed comparisons between the automotive Ethernet cables are performed for the first time in this work.

In the next chapter, the RF immunity and emission characteristics of the STP cable are studied and investigated by in-vehicle measurements.

The contents of this chapter are published in the following two articles:

1. IEEE International Symposium on Electromagnetic Compatibility and IEEE Asia-Pacific Symposium on Electromagnetic Compatibility (EMC/APEMC), Singapore (2018) under the following title:

   S. Mortazavi, D. Schleicher and F. Gerfers, "Characterization and verification of Gigabit ethernet-based bus systems in vehicles," IEEE International Symposium on Electromagnetic Compatibility and IEEE Asia-Pacific Symposium on Electromagnetic Compatibility (EMC/APEMC), Singapore, 2018, pp. 428-433. doi: 10.1109/ISEMC.2018.8393814.

2. IEEE International Symposium on Electromagnetic Compatibility, EMC EUROPE Amsterdam (2018) under the following title:

   S. Mortazavi, D. Schleicher, F. Schade, C. Gremzow and F. Gerfers, "Toward Investigation of the Multi-Gig Data Transmission up to 5 Gbps in Vehicle and Corresponding EMC Interferences," International Symposium on Electromagnetic Compatibility (EMC EUROPE), Amsterdam, 2018, pp. 60-65. doi: 10.1109/EMC Europe.2018.8485142.

3. IEEE international symposium on electromagnetic compatibility, signal & power integrity, New Orleans (2019) under the following title:

   S. Mortazavi, D. Schleicher, A. Stieler, A. Sinai, F. Gerfers, M. Hampe, "EMC Analysis of Shielded Twisted Pair and Shielded Parallel Pair Transmission Lines for Automotive Multi-Gig Ethernet," IEEE international symposium on electromagnetic compatibility, signal & power integrity (2019).

   This paper won the best student paper award.

Contribution

I provided the basic ideas of the publications. The measurements of Section 5.3 are performed in cooperation with Matthias Hampe and Alexander Stieler. Matthias Hampe and I wrote the resulting publication in cooperation. The measurements of Section 5.4 were performed by Detlef Schleicher and me. Carsten Gremzow implemented FPGA programming and was involved in measurements of Section 5.5. I made the related data processing and wrote the publications. The other authors gave constructional advice and reviewed the publications.

5.1 Introduction

With the ever-increasing data rates in today's digital world, the automotive industry is also pursuing the usage of the fastest possible data communication systems in vehicles. The developments of the semiconductor industry in past decades have helped the implementation of new technologies, such as autonomous driving, in on-road vehicles. The newest processor units are capable of running the complicated machine learning algorithms for self-driving cars. The inputs of such algorithms are prepared from various modern sensors, which replace human's senses. The data from different sensors are fused in the algorithms, and their outputs are the commands on the corresponding electronic components units (ECUs) of the car, which control the motion of the vehicle.

The objectives of the automotive industry are the implementation of fully automated driving, where all the decisions are made by artificial intelligence (AI) in all situations and even at high speeds. This means that the AI has to communicate in real-time, i.e., nanoseconds latency, with the available sensors and actuators using communication signals with high frequencies, e.g., in the gigahertz range. This reveals the importance of the presence of a high-speed communication system that transfers the data both safely and reliably.

The traditional automotive communication systems like LIN, CAN, CAN-FD, and MOST with data rates of 19.2 kbit/s, 500 kbit/s, 2 Mbit/s (5 Mbit/s), and 150 Mbit/s, respectively, cannot meet the requirements of Multi-Gig automotive networks. That is why the internet protocol (IP)-based Ethernet network was chosen as the appropriate solution for higher data rates [162].

One of the main challenges of the automotive Ethernet is the use of a single twisted pair in a full-duplex operation mode. The use of one lane in automotive Ethernet in comparison to the other Ethernet standards, e.g., 1000BASE-T, which uses four parallel lanes, leads to the reduction of possible EMC interferences, cost, and weight.

The objective of the automotive Ethernet is the implementation of different data rates, i.e., 100 Mbit/s, 1000 Mbit/s, 2.5 Gbit/s, 5 Gbit/s, and 10 Gbit/s. Additionally, the further increase of data rates to 25 Gbit/s, 50 Gbit/s, and even 100 Gbit/s, is currently in the focus of the automotive industry worldwide. These high data rates lead to the next challenge of this technology in the automotive industry, which is dealing with signal frequencies and bandwidths in gigahertz range over one lane.

The further challenge of the automotive Ethernet is the use of the discussed high-frequency single lane network in a car with a continuously changing EMC environment. The EMC issues between the internal components of the network could be considered in the design phase using laboratory measurements. However, the system immunity regarding unknown environmental noise in the "real world" plays a vital role in future vehicles, which are controlled by AI, sensors, and actuators.

Therefore, the study of the EMC behavior of the network's components plays a crucial role in automotive Ethernet technology.

The implementation of gigabit data rates (2.5 Gbit/s, 5 Gbit/s, and 10 Gbit/s) will be standardized by IEEE 802.3ch Multi-Gig automotive Ethernet PHY task force. The differential signaling operation should be implemented using at least one of the following cables as the medium of the network: UTP, shielded twisted quad (STQ), STP, SPP, Coax, or Twinax [163].

The EMC investigations of the communication cables play a vital role in the safety and reliability of the gigabit Ethernet networks. Three major EM aspects should be investigated. The first is the emission of the medium. The noise immunity and signal integrity tests are the next two critical issues of the cables. Signal integrity tests of STP vs. UTP cables are reported in [164, 165]. In [165], the in-vehicle emissions of the STP cable with data rates up to 5 Gbit/s are reported.

In Section 5.2, possible automotive Ethernet cable options are presented in the initial step. The physical structures of the possible automotive Multi-Gig cables are briefly explained .

In Section 5.3, the measurements of the medium dependent interface (MDI) test heads are discussed. After describing the measurement setups in Section 5.3, the frequency domain measurements of the STP and SPP cables, based on the mixed-mode S-parameters for frequencies up to 8 GHz, are discussed. Two different lengths are examined for each STP and SPP cable, i.e., 1.0 m and 10.0 m. In order to consider the manufacturing tolerances, four different cables of the same length and type are measured. Furthermore, the screening attenuation, coupling attenuation, and the unbalanced attenuation of both cables are investigated and compared using a triaxial measurement setup. Utilizing a bit error rate tester, the time-domain characteristics of the cables for different gigabit data rates are compared.

In Section 5.4, a comparison between UTP and STP cable based on laboratory-level measurements is performed in two steps. First, the mixed-mode S-parameters of the mentioned cables are determined. Second, the coupling between different cables, i.e., UTP, STP, and coax, is examined. Finally, based on the measurement results, the application frequency range of each cable is discussed.

The signal integrity of the STP channel is investigated in Section 5.4. In this regard, two Xilinx Kintex-7 FPGA boards are configured as the transmitter and receiver of the gigabit data communication link. The Multi-Gig communication path is constructed on the lab bench using the FPGA boards and STP cable. The signal integrity of the channel is discussed using different cable lengths and data rates. The investigations include the associated statistical eye diagrams. Finally, Section 5.6 summarizes and concludes this chapter.

5.2 Automotive Ethernet cable options

A. UTP

The unshielded twisted-pair cable consists of two twisted cables without additional shielding, which leads to susceptibility against noise (Figure 5.1a). UTP cables are implemented in 100BASE-T1 for data rates of 100 Mbit/s.

B. STP

The Shielded twisted pair cable (Figure 5.1b) has an additional shielding around both twisted cables that can prevent the interference of external noise with data lines.

C. SPP

As it is shown in Figure 5.1c, the shielded parallel pair cable includes two parallel cables, which are shielded. As the pairs are not twisted, the skew of SPP is lower than the STP.

D. Coaxial

The coaxial cable (Figure 5.1d) has the advantage of low costs compared to the other cables. This cable's drawback is the common-mode current on its shield and the associated radiation and immunity issues.

E. STQ

Figure 5.1e illustrates the cross-section of STQ cables. Two opposite conductors carry the differential signal. The other two perpendicular lines build a virtual ground for the signal lines. A copper layer around the whole line shields the cable separately.

F. Twinax

The twin-axial cable consists of two parallel cables with a joint shielding. A coaxial cable has one inner conductor, but the Twinax includes two conductors for differential signaling (Figure 5.1f).

5.3 Measurement of STP and SPP cables

In this section, measurements of STP and SPP cables are presented. As there are still no standardized limit lines for Multi-Gig networks, the predefined setups and limits of 1000BASE-T1 build the theoretical background of the following measurements. According to the IEEE 802.3ch taskforce, using pulse amplitude modulation level 4 (PAM-4) seems to be an interesting approach for Multi-Gig automotive Ethernet.

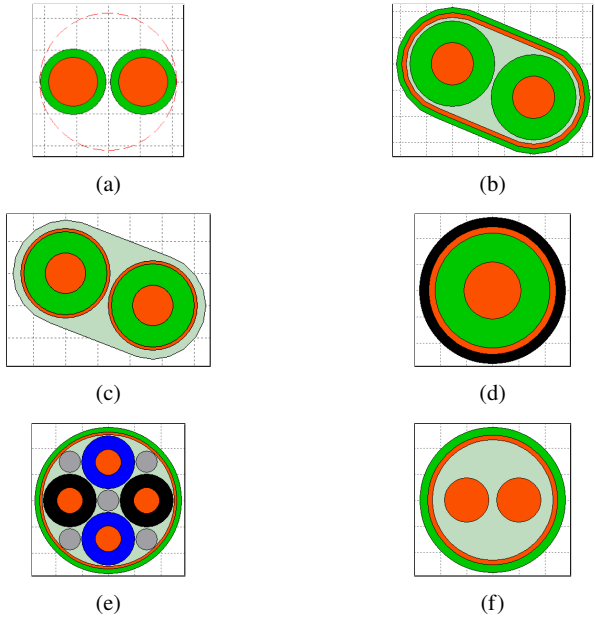

Fig. 5.1: Possible cables for automotive Multi-Gig Ethernet networks (a) UTP (b) STP (c) SPP (d) coaxial (e) STQ (f) Twinax - ©2019 IEEE

Using PAM-4 the required channel bandwidth for 2.5 Gbit/s, 5 Gbit/s and 10 Gbit/s is 0.69 GHz, 1.38 GHz, and 2.75 GHz, respectively [166]. Hence, in the following measurements, the behavior of the examined cables up to 3 GHz as an approximation for gigabit Ethernet plays a key role.

For each STP and SPP cable, two different lengths are examined, i.e., 1.0 m and 10.0 m. To consider the manufacturing tolerances, four different cables of the same length and type are measured. In total sixteen cables are studied. For reasons of clarity, only the results of one sample from each cable type and length are displayed. The results of the remaining samples are quite the same. In the first step, the required MDI test heads are measured regarding their differential impedance.

5.3.1 Measurement of MDI test head

To connect the under test STP and SPP transmission lines to different measurement instruments, specific MDI test heads (adapters) have to be used. These adapters need to have low insertion loss and good matching to 50 Ω single-ended as well as 100 Ω differential-mode line impedance. To ensure this property, time domain

reflectometry (TDR) measurement setup (Figure 5.2) is applied. As illustrated, a vector network analyzer (VNA) with TDR option is connected via two low loss and phase stable coaxial cables to the adapter. The test head is not terminated on the other side. According to [167], following settings are applied: frequency range from 10 MHz to 20 GHz, linear sweep with 2000 points, output power 0 dBm, measurement bandwidth 1 kHz, differential-mode port impedance 100 Ω, TDR step impulse, filtering with Hanning window.

The measurement results of both adapters are illustrated in Figure 5.2. The differential-mode line impedance $|Z_{dd11}|$ of these test heads should be within the range of 95 Ω to 105 Ω (±5%) [167]. A tolerance of ± 10 % is allowed on the coaxial connectors side, for a time duration smaller than 120 ps round trip time or 60 ps propagation time [167]. As shown in Figure 5.2, both MDI test heads fulfill the aforementioned requirements with a minimum value of 98.1 Ω and a maximum value of 102.6 Ω .

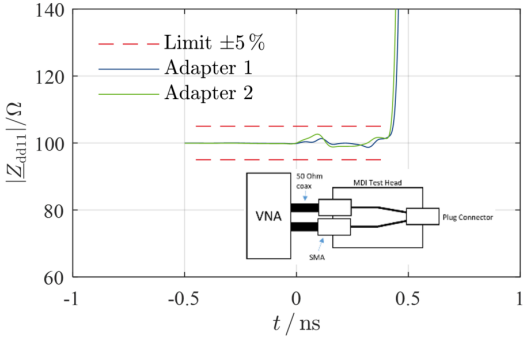

Fig. 5.2: TDR measurement of differential-mode line impedance $|Z_{dd11}|$ of both MDI test heads, which is within the allowed range of 95 Ω and 105 Ω. - ©2019 IEEE

5.3.2 Measurement settings

For the measurements in frequency domain, the following settings for the VNA are performed [167]: frequency range from 1 MHz to 8 GHz, logarithmic sweep, 2001 sweep points, output power 0 dBm, measurement bandwidth 100 Hz, differential-mode port impedance 100 Ω, common-mode port impedance 25 Ω. The VNA has been calibrated using an appropriate four-port calibration unit. The phase reference plane of each port has been moved to the end of the MDI test heads by defining an adequate port extension. According to [167], the VNA calibration accuracy is validated by measuring the return loss (RL) of a direct through/through connection between the two mixed-mode ports at the calibration plane. Figure 5.3 shows the corresponding measurement results. As is shown, the RL is below the specified limit at all frequencies for both mixed-mode ports.

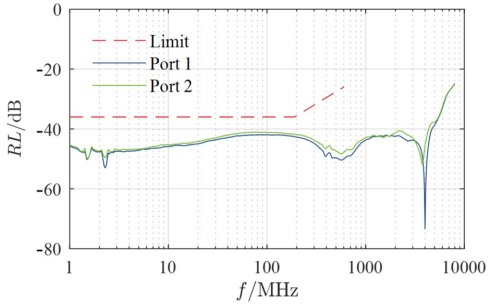

Fig. 5.3: Return loss (RL) parameters for a direct through/through connection between the two mixed-mode ports at the calibration plane. - ©2019 IEEE

5.3.3 Measurement results in frequency domain

In this section, the mixed-mode scattering parameters for both STP and SPP transmission lines are presented. The measurement setup, shown in Figure 5.4, is established. The transmission line under testing is connected to four-port VNA through the MDI test heads and the corresponding coaxial cables. The cables under testing are placed on an isolation material with a relative permittivity less than 1.4 and with a height of 10 mm above a wooden table. To avoid unwanted coupling, the minimum distance between adjacent sections of the transmission line is 30 mm.

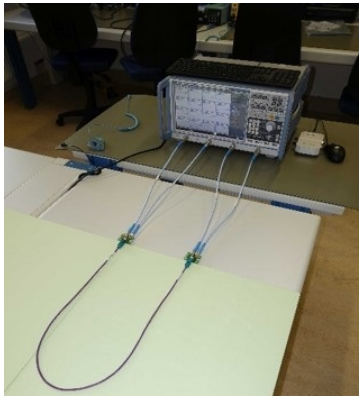

Fig. 5.4: Mixed-mode measurement setup with VNA, low loss and phase stable cables, measurement fixtures and transmission line under test. - ©2019 IEEE

The mixed-mode S-parameters have been measured for both STP and SPP transmission lines, each with two different lengths. The measured RL (S_{dd11}) of short (1 m) and long (10 m) cables are presented in Figure 5.5a and 5.5b, respectively. The measurement results of all cables are below the predefined limits in [167]. For lower frequencies, the shorter cables show smaller RL (-12.2 dB at 1 MHz), and therefore a better matching is provided. Even though all cables are electrically short

- at 1 MHz - this effect can be explained due to the mismatch of line impedance and port load 100 Ω. Hence, for cable with a length of 10.0 m, the transformation of the load down the transmission line gives a larger additional capacitive part than for the line with a length of 1.0 m. However, at higher frequencies, RL is similar for both cable lengths. A comparison between both cable types STP and SPP reveals that STP cables generally show smaller RL at higher frequencies. Note that the RL of both cable types is still below -20 dB up to 3.5 GHz.

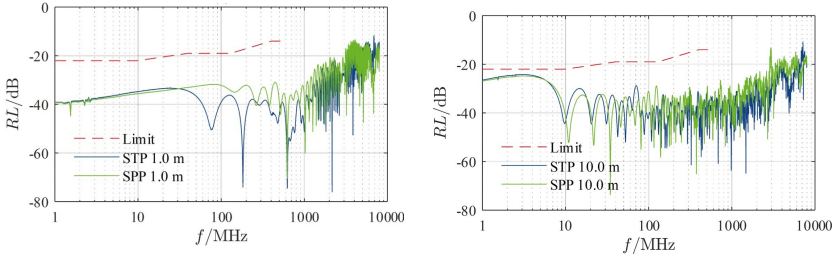

Fig. 5.5: Measured RL for both STP and SPP cables: (a) line length 1.0 m, (b) line length 10.0 m - ©2019 IEEE

Figure 5.6a illustrates the insertion loss (S_{dd21}) of both cable types with a length of 1 m. The insertion loss (IL) of the longer cables, Figure 5.6b, is slightly larger than that of shorter cables. The reason for this is the attenuation due to the measurement fixtures, which has not been compensated and is more predominant when cable lengths are short. Overall, the SPP cable shows little better IL. At 1 GHz, the difference between both cable types is 0.03 dB/m. The longer cables (10.0 m) hold the limit according to [167], whereas the cables with a length of 1.0 m are below the defined limit for lower frequencies. Again, this effect is most probably caused by the measurement fixtures. Concerning Multi-Gig data transmissions, both cable types show sufficiently good IL. Figure 5.6b shows an IL around - 1.75 dB/m at 3 GHz.

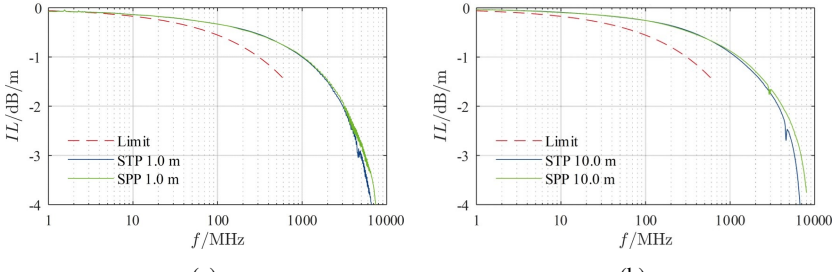

Fig. 5.6: Measured insertion loss (IL) for both STP and SPP cables: (a) line length 1.0 m, (b) line length 10.0 m. - ©2019 IEEE

Finally, results for the longitudinal conversion loss (LCL) are presented in Figure 5.7. Generally, larger LCL (S_{dc11}) is observed for longer cables, since the asymmetry and the corresponding mode conversion tends to increase with transmission line length. Based on the measurement, the STP cables show better LCL results than SPP cables. At 80 MHz, the difference between both cable types is about 16.8 dB, while around 3 GHz, both cables present similar mode conversion values. Comparable results have been obtained for the transverse conversion loss (TCL), which is not shown in this chapter for reasons of simplicity. Merely the STP cable with a length of 1.0 m holds the limit as defined in [167]. Note that the LCL and TCL are very sensitive to external influences. For example, the presence of a ground plane fundamentally changes the results.

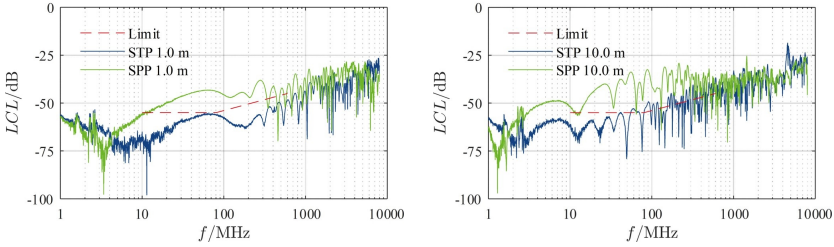

Fig. 5.7: Measured LCL for both STP and SPP cables: (a) line length 1.0 m, (b) line length 10.0 m. - ©2019 IEEE

5.3.3.1 Measurement of coupling attenuation

In this section, the screening of both STP and SPP cables is investigated in detail. For this purpose, the triaxial measurement setup is used (Figure 5.8). Here, the triaxial test procedure is well known and widely used [168]. Again, the four-port VNA with low loss and phase stable cables are used. Two ports of the VNA are used in mixed-mode while a third port is used single-ended. The fourth port of the VNA is not needed. The settings of the VNA are as follows: frequency range from 1 MHz to 8 GHz, logarithmic sweep, 10001 sweep points, output power 0 dBm, measurement bandwidth 1 kHz, differential-mode port impedance 100 Ω, common-mode port impedance 25 Ω, single-ended impedance 50 Ω.

The VNA is calibrated using an appropriate four-port calibration unit. Further, the phase reference plane of the mixed-mode port is moved to the end of the MDI test head by defining an adequate port extension. The transmission line under test is placed within the tube with a length of 3.0 m and connected to the mixed-mode port of the VNA at the near end.

At the far end, the line under test is connected to a specific termination network, which shows 100 Ω for differential-mode and 25 Ω for common-mode. The shielding of the line under test forms a second transmission line together with the tube. This coaxial line is connected to the single-ended port of the VNA at the far end. At the near end, this line is short-circuited. This setup allows the measurement of screening attenuation (a_s) and coupling attenuation (a_c) [123, 169–171], where these quantities are derived from scattering parameters S_{sc21} as well as S_{sd21}. Further, the unbalanced attenuation (a_u) is obtained from the results of the previous section. Here, a_u is given at the far end as transverse conversion transfer loss (TCTL), which is obtained from scattering parameter S_{cd21}.

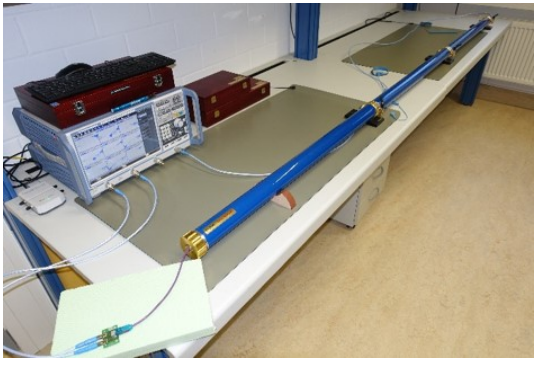

Fig. 5.8: Measurement setup with VNA and triaxial tube to measure the shielding effectiveness of the transmission lines under test. - ©2019 IEEE

The measurement results for a_u, a_s and a_c are shown in Figure 5.9. As shown in Figure 5.9a, the unbalanced attenuation of the STP cable under test is generally higher and thus better than that of the SPP cable. This means that along the SPP line, a greater proportion of the injected differential-mode signal is converted into common-mode. At 100 MHz, the difference between both cables is 4.1 dB. Note that in the frequency range around 1 GHz, the SPP line under test has slightly better a_u than the STP line, while at higher frequencies around 3 GHz the STP cable shows a better performance regarding a_u. Furthermore, the measured screening attenuation a_s of both cables is shown in Figure 5.9b. Except for very low and very high frequencies, the SPP line under test shows lower a_s than the STP line and thus lower effectiveness of its screening. At frequency 100 MHz, the difference between both cable types is 12.4 dB. Finally, the measured coupling attenuation a_c is illustrated in Figure 5.9c. According to [170, 171], this quantity can be considered in a first approach as the sum of unbalanced attenuation a_u as well as screening attenuation a_s. Consequently, the results of the SPP line under test are generally worse than that of the STP line. Note that the SPP line shows better behavior than the STP line for the frequency range around 1 GHz, which probably results from the higher unbalanced attenuation a_u of the SPP line in this frequency band.

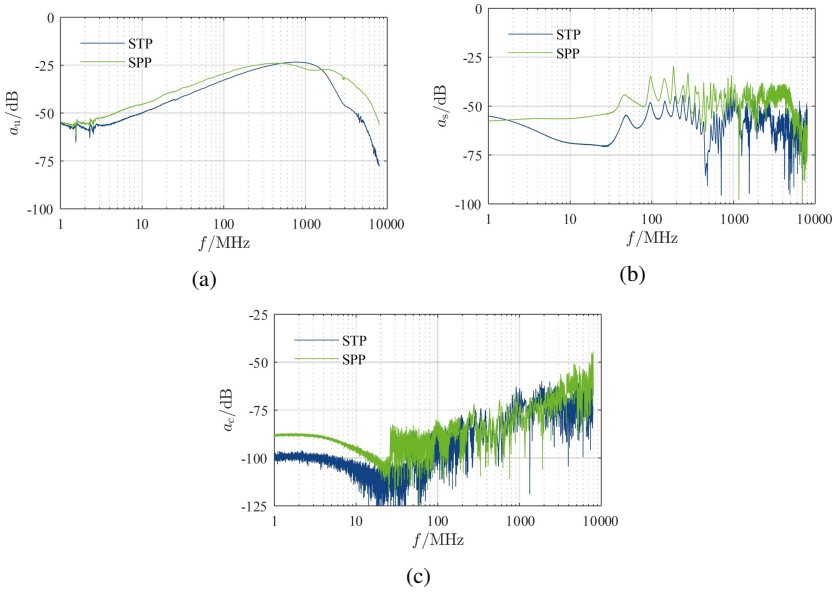

Fig. 5.9: Measured attenuation for both STP and SPP cables: (a) unbalanced attenuation a_u, (b) screening attenuation a_s, (c) coupling attenuation a_c. - ©2019 IEEE

5.3.4 Measurement results in time domain

To assess the impact of STP and SPP cables on the signal integrity of Multi-Gig data transmissions, the time domain measurements are performed in this subsection. Figure 5.10 shows the measurement setup with a bit error rate tester (BERT). The differential output signal of the pulse pattern generator is connected via two relatively short and high-performance coaxial cables and the MDI test head to one side of the transmission line under test. The second side of the cable is connected to the differential error detector port of the BERT through the second adapter and the corresponding coaxial cables. For this measurement, the PAM-2 modulated signal is used, as the BERT does not support the higher PAM levels. The test signal is generated as a pseudorandom binary sequence with length 2^{23}-1, and peak-to-peak voltage of 0.8 V. The bit rate (BR) is gradually increased, and the related bit error rate (BER) of each transmission line is measured.

Measurement results of the STP and SPP cables with a length of 10.0 m are listed in Table 5.1. The SPP cable shows smaller BER for any data rate. Further, the maximum data rate for SPP cable is 5.2 Gbps (PAM-2) before the loss of synchronization (SYNC), while the maximum data rate for STP is 4.7 Gbps (PAM-2). Together with the results of the previous subsections, the marginally better performance of STP cables up to frequency 3 GHz could be shown. For frequencies beyond the mentioned ranges, the SPP cables may be preferred. However, as described at the beginning of

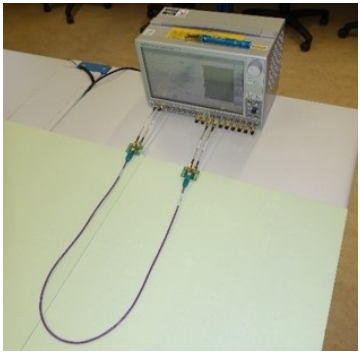

Fig. 5.10: Time domain measurement setup with BERT, low loss and phase matched cables, MDI test heads and transmission line under test. - ©2019 IEEE

this section, the automotive Multi-Gig Ethernet can be realized with 3 GHz cable bandwidth and PAM-4 modulation. Please note that data transmission with STP and SPP cables with a length of 1.0 m does not show any bit error up to 10.0 Gbps. Therefore, these results are not presented further.

Table 5.1: Bit error rate of STP and SPP cables - ©2019 IEEE

Data rate	**Bit Error Rate**	
	STP 10.0 m	**SPP 10.0 m**
2.0 Gbps	0.0	0.0
2.5 Gbps	0.0	0.0
3.0 Gbps	$6.30 \cdot 10^{-8}$	0.0
3.5 Gbps	$1.63 \cdot 10^{-4}$	$8.36 \cdot 10^{-6}$
4.0 Gbps	$3.85 \cdot 10^{-3}$	$7.52 \cdot 10^{-4}$
4.5 Gbps	$1.38 \cdot 10^{-2}$	$5.45 \cdot 10^{-3}$
5.0 Gbps	SYNC loss	$1.41 \cdot 10^{-2}$
5.5 Gbps	SYNC loss	SYNC loss
6.0 Gbps	SYNC loss	SYNC loss

5.4 Measurement of UTP and STP cables

As previously described, the data transmission for 100 Mbit/s is established via UTP lines. The characterization of the transmission channel helps to implement methods such as forward error correction, and equalization at the chip level [172]. In the next generation of Ethernet communication, the goal is to increase data rates to 1 Gbit/s. With increasing frequencies, the data lines become more susceptible to interference [139]. Therefore, the use of UTP lines for gigabit communication is doubted, and alternative transmission media such as STP, SPP, or coaxial lines are examined for their suitability. These cables have better noise immunity and noise emission than UTP cables.

In this section, a comparison between a UTP and an STP cable, based on laboratory-level measurements, is performed in two steps. First, the mixed-mode S-parameters of the STP and UTP line with a length of 6 m are determined using the test setup described in [173]. This is shown in Figure 5.11. The corresponding measurement results are shown in Figure 5.11b and 5.11c. In the second step, the shielding attenuation between three different cables (i.e., STP, UTP, and RG58) under the same measuring conditions is examined.

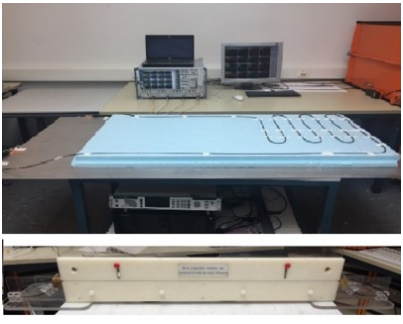

(a)

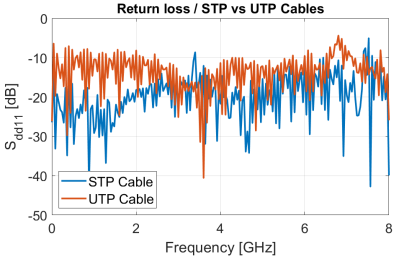

(b)

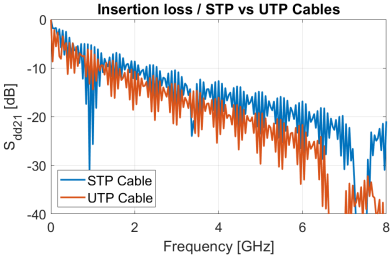

(c)

Fig. 5.11: Mixed-mode S-parameter for UTP - vs. STP (a) measurement setup for S-parameter measurement and shielding attenuation of the cables (b) differential-mode return loss (c) differential-mode insertion loss - ©2018 IEEE

Note that the performed measurements of this section are done using an STP cable from a different vendor compared to the used STP cable for the previously presented results in Figure 5.5. Figure 5.11b shows the differential return loss (S_{dd11}) of the both examined UTP and STP cables. The line in red the measurement result of UTP, while the line in blue is the return loss result of STP cable. Both cables are at the same length of 6 m. A comparison of these two cables shows that the STP cable has better performance in the entire frequency range up to 8 GHz. The performance of both cables deteriorates in the higher frequency range.

The insertion loss of the STP and UTP cables, up to 8 GHz, is illustrated in Figure 5.11c. Generally, the STP cable shows a better performance than the UTP

cable over the measured frequency range. As mentioned, the UTP cable is used for 100BASE-T1 with a frequency range of up to 33.3 MHz. The measurements show that the UTP cable has an acceptable insertion loss for 100BASE-T1.

The presented measurement results show that the UTP cable is not suitable for higher frequency ranges. The 6 m STP cable used has an insertion loss of approx. 11 dB at 2.75 GHz, which is the required channel bandwidth for 10 Gbit/s automotive Ethernet using PAM-4. Considering the presented limits in section 2.3.4, the measured STP cable can fulfill the requirements.

The following results are obtained by comparing the coupling measurements. The measured coupling between STP and UTP lines of equal length is less than -65 dB. The coupling between an STP line and an RG58 cable is less than -50 dB. Finally, the coupling of two STP lines has a value of less than -90 dB. These measurements show the effectiveness of the twisting and especially the shielding of the tested lines.

5.5 Signal integrity of STP cable

Using two Xilinx Kintex-7 FPGA boards (Figure 5.12a), the gigabit data communication with an STP cable is investigated. To realize the communication between two FPGA boards and to transmit the desired data rate, the first board was configured as Tx and the second one as Rx. The pattern generator of the GTX transceiver enables the generation of a PRBS 2^5-1 bits. The differential signaling is realized over GTX SMA I/O connectors. The peak-to-peak voltage level is equal to 1 V. Data rates of 2.5 Gbit/s and 5 Gbit/s are generated. A Rosenberger H-MTD adapter (Figure 5.12b) realizes the interface between SMA connectors of the FPGA board and the medium (TP line).

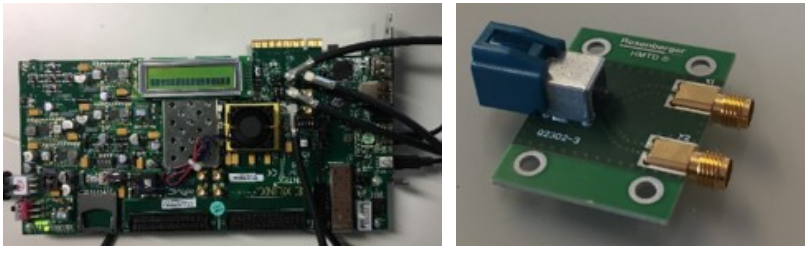

(a) (b)

Fig. 5.12: (a) Kintex-7 FPGA Board (b) The Rosenberger H-MTD adapter - ©2018 IEEE

The signal attenuation, e.g., from the transmission channel, can lead to a very closed eye diagram at the receiver input ports. However, the negative impacts of the channel can be calculated and used to reconstruct the received signal (equalization). The Rx eye scan in GTX transceivers of FPGA-board provides a method to measure and visualize the receiver eye margin after the equalizer (statistical eye). By using this method, it is possible to calculate the BER over time and the voltage offset at the post-equalization data sampling point within Rx [174].

In the following figures, the BER is presented by different color codes, all illustrated on the right side of the diagrams. The vertical axis of the diagram is the so-called 'voltage code'. It includes 256 vertical taps. Each tap corresponds to around 3.9 mV (for the measurements of this section). The horizontal axis is the unit interval width of the eye diagram [174].

In addition to the data rate, the next important aspect that affects BER is the length of the STP line. In general, the length of the lines and the attenuation are proportional to each other. This fact leads to the degradation of data transmission quality and the increase in data loss over longer cables [158]. Consequently, it also affects the opening of the eye diagram, deteriorates the signal-to-noise ratio, and increases the BER. To examine the effect of the cable length, three STP cables with different lengths (i.e., 2 m, 6 m, and 15 m) are used for the measurements. Figures 5.13 - 5.21 show the effect of data rate and cable length on signal quality.

With a data rate of 1 Gbit/s, while varying the STP cable lengths, the degradation of signal quality concerning BER is illustrated in Figures 5.13 - 5.15. Among the mentioned figures, Figure 5.15, which illustrates the results of 15 m cable, has the closest statistical eye diagram. A comparison between Figures 5.14, 5.17, and 5.20 confirms the influence of increasing data rates (1 Gbit/s to 5 Gbit/s) on statistical eye-opening, and BER. In the mentioned figures, the cable length remained constant (6 m). Consequently, Figure 5.21 implies the closest statistical eye diagram. The illustrated eye diagram is the worst case. For this test, the longest cable (STP with a length of 15 m) and the highest data rate (5 Gbit/s) was implemented. The impact of cable length and the data rate on signal quality is illustrated.

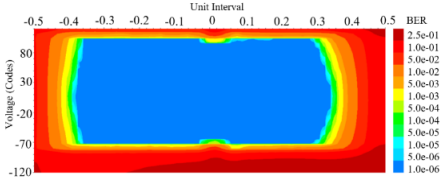

Fig. 5.13: Statistical Eye of 1 Gbps over 2 m STP Cable - ©2018 IEEE

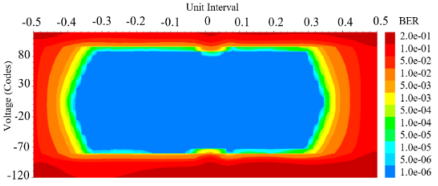

Fig. 5.14: Statistical Eye of 1 Gbps over 6 m STP Cable - ©2018 IEEE

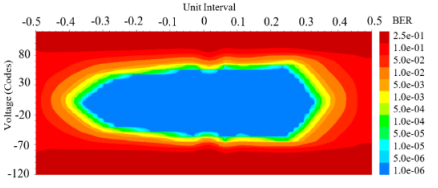

Fig. 5.15: Statistical Eye of 1 Gbps over 15 m STP Cable - ©2018 IEEE

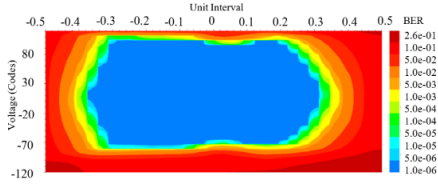

Fig. 5.16: Statistical Eye of 2.5 Gbps over 2 m STP Cable - ©2018 IEEE

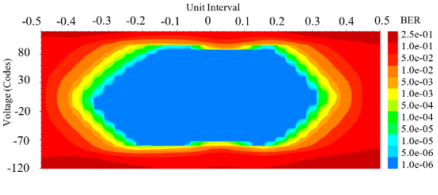

Fig. 5.17: Statistical Eye of 2.5 Gbps over 6 m STP Cable - ©2018 IEEE

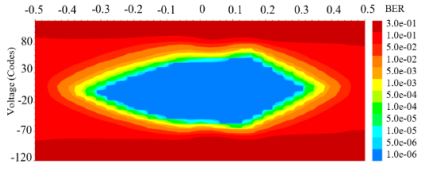

Fig. 5.18: Statistical Eye of 2.5 Gbps over 15 m STP Cable - ©2018 IEEE

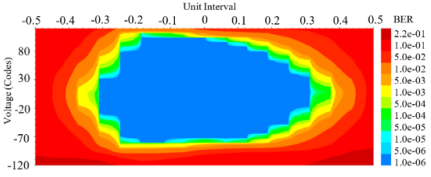

Fig. 5.19: Statistical Eye of 5 Gbps over 2 m STP Cable - ©2018 IEEE

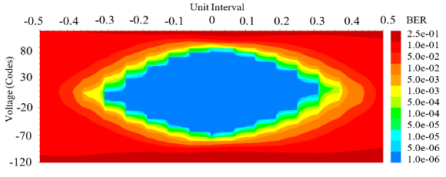

Fig. 5.20: Statistical Eye of 5 Gbps over 6 m STP Cable - ©2018 IEEE

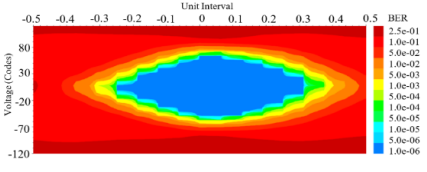

Fig. 5.21: Statistical Eye of 5 Gbps over 15 m STP Cable - ©2018 IEEE

5.6 Conclusion

For the realization of fully automated vehicles, there is a requirement for high-speed communication networks. According to IEEE 802.3ch, Ethernet is the superior technology. Data rates of 1 Gbit/s, 2.5 Gbit/s, 5 Gbit/s, and 10 Gbit/s have to be implemented in the vehicles. For the implementation of Level 5 autonomous driving, even higher data rates (up to 100 Gbit/s) are required. The realization of the mentioned Ethernet networks is currently at the focus of the automotive industry. EMC investigation of the automotive Ethernet plays a crucial role, as the safety and reliability of the whole system depends on it.

The signal integrity of STP and SPP cables, as the favorable channel choices for Multi-Gig applications, have been investigated in this chapter. The automotive Multi-Gig Ethernet can be implemented with 3 GHz cable bandwidth and PAM-4 modulation. The marginally better performance of STP cables up to 3 GHz was shown using mixed-mode S-parameter measurements (return loss, insertion loss, longitudinal conversion loss, and transverse conversion loss). With the triaxial measurement setup, the screening attenuation, coupling attenuation, and the unbalanced attenuation of the mentioned transmission lines were measured. The STP cable showed a better performance again up to 3 GHz. Finally, using a bit error rate tester,

the time domain performance of both cables were examined. According to the latter mentioned measurement and the other presented measurement, the SPP cable showed lower BER for data rates beyond 3 Gbaud (PAM-2) and better performance for higher frequencies above 3 GHz.

Further, using the statistical eye diagram of Xilinx GTX transceivers, the BER over STP cable for different lengths and data rates were measured in the laboratory. The measurement results of a 15 m long cable showed a poor statistical eye-opening, while the 6 m cable showed acceptable results for three different data rates. The best result was measured from the lowest data rate (1 Gbit/s) and the shortest cable length (2 m).

Chapter 6
Toward Investigation of the Electromagnetic Radiation and Immunity of the STP Cable by In-Vehicle Measurements

As described in Chapter 2, electromagnetic radiation and RF immunity are two of the critical EMC issues which should be tested at component and vehicle level. The communication link should ensure reliable performance under harsh automotive EMC conditions and should not disturb the functionality of the surrounding components. The measurements of the previous chapter have shown the suitability of the STP cable for the use as automotive Multi-Gig Ethernet link for the IEEE 802.3ch standard.

This chapter consists of two parts. The first part presents the in-vehicle immunity tests of the 10 m STP cable with four in-line connectors. The measurement setup includes a worst-case situation, which should be considered for a reliable ECU design. The RF ingress of the STP cable is measured up to 6 GHz. The second part of this chapter deals with the in-vehicle electromagnetic emission of the STP link. Again, a worst-case routing for STP cable is implemented. The measured emission of the STP cable should be regarded; otherwise, the radiation of the automotive Multi-Gig channel can disturb other E/E components of the vehicle. The measurements include the electromagnetic coupling of STP cable to different receivers (antennas).

In the next chapter, a simulation methodology for calculating the RF emission of STP cable is introduced that facilitates the network design and harness routing.

The in-vehicle immunity test results of this chapter complete the IEEE 802.3ch studies and propose new limits for this standard. Furthermore, a novel idea in this chapter is the use of FPGA as a temporary alternative to a Multi-Gig automotive PHY for data communication over one twisted pair. By using this method, early investigation and characterization of possible EMC issues in the vehicle can be made possible.

The contents of this chapter are published in the following two articles:

1. IEEE International Symposium on Electromagnetic Compatibility, EMC EUROPE Amsterdam (2018) under the following title:

   S. Mortazavi, D. Schleicher, F. Schade, C. Gremzow and F. Gerfers, "Toward Investigation of the Multi-Gig Data Transmission up to 5 Gbps in Vehicle and Corresponding EMC Interferences," International Symposium on Electromagnetic Compatibility (EMC EUROPE), Amsterdam, 2018, pp. 60-65. doi: 10.1109/EMCEurope.2018.8485142.

2. IEEE international symposium on electromagnetic compatibility, signal & power integrity, New Orleans (2019) under the following title:

   S. Mortazavi, D. Schleicher, A. Sinai, F. Gerfers, "RF Ingress Automotive Immunity Measurement on STP Cable in the Vehicle up to 6 GHz," 2019 IEEE international symposium on electromagnetic compatibility, signal & power integrity (2019).

Contribution

The measurements of Section 6.5 were performed by Detlef Schleicher and myself. The measurements of Section 6.7 are performed by both Detlef Schleicher, Carsten Gremzow, and myself. Carsten Gremzow has implemented FPGA programming. I made the related data processing and wrote the publications. The other authors gave constructional advice and reviewed the publications.

6.1 Introduction

Electrical-based technical progress in the automotive area creates new challenges for OEMs. The audio and video communication in the car has been gaining remarkable importance. The infotainment devices now play a key role in today's cars with high bandwidth (BW) requirements, and they bring the classic vehicle bus systems to the limit of their potential.

The demand for real-time audio and video-based driver assistance systems has received considerable attention. Sensor systems containing multimode radars, long range radars, ultrasonic sensors, and multi-purpose cameras belong to this category. The upcoming implementation of 5G mobile technology with data rates of up to 10 Gbit/s should also be available in the next generation of cars. Furthermore, the automotive industry is preparing itself to fully implement autonomous driving (including machine learning, artificial intelligence) as well as vehicle-to-vehicle (V2V) and vehicle-to-infrastructure (V2I) communication. This is why the number of ECUs in modern automobiles has increased significantly in recent years. This, in turn, leads to increasing data rates in the communication network. Realizing these functions requires high-performance network technologies with a high data rate and, consequently, higher bandwidth.

The existing automotive communication networks, e.g., LIN, CAN, FlexRay, and MOST cannot satisfy the mentioned expectations, and are limited regarding the maximum possible data rates. This is why Ethernet should enable the high-speed intentions of the automotive industry. IP-based Ethernet networks represent high transmission capacities and can fulfill the mentioned bandwidth requirements in the automotive industry. With these bus systems, HD media quality, low latency, and low jitter data communication are possible [175, 176]. Cost reduction and simplifying complex communication structures are other advantages of Ethernet in the car [176]. The integration of different automotive components on a single shared physical infrastructure facilitates the implementation of the mentioned complex system with more than 100 ECUs [177]. The first automotive Ethernet standard, 100BASE-T1, provides data rates of up to 100 Mbit/s, while the following 1000BASE-T1 standard offers a ten-times higher data rate of 1000 Mbit/s. Even a data rate of 1 Gbit/s cannot satisfy the automotive objectives, and this had led to the formation of IEEE 802.3ch to achieve the realization of data rates up to 10 Gbit/s.

The Ethernet communication over copper lines has EMC issues. The essential large BW may lead to interference, electromagnetic emissions, and deterioration of system immunity. Ethernet over optical fiber, as specified by IEEE 802.3bv, has fewer problems regarding EMC. However, this technology has other drawbacks which have to be overcome. For example, power delivery to the ECUs has to be fulfilled by a separate medium [43]. The transmission directivity and the number of connections affect the bandwidth performance of optical automotive Ethernet [41].

The early EMC investigations of automotive gigabit networks play a crucial role in the safety and reliability of such systems. Because the electromagnetic environment of a car is not predictable, and the gigabit networks are more susceptible to RF noise, the study of worst-case situations is of great importance. The data rate of 10 Gbit/s using pulse amplitude modulation with four levels (PAM-4)[178] requires a bandwidth of around 3 GHz [158]. The physical structures of such microwave networks are sensitive to noise and have more radiation simultaneously. The packaging of ECUs, choice of the associated cables, and the structure of the related interconnections play a vital role in the EMC considerations of automotive Multi-Gig networks. To reduce the possible EMC issues, caused by the channel, the IEEE 802.3ch task force has suggested the use of one pair cables as the transfer medium. The implementation of full-duplex gigabit data rates over one differential pair line is a new challenge for the semiconductor industry. The lack of experience regarding EMC characteristics of automotive gigabit lines complicates the network design procedure.

This chapter presents the results of in-vehicle immunity and emission measurements for the implementation of Multi-Gig networks. In the previous chapter, the suitability of the STP and SPP cables for gigabit networks were examined. Because the laboratory measurements of STP cables have shown good signal integrity characteristics regarding 2.5 Gbit/s, 5 Gbit/s, and 10 Gbit/s data links [179], the RF immunity and emission of these cables were studied in a car using worst-case routing.

This chapter is organized as follows: Section 6.2 explains the two established automotive Ethernet standards (IEEE 802.3bw and IEEE 802.3bp) and the next generation of the Multi-Gig data communication (IEEE 802.3ch) briefly. In Section 6.3, the important topics of Multi-Gig data transmission, i.e., bandwidth requirements, appropriate medium, and the operation modes, are described. Section 6.4 briefly explains the existing automotive EMC standards. Based on the automotive EMC standards, the measurement of the Multi-Gig network channel is performed. The measurement setup of the immunity test and the vehicle emission measurements of the Multi-Gig transmission and the corresponding results are described in Sections 6.6 and 6.7, respectively. Finally, Section 6.8 summarizes and concludes this chapter.

6.2 Automotive Ethernet standards

As described, the high-speed data transmission via Ethernet, as a prerequisite for the implementation of “big data” in the vehicle, requires a large bandwidth in the frequency spectrum. To realize the automotive Ethernet communication with different data rates, the corresponding standards are defined. The established automotive Ethernet standards are a) IEEE 802.3bw (100BASE-T1) and b) IEEE 802.3bp (1000BASE-T1).

IEEE 802.3bw / 100BASE-T1

In this standard, the 100 Mbit/s data communication is specified, which enables the integration of different applications in a compact automotive Ethernet network over a single-pair cable. A full-duplex communication over a UTP cable can be realized. This standard uses PAM-3 signaling at 66.66 MBd, which limits the signal bandwidth to 33.3 MHz [43, 154]. This communication standard is currently established and is used for driver assistance systems, such as camera links.

IEEE 802.3bp / 1000BASE-T1

To increase the data rates up to 1 Gbit/s, the 1000BASE-T1 automotive standard was introduced. This communication technology is based on a point-to-point full-duplex data transmission over a twisted pair line [180]. A Significant improvement, by using 1000BASE-T1 over 1000BASE-T, is the reduction of four transmission channels to a single channel. In this standard, the established PAM-3 modulation method is also used, which provides a better SNR and requires a baud rate of 750 Mbaud.

As explained, the rapid technological progress encounters the OEMs with the need for more BW and higher data rates. Therefore, IEEE 802.3 initiated the next task force for specifying the requirements of data rates of up to 10 Gbit/s.

IEEE 802.3ch Multi-Gig automotive Ethernet PHY

In the next generation of automotive Ethernet standard data rates of 2.5 Gbit/s, 5 Gbit/s and 10 Gbit/s have to be standardized. Data lines with up to four in-line connectors for at least 15 m on one type of automotive cabling (e.g., UTP, STQ, STP, SPP, coax, etc.) could be used [157]. Autonomous driving (artificial intelligence), new 5G communication standards, and V2V or V2I technologies are the goal of OEMs worldwide. These technologies assume a new broadband Multi-Gig network in the car, which supports a high number of sensors and HD-video streaming.

6.3 Important issues of the Multi-gig data transmission

Estimation of the required RF bandwidth, which depends on the PAM-Level, the choice of the appropriate cable, and the type of operation mode, is a decisive criterion that should be considered for high-speed transmission.

Bandwidth and the efficient modulation format

To increase the transmission capacity, a higher BW is needed, which leads to more frequency-dependent losses. Due to the limited bandwidth of electrical components such as cables, the use of multilevel signaling (PAM modulation) reduces the required bandwidth and increases the data rate. On the other hand, higher PAM levels decrease EMC robustness [53].

The Shannon-Hartley theorem, shown in 6.1, limits the maximum amount of information transmitted over the Gaussian channel in terms of signal-to-noise ratio [181].

$$C = BW \cdot \log_2(1 + SNR) \tag{6.1}$$

Where C is the data rate in bits per second, BW is bandwidth in Hz, and SNR is the signal-to-noise ratio. In terms of non-return to zero (NRZ) signaling, the 6.1 could be roughly simplified to 6.2.

$$BW = 0.75 \cdot C \tag{6.2}$$

For the PAM modulation format, the equation between channel capacity and bandwidth is given in (6.3).

$$BW = \frac{0.75}{ld(N)} \cdot C \tag{6.3}$$

Where N is the PAM level and *ld* is the logarithm base 2.

In following, the required BW for 10 Gbit/s data transmission as a function of different PAM levels (N) is calculated (Table 6.1).

Table 6.1: Required BW for 10 Gbit/s data transmission - ©2018 IEEE

N	2	3	4	8	16
BW [GHz]	7.5	4.73	3.75	2.5	1.88

Appropriate medium for future automotive Multi-Gig applications

High-Speed bus systems with data rates of up to 10 Gbit/s are planned as the future standards of automotive communication systems. This kind of data transmission requires secure interfaces and links. Choosing the right cable for Multi-Gig communication depends on several parameters. The weight of wires, cost, and the EMC properties are some critical aspects. In addition, the channel behavior as a function of S-parameter depends on the frequency and data rate, which have to be considered as well.

Camera applications in vehicles have so far used the LVDS principle. This traditional signaling principle is expensive and has severe electromagnetic issues. Therefore, they are no longer a practical installation in a motor vehicle.

The proper Ethernet channels could be the UTP, STQ, STP, SPP, and coaxial cables. UTP cables cannot adequately meet the requirements of Multi-Gig communication. Because of the missing shielding, they generate EMC problems, such as emissions in higher frequency ranges. UTP cables are implemented in the 100BASE-T1 standard. STQ cables seem to be unsuitable for Multi-Gig. The measured performance of STQ, e.g., insertion loss (S_{21}), indicates high signal attenuation for higher frequencies. The drawbacks of coaxial cables are high weight and cost for extensive use in the vehicle. However, due to the good RF performance, they could be used for future high-speed networks. STP and SPP cables appear to be the appropriate alternatives, as these lines have a reasonable high-frequency characteristic (Chapter 5).

The choice of operation mode

There are three kinds of operation modes for data transmission over one channel, i.e., simplex, half-duplex, and full-duplex mode. The typical 10BASE-T link has a simplex operation where the transmission is only in one direction. The physical layers of the mentioned standard can support either half-duplex or full-duplex operation [180].

The 100BASE-TX standard operates in half-duplex (unidirectional) mode. In this standard, at least two wire pairs (4 wires) are required for full-duplex data transmission. In full-duplex mode, the transmitter (Tx) and receiver (Rx) operate simultaneously. In comparison with the other two mentioned modes, the full-duplex operation has the following advantages. Firstly, there is no need for alternating operation of Tx and Rx. Secondly, due to the simultaneous operation, the maximum available data rate can be theoretically achieved (e.g., for 100BASE-T1 the maximum throughput is 200 Mbps). The third advantage is the possibility of simultaneous conversations between different pairs of devices on a single shared IP-based link [180].

The full-duplex operation mode is used in 100BASE-T1 and 1000BASE-T1 standards. In the case of Multi-Gig data transmission, the full-duplex operation mode will be used as the proper mode in the future (Figure 6.1).

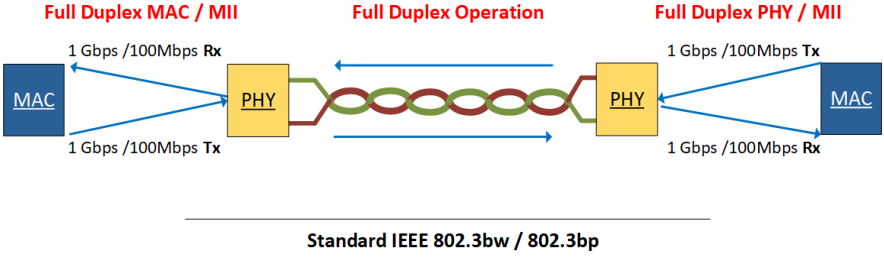

Fig. 6.1: Ethernet data transmission with full-duplex operation mode - ©2018 IEEE

6.4 Definition of EMC issues and corresponding standards

Definition of most important automotive EMC issues

The most critical issues of automotive EMC, which have to be considered by vehicle and component test, are emission, immunity, and ESD test. The emission test can be understood as the measurement of unwanted interferences on the radio receivers of the same vehicle (near-field) or the off-road infrastructures (far-field) due to the electromagnetic emissions of one or more components. The immunity test deals with the investigation of the malfunctioning, or total failure of car components caused by external or internally generated RF fields or pulses. The test of immunity to electrostatic discharges toward different electrical components and units is the subject of ESD tests.

Definition of EMC standards

The future standards regarding Multi-Gig networks should be compatible with the existing standards. Therefore, in this section, a brief overview of the existing automotive EMC standards is given.

1) Automotive emission tests:

CISPR 12: Vehicles, boats and internal combustion engines – Radio disturbance characteristics – Limits and methods of measurement for the protection of off-board receivers. The CISPR 12 standard concerns the vehicle level far field emissions [12, 182].

CISPR 25: Limits and methods of measurement of radio disturbance characteristics for the protection of receivers used on board vehicles. Additionally, the component level measurement is discussed in CISPR 25 [13, 182].

2) Vehicle immunity tests:

ISO 11451: Road vehicles - Vehicle test methods for electrical disturbances from narrowband radiated electromagnetic energy. This standard consists of the following parts [183]:

- Part 1: General principles and terminology
- Part 2: Off-vehicle radiation sources
- Part 3: On-board transmitter simulation
- Part 4: Bulk current injection (BCI)

3) Component immunity tests:

ISO 11452: Road vehicles - Component test methods for electrical disturbances from narrowband radiated electromagnetic energy. This standard consists of the following parts [184]:

- Part 1: General principles and terminology
- Part 2: Absorber-lined shielded enclosure
- Part 3: Transverse electromagnetic mode (TEM) cell
- Part 4: Bulk current injection (BCI)
- Part 5: Stripline
- Part 6: Parallel plate antenna
- Part 7: Direct radio frequency power injection (DPI)
- Part 8: Immunity to magnetic fields
- Part 9: Portable transmitter
- Part 10: Immunity to conducted disturbances in the extended audio frequency range
- Part 11: Reverberation chamber

4) Automotive electrostatic discharge tests:

ISO 10605: Road vehicles - Test methods for electrical disturbances from electrostatic discharge. In this standard, the test methods for the immunity compliance of electronic components are described.

By OEMs defined standards

The original OEMs have defined their specific EMC standards, limits, with higher requirements. Germany's automotive EMC standards are listed as follow:

- **GS 95002**: BMW Group – Electromagnetic Compatibility (EMC) requirements and tests (October 2001)
- **MBN LV 214, MBN 10384, MAN M 3285**: The EMC requirements and test for Daimler AG.
- **TL 81000**: The EMC requirements and test for VW AG, which includes the corresponding limits of emission, immunity and ESD tests.

6.5 In-vehicle immunity measurement setup

This section focuses on the immunity test of Multi-Gig Ethernet cables in the vehicle. The design of gigabit PHYs assumes that the EMC issues of the channel and AFE are known. Based on the knowledge of channel interferences and attenuations,

the forward error correction (FEC) methods could be implemented. Using the FEC method, the receiver can correct the disturbed transmitted signals. As an example, the signal attenuation caused by AFE components (LPF, CMC, CM termination, cables or interconnections) can be considered.

One of the critical EMC measurements for the future Multi-Gig automotive networks is the radio frequency interference (RFI) ingress limit. This measurement deals with the coupled voltage on a transmission channel caused by an external source. Such coupled voltages act as noise signals for the transmitted signal and could lead to malfunctioning of the receiver. Because the automotive Ethernet networks have a bandwidth in the gigahertz range, the susceptibility to the external high-frequency interferences is more significant.

In [185], the RF ingress limit for automotive links based on ISO 11452-2 is presented. This component immunity test setup, which is based on an ALSE measurement, investigates the susceptibility of an STP cable with an H-MTD connector to RF interferences. For frequencies up to 5 GHz, an RF ingress limit line at PHY input of 73 dBµV (4.5 mV_{RMS}) is suggested [185]. The mentioned limit is a maximum of coupled noise voltage that could be added to data. The receiver should be capable of processing the signal with this defined noise level. However, the proposed limit is based on the component measurement and has to be verified by vehicle measurements. The final limits, which should be considered for the design of Multi-Gig PHY, are composed of both component and vehicle test limits.

In this chapter, the in-vehicle immunity tests of the STP cable in a 'worst-case' configuration are presented. The STP cable has a total diameter of 3.8 mm. The twisted-pair cable includes two wires- each with a diameter of 0.5 mm, which are surrounded by polypropylene insulation with a thickness of 0.365 mm. The cable consists of a layered shield. The thickness of the shield is 0.301 mm, and the corresponding inner diameter is 2.47 mm. The coverage of the whole cable is from PVC insulating material.

The measurement setup, Figure 6.2, consists of five STP cables, which are joined with four shielded in-line connectors. The cable section has a total length of 10 m. The implemented route of the cable starts near to the dashboard on the passenger side, Figure 6.2b, and goes along the dash panel to the driver's side and along the chassis. Finally, the cable terminates near the rear window antenna, Figure 6.2c. The described routing is a worst-case choice, as the cable is very close to the online communication unit (OCU) and rear window antenna. Because there has been no predefined routing for the vehicle test of Multi-Gig networks until now, the mentioned routing is chosen.

The far end of the STP cables, on the back-side, is connected with an H-MTD adapter and is 100 ohms terminated. Termination and adapter are shielded using a prefabricated shielded box. On the front side, the near end of the STP cable is con-

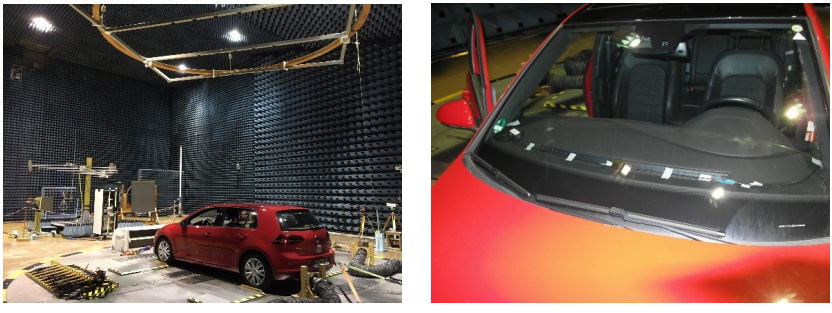

(a) (b)

(c)

Fig. 6.2: (a) Measurement setup in absorber hall (b) starting position of cable route (c) end of the cable route. - ©2019 IEEE

nected to the measuring coaxial cable through the second shielded H-MTD adapter and a balanced to unbalanced transformer (Balun). The Balun is needed as the EMI test receiver has single-ended input, while the STP cable is differential. The bandwidth of the Balun is from 150 kHz to 6 GHz. The common to output port insertion loss of the Balun is ca. -4 dB, -5 dB, and -6 dB at 150 kHz, 3 GHz, and 6 GHz, respectively.

The connection to the EMI receiver is established using three coaxial cables. The first coaxial cable, connected to the near end of the STP cable, has a length of 10 m and is double-shielded. To reduce the common-mode noise, several ferrite cores are placed around the first coaxial cable. The second coaxial cable has a length of 17 m and is embedded under the flooring. The second cable is connected to the third one (4 m), which is connected to the EMI receiver. A separate attenuator (limiter) as protection against high induced voltages is connected between the third cable and the input of the measurement device. The attenuation of the described 31 m coaxial cable and of the Balun is an important parameter, to be considered for the evaluation of the coupled voltage on the STP lines. Figure 6.3 shows the total measured attenuation, which is around 7 dB at 150 kHz and is increased to 30 dB at 6 GHz.

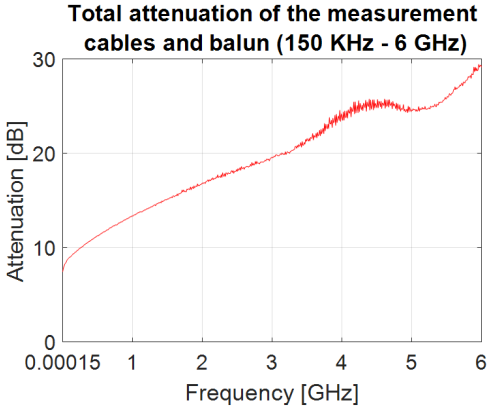

Fig. 6.3: Total attenuation of the measurement cables and Balun - ©2019 IEEE

The absorber hall is equipped with different antennas for different frequency ranges, Figure 6.2a. Using these antennas, vehicle immunity tests are performed. The used antennas and the corresponding frequency ranges are noted in Table 6.2. According to the ISO 11451-2 / TL81000, the distance between the antenna and the chassis varies with different frequency ranges. To study all possible coupling situations, the vertical and horizontal polarization has to be considered. Therefore, the orientation of antennas has to be changed correspondingly for each frequency range.

Table 6.2: Investigated frequency ranges and the related antennas, radiated field strength, and the modulation type - ©2019 IEEE

Freq. range	**Antenna type**	**Radiation direction**	**field strength [V/m]**	**Modulation**
1 MHz - 30 MHz	stripline	unidirectional	70	AM
30 MHz -220 MHz	log-periodic	H* / V*	70 & 100	AM
220 MHz - 400MHz	horn	H* / V*	70	AM
400 MHz -1 GHz	horn	H* / V*	70 & 100	AM
1 GHz - 3 GHz	horn	H* / V*	70 & 100	CW
3 GHz – 4 GHz	horn	H* / V*	50	PA
4 GHz – 6 GHz	horn	H* / V*	30	CW

H* : Horizontal direction / V* : Vertical direction

According to TL81000, the field strength for the immunity test is illustrated in Figure 6.4. However, to protect the measurement devices, the maximum power is not radiated in all frequency ranges. As an example, in the frequency range from 100 kHz to 30 MHz, instead of 140 V/m half of the field strength is chosen.

As the car can be rotated by 360 degrees, radiation is possible from all sides, i.e., the front, back, driver, and passenger side of the vehicle. Due to the metal car body,

radiations from the driver's and passenger's side could be reflected more severely than the other two sides. However, radiations from the front and back-side could be coupled to the STP lines through the front and rear windows. In the following, both front and back-side radiations are investigated.

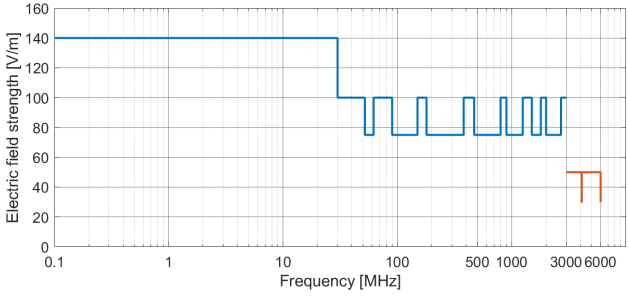

Fig. 6.4: Radiation strength for different frequency ranges for the immunity test according to TL81000 - ©2019 IEEE

6.6 In-vehicle immunity measurement results

In this section, the measurement results of the immunity test of predescribed STP cables with four shielded in-line connectors are presented. The attenuation of the measurement cables, shown in terms of dB in Figure 6.3, is subtracted from the measurement results (expressed in dBµV) of this section in post-processing. This is why in all the following diagrams, the minimum value of the induced RMS voltage is not zero, and a white region under the measurement lines is present.

This first studied frequency range is from 100 kHz to 30 MHz. Using a stripline antenna, a unidirectional field is generated. The antenna is positioned above the car, Figure 6.2a. The corresponding measurement results are shown in Figure 6.5. The coupled voltage to the STP cable is more than 80 dBµV and less than 103 dBµV.

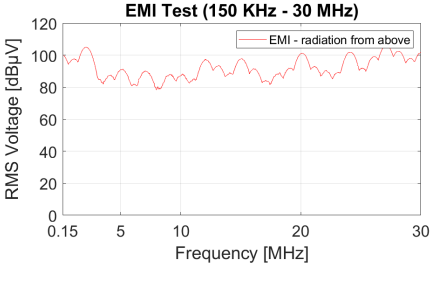

Fig. 6.5: EMI test of STP cable in frequency range of 150 KHz - 30 MHz - ©2019 IEEE

The second investigated frequency range is 30 MHz – 220 MHz. A log-periodic antenna is used for this frequency range in a vertical and horizontal polarization (Figure 6.2a). The generated field strength pattern is presented in Figure 6.4, which varies between 70 V/m and 100 V/m. Figures 6.6a and 6.6b show the measurement results of the coupled voltage in both horizontal and vertical polarization and reveal a voltage limit of less than 80 dBµV for the radiation from the front and back-side. The comparison of Figure 6.5 and Figure 6.6 shows that the coupled voltage in frequencies up to 30 MHz is larger than the frequency range of 30 MHz – 220 MHz.

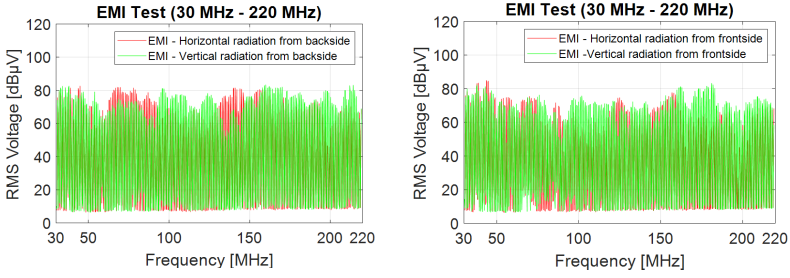

(a) (b)

Fig. 6.6: EMI test of STP cable in the frequency range of 30 MHz – 220 MHz (a) horizontal and vertical radiation from the backside of the vehicle (b) horizontal and vertical radiation from the front side of the vehicle - ©2019 IEEE

Using a horn antenna, the EMI test of the next frequency range, i.e., 220 MHz to 400 MHz, is performed. Figure 6.7a and 6.7b illustrate the results of these measurements of the radiation from the back-side and front-side correspondingly. The coupled voltage is less than 75 dBµV for the radiation from the back-side and front-side. The comparison of the measurement results of Figure 6.6 and Figure 6.7 shows that the overall coupled voltage in frequency 220 MHz – 400 MHz is less than the frequency range of 30 MHz – 220 MHz.

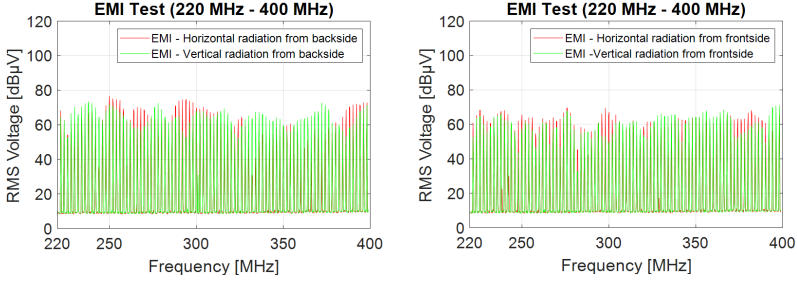

(a) (b)

Fig. 6.7: EMI test of STP cable in the frequency range of 220 MHz – 400 MHz (a) horizontal and vertical radiation from the backside of the vehicle (b) horizontal and vertical radiation from the front side of the vehicle - ©2019 IEEE

Figure 6.8 and 6.9 present the measurement results of 400 MHz – 1000 MHz and 1 GHz – 3 GHz, respectively. A coupled voltage above 80 dBµV from the back-side radiation with a vertical field direction is observed between 400 MHz – 1000 MHz. Toward 3 GHz, the coupled voltage becomes smaller.

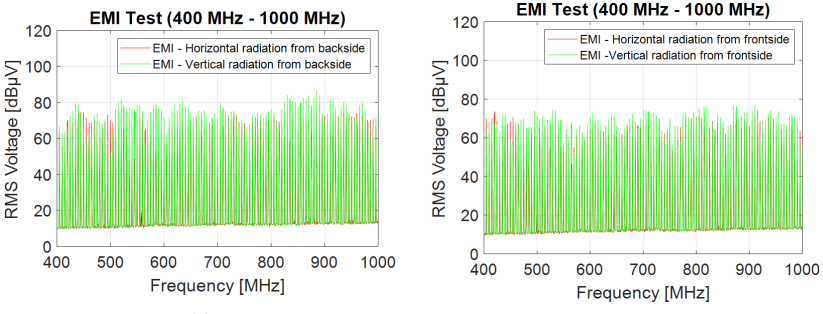

(a) (b)

Fig. 6.8: EMI test of STP cable in the frequency range of 400 MHz – 1000 MHz (a) horizontal and vertical radiation from the backside of the vehicle (b) horizontal and vertical radiation from the front side of the vehicle - ©2019 IEEE

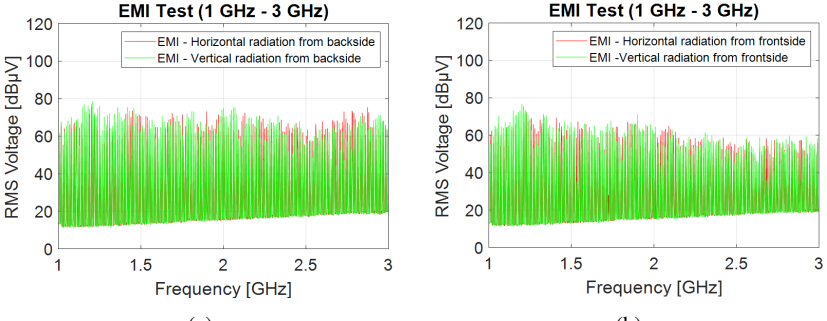

(a) (b)

Fig. 6.9: EMI test of STP cable in the frequency range of 1 GHz – 3 GHz (a) horizontal and vertical radiation from the backside of the vehicle (b) horizontal and vertical radiation from the front side of the vehicle - ©2019 IEEE

The results of the EMI tests for the frequencies between 3 GHz – 4 GHz and 4 GHz – 6 GHz, Figure 6.10 and 6.11, show that the coupled voltage is less than 70 dBµV and decreases toward higher frequencies. However, as shown in Figure 6.4, the generated field strength in these ranges is also smaller when compared to the previous measurements.

The presented measurements do not show any vital difference between the front side and back-side radiation. The main significant difference is just observed from the above-placed stripline antenna.

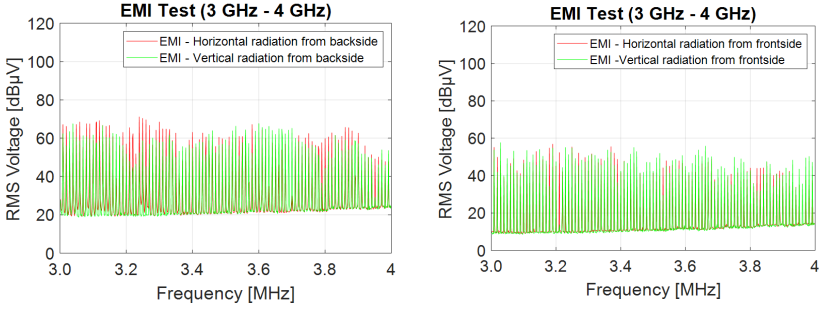

(a) (b)

Fig. 6.10: EMI test of STP cable in the frequency range of 3 GHz – 4 GHz (a) horizontal and vertical radiation from the backside of the vehicle (b) horizontal and vertical radiation from the front side of the vehicle - ©2019 IEEE

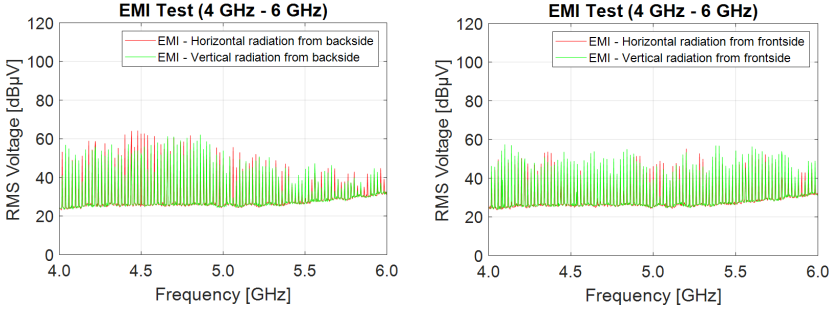

(a) (b)

Fig. 6.11: EMI test of STP cable in the frequency range of 4 GHz – 6 GHz (a) horizontal and vertical radiation from the backside of the vehicle (b) horizontal and vertical radiation from the front side of the vehicle - ©2019 IEEE

As described in the previous section, the discussed measurements determine a limit for the maximum possible noise voltage that can be coupled to the Ethernet Multi-Gig channel. In [185] the suggested limit of 73 dBµV cannot be approved by vehicle measurements. For the low frequencies of up to 30 MHz, a limit line with a voltage of 103 dBµV is suggested, and for the higher frequencies of up to 6 GHz, the limit line of 90 dBµV is suggested.

6.7 In-vehicle emission measurement results

Multi-Gig Ethernet transceiver

The IEEE 802.3 standardized IP based Ethernet technology and defined the requirements of the physical layer and the MAC of the data link layer. The digital data flowing from MAC is prepared in PHY for the transmission [186]. The PHY in a full-duplex mode includes the digital-analog converter (DAC) and the analog-digital converter (ADC). The data modulation (e.g., PAM) is implemented in PHY. With forward error correction in PHY, an extra redundancy is added to the original data. In case of bit errors caused by the channel, the receiver can correct the data without the need for the data being resent. For this reason, the channel EMC investigation plays a key role in the design of the PHY.

The chip industry has already presented 100BASE-T1 PHYs for automotive Ethernet [154, 187]. These transceivers are intended for applications like backbone networks, driver assistance systems, entertainment, and IP camera links. The prototypes of Ethernet transceiver PHY for the 1000BASE-T1 standard have already been produced [67]. Using 1 Gbit/s automotive Ethernet will pave the way for the implementation of high-tech driver assistance systems, HD-video streaming, and advanced sensor systems, etc. One of the primary tasks for the development of these chips is to investigate the EMC issues in advance.

In literature, different articles report the use of Ethernet IP core using field programmable gate array (FPGA) in aerospace and defense communication systems. A novel idea of this section is the use of FPGA as a temporary alternative to a Multi-Gig automotive PHY for data communication over one twisted pair. By using this method, early investigation and characterization of possible EMC issues in the vehicle can be enabled. Using two Xilinx Kintex-7 FPGA boards (Figure 6.12), the gigabit data communication is investigated at component and vehicle-level. The component-level measurements deal with the signal integrity of the STP cable on the lab bench, as discussed in the previous chapter. The vehicle-level measurements are presented in this section. In this context, the STP cable is routed in the car, and the corresponding emissions using different gigabit data rates are measured.

To realize the data communication between two FPGA boards and to transmit the desired data rate, the first board was configured as Tx and the second one as Rx. The pattern generator of the GTX transceiver enables the generation of a PRBS 127-bit data sequence. The differential signaling is realized over GTX SMA I/O connectors. The peak-to-peak voltage level is equal to 1 V. Data rates of 2.5 Gbit/s and 5 Gbit/s are generated. A Rosenberger H-MTD adapter (Figure 6.12b) realizes the interface between SMA connectors of the FPGA boards and the medium (STP cable). Note that the FPGAs use PAM-2 signaling. The corresponding emissions of the STP cable are measured with different antennas up to 6 GHz.

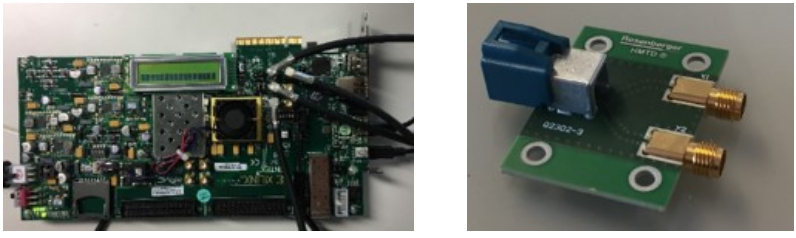

(a) (b)

Fig. 6.12: (a) Kintex-7 FPGA Board (b) The SMA-TP Adapter - ©2018 IEEE

The discrete spectrum of the PRBS data sequence

The investigation of the discrete spectrum of the corresponding PRBS data sequences is necessary to analyze the measurement results of this section. To this regard, the power spectrum of PRBS data sequences - with the data rate of 2.5 Gbit/s and 5 Gbit/s - are examined in MATLAB.

Figure 6.13a shows a PRBS data sequence, including 2^7-1 bits, with a data rate of 2.5 Gbit/s. Each bit has a period (T_0) of 0.4 ns. The assumption for the simulations is that the sampling frequency is eight times the signal frequency. Hence, each bit is presented with eight samples in the time domain. The discrete Fourier transform of the signal illustrates the frequency-dependent power distribution (Figure 6.13b). For reasons of simplicity, the DC part of the spectrum is removed. The nulls of the spectrum occur at the signal frequency, i.e., 2.5 GHz, and its integer multiples. The distance between the spectral lines (around 20 MHz) can be calculated by dividing of the signal frequency by the number of bits. The inverse of the pattern length, i.e., 2^7-1 bits multiplied by T_0, can also be used for the calculation of the spacing between the spectral lines [188]. These spectral lines of the data sequence are also present in the measurements of this section.

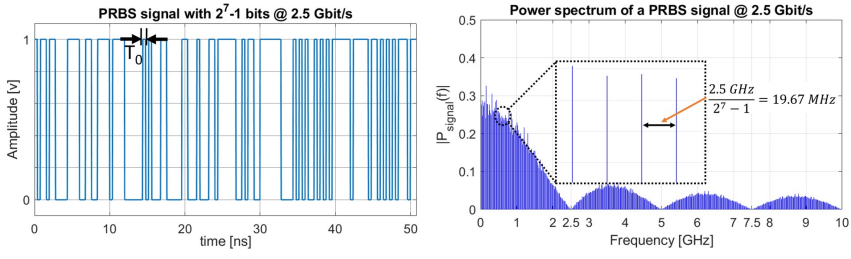

(a) (b)

Fig. 6.13: (a) a PRBS signal with 2^7-1 bits with a data rate of 2.5 Gbit/s and (b) the corresponding power spectrum

The PRBS signal, with a data rate of 5 Gbit/s, is illustrated in Figure 6.14a. The signal frequency of this signal is 5 GHz, and the bit period T_0 is 0.2 ns. Again, the number of used bits is 2^7-1. The frequency spectrum of the 5 Gbit/s bitstream is shown in Figure 6.14b. The DC part of the spectrum is also removed in this diagram. The nulls of the spectrum are at 5 GHz and its integer multiples. The distance between the spectral lines is 39.37 MHz.

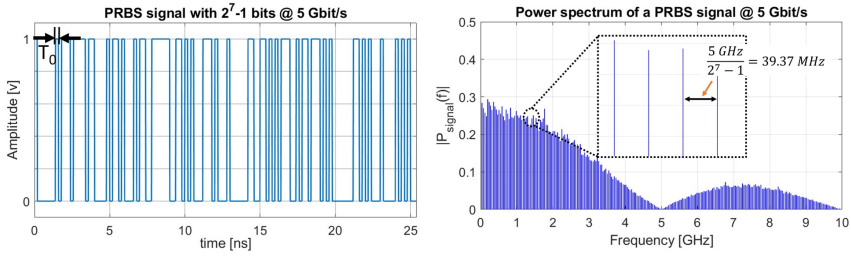

(a) (b)

Fig. 6.14: (a) a PRBS signal with 2^7-1 bits with a data rate of 5 Gbit/s and (b) the corresponding power spectrum

Emission measurement results

As previously mentioned , the use of high-speed bus systems with higher data rates require higher bandwidth. This increases the risk of interference between different frequency bands. To clarify this issue, the emission test is carried out on the vehicle (VW Golf) in the absorber hall. For the measurement, the engine and the ignition were off. Thus, only the spurious radiation of high-speed data transmission is examined and evaluated. For this measurement, one FPGA board is used as Tx and the other one as Rx. The transmitting data rates are 2.5 Gbit/s and 5 Gbit/s. To reduce the parasitic radiation from FPGA boards, they were mounted in a closed metal box. The STP cable, with the length of 6 m, was placed close to the rear window antenna. This is one of the worst cases for the emissions test due to the very short distance to the antenna. Measurements with in-line connectors were also necessary. The real routing of the Ethernet bus system in the car has a more considerable distance to the antenna. The measurement was repeated for different frequency bands. The measured frequency ranges and the associated antennas are listed in Table 6.3.

Table 6.3: Examined frequency ranges and the related antennas - ©2018 IEEE

Designation	Frequency range [MHz]	Antenna
FM1-FM2	76 – 108	Rear window Antenna
DAB	174 – 230	Monopol Antenna
TV IV - V	470 – 806	Monopol Antenna
Wi-Fi	2400 - 2500	Omnidirectional Antenna
DSRC	5900 - 6000	Omnidirectional Antenna

The antenna of the measured car could cover the radio frequency ranges FM1 and FM2. For the other frequency bands, the monopole or omnidirectional antenna was used (Figure 6.15).

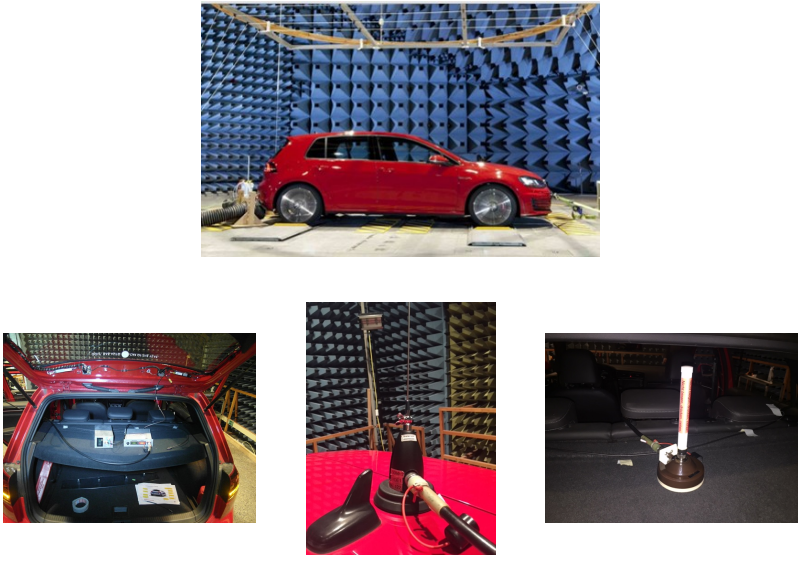

Fig. 6.15: Emission test of STP cable with different antennas - ©2018 IEEE

The first tested frequency range is FM1 and FM2 (76 - 108 MHZ). For this frequency band, the rear window antenna with high sensitivity was used. The measurement results are shown in Figure 6.16. For the 2.5 Gbit/s data link, two spectral lines at 78 MHz and 98 MHz were simulated in MATLAB. The mentioned spectral lines have a distance of around 20 MHz and are also captured in measurements. The measured emission at the mentioned frequencies is larger than the 7 dBµV Quasi-peak limit. The used STP cable can not fully satisfy the expectations in the VHF band. The spectral peak of 5 Gbit/s at 78 MHz generates an emission of around 7 dBµV.

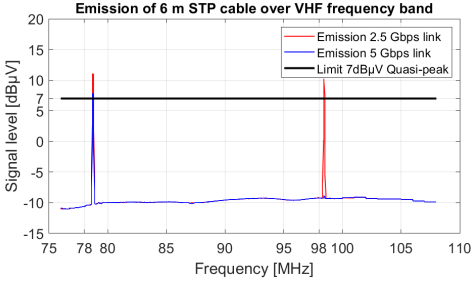

Fig. 6.16: Emission of 6 m STP cable over FM1-FM2 frequency band - ©2018 IEEE

The second measured frequency range is DAB (TV III / 174 - 240 MHz), where a 200 MHz monopole antenna is used. The results are illustrated in Figure 6.17. For the 2.5 Gbit/s data link, the MATLAB simulations show spectral lines at 177 MHz, 197 MHz, 217 MHz, and 237 MHz that are also measured at the same frequencies. The spectral lines of 5 Gbit/s data communication are placed in a distance of 40 MHz. The measurements show the spectral lines at 197 MHz and 237 MHz. The measured radiation curve is slightly over the 10 dBµV limit. Note again, the measurements are done in a worst-case situation. Further measurements are needed to define the minimum allowed distances.

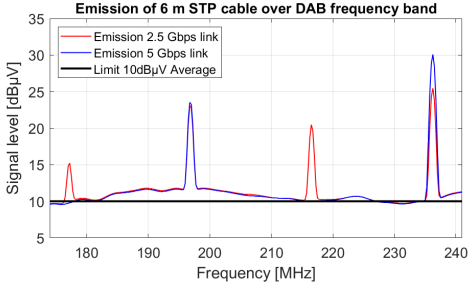

Fig. 6.17: Emission of 6 m STP cable over DAB frequency band - ©2018 IEEE

The measurement results of 2.5 Gbit/s and 5 Gbit/s links over the next frequency band, i.e., TV IV-V, are shown in Figure 6.18. From 470 MHz to 806 MHz, seventeen spectral lines with a distance of 20 MHz are measured for 2.5 Gbit/s data link. In the same frequency span and for the 5 Gbit/s data rate, nine spectral peaks are expected, which are verified in the measurements. The measurements of the TV IV-V frequency range do not comply with the 10 dBµV limit line.

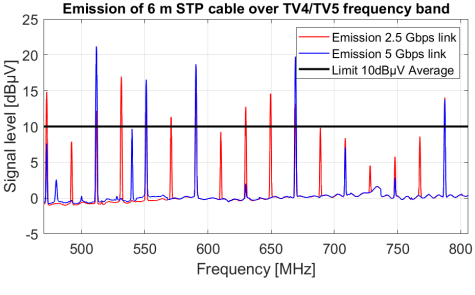

Fig. 6.18: Emission of 6 m STP cable over TV IV-TV V frequency band - ©2018 IEEE

The final diagrams (Figure 6.19 and 6.20) show the test results in the range of Wi-Fi and DSRS. In Figure 6.19, the injected radiation from the Multi-Gig data transmission in the entire examined frequency band is continuously below the defined 10 dBµV average limit. The measurement results show a good agreement with the simulations. As illustrated in Figure 6.13b, the first null of the 2.5 Gbit/s spec-

trum is at 2.5 GHz. Around this frequency, the spectral lines have a small amplitude. Therefore, no spectral peaks are recorded in the measurements for the Wi-Fi range. According to the simulation results of Figure 6.13b, the spectral lines of 2.5 Gbit/s should also have a small amount of power in the DSRC range, which is also not detected by the corresponding antenna. However, in the DSRC band, the radiation is slightly over the average limit (Figure 6.20).

Because the first spectral null of the 5 Gbit/s data link is at 5 GHz, the associated spectral lines in the Wi-Fi range have more significant power than the spectral lines of 2.5 GBit/s data link. According to the simulations, three spectral lines at a distance of 40 MHz are expected between 2400 MHz and 2500 MHz for the 5 Gbit/s data rate. In Figure 6.19, two spectral lines for the latter mentioned data rate are recorded. In the DSRC range, the spectral lines of 5 Gbit/s have low power and are not measured with the antenna (Figure 6.20).

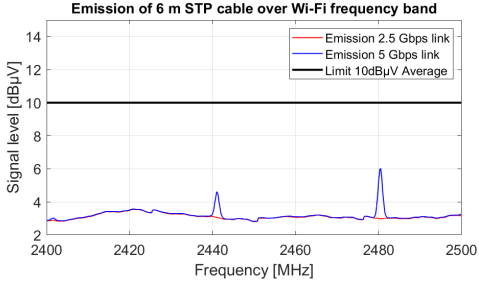

Fig. 6.19: Emission of 6 m STP cable over Wi-Fi frequency band - ©2018 IEEE

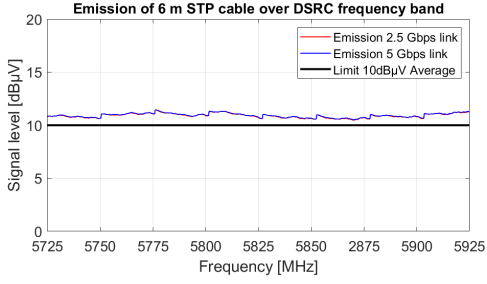

Fig. 6.20: Emission of 6 m STP cable over DSRC frequency band - ©2018 IEEE

The presented measurements in this section show the emission of a 6 m STP cable with different data rates and over various frequency ranges. To reach a definitive conclusion about the STP cables, further measurements are required. A real in-car routing of the cable with different in-line connectors has to be implemented. However, the first worst-case measurements of this chapter show the possible suitability of STP cable for Multi-Gig communication.

6.8 Conclusion

The high-speed data transmission via Ethernet as a prerequisite for the implementation of "big data" in the vehicle requires a large bandwidth in the frequency spectrum. As the safety and reliability of the modern technologies are of primary importance for the OEMs, the EMC investigations of these networks play a significant role in the design stages.

At the beginning of this chapter, the established automotive Ethernet standards (100BASE-T1 and 1000BASE-T1), as well as the next generation of Multi-Gig automotive Ethernet (NBASE-T1), were briefly discussed. The three critical aspects of Multi-Gig communication; namely bandwidth, medium, and mode of operation, have been described. The definitions of different automotive EMC standards for emission, immunity, and ESD tests were briefly described .

In the further course of the chapter, the immunity test of STP, as a solution for the automotive Multi-Gig Ethernet network channel, was performed. In the first step, the details of the measurement setups were presented and discussed. All in all a total of seven different frequency ranges - from 150 kHz to 6 GHz - were measured using different antennas. The vehicle emission was performed at the front and back-side of the car. The coupled voltage to the STP cable was discussed using measurement results. These measurements can help the semiconductor industry for the fabrication of the corresponding PHYs. The measurements of this work show the maximum possible coupled noise voltage, which can lead to signal distortion and malfunctioning. For the low frequencies of up to 30 MHz, a line line with a voltage of 103 dBµV. For the higher frequencies up to 6 GHz, the limit of 90 dBµV was suggested.

Further, by using FPGAs instead of Multi-Gig PHYs, the emission measurements in the vehicle were performed. The use of FPGAs for EMC characterization of the automotive Multi-Gig Ethernet communication was one of the novelties of this chapter. Different data rates (2.5 Gbit/s and 5 Gbit/s) were transmitted over an STP line with a length of 6 m, and the corresponding emissions were recorded over different frequency bands with the related antennas. It was shown that the corresponding measured spectral lines do not comply with the limit lines of the TL 81000 standard. However, the performed measurements are a worst-case study. Further measurements with in-line connectors and with other routings are still necessary.

Chapter 7
Investigation of Possible EMC Interferences between automotive Multi-Gig Communication link and in-vehicle Applications Using 3D Field Simulation

The STP cable as the possible suitable channel for the Multi-Gig automotive Ethernet link was investigated in the previous chapter. The in-vehicle immunity and emission measurements considering a worst-case routing were also studied.

The increase of computational data processing in recent years has enabled the 3D electromagnetic field calculation for the complex structures. The calculation and simulation of the radiated emission, and the coupled electrical field of the STP cables to other in-vehicle receivers, are introduced in this chapter. The use of the provided simulation method enables the OEMs to consider the RF emission of the gigabit data links in the car.

This chapter describes the mentioned 3D field simulation results in the FM (76 - 108 MHz), DAB (174 - 230 MHz), TV IV – V (470 – 806 MHz), GPS (1580 – 1650 MHz), WLAN (2400 – 2500 MHz), and DSRC (5900 – 6000 MHz) frequency bands.

The contents of this chapter are published in the following two articles:

1. IEEE International Symposium on Electromagnetic Compatibility and Asia-Pacific International Symposium on Electromagnetic Compatibility (2019), Sapporo under the following title:

   S. Mortazavi, D. Schleicher, D. Eremyan, A. Gheonjian, I. Badzagua, I. Danelyan, R. Jobava, A. Sinai, F. Gerfers, "Investigation of Possible EM Interference of Auto-motive Multi-Gig Communication Link in the FM and DAB Ranges Using 3D Field Simulation," 2019 Joint International Symposium on Electromagnetic Compatibility and Asia-Pacific International Symposium on Electromagnetic Compatibility, Sapporo (EMC Sapporo & APEMC 2019).

2. IEEE International Symposium on Electromagnetic Compatibility, EMC EUROPE Barcelona (2019) under the following title:

   S. Mortazavi, D. Schleicher, D. Eremyan, A. Gheonjian, R. Jobava, A. Sinai, F. Gerfers, "Investigation of Possible EMC Interferences between Multi-Gig Communication link and RF Applications in Vehicle," International Symposium on Electromagnetic Compatibility (EMC EUROPE), Barcelona, (2019).

Contribution

The first author (Sanaz Mortazavi) provided the basic idea of the publications. Detlef Schleicher and Sanaz Mortazavi performed the required measurements for modeling of the simulation components. The authors from EMCoS company generated and assembled simulation models, performed simulations and analysis of results (Ilona Danelyan: Modeling of antennas; lskander Badzagua: Modeling of signals; Diana Eremyan: Modeling of the complete system). Diana Eremyan and Sanaz Mortazavi wrote the publications in cooperation. The other authors, Ali Sinai, Friedel Gerfers, Anna Gheonjian, and Roman Jobava, gave constructional advice and reviewed the publications.

7.1 Introduction

Toward digitalization and together with the other industry branches, the automotive industry is switching to digital cars. Most of the mechanical components of the vehicles are being replaced by electronic ones. The future digital car will contain an ultra-high-speed network for in-car communication as well as for communicating with the outside world.

The driving automation system for on-road vehicles consists of six levels [189]. The realization of the last two levels of autonomous driving, i.e., high and fully automated, requires a highly connected car that can communicate with its surrounding world and internal components in real-time. On the other hand, communicating with other cars (car-2-car) and infrastructure (car-2-x) uses WLAN technology with an operating frequency of 5 GHz [190]. Applying these microwave frequencies in an "unknown" environment, regarding EMC characteristics, and transferring the high-speed data to the central processing unit of the car, is a challenge of the automotive industry.

Advanced driver-assistance systems should improve the driving safety [191]. ADAS uses different high definition cameras, radars, lidars, and map databases [191], which enable the smart car to analyze the situation and take the corresponding actions. They are used for pedestrian and vehicle detection, ground plane recognition, tracking barriers, traffic signs, and lights [192]. The multi-mode radar, multi-purpose high-resolution cameras, short-range radar with 24 GHz operation frequency, long-range radars operating at 77 GHz, ultrasonic sensors, etc. enable object detection, distance and velocity measurements [193]. Using lidar sensors for measurement ranges between 1 and 10 m enables the vehicle to gain further environmental information utilizing laser light [193]. The gathered information, together with interior and exterior states and conditions, should be directly involved in decision-making algorithms.

The objectives mentioned above require a high-speed, reliable, and safe in-vehicle network (IVN), which is capable of transferring gigabits of data in one second (Multi-Gig). The communication of the mentioned technologies with the central processing unit of the car should be realized through a stable, high-speed, and modular network. The fusion of various sensor information assumes a reliable network with low redundancy and error rate. The past investigations of the automotive industry, together with semiconductor manufacturers, led to the choice of the Ethernet-technology for Multi-Gig communication as a favorable cost-performance system [194]. IP-based Ethernet technology should pave the way for the future of a fully automated vehicle. According to the IEEE 802.3ch working group, data rates of 2.5 Gbps, 5 Gbps, and 10 Gbps are the next generations of automotive Ethernet standards [71].

Two critical factors make these systems susceptible to environmental noise. The first one is the increasing signal frequency, which is in the microwave range. The cost and weight reduction is the second factor that leads to the use of components, which are more sensitive regarding EMC issues. The EMC issue of the Multi-Gig Ethernet networks in different frequency ranges is an essential factor, which ensures the safety and reliability of the future fully automated cars. The main automotive application frequency bands are FM (76 – 108 MHz), DAB (174 – 230 MHz), TV IV – V (470 – 806 MHz), GPS (1580 – 1650 MHz), WLAN (2400 – 2500 MHz), and DSRC (5900 – 6000 MHz).

The Multi-Gig Ethernet networks should be examined using simulations in a primary stage and be verified by measurements. In this chapter, the emission of the Ethernet channel for frequency ranges between 76 MHz and 6 GHz are simulated and discussed. The use of 3D-field simulation of Multi-Gig automotive cabling, i.e., shielded twisted pair (STP), and the corresponding EM interference based on a real car model and a worst-case routing are presented. To the authors' knowledge, this is one of the first works to deal with the simulation of automotive Multi-Gig EMC issues. The results of this work can help the industry to study the continuing challenges of the physical layer in the first stages of the design.

Figure 7.1 illustrates a general procedural overview, which is used for the simulation of the coupled voltage of the STP cable to the vehicle antennas. To calculate the coupled disturbance voltage, the transfer function between the STP cable and antennas should be defined. The transfer function is calculated using the CM current, which flows in the STP cable. To calculate the CM current, the transfer impedance of the cable is needed. Knowing the transfer impedance of the cable, the CM current of a sine-wave sweep in the STP cable can be calculated. Then, transfer function between STP cable and antenna is determined. The further course of this chapter discusses the convolution of the PAM-N signal with the transfer function (in the frequency domain) that enables the calculation of the coupled voltage at the port of the antenna. A detailed discussion regarding the mentioned procedure is provided in the following sections of this chapter.

This chapter is organized as follows: Section 7.2 concerns the suitability of the pulse amplitude modulation with N-levels (PAM-N) as the proper modulation format for the Multi-Gig Ethernet standard. Furthermore, the generation of the PAM-N signal for 5 Gbit/s data rates is simulated. The results of the discrete spectrum of PAM-N signals are also presented. The modeling of STP cable as a proper medium for Multi-Gig networks and the corresponding in-vehicle routing is described in Section 7.3. Additionally, the generated CM current of STP cable is discussed in this section. The model of different in-car antennas and the corresponding reflection coefficients are discussed in Section 7.4. The emission of the STP cable and the coupled voltages on the different antennas are discussed in Section 7.5. Finally, Section 7.6 summarizes and concludes this chapter.

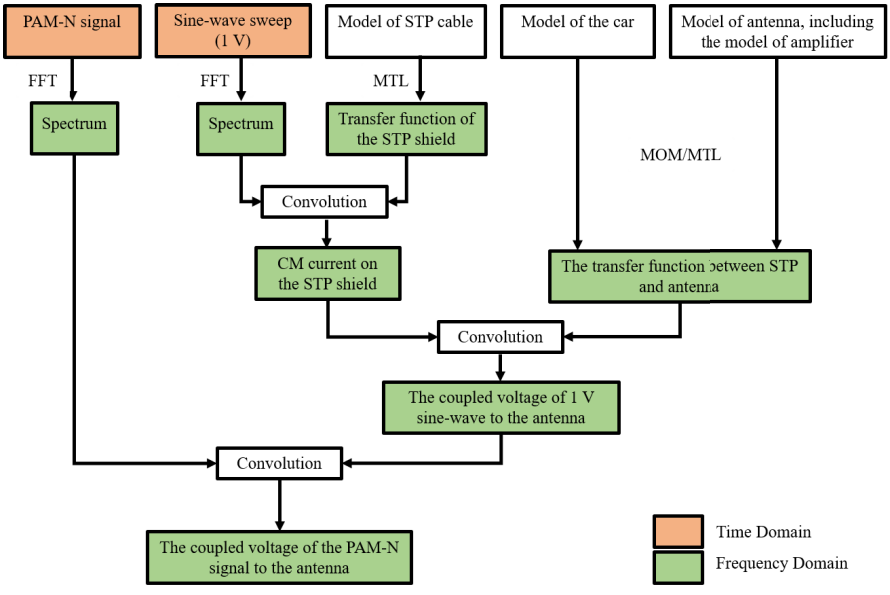

Fig. 7.1: General overview of the used procedure for the simulation of the coupled voltage of the STP cable to the antennas.

7.2 PAM-N signaling for Multi-Gig automotive networks

In this section, the generation of the PAM-N signal is described. Furthermore, the discrete spectrums of the PAM-N signals with different data rates are discussed.

The generation of PAM-N signals for different data rates

As previously mentioned, the implementation of Multi-Gig communication requires considerable bandwidth (BW) in the gigahertz range. In order to limit the BW, the use of differential PAM-N is suggested in the IEEE 802.3 Multi-Gig automotive Ethernet PHY task force [194, 195]. The first step toward the simulation of the Multi-Gig networks is the generation of PAM-N signals. Although the PAM-4 signaling is the preferred modulation, other formats, like PAM-2, PAM-3, and PAM-5 are simulated as well. For the simulations, 31-bit PRBS signals [196] are generated with data rates corresponding to 1 Gbit/s, 2.5 Gbit/s, 5 Gbit/s, and 10 Gbit/s. Because of the forward error correction, an overhead of around 10% has to be added to the data rate. The symbol duration (T_s) of PAM-N signals is calculated using 7.1. T_s is the time interval during which the value of the corresponding symbol remains constant.

$$T_s = \frac{1}{BR} \tag{7.1}$$

Where BR is the baud rate of PAM signal with N modulation levels and is defined in 7.2. The rise and fall times of generated time signals are considered as t = 0.35/BR.

$$BR = \frac{DataRate}{log_2 N} \tag{7.2}$$

Using the above equations, the main parameters for time signals are estimated. One period of the generated signal with 5 Gbit/s data rate for each PAM level is presented separately in Figure 7.2. The same PAM-N signals are generated for other data rates. The peak-to-peak voltage level is equal to 1 V.

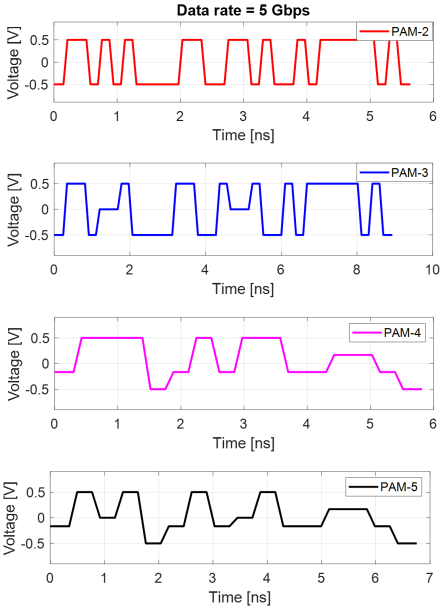

Fig. 7.2: PAM-N signals with 5 Gbit/s data rate - ©2019 IEEE

Discrete spectrums of the PAM-N signal with the different data rates

Using PAM-N signaling has the advantage of reducing the baud rate, which consequently reduces the required bandwidth. Furthermore, the channel insertion loss will be decreased [197]. As the number of bit per symbols increases in PAM-N signaling, the eye diagram of the signal gets smaller, and therefore a higher SNR is required. Thus, better noise protection, e.g., using shielded cables, should be provided [197].

In the previous chapter, the discrete spectrum of the PAM-2 signal for data rates of 2.5 Gbit/s and 5 Gbit/s was discussed. In this chapter, the discrete spectrums of the periodic PAM-N signals, depending on the data rate, are examined. The calculation of the corresponding spectrums of PAM-N signals for different data rates is based on the discrete Fourier transform. The sequences of 31-bit PRBS signals for data rates

of 1 Gbps, 2.5 Gbps, 5 Gbps, and 10 Gbps are generated. The calculated spectra in the FM (76 - 108 MHz) and DAB (174 - 230 MHz) frequency ranges are studied and illustrated in Figure 7.3.

For the frequency range of 470 MHz to 6000 MHz, only the discrete spectra of the PAM-4 signals with different gigabit data rates are calculated and visualized in Figure 7.4. For reasons of simplicity, the spectrum of other PAM-N levels, i.e., N equal to 2, 3, 5, and 8, are not shown. The investigations of the PAM-4 signaling are of primary importance because this modulation type seems to be the choice of the IEEE 802.3ch task force group. The illustrated peaks of the PAM-4 signals have a significant impact on the radiation of the STP cable, as explained in the previous section. The resulting spectra are used for the normalization of the coupled voltages in Section 7.5.

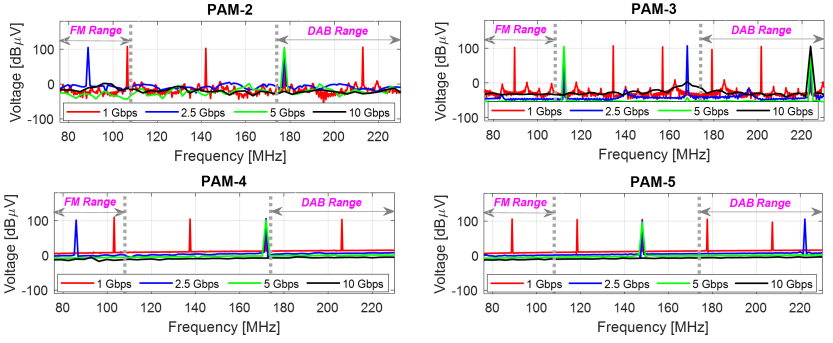

Fig. 7.3: Spectrums of the PAM-N signals in FM and DAB ranges - ©2019 IEEE

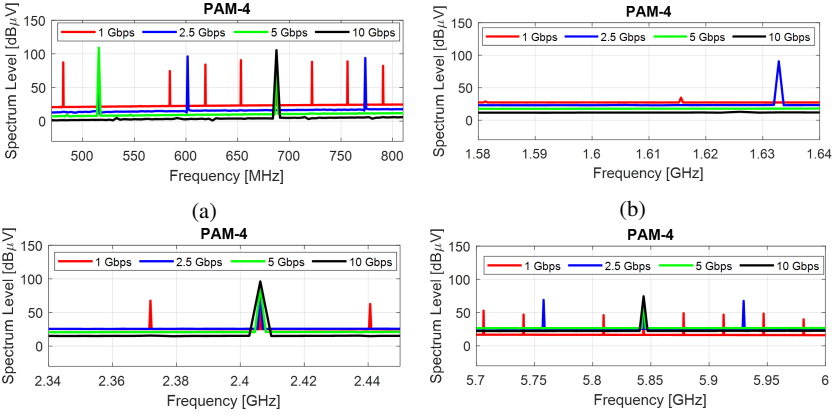

Fig. 7.4: Discrete spectrum of PAM-4 signaling in frequency range of (a) TV band (b) GPS (c) WLAN (d) DSRC - ©2019 IEEE

7.3 Transmission medium and its radiation

STP cable as the medium and its routing

The Multi-Gig Ethernet bus system in the vehicle is realized with the model of the high-speed STP cable. Realistic routing of the cable with a length of 5.75 m in the car body is selected to simulate the worst-case situation and to study the corresponding EMC issues.

The model of the STP cable is performed using hybrid method of moments (MoM) and multi-conductor transmission lines (MTL) theory approach [198, 199]. Cables are modeled with MTL (considering transfer impedance of multi-shields), and interaction with the 3D environment is simulated using MoM. For reasons of the clarification, the mentioned STP cable is briefly presented in this section .

The cross-view of the STP cable is illustrated in Figure 7.5a. Inner conductors of the twisted pair cable are considered as copper wires with a diameter equal to 0.5 mm and polypropylene (PP) insulation with 0.365 mm thickness. The inner layer is represented as Alu-PET foil with metallization thickness 1 µm, and the outer layer is a braided shield with 16 carriers, 6 copper filaments with a diameter of 0.15 mm per carrier. The inner diameter of the shield is 2.47 mm, and the total thickness is 0.301 mm. The cable has outer coverage made of PVC insulating material with an overall diameter of 3.8 mm. The twisting pitch for the considered STP cable is equal to 25 mm. Transfer impedance of the braided shield (Figure 7.5b) is calculated with the analytical Kley model [200, 201].

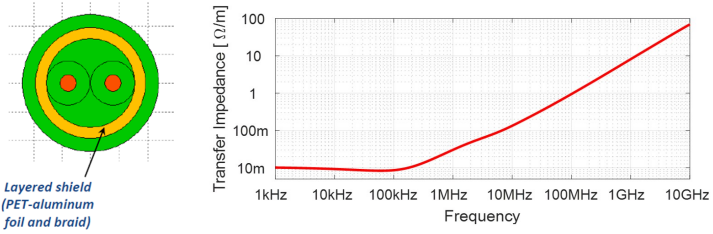

(a) (b)

Fig. 7.5: (a) Cross view of the modeled STP cable and (b) transfer impedance of the layered shield - ©2019 IEEE

The selected route of the cable starts close to the metallic edge of the dashboard. It then runs along the vehicle and terminates near to the rear window antenna, as it is shown in Figure 7.6. The total length of the modeled STP cable is 5.75 m. The distance between the cable and ground plane, car body, varies between 1.5 cm and 3 cm. Mesh of the car body consists of 30,000 metallic triangles.

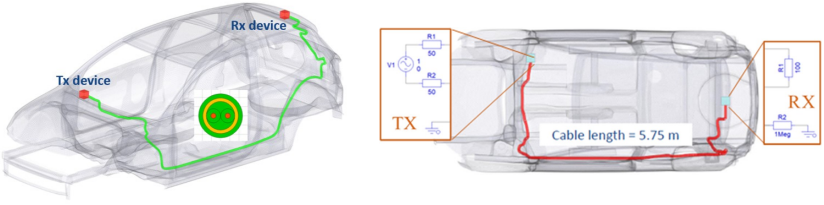

Fig. 7.6: The routing of the STP cable along the vehicle in the simulation model - ©2019 IEEE

As shown in Figure 7.6, the differential PAM-N transmitter (Tx device) is located near the dashboard, and the receiver (Rx device) is inside the spoiler. The system diagram with Tx and Rx devices at the ends of the STP cable is presented in Figure 7.7. The transmitter generates signals with 1 V peak-peak. The shield of the cable is grounded at the Tx side and floats at the far end, using a series resistor of 1 MOhm to ground. The differential voltage source is connected between the inner conductors of the STP through two 50 Ω resistors. At the Rx device, a 100 Ω load is placed between the differential lines.

Fig. 7.7: System diagram with Tx, Rx devices and STP cable - ©2019 IEEE

Simulation of the generated CM current

Common-mode radiation is an important source of the overall radiations from electronic hardware [202]. Therefore, the calculation of CM currents has a significant impact on the simulation of the coupling between STP cable and antennas. In order to calculate the overall CM current of the whole cable with the MTL method, the STP line is divided into sub-segments. The chosen length of each segment depends on the examined frequency range, e.g., 18.6 mm for TV band and 2.5 mm for the DSRC frequency range. Mesh-contours of the metallic surfaces of the car body are considered as a reference during the calculation of per-unit length parameters. Considering a voltage source of 1 V, the CM mode current of each segment that is caused over the data line and the shield is simulated. The CM current is used as the source of radiation for the estimation of interference voltage at ports of the antenna.

Figure 7.8 illustrates the result of CM current simulations. Depending on the segment length, frequency range, and the current return path, the resonance frequencies are observed. In Section 7.5, it is shown that coupled voltage to the antennas is the

result of the discussed resonance frequencies of the CM current and the spectral lines of the communication signal.

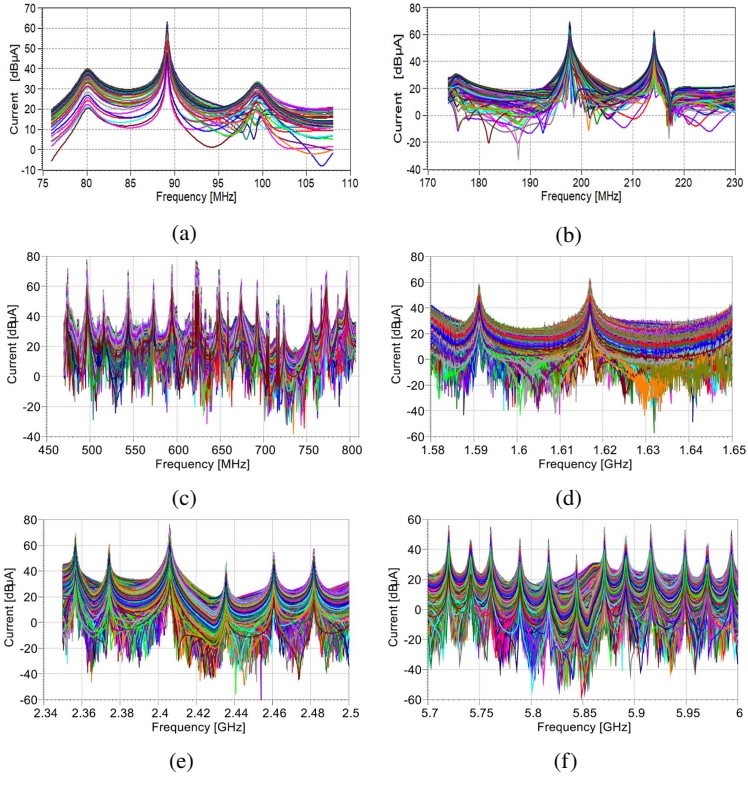

Fig. 7.8: Simulation of generated CM current in all segments of the STP cable in frequency range of (a) FM (b) DAB (c) TV band (d) GPS (e) WLAN (f) DSRC - ©2019 IEEE

7.4 Simulation models of different antennas

FM, DAB and TV IV – V frequency ranges

The simulation model of the vehicle with impressed current sources and rear window glass antenna is shown in Figure 7.9. Modeling of the glass antenna is performed with full-wave MoM solver utilizing special Green's function approach implemented in EMCoS Studio software [203]. This methodology was validated on some automotive glass antennas by comparing simulation results with measurements [204, 205]. For the considered antenna model (Figure 7.9c), the thickness of the glass is 3 mm, and the width of the strips of the antenna pattern is 1 mm. The permittivity of the glass is 7, with a dielectric loss equal to 0.02. Additional chokes are used for the connection of a heating structure to the car model. These chokes are modeled using 3 µH lumped elements. The length of the pigtail wires is equal to 8 cm.

Ports of the antenna are connected to the car body through non-radiating networks representing measured S-parameters of amplifiers. The related reflection coefficient of this antenna is presented in Figure 7.9e.

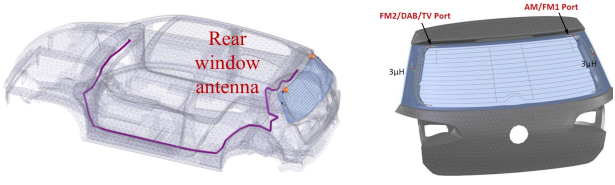

(a)

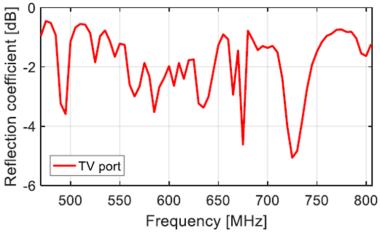

(b)

Fig. 7.9: (a) Model of rear window glass antenna for the frequency bands FM, DAB, and TV (b) The corresponding reflection coefficient in TV IV and TV V frequency range - ©2019 IEEE

GPS frequency range

Figure 7.10a represents the modeled GPS antenna, which is placed in the head unit in the simulated car model. This patch antenna is implemented using a substrate with a permittivity of 20.31. The feeding point of the antenna is connected to an SMA connector model with 50-Ohm impedance. The related reflection coefficient of this antenna is presented in Figure 7.10b. Simulation is done using the method of moments where dielectric parts of the antenna are modeled using surface integral equations. Validation of the modeling approach against measurements is demonstrated in [206].

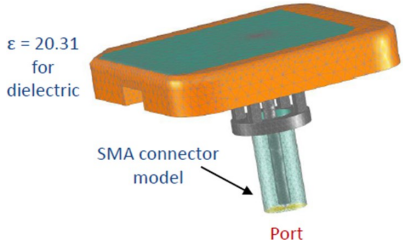

(a)

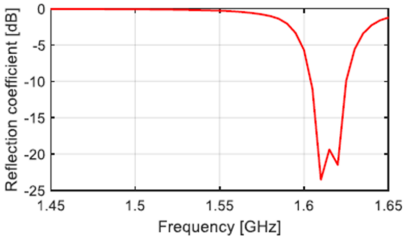

(b)

Fig. 7.10: (a) Model of the GPS antenna (b) The corresponding reflection coefficient - ©2019 IEEE

WLAN frequency range

The WLAN antenna is placed under the roof near the rear window of the car model. The simulation model of this antenna, Figure 7.11a, has a length of 58.5 mm. The reflection coefficient of the antenna is presented in Figure 7.11b. In the latter figure, the simulation results obtained using EMCoS Software (MoM solver) are verified by the measurements of the corresponding antenna.

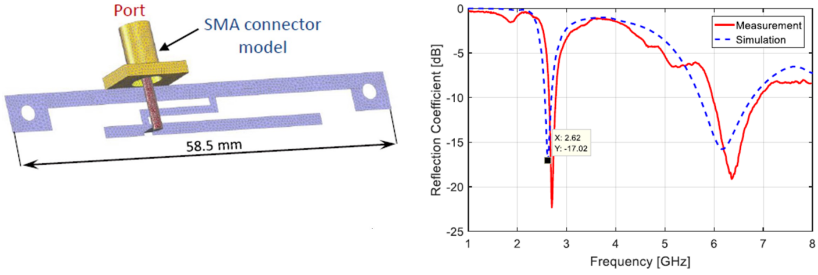

(a) (b)

Fig. 7.11: (a) Model of the WLAN antenna (b) The corresponding reflection coefficient - ©2019 IEEE

DSRC frequency range

The DSRC operation frequency, used for short-range applications like car-2-car and car-2-x communication, is around 5.9 GHz [207]. The modeled lambda-quarter monopole antenna has a length of 12.7 mm and is placed in the front window of the car model, Figure 7.12a. The corresponding reflection coefficient of this antenna is shown in Figure 7.12b. This antenna shows a broadband characteristic.

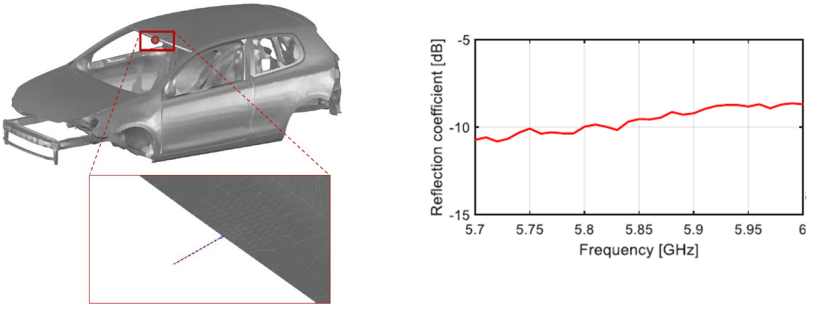

(a) (b)

Fig. 7.12: (a) Model of the DCRS antenna (b) The corresponding reflection coefficient - ©2019 IEEE

7.5 Emission of STP cable and coupling on the antennas over different frequency bands

For the calculation of the desired coupled voltage, the transfer function between the STP cable and the receiver antenna should be calculated. Once the transfer function is known, the radiation due to CM current and spectral lines of the signal, can be simulated.

For the calculation of the transfer function, a broadband signal with a known amplitude is required. Since CM currents are calculated from 1 V voltage source, these disturbance voltages (Figure 7.8) will be used as the source signal. The hybrid solution, which is based on the multi-transmission line theory and method of moments (MTL/MoM) [203], is applied for the calculation of transfer function between the cable and antenna. Using CM currents and MTL/MoM, the transfer function between the STP cable and different antennas for various frequency bands are calculated and illustrated in Figure 7.13.

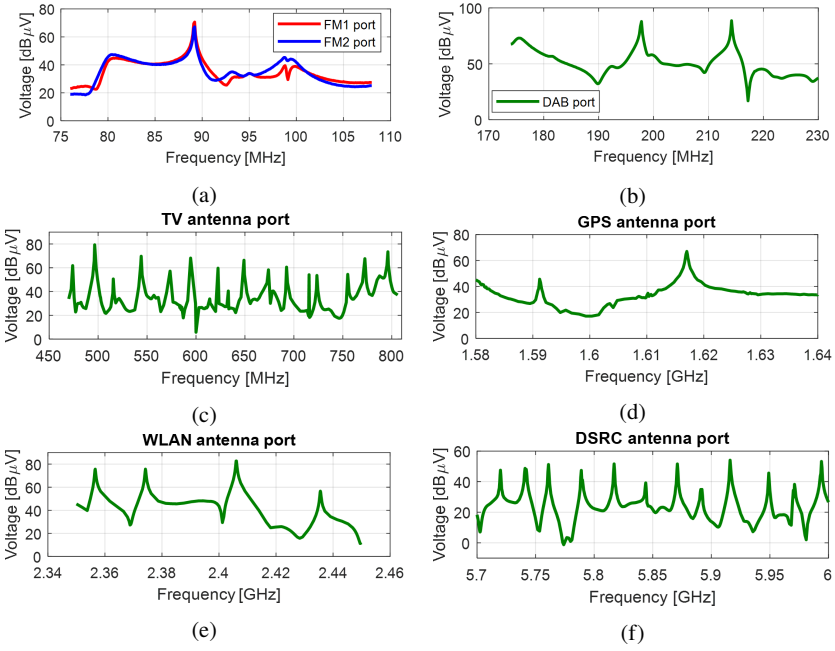

Fig. 7.13: Transfer functions between radiating cable and corresponding ports of antennas (a) FM1, FM2 (b) DAB (c) TV IV-V (d) GPS (e) WLAN (f) DSRC - ©2019 IEEE

The disturbance voltages at the rear window glass antenna ports, coupled from the radiating STP cable, are shown in Figure 7.14. The STP cable carries PAM-N signals with different data rates. Analysis of calculated disturbance voltages at rear window

antenna ports allows for the distinguishing of two types of peaks. Dominant peaks correlate with spectrum lines of PAM-N signals (Figure 7.3). Minor peaks observed in DAB range around 198 MHz, and 214 MHz are caused by cable resonances and correlate with CM current peaks shown in Figure 7.8. In FM frequency range, a minor peak at 89 MHz is also presented, but for PAM-2, PAM-3 and PAM-5 signals it is overlapped by the dominant peak.

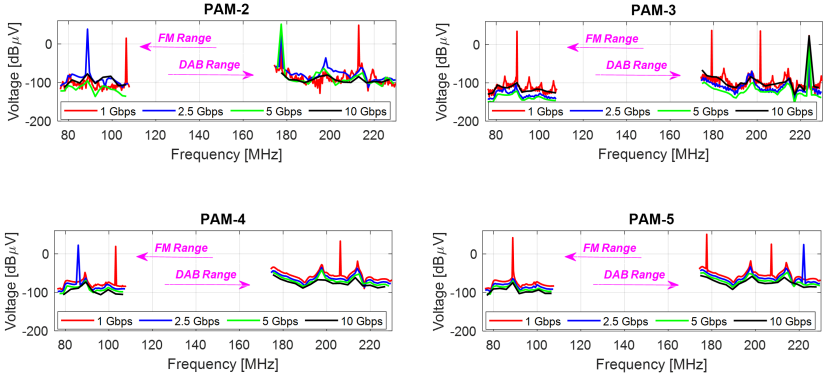

Fig. 7.14: Calculated coupled voltage at rear window antenna FM port - ©2019 IEEE

The results of the normalized coupled voltages are shown in Figure 7.15 and Figure 7.16. The normalization is performed using the calculated spectrum of PAM-N signals, as discussed in Section 7.2, and convolution of them with transfer functions between cable and corresponding antennas (Figure 7.13).

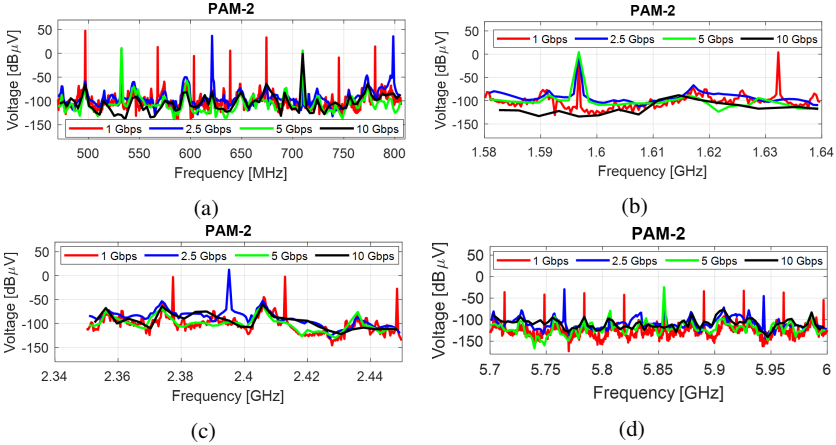

Fig. 7.15: Coupling of STP cable carrying PAM-2 signals with different data rate on the antenna in frequency range of (a) TV band (b) GPS (c) WLAN (d) DSRC - ©2019 IEEE

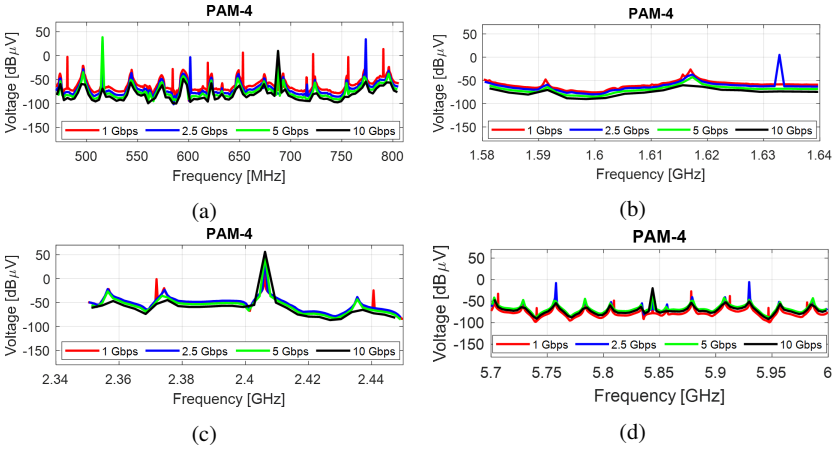

Fig. 7.16: Coupling of STP cable carrying PAM-4 signals with different data rate on the antenna in frequency range of (a) TV band (b) GPS (c) WLAN (d) DSRC - ©2019 IEEE

The simulation results presented in Section 7.2, and Section 7.3 reveal that the peaks of PAM-4 signal spectrum, together with the CM mode current resonances, lead to the major and minor peaks of coupled voltage, respectively.

The presented simulation methods can help the chip industry and the OEMs to design the characteristics of the related PHYs, defining the optimum cable routings, forecasting maximum radiations limits, and studying the behavior of future vehicle networks.

7.6 Conclusion

This chapter presented the 3D field simulation of the Multi-Gig Ethernet networks considering EM radiations. The generation of PAM-N (N=2,3,4,5) signals with their corresponding discrete spectrums were discussed. The simulation model of an STP cable with a length of 5.75 m was also described in detail. To study the radiation of the cable, a realistic in-car routing was chosen. The different antennas of a car were modeled. Based on the explained routing of the cable, the common-mode currents of the cable were calculated in the investigated frequency ranges. The EM interferences of the cable, carrying signals with data rates of 1 Gbit/s, 2.5 Gbit/s, 5 Gbit/s, and 10 Gbit/s, with different antennas, were both simulated and studied. The corresponding coupled voltages at the passive FM1, FM2, DAB, TV IV-V, GPS, Wi-Fi, and DSRC ports of the antennas were calculated.

The simulated coupled voltages at the ports of corresponding antennas show that the common-mode current resonances and the peaks of PAM-4 spectra lead to the

main coupled resonances. Analysis of disturbances demonstrates dominant voltage peaks that correlate with signal spectral lines and minor peaks that originate from cable resonances.

The qualitative comparison of the simulation results of this chapter and measurements, discussed in Chapter 6, prove the effectivity of the simulation method and the corresponding results. The proposed simulation model is a novel methodology for investigating the EMC issues of automotive Multi-Gig networks. This approach could be expanded for the use of other routing topologies.

Chapter 8
Summary and Conclusions

In this work, the EMC issues of the automotive Multi-Gig Ethernet communication networks have been investigated and discussed. The mentioned EMC investigations are of paramount importance, as the required frequency bands for the implementation of automotive gigabit Ethernet are in the gigahertz range, which encounters the automotive industry with new EMC challenges. The automotive Ethernet, with data rates of up to 100 Gbit/s (and even higher), is the prerequisite for the implementation of fully autonomous driving, car-2-car, car-2-x, and the use of 5G communication technology in the car. If the related EMC issues are not well thought out, then driving safety can deteriorate.

The introductory discussions included different automotive EMC tests and communication networks. It was shown that CISPR and ISO standards define the most important guidelines for EMC testing. While the emission tests are handled in CISPR, the ISO standards discuss the immunity and ESD tests. CISPR 12 characterizes the interference tests for examining the emission of automotive components on the objects around the vehicle (10 m distance from the car). As a result of the emission, the automotive electric and electronic components can interfere with each other's functionality. The in-vehicle emission tests are described in CISPR 25. In this standard, the measurement methods of conducted and radiated emission are explained. The immunity of the vehicle's components can be tested in the vehicle (ISO 11451) or in the laboratory (ISO 11452). The latter mentioned standard has ten parts and includes important immunity tests like ALSE-test, harness excitation methods, and DPI-test. The automotive ESD test was discussed in ISO 10605, which is an adapted version of the IEC 61000-4-2 standard.

It was discussed that the traditional automotive communication networks could not fulfill the requirements of future cars. To introduce the shortcomings of these technologies, the most important traditional communication networks were discussed with the focus on the physical layer. It was shown that LIN technology could support applications that do not need real-time response and high-data rates. The supported data rate of the LIN bus is 20 kbit/s. The CAN bus system was the next generation

of the automotive communication networks, with which data rates between 10 kbit/s and 1 Mbit/s over unshielded twisted pair cables are realizable. The CAN bus is not suitable for real-time and safety-critical applications. The extended version of the CAN-bus, with data rates up to 10 Mbit/s, was the CAN with flexible data rates (CAN FD).

For safety-critical applications in the powertrain and chassis, the FlexRay communication network was introduced. FlexRay has enabled the automotive industry to implement the 10 Mbit/s communication networks. The use of a time-triggered protocol facilitates the realization of a communication network with constant latency and jitter. Using the LVDS communication principle, which is based on a point-to-point link, significant advances in infotainment and camera systems can be achieved. This communication principle supports data rates of up to 655 Mbit/s. MOST communication network profits from a fiber optic channel, which is not affected by electromagnetic interferences. With a data rate of 150 Mbit/s, the infotainment and multimedia applications are realizable using MOST communication technology. The digitalization of the automotive components, on the one side, and the implementation of new technologies and applications, on the other, have introduced the need for a communication network with flexible data rates. With automotive Ethernet, data rates from 10 Mbit/s up to 100 Gbit/s, or even higher, can be realized.

For applications where lower data rates and a simple bus structure are needed, the 10 Mbit/s Ethernet should be applied. The IEEE 802.3cg working group is currently (mid-2020) working on the standardization of 10BASE-T1S.

The next discussed automotive Ethernet was 100BASE-T1. This standard (IEEE 802.3bw) covers the implementation of automotive Ethernet with a data rate of 100 Mbit/s. The analog front-end of 100BASE-T1 includes the transceiver, common-mode choke, DC-block capacitors, common-mode termination, ESD-protection device, and the medium dependent interface. The corresponding PHY of the 100BASE-T1 can operate in master or slave mode. Using PAM-3 signaling the implementation of 100 Mbit/s over a UTP cable is realizable. In order to avoid discrete spectral lines in the signal spectrum, the data scrambling method is applied. Using data switches, the data packets are transferred between different network participants. The use of PoE is foreseen in the IEEE 802.3bw standard, as well. As 100BASE-T1 uses a full-duplex communication mode, echo-cancellation circuitry for distinguishing the transmitted and received signals is needed. Various test methods for examining the proper functionality of the corresponding PHY regarding transmitter droop, jitter, distortion, and PSD mask are suggested in IEEE 802.3bw. The immunity of the PHY should be tested with the DPI test method. By applying the 150-ohm test method, the RF emission of the PHY can be measured. Further test methods for transients and ESD immunity are explained in the standard. Furthermore, the PHY immunity against alien crosstalk should be performed using the suggested measurement setup proposed in the IEEE 802.3bw standard. Two companies, i.e., Broadcom and Marvel, have introduced the corresponding PHYs of the 100BASE-T1 till now (mid-2020).

The channel and MDI connector of the IEEE 802.3bw standard should fulfill the specified limits concerning differential impedance, insertion loss, return loss, and mode conversion.

Further, it was discussed that the implementation of 1000 Mbit/s over an automotive Ethernet network is standardized in IEEE 802.3bp. Using PAM-3 modulation and a baud rate of 750 Mbaud/s, the mentioned data rate is achievable. The difference between the structure of the physical layer of 1000BASE-T1 and 100BASE-T1 is the use of the gigabit medium independent interface (GMII) and the optional use of the auto-negotiation sublayer. The latter sublayer controls the master or slave mode of the PHY. As there is a similarity between the described test methods of 100BASE-T1 and 1000BASE-T1, the corresponding measurement methods are not explained here again. Because of the higher signal frequency, the related EMC issues of this communication standard could be overcome using shielded twisted pair cable.

In the further course of the introductory discussions of this work, the state of the knowledge of the automotive Multi-Gig Ethernet was presented. The IEEE 802.3ch task force is currently working on the NGBASE-T1 standard. In this standard, the realization of the data rates of 2.5 Gbit/s, 5 Gbit/s, and 10 Gbit/s will be defined. The proposed information is based on the publicly accessible presentations of the mentioned task force. According to the objectives of the task force, the Ethernet frame format and the frame size of the IEEE 802.3 should be preserved. The gigabit data communication should have a BER better than 10^{-12} and support the harsh automotive EMC conditions. To reduce power consumption and computation capacity, the use of asymmetrical data transmission is of interest to the Multi-Gig automotive networks. Using FEC, the BER of the communication link can be improved.

The bandwidth of the NGBase-T1 communication system plays a significant role in the overall system performance. The use of a suitable signal modulation can reduce the bandwidth and ease the strict requirements of the corresponding cables. Considering SNR, PHY complexity, power consumption, etc. the PAM-4 modulation format is suggested. Furthermore, the use of data scrambling and energy-efficient Ethernet (EEE) is foreseen in IEEE 802.3ch. The Tx-PSD mask of this standard contains the peak emission requirements of OEMs. With the measurement of the coupling attenuation, the emission can be defined. The corresponding PSD-mask limits for the NGBase-T1 were presented. The choice of a suitable channel for the automotive Multi-Gig Ethernet is of primary importance for the implementation of this network. Considering RF immunity, radiation, insertion loss, and return loss, the use of STP cables seems to be the appropriate solution.

The next generation of the future automotive Ethernet should cover data rates beyond 10 Gbit/s. Through using the mentioned data rates, the implementation of fully autonomous driving is realizable. A large number of sensors and cameras should prepare the required data of the artificial intelligence. The data processing and decision making can be performed in one or more central units. In a zonal architecture,

multiple central units control specific zones, which in turn are connected via related switches.

The implementation of automotive Ethernet with different data rates requires accurate interaction between the involved components of the network. Two main parts of the whole network are, among other things, the analog front-end (AFE), and channel. Considering the EMC issues of the mentioned two components is of primary importance in the design stages of the networks. In the first part of this work, the components of the AFE regarding their high-frequency EMC characteristics were investigated. Based on measurements, novel simulation models were presented and discussed. The second part of this work contains the investigations of the channel. The IEEE 802.3ch task force suggestions are mainly based on lab measurements. Some of the most important in-vehicle measurements, i.e., RF immunity and emission of Multi-Gig channel, were performed in this work. Based on the measurements, new limit lines were suggested. Furthermore, a new simulation method was proposed, helping the OEMs choose the proper routing topology. In the following, a summary of the provided contents is presented.

Due to asymmetries in the communication system or external disturbances, common-mode (CM) noise can be generated. CM degrades the signal quality and leads to unwanted emissions. To suppress the CM noise, a common-mode choke (CMC) is used in the AFE of the Ethernet communication link. A CMC comprises two coupled inductors sharing the same core. The CMC has a low resistive impedance to differential signals and shows a high impedance against the common-mode currents. In this work, a simple HF simulation model of the automotive CMC was developed and verified by measurements. The equivalent circuit model contains two parts, i.e., CM and differential-mode (DM). The CM part of the circuit includes the self-inductance, the windings capacitance, and the resistance of the coil. The DM part represents the parasitic parameters of the CMC, which are contributed from DM signaling. The isolation of the inductors is modeled using the corresponding resistors and capacitors. The values of the circuit components were derived from the performed impedance measurements and the datasheet of the CMC, which is suitable for the 100BASE-T1 link.

For measuring the impedance of the CMC in the case of CM, both inductors of the choke were connected in parallel. The measurement of DM impedance was performed through connecting both inductors of the CMC in series. Considering the resonance frequencies in CM and DM, the related equivalent circuit values were calculated. The presented measurements were performed for three CMCs. The first one was suitable for 100BASE-T1. The other two CMCs, which were from various vendors, were applicable for 1000BASE-T1.

The verification of the equivalent circuit model was performed by mixed-mode S-parameter measurements. The used parameters were DM and CM insertion loss (S_{dd21}, S_{cc21}), DM and CM return loss (S_{dd11}, S_{cc11}), common to differential-mode

rejection (S_{ds21}, S_{ds12}), and differential to common-mode rejection (S_{sd21}, S_{sd12}). The measurement and simulation results, using the equivalent circuit model, have shown a good agreement, and proved the developed methodology.

As explained previously, the AFE contains other components, e.g., CM termination, low-pass filter, and PHY. In Chapter 4, the simulation models of the mentioned components were developed and discussed. In the first step, the equivalent circuit model of the PHY was discussed.

The presented simple equivalent circuit model of the PHY contains the Tx, Rx, and echo-cancellation circuit. The differential input signal of Tx is realized by two PAM-3 voltage sources with a phase difference of 180°. An echo-cancellation helps to distinguish the transmitted and received signals, which are added together on the channel side in a full-duplex operation mode. Therefore the Tx signal has to be subtracted internally from the whole signal. The circuit model was used for further investigations. Using the developed PHY circuit model, the PSD of 100 Mbit/s, 1000 Mbit/s, and 2.5 Gbit/s Ethernet communication were investigated. In this regard, the developed circuit model was fed by a PAM-3 PRBS data sequence. The PSD diagram of the circuit model was examined in three different stages, i.e., after the Tx circuit, after LPF, and at the end of the AFE circuit. The simulation results of 100 Mbit/s and 1000 Mbit/s PHY were compared to the corresponding defined limits of 100BASE-T1 and 1000BASE-T1. The simulation results complied with the standardized limits. Hence, the validity of the simulation model was verified. Using the PHY circuit model, the PSD of Multi-Gig Ethernet PHY (with a data rate of 2.5 Gbit/s) could be predicted.

In a further step, the low-pass filter of the automotive Ethernet AFE was studied. The corresponding circuit model was presented and discussed. The associated values for the lumped components were defined for three different data rates (i.e., 100 Mbit/s, 1000 Mbit/s, and 2.5 Gbit/s). To verify the circuit model, the corresponding PCBs were fabricated and tested. The measurements have shown a good agreement with the simulation results.

The next investigated AFE component was the CM termination. This component helps to reduce EMI and sensitivity to common-mode noise in predefined frequency ranges. The circuit model of the CM termination was illustrated and explained. The related values of the lumped components were calculated and simulated for the three examined date rates. The functionality of the CM termination is measured together with corresponding CMCs.

In the last step, the circuit model of the whole AFE is examined. For this, the individual circuit models of the components were connected, and the overall functionality of the AFE was simulated. Three different AFE PCBs with the previously calculated lumped components values were fabricated and measured. The measurements and simulation results were compared. The good agreement between simulations and

measurements have proven the suitability of the AFE circuit model. The presented circuit model paves the way for the characterization of the automotive Ethernet networks in the early design stages.

In the second part of this work, the EMC of the automotive Multi-Gig Ethernet channel was investigated. The focus of the investigations was on the emission, the noise immunity, and the signal integrity of the cables. According to IEEE 802.3ch, the implementation of gigabit data rates (2.5 Gbit/s, 5 Gbit/s, and 10 Gbit/s) should be realized using at least one of the following cables as the medium of the network: UTP, STQ, STP, SPP, coax, or Twinax. Hence, the physical structures of the mentioned cables were explained briefly. STP and SPP cables seem to be the choice of the IEEE 802.3ch task force group.

The STP and SPP cables were at the focus of this work. The measurements of these cables assume the use of the H-MTD adapters. Hence, the suitability of the adapters was studied in the first step. Using TDR measurement, the differential-mode line impedance of both used adapters were defined. The results were within the allowed range of 95 Ω - 105 Ω. Using verified H-MTD adapters, different STP, and SPP cables were measured. For each STP and SPP cable, two different lengths were examined, i.e., 1.0 m and 10.0 m. To consider the manufacturing tolerances, four different cables of the same length and type were measured. In total, sixteen cables were studied.

After describing the measurement setups, the frequency domain measurements of the STP and SPP cables, based on the mixed-mode S-parameters for frequencies up to 8 GHz, were discussed. The first investigated parameter was DM return-loss (S_{dd11}). For lower frequencies, the shorter cables have shown smaller RL. However, at higher frequencies, RL was found to be similar for both cable lengths. A comparison between both cable types STP and SPP revealed that STP cables generally show smaller RL at higher frequencies. It should be noted that the RL of both cable types were still below -20 dB up to 3.5 GHz.

The DM insertion loss (S_{dd21}) of both cable types was also measured. Overall, the SPP cable has shown a little better IL. However, concerning Multi-Gig data transmissions, both cable types have shown sufficiently good IL. The longitudinal conversion loss (LCL) of the cables was compared in further measurements. Generally, larger LCL (S_{dc11}) was observed for longer cables, since the asymmetry and the corresponding mode conversion tends to increase with transmission line length. Based on the measurement, the STP cables show better LCL results than SPP cables.

Furthermore, the screening attenuation, coupling attenuation, and the unbalanced attenuation of both cables were investigated and compared using a triaxial measurement setup. The unbalanced attenuation of the STP cable under testing was generally higher and thus better than that of the SPP cable. This means that along the SPP line, a higher proportion of the injected differential-mode signal is converted into CM. The same behavior was observed for the screening attenuation. Except for very

low and very high frequencies, the SPP line under testing showed lower screening attenuation than the STP line and thus lower effectiveness of its screening. Generally, the results of the SPP line under testing were worse than that of the STP line.

Utilizing a bit error rate tester, the signal integrity of the STP and SPP cables for different gigabit data rates was compared. The corresponding time-domain measurements were implemented using PAM-2 modulated PRBS signals with a length of 2^{23}-1 bits. The cables were tested with data rates from 2 Gbit/s up to 6 Gbit/s. The SPP cable showed a smaller BER for any data rate. The maximum reachable data rate for SPP cable was 5.2 Gbit/s (PAM-2) before the loss of synchronization happened. The maximum applicable data rate for STP was 4.7 Gbit/s (PAM-2).

A comparison between UTP and STP cable, based on laboratory level measurements, was also performed. The DM return loss of both examined cables, each having 6 m length, revealed the better functionality of the STP cable. The DM insertion loss of the STP and UTP cables, up to 8 GHz, also showed a better performance of the STP cable. However, the measurements demonstrated the suitability of the UTP cable for 100BASE-T1 with a frequency range of up to 33.3 MHz.

The signal integrity of the STP cable was also investigated using two Xilinx Kintex-7 FPGA boards. The use of FPGAs for the EMC investigations of the automotive Multi-Gig Ethernet is a novelty of this work. In this regard, one FPGA was configured as the transmitter and the other one as the receiver of the gigabit data communication link. The Multi-Gig communication path was constructed on the lab bench using the FPGA boards and STP cable. The signal integrity of the channel was discussed using the statistical eye diagram provided by Xilinx. Different cable lengths and data rates were studied for the measurements. The most extended cable (STP with a length of 15 m) and the highest data rate (5 Gbit/s) led to the most closed statistical eye diagram. On the contrary, the best results were achieved with the shortest cable with a length of 1 m. The provided measurement method enables the investigation of the cables, while the corresponding PHYs have not yet been developed.

The EMC investigations of the channels were continued by the in-vehicle immunity and emission measurements. The in-vehicle immunity test was performed using a 10 m STP cable route with four in-line connectors. The measurement setup included a worst-case situation, which must be considered for a reliable ECU design. The RF ingress of the STP cable was measured up to 6 GHz within seven frequency spans. Correspondingly, seven different antennas were used.

This first studied frequency range was from 100 kHz to 30 MHz. A stripline antenna, which was positioned above the car, has generated a unidirectional field. The coupled voltage to the STP cable was less than 103 dBµV. Using a log-periodic antenna, the frequency range of 30 MHz – 220 MHz was investigated. The ingressed voltage in the mentioned frequency range was less than 80 dBµV. The frequency

band of 220 MHz to 400 MHz was studied with a horn antenna. For the immunity of the STP cable in the mentioned frequency range, a limit of 75 dBµV was measured. The horn antenna was also used for the remaining measurements up to 6 GHz. The coupled voltage to the STP cable was less than 80 dBµV from 400 MHz to 1000 MHz. Towards 3 GHz, the coupled voltage has become smaller and was around 75 dBµV. The results of the EMI tests for the frequencies between 3 GHz – 4 GHz and 4 GHz – 6 GHz show that the coupled voltage was less than 70 dBµV.

The RF ingress measurement results of this work did not comply with the introduced component test results of the IEEE 802.3ch task force group. The components test has led to a limit of 73 dBµV. The performed in-vehicle measurements of this work point to a limit of 103 dBµV (for the low frequencies up to 30 MHz) and 90 dBµV (for the higher frequencies up to 6 GHz).

The in-vehicle emission measurement of the Multi-Gig Ethernet channel is associated with the problem that the Multi-Gig Ethernet PHYs are still not yet available. To overcome the mentioned issue, FPGAs boards were used as Tx and Rx of the communication link. Unfortunately, just PAM-2 signals could be realized with the FPGA boards. For the in-vehicle electromagnetic emission measurement of the STP cable, a worst-case routing was chosen. The measurements included the electromagnetic coupling of STP cable to different vehicle antennas. The measured frequency ranges were FM1-FM2 (using rear window antenna), DAB (using a monopole antenna), TV IV - V (using a monopole antenna), Wi-Fi (using an omnidirectional antenna), and DSRC (using an omnidirectional antenna). The evaluation of the measurements was performed by comparing the results with the provided limits in the specification TL 81000.

To evaluate the emission measurement results, the spectra of the PAM-2 signals for data rates of 2.5 Gbit/s and 5 Gbit/s were studied by MATLAB simulations. The distance between the spectral lines of the mentioned signals could be calculated by the inverse of the pattern length, i.e., 2^7-1 bits, multiplied by the associated bit period. The knowledge of the exact position of the spectral lines helps to interpret the measurement results. It was shown that the spectral distance for 2.5 Gbit/s and 5 Gbit/s data link is around 20 MHz and 40 MHz, respectively.

For all mentioned frequency ranges, the simulated spectral lines were observed in the measurements on the same frequencies. In the FM1-FM2, DAB, TV IV-TV V, and DSRC frequency bands, the limits of the TL 81000 could not be satisfied. On the contrary, the results of the WLAN frequency band complied with the limits. It should be considered that the presented results were for the worst-case routing. To reach a definitive conclusion about the STP cables, further measurements are obligatory. A real in-car routing of the cable with different in-line connectors has to be implemented.

The in-vehicle EMC measurements are very time-consuming. Therefore, corresponding simulation methods can be beneficial in the early design stages. For this, a simulation method for the emission of the STP cable was provided. The provided 3D field simulation method is a further novelty of this work. Using the introduced method, the emission of the STP cable in the form of coupled voltage to different vehicle antennas can be simulated. To calculate the coupled disturbance voltage, the transfer function between the STP cable and antennas was defined. The transfer function was calculated using the CM current, which flows in the STP cable. The convolution of the PAM-N spectrum with the transfer function has enabled the calculation of the coupled voltage at the port of the antenna. The reflection coefficients of the antennas were also defined, with which the coupled voltage to the antennas could be simulated.

It was demonstrated that the significant peaks in simulation results were because of the spectral lines of the transmitted PRBS signal. The minor peaks of the simulation results were because of the CM current resonances. The provided simulation results have shown a good agreement with the measurement results of the STP cable emission.

Outlook and perspectives

The presented AFE circuit models should be validated by further measurements, which contain components from different vendors. Various automotive CMCs from multiple manufacturers and suitable for different data rates should be tested. Because the corresponding Multi-Gig PHYs were not available, the functionality of the presented PHY circuit model could not be compared with the measurements. The presented circuit model can be adopted should the associated PHYs be available. If the CMC and the low-pass filter are implemented on-chip, the presented circuit model should also be validated.

As soon as the related Multi-Gig automotive Ethernet PHYs are available, the discussed EMC channel investigation should also be repeated and examined. The signal integrity measurements of the STP and SPP cables have to be examined using the corresponding PAM-4 signals. The in-vehicle immunity and emission measurements should be performed with the related PHYs. The mentioned EMC measurements should also be repeated with the corresponding Multi-Gig Ethernet ECUs.

References

[1] N. Navet and F. Simonot-Lion, *In-vehicle communication networks-a historical perspective and review*, University of Luxembourg, Ed., 2013. [Online]. Available: https://orbilu.uni.lu/handle/10993/5540.

[2] T. Nolte, H. Hansson, and L. Lo Bello, "Automotive Communications - Past, Current and Future", in *Emerging Technologies and Factory Automation, 2005. ETFA 2005. 10th IEEE Conference on*, s.l.: IEEE, 2005, pp. 985–992. DOI: 10.1109/ETFA.2005.1612631.

[3] L. Braun, M. Armbruster, and F. Gauterin, "Trends in Vehicle Electric System Design: State-of-the Art Summary", in *2015 IEEE Vehicle Power and Propulsion Conference (VPPC)*, Piscataway, NJ: IEEE, 2015, pp. 1–6. DOI: 10.1109/VPPC.2015.7353035.

[4] V. Manoj and J. Niresh, "Automotive Networks : A Review", *International Journal of Advanced engineering, Management and Science*, vol. 3, no. 5, pp. 504–509, 2017. DOI: 10.24001/ijaems.3.5.15.

[5] S. Tuohy, M. Glavin, C. Hughes, E. Jones, M. Trivedi, and L. Kilmartin, "Intra-Vehicle Networks: A Review", *IEEE Transactions on Intelligent Transportation Systems*, vol. 16, no. 2, pp. 534–545, 2015. DOI: 10.1109/TITS.2014.2320605.

[6] A. Amerasekera and N. Da Dalt, "High-Speed Communications on Four Wheels: What is in Your Next Car?", *IEEE Solid-State Circuits Magazine*, vol. 5, no. 2, pp. 79–80, 2013.

[7] L. Reger, "1.4 The road ahead for securely-connected cars", in *2016 IEEE International Solid-State Circuits Conference*, L. C. Fujino and J. H. Anderson, Eds., Piscataway, NJ: IEEE, January 2016, pp. 29–33. DOI: 10.1109/ISSCC.2016.7417892.

[8] K. Matheus and T. Königseder, *Automotive ethernet*, Second edition, 2017. Cambridge: Cambridge University Press, 2017. DOI: 10.1017/9781316869543. [Online]. Available: https://doi.org/10.1017/9781316869543.

[9] K. Borgeest, "Practical papers, articles and application notes: EMC aspects of car communication systems", *IEEE Electromagnetic Compatibility Magazine*, vol. 1, no. 1, pp. 35–41, 2012. DOI: 10.1109/MEMC.2012.6244943.

[10] S. Buntz, B. Körber, D. Bollati, *100BASE-T1 System Implementation Specification*, Open Alliance, Ed. [Online]. Available: http://www.opensig.org/download/document/231/OA+100BASE-T1+system+implementation+specification_D1.0_final_18.pdf.

[11] C. Fanning, “An Overview of Automotive EMC Standards and Emerging Requirements”, in *2018 IEEE Symposium on Electromagnetic Compatibility, Signal Integrity and Power Integrity (EMC, SI & PI)*, Piscataway, NJ: IEEE, 2018, pp. 1–43. DOI: 10.1109/EMCSI.2018.8495352.

[12] IEC, *CISPR 12, Vehicles, boats and devices with internal combustion engines or traction batteries – Radio disturbance characteristics – Limits and methods of measurement for the protection of off-board receivers*, 3.10.2009. [Online]. Available: https://www.sis.se/api/document/preview/568773/.

[13] ——, *CISPR 25:2016 - Vehicles, boats and internal combustion engines - Radio disturbance characteristics - Limits and methods of measurement for the protection of on-board receivers*, 2016-10.

[14] JIN JIA, *Current Scan Methods to Predict Radiated Emissions of Automotive Components According to CISPR 25*. Dortmund: Technische Universität Dortmund, 2015. [Online]. Available: https://core.ac.uk/download/pdf/46916292.pdf.

[15] Mayerhofer, *Application Note - Conducted emission measurement using the Tekbox 5µH LISN TBOH01*, ALLDAQ, Ed. [Online]. Available: https://www.alldaq.com/fileadmin/user_upload/files/manuals/tekbox/AN_Conducted_Noise_Measurement_Tekbox_LISN_TBOH01_and_EMCview_ALLDAQ.pdf.

[16] E. Panholzer, M. Spagele, H. Leier, and S. Lindenmeier, “In-Car Emission Prediction for a Real Communication System Based on a Component Level Test”, in *2018 International Symposium on Electromagnetic Compatibility*, Piscataway, NJ: IEEE, 2018, pp. 72–77. DOI: 10.1109/EMCEurope.2018.8484957.

[17] ISO, *ISO 11451-1:2015 - Road vehicles – Vehicle test methods for electrical disturbances from narrowband radiated electromagnetic energy – Part 1: General principles and terminology*, 6.2015.

[18] ——, *ISO 11451-2:2015 - Road vehicles – Vehicle test methods for electrical disturbances from narrowband radiated electromagnetic energy – Part 2: Off-vehicle radiation sources*, 6.2015.

[19] ——, *ISO 11451-3:2015 - Road vehicles – Vehicle test methods for electrical disturbances from narrowband radiated electromagnetic energy – Part 3: On-board transmitter simulation*, 6.2015.

[20] ——, *ISO 11451-4:2013 - Road vehicles – Vehicle test methods for electrical disturbances from narrowband radiated electromagnetic energy – Part 4: Bulk current injection (BCI)*, 4.2013.

[21] ——, *ISO 11452-1:2015 - Road vehicles – Component test methods for electrical disturbances from narrowband radiated electromagnetic energy – Part 1: General principles and terminology*, 6.2015.

[22] ——, *ISO 11452-2:2019 - Road vehicles – Component test methods for electrical disturbances from narrowband radiated electromagnetic energy – Part 2: Absorber-lined shielded enclosure*, 1.2019.

[23] H. Rakouth, C. Cammin, L. Comstock, and J. Ruiz, "Automotive EMC: Key Concepts for Immunity Testing", in *IEEE International Symposium on Electromagnetic Compatibility, 2007*, Piscataway, NJ: IEEE Operations Center, 2007, pp. 1–7. DOI: 10.1109/ISEMC.2007.168.

[24] ISO, *ISO 11452-3:2016 - Road vehicles – Component test methods for electrical disturbances from narrowband radiated electromagnetic energy – Part 3: Transverse electromagnetic (TEM) cell*, 9.2016.

[25] ——, *ISO 11452-4:2011 - Road vehicles – Component test methods for electrical disturbances from narrowband radiated electromagnetic energy – Part 4: Harness excitation methods*, 12.2011.

[26] P. DeRoy, N. Toscani, F. Grassi, W. Schulz, and C. Rostamzadeh, "Sensitivity Analysis of RF Current Injection Techniques for Immunity Testing of Automotive Ethernet", in *2018 IEEE Symposium on Electromagnetic Compatibility, Signal Integrity and Power Integrity (EMC, SI & PI)*, Piscataway, NJ: IEEE, 2018, pp. 461–466. DOI: 10.1109/EMCSI.2018.8495370.

[27] ISO, *ISO 11452-5:2002 - ROAD VEHICLES – COMPONENT TEST METHODS FOR ELECTRICAL DISTURBANCES FROM NARROWBAND RADIATED ELECTROMAGNETIC ENERGY – PART 5: STRIPLINE*, 4.2002.

[28] ——, *ISO 11452-7:2003 - ROAD VEHICLES – COMPONENT TEST METHODS FOR ELECTRICAL DISTURBANCES FROM NARROWBAND RADIATED ELECTROMAGNETIC ENERGY – PART 7: DIRECT RADIO FREQUENCY (RF) POWER INJECTION*, 11.2003.

[29] A. H. van Roermund, H. Casier, and M. Steyaert, *Analog Circuit Design: High-Speed A-D Converters, Automotive Electronics and Ultra-Low Power Wireless*. Dordrecht: Springer, 2006. DOI: 10.1007/1-4020-5186-7. [Online]. Available: http://gbv.eblib.com/patron/FullRecord.aspx?p=323049.

[30] C. Rostamzadeh, "Correlation of radio frequency interference tests with low dropout voltage regulators", in *2006 IEEE International Symposium on Electromagnetic Compatibility, 2006*, Piscataway, NJ: IEEE Operations Center, 2006, pp. 191–195. DOI: 10.1109/ISEMC.2006.1706290.

[31] Schwarzbeck Mess - Elektronik, *Broadband Artificial Network BAN 8508*, Schwarzbeck Mess - Elektronik, Ed., Schoenau, Germany. [Online]. Available: http://www.schwarzbeck.de/Datenblatt/k8508.pdf.

[32] ISO, *ISO 11452-8:2015 - ROAD VEHICLES – COMPONENT TEST METHODS FOR ELECTRICAL DISTURBANCES FROM NARROWBAND RADIATED ELECTROMAGNETIC ENERGY – PART 8: IMMUNITY TO MAGNETIC FIELDS*, 6.2015.

[33] ——, *ISO 11452-9:2012 - ROAD VEHICLES – COMPONENT TEST METHODS FOR ELECTRICAL DISTURBANCES FROM NARROWBAND RADIATED ELECTROMAGNETIC ENERGY – PART 9: PORTABLE TRANSMITTERS*, 5.2012.

[34] ——, *ISO 11452-10:2009 - ROAD VEHICLES – COMPONENT TEST METHODS FOR ELECTRICAL DISTURBANCES FROM NARROWBAND RADIATED ELECTROMAGNETIC ENERGY – PART 10: IMMUNITY TO CONDUCTED DISTURBANCES IN THE EXTENDED AUDIO FREQUENCY RANGE*, 4.2009.

[35] ——, *ISO 11452-11:2010 - ROAD VEHICLES – COMPONENT TEST METHODS FOR ELECTRICAL DISTURBANCES FROM NARROWBAND RADIATED ELECTROMAGNETIC ENERGY – PART 11: REVERBERATION CHAMBER*, 9.201.

[36] B. Adamczyk, *Foundations of Electromagnetic Compatibility with Practical Applications*. Newark: John Wiley & Sons Incorporated, 2017. [Online]. Available: https://ebookcentral.proquest.com/lib/gbv/detail.action?docID=4816187.

[37] S. H. Voldman, *ESD testing: From components to systems*, ser. ESD series. Chichester, West Sussex, United Kingdom: Wiley, 2017.

[38] ISO, *ISO 10605:2008 - Road vehicles — Test methods for electrical disturbances from electrostatic discharge*, 7.2008.

[39] M. Hampe, "Accurate measurement of transmission line parameters for automotive ethernet", in *IEEE International Symposium on Electromagnetic Compatibility (EMC), 2015*, Piscataway, NJ: IEEE, 2015, pp. 1363–1368. DOI: 10.1109/ISEMC.2015.7256370.

[40] G. W. d. Besten, "30.1 Single-Pair Automotive PHY Solutions from 10Mb/s to 10Gb/s and Beyond", in *2019 IEEE International Solid- State Circuits Conference - (ISSCC)*, IEEE, 2/17/2019 - 2/21/2019, pp. 474–476. DOI: 10.1109/ISSCC.2019.8662539.

[41] S. Kobayashi and C. Almeida, “Fiber optic interconnection devices for in-vehicle communication”, in *MOC2017*, Yokohama: The Microoptics Group, 2017, pp. 30–31. DOI: 10.23919/MOC.2017.8244481.

[42] D. Kraus, E. Leitgeb, T. Plank, and M. Loschnigg, “Replacement of the Controller Area Network (CAN) protocol for future automotive bus system solutions by substitution via optical networks”, in *2016 18th International Conference on Transparent Optical Networks (ICTON)*, Piscataway, NJ: IEEE, 2016, pp. 1–8. DOI: 10.1109/ICTON.2016.7550335.

[43] H. Pan *et al.*, “10.3 An analog front-end for 100BASE-T1 automotive Ethernet in 28nm CMOS”, in *2016 IEEE International Solid-State Circuits Conference*, L. C. Fujino and J. H. Anderson, Eds., Piscataway, NJ: IEEE, January 2016, pp. 186–187. DOI: 10.1109/ISSCC.2016.7417969.

[44] *802.3bv-2017 - IEEE standard for ethernet amendment 9: physical layer specifications and management parameters for 1000 mb/s operation over plastic optical fiber: IEEE Standard for Ethernet Am.* NY: IEEE, 2017. [Online]. Available: http://ieeexplore.ieee.org/servlet/opac?punumber=7875373.

[45] O. Ciordia, R. Perez, and C. Pardo, “Optical communications for next generation automotive networks”, in *MOC2017*, Yokohama: The Microoptics Group, 2017, pp. 24–25. DOI: 10.23919/MOC.2017.8244478.

[46] M. Meier, “Local interconnect network”, 2007. [Online]. Available: https://ess.cs.tu-dortmund.de/Teaching/PGs/autolab/ausarbeitungen/Meier-LIN-Ausarbeitung.pdf.

[47] T. Steinbach, “Ethernet-basierte Fahrzeugnetzwerkarchitekturen für zukünftige Echtzeitsysteme im Automobil”, Dissertation / Dissertation. DOI: 10.1007/978-3-658-23500-0.

[48] S. Kang, S. Han, S. Cho, D. Jang, H. Choi, and J.-W. Choi, “High speed CAN transmission scheme supporting data rate of over 100 Mb/s”, *IEEE Communications Magazine*, vol. 54, no. 6, pp. 128–135, 2016. DOI: 10.1109/MCOM.2016.7498099.

[49] Y. B. Pradeep, “CAN-FD and ethernet create fast reliable automotive data buses for the next decade”, *Automotive Compilation*, vol. 10, 2013.

[50] W. Lawrenz, Ed., *CAN System Engineering: From Theory to Practical Applications*, 2nd ed. 2013. London and s.l.: Springer London, 2013. DOI: 10.1007/978-1-4471-5613-0. [Online]. Available: http://gbv.eblib.com/patron/FullRecord.aspx?p=1592327.

[51] O. Strobel, *Communication in transportation systems*. Hershey, Pa: IGI Global (701 E. Chocolate Avenue Hershey Pennsylvania 17033 USA), 2013.

DOI: 10.4018/978-1-4666-2976-9. [Online]. Available: http://services.igi-global.com/resolvedoi/resolve.aspx?doi=10.4018/978-1-4666-2976-9.

[52] M. Jones, *Time is Right for Automotive Ethernet*, Micrel Inc., Ed., San José, USA, 2012. [Online]. Available: https://pdfs.semanticscholar.org/475c/b1fdac70f7bd501193%2003146e6495e94d8d88.pdf.

[53] W. Steiner, P. Heise, and S. Schneele, "Recent IEEE 802 developments and their relevance for the avionics industry", in *IEEE/AIAA 33rd Digital Avionics Systems Conference (DASC), 2014*, Piscataway, NJ: IEEE, 2014, 2A2-1-2A2–12. DOI: 10.1109/DASC.2014.6979419.

[54] *IEEE Standard for Information Technology - Telecommunications and information exchange between systems - Local and Metropolitan Area Networks - Part 3: Carrier Sense Multiple Access with Collision Detection (CSMA/CD) Access Method and Physical Layer Specifications - Physical Layer Parameters and Specifications for 1000 Mb/s Operation over 4 pair of Category 5 Balanced Copper Cabling, Type 1000BASE-T*, Piscataway, NJ, USA. DOI: 10.1109/IEEESTD.1999.90568.

[55] V. A. Pedroni, *Digital electronics and design with VHDL*. Amsterdam: Elsevier, 2008. [Online]. Available: http://site.ebrary.com/lib/alltitles/docDetail.action?docID=10520768.

[56] M. Moussavi, *Data communication and networking: A practical approach*. Clifton Park, N.Y.: Delmar, 2012.

[57] C. E. Spurgeon and J. Zimmerman, *Ethernet*, 2nd ed. Sebastopol: O'Reilly Media, 2014.

[58] A. Elefsiniotis and S. Hahn, "Aircraft harness measurement campaign and investigations on introducing one pair Ethernet", in *2016 17th International Telecommunications Network Strategy and Planning Symposium (Networks)*, Z. Dziong, J.-C. Grégoire, and J. Rak, Eds., Piscataway, NJ: IEEE, 2016, pp. 207–212. DOI: 10.1109/NETWKS.2016.7751177.

[59] S. Liu, J. Tang, Z. Zhang, and J.-L. Gaudiot, "Computer Architectures for Autonomous Driving", *Computer*, vol. 50, no. 8, pp. 18–25, 2017. DOI: 10.1109/MC.2017.3001256.

[60] Adam Grzywaczewski, *Training AI for Self-Driving Vehicles: the Challenge of Scale*, Nvidia, Ed., 2017. [Online]. Available: https://devblogs.nvidia.com/training-self-driving-vehicles-challenge-scale/.

[61] B. Sander, B. Sander, Y. Asheshov, *Migrating From CAN(-FD) to 10BASE-T1S*, Microchip, Ed., Munich, Germany, 2019.

[62] Broadcom Corporation, *OPEN Alliance BroadR-Reach (OABR) . Physical Layer Transceiver Specification For Automotive Applications - V3.2*, Broadcom Corporation, Ed.

[63] Bernd Körber, *100BASE-T1 EMC Measurement Specification for Transceivers*, Open Alliance, Ed. [Online]. Available: http://www.opensig.org/download/document/212/OA+100Base-T1_Transceiver+EMC+Specification_v1.0_17.pdf.

[64] H. Leier, L. Reiter, S. Lindenmeier, M. Spägele, and S. Buntz, "Reduction of differential-mode to common-mode conversion by means of analytic description in common-mode chokes used for an automotive communication bus system", *IET Science, Measurement & Technology*, vol. 8, no. 2, pp. 74–80, 2014. DOI: 10.1049/iet-smt.2013.0055.

[65] M. Spägele *et al.*, Eds., *Radiated Emission of automotive communication bus systems caused by mode-conversion of common-mode chokes and in-line-connectors*, IEEE, 2013.

[66] T. Makharashvili, B. Booth, K. Martin, J. Drewniak, and D. G. Beetner, "Study of alien crosstalk to a BroadR-Reach protocol based system", in *2016 IEEE International Symposium on Electromagnetic Compatibility (EMC 2016)*, Piscataway, NJ: IEEE, 2016, pp. 379–384. DOI: 10.1109/ISEMC.2016.7571677.

[67] MARVELL®, *88Q2110/88Q2112 100/1000BASE-T1 PHY - 100/1000Mbps IEEE 802.3bp compliant Automotive Ethernet PHY*, MARVELL®, Ed. [Online]. Available: https://www.marvell.com/documents/a4xrw9eplode5btwxs7k/.

[68] IEEE Standard 1Gbit/s, *IEEE Standard for Ethernet Amendment 4: Physical Layer Specifications and Management Parameters for 1 Gb/s Operation over a Single Twisted-Pair Copper Cable*, Piscataway, NJ, USA. DOI: 10.1109/IEEESTD.2016.7564011.

[69] Bernd Körber, *1000BASE-T1 EMC Measurement Specification for Transceivers*, Open Alliance, Ed. [Online]. Available: http://www.opensig.org/download/document/229/OA+1000Base-T1_Transceiver+EMC+Specification_v1.0_18.pdf.

[70] ——, *1000BASE-T1 EMC Test Specification for Common Mode Chokes*, Open Alliance, Ed. [Online]. Available: http://www.opensig.org/download/datasets/2904/OA-1000Base-T1_CMC-Test-Specification-v1.0.pdf.

[71] IEEE 802.3 MULTI-GIG AUTOMOTIVE ETHERNET PHY, *Adopted Objectives Approved by 802.3 WG 16 March 2017*. [Online]. Available: http://www.ieee802.org/3/ch/0317_approved_objectives_3NGAUTO.pdf.

[72] Jim Graba, Tom Souvignier, and Mike Tu, *PCS Changes For Asymmetrical Data Transmission*, IEEE 802.3ch Multi-gig Automotive Ethernet PHY Task Force, Ed., Spokane, WA, USA. [Online]. Available: http://www.ieee802.org/3/ch/public/sep18/souvignier_3ch_01_0918.pdf.

[73] Mike Tu, *RS FEC Proposal for Multi-Gigabit Automotive PHY*, IEEE 802.3ch Multi-gig Automotive Ethernet PHY Task Force, Ed., San Diego, CA, USA. [Online]. Available: http://www.ieee802.org/3/ch/public/jul18/tu_3ch_01b_0718.pdf.

[74] Paul Langner, *802.3ch PCS + FEC Design*, IEEE 802.3ch Multi-gig Automotive Ethernet PHY Task Force, Ed., Spokane, WA, USA. [Online]. Available: http://www.ieee802.org/3/ch/public/sep18/langner_3ch_01a_0918.pdf.

[75] Sujan Pandey, *Multi-Gig PHYs Channel Code Proposal*, IEEE 802.3ch Multi-gig Automotive Ethernet PHY Task Force, Ed., San Diego, CA, USA.

[76] Thomas Müller, *802.3ch channel options*, IEEE 802.3ch Multi-gig Automotive Ethernet PHY Task Force, Ed., Berlin, Germany. [Online]. Available: http://www.ieee802.org/3/ch/public/jul17/mueller_channel_options_01a_0717.pdf.

[77] Ramin Farjadrad, *Channel Requirements for Optimum/Robust PHY Design Beyond 1000BASE-T1*, IEEE 802.3ch Multi-gig Automotive Ethernet PHY Task Force, Ed., Orlando, FL, USA. [Online]. Available: http://www.ieee802.org/3/ch/public/nov17/Farjadrad_3ch_01b_1117.pdf.

[78] Hossein Sedarat and Ramin Shirani, *Considerations for Coding and Baud Rate of a Multi -Gig Phy for Automotive*, IEEE 802.3ch Multi-gig Automotive Ethernet PHY Task Force, Ed., Berlin, Germany. [Online]. Available: http://www.ieee802.org/3/ch/public/jul17/Sedarat_Shirani_3ch_02_0717.pdf.

[79] Peter Wu, *Multi-level PAM Study for M-Gig Automotive PHYs*, IEEE 802.3ch Multi-gig Automotive Ethernet PHY Task Force, Ed., Charlotte, NC, USA. [Online]. Available: http://www.ieee802.org/3/ch/public/sep17/wu_3ch_01_0917.pdf.

[80] Ramin Farjadrad, *Channel Selection Tradeoffs for Automotive 2.5G/5.0G/10Gbps*, IEEE 802.3ch Multi-gig Automotive Ethernet PHY Task Force, Ed., Rosemont, IL, USA. [Online]. Available: http://www.ieee802.org/3/ch/public/mar18/Farjadrad_3ch_01d_0318.pdf.

[81] OLAF GRAU, *3GHZ BANDWITDH STP CABLES USE FOR 2,5/5/10GB/S SPEED GRADES*, IEEE 802.3ch Multi-gig Automotive Ethernet PHY Task Force, Ed., Rosemont, IL, USA. [Online]. Available: http://www.ieee802.org/3/ch/public/mar18/grau_3ch_01c_0318.pdf.

[82] Mike Tu, *Proposal for 2.5G/5G/10GBASE-T1 Transmit Voltage Level*, IEEE 802.3ch Multi-gig Automotive Ethernet PHY Task Force, Ed., Pittsburgh, PA, USA. [Online]. Available: http://www.ieee802.org/3/ch/public/may18/tu_3ch_02a_0518.pdf.

[83] Tom Souvignier, *Bandwidth, Modulation and SNR Comparison for Multi-Gigabit Automotive PHY*, IEEE 802.3ch Multi-gig Automotive Ethernet PHY Task Force, Ed., Pittsburgh, PA, USA. [Online]. Available: http://www.ieee802.org/3/ch/public/may18/souvignier_3ch_01c_0518.pdf.

[84] Ramin Farjadrad, *2.5Gbps Implementation Considerations*, IEEE 802.3ch Multi-gig Automotive Ethernet PHY Task Force, Ed., San Diego, CA, USA. [Online]. Available: http://www.ieee802.org/3/ch/public/jul18/farjarad_3ch_02c_0718.pdf.

[85] Hideki Goto *et al.*, *End User PHY Preferences*, IEEE 802.3ch Multi-gig Automotive Ethernet PHY Task Force, Ed., San Diego, CA, USA. [Online]. Available: http://www.ieee802.org/3/ch/public/jul18/wienckowski_3ch_01a_0718.pdf.

[86] Sujan Pandey, *2.5G and 10G PHYs Modulation Scheme Proposal*, IEEE 802.3ch Multi-gig Automotive Ethernet PHY Task Force, Ed., Pittsburgh, PA, USA. [Online]. Available: http://www.ieee802.org/3/ch/public/may18/Pandey_3ch_01c_0518.pdf.

[87] Ramin Farjadrad and George Zimmerman, *Power/Area Tradeoffs in Multi-Gig BASE-T1 PHYs*, IEEE 802.3ch Multi-gig Automotive Ethernet PHY Task Force, Ed., Pittsburgh, PA, USA. [Online]. Available: http://www.ieee802.org/3/ch/public/may18/Farjadrad_3ch_01a_0518.pdf.

[88] Gerrit W. den Besten, *Line modulation considerations for 2.5Gbps and 5/10Gbps Automotive Ethernet*, IEEE 802.3ch Multi-gig Automotive Ethernet PHY Task Force, Ed., San Diego, CA, USA. [Online]. Available: http://www.ieee802.org/3/ch/public/jul18/DenBesten_3ch_01a_0718.pdf.

[89] Sujan Pandey, *Scrambler Options for Multi-Gig PHYs*, IEEE 802.3ch Multi-gig Automotive Ethernet PHY Task Force, Ed., Bangkok, Thailand. [Online]. Available: http://www.ieee802.org/3/ch/public/nov18/Pandey_3ch_01_1118.pdf.

[90] George Zimmerman, *Energy Efficient Ethernet, Wake Signals and Deep Sleep for Automotive Ethernet*, IEEE 802.3ch Multi-gig Automotive Ethernet PHY Task Force, Ed., Berlin, Germany. [Online]. Available: http://www.ieee802.org/3/ch/public/jul17/zimmerman_3ch_02a_0717.pdf.

[91] Natalie A. Wienckowski, *AUTOMOTIVE WAKEUP METHODS*, IEEE 802.3ch Multi-gig Automotive Ethernet PHY Task Force, Ed., Charlotte,

NC, USA. [Online]. Available: http://www.ieee802.org/3/ch/public/sep17/Wienckowski_3ch_01a_0917.pdf.

[92] Saied Benyamin, Paul Langner, and George Zimmerman, *EEE Ultra Low Power Mode*, IEEE 802.3ch Multi-gig Automotive Ethernet PHY Task Force, Ed., Bangkok, Thailand. [Online]. Available: http://www.ieee802.org/3/ch/public/nov18/Benyamin_Langner_Zimmerman_3ch_01_1118.pdf.

[93] Tom Souvignier, Mike Tu, and Jim Graba, *Asymmetrical Data Transmission*, IEEE 802.3ch Multi-gig Automotive Ethernet PHY Task Force, Ed., San Diego, CA, USA. [Online]. Available: http://www.ieee802.org/3/ch/public/jul18/souvignier_3ch_01a_0718.pdf.

[94] Natalie Wienckowski, *P802.3ch PHY Power and PoDL*, IEEE 802.3ch Multi-gig Automotive Ethernet PHY Task Force, Ed., Rosemont, IL, USA. [Online]. Available: http://www.ieee802.org/3/ch/public/mar18/wienckowski_3ch_03_0318.pdf.

[95] Sujan Pandey, *Multi-Gig PHY Emission Performance Investigation*, IEEE 802.3ch Multi-gig Automotive Ethernet PHY Task Force, Ed., Geneva, Switzerland. [Online]. Available: http://www.ieee802.org/3/ch/public/jan18/Pandey_3ch_01_0118.pdf.

[96] Gerrit W. den Besten, *Transmit PSD mask*, IEEE 802.3ch Multi-gig Automotive Ethernet PHY Task Force, Ed., Warren, MI, USA. [Online]. Available: http://www.ieee802.org/3/ch/public/apr19/DenBesten_3ch_01_0419.pdf.

[97] Ramin Farjadrad, *Transmit Power Spec*, IEEE 802.3ch Multi-gig Automotive Ethernet PHY Task Force, Ed., Vienna, Austria. [Online]. Available: http://www.ieee802.org/3/ch/public/jul19/Farjadrad_3ch_03a_0719.pdf.

[98] Kadir Dinc and Tom Souvignier, *Transmitter PSD Masks*, IEEE 802.3ch Multi-gig Automotive Ethernet PHY Task Force, Ed. [Online]. Available: http://www.ieee802.org/3/ch/public/nov18/souvignier_3ch_04_1118.pdf.

[99] Gerrit den Besten, *Transmit PSD mask*, IEEE 802.3ch Multi-gig Automotive Ethernet PHY Task Force, Ed., Vienna, Austria. [Online]. Available: http://www.ieee802.org/3/ch/public/apr19/DenBesten_3ch_01_0419.pdf.

[100] Thomas Müller, *802.3ch alien crosstalk rejection*, IEEE 802.3ch Multi-gig Automotive Ethernet PHY Task Force, Ed., Vancouver, BC. [Online]. Available: http://www.ieee802.org/3/ch/public/mar19/mueller_3ch_02a_0319.pdf.

[101] B. B. Eric DiBiaso, *Media Considerations - Insertion Loss and EMC*, IEEE 802.3ch Multi-gig Automotive Ethernet PHY Task Force, Ed., New Orleans, LA, USA. [Online]. Available: http://www.ieee802.org/3/ch/public/may17/DiBiaso_3NGAUTO_01_0517.pdf.

[102] OLAF GRAU, *SOME REMARKS/THOUGHTS ABOUT AUTOMOTIVE MULTIGIG LINK SEGMENTS: (SINGLE ENDED SIGNALING, E.G. COAX OR DIFFERENTIAL SIGNALING, E.G. STP)*, IEEE 802.3ch Multi-gig Automotive Ethernet PHY Task Force, Ed., New Orleans, LA, USA. [Online]. Available: http://www.ieee802.org/3/ch/public/may17/grau_3NGAUTO_02_0517.pdf.

[103] Olaf Krieger, Christoph Wechsler, and Keld Lange, *Typical Automotive Harness Topologies*, IEEE 802.3ch Multi-gig Automotive Ethernet PHY Task Force, Ed., Rosemont, IL, USA. [Online]. Available: http://www.ieee802.org/3/ch/public/mar18/krieger_3ch_01a_0318.pdf.

[104] Natalie A. Wienckowski, *POTENTIAL MULTI-GIG ETHERNET TOPOLOGIES FOR GENERAL MOTORS*, IEEE 802.3ch Multi-gig Automotive Ethernet PHY Task Force, Ed., Rosemont, IL, USA. [Online]. Available: http://grouper.ieee.org/groups/802/3/ch/public/adhoc/wienckowski_3ch_01a_022118.pdf.

[105] Doug Oliver and James Lawlis, *POTENTIAL MULTI-GIG ETHERNET TOPOLOGIES*, IEEE 802.3ch Multi-gig Automotive Ethernet PHY Task Force, Ed., Rosemont, IL, USA. [Online]. Available: http://www.ieee802.org/3/ch/public/mar18/oliver_3ch_01_0318.pdf.

[106] Larry Cohen and Ramin Shirani, *Initial RF Ingress Measurements for Coaxial and UTP Cables from Automotive BCI Test*, IEEE 802.3ch Multi-gig Automotive Ethernet PHY Task Force, Ed., New Orleans, LA, USA. [Online]. Available: http://www.ieee802.org/3/ch/public/may17/cohen_shirani_3ch_01_0517.pdf.

[107] ——, *RF Ingress Measurements for Shielded Twisted Pair (STP) Cables from Automotive BCI Test*, IEEE 802.3ch Multi-gig Automotive Ethernet PHY Task Force, Ed., Berlin, Germany. [Online]. Available: http://www.ieee802.org/3/ch/public/jul17/cohen_shirani_3ch_01_0717.pdf.

[108] Thomas Müller, *802.3ch coupling attenuation and BCI ingress noise*, IEEE 802.3ch Multi-gig Automotive Ethernet PHY Task Force, Ed., Orlando, FL, USA. [Online]. Available: http://www.ieee802.org/3/ch/public/nov17/mueller_3ch_01_1117.pdf.

[109] Larry Cohen and Ramin Shirani, *RF Ingress Measurements for STP Cables from Automotive ALSE Test*, IEEE 802.3ch Multi-gig Automotive Ethernet PHY Task Force, Ed., Berlin, Germany. [Online]. Available: http://www.ieee802.org/3/ch/public/nov17/Cohen_Shirani_3ch_01_1108.pdf.

[110] Thomas Müller, *802.3ch ALSE ingress noise*, IEEE 802.3ch Multi-gig Automotive Ethernet PHY Task Force, Ed., Pittsburgh, PA, USA. [Online]. Available: http://www.ieee802.org/3/ch/public/may18/mueller_3ch_03_0518.pdf.

[111] Ramin Farjadrad and Larry Cohen, *A Proposed Specification for RFI Ingress Limit in 802.3ch Automotive Links*, IEEE 802.3ch Multi-gig Automotive Ethernet PHY Task Force, Ed., Spokane, WA, USA. [Online]. Available: http://www.ieee802.org/3/ch/public/sep18/farjarad_3ch_01b_0918.pdf.

[112] Taketo Kumada, *STP cable in automotive environment*, IEEE 802.3ch Multi-gig Automotive Ethernet PHY Task Force, Ed., Orlando, FL, USA. [Online]. Available: http://www.ieee802.org/3/ch/public/nov17/kumada_3ch_01_1117.pdf.

[113] ——, *STP cable - Analysis of insertion loss degradation in high temperature atmosphere*, IEEE 802.3ch Multi-gig Automotive Ethernet PHY Task Force, Ed., Geneva, Switzerland. [Online]. Available: http://www.ieee802.org/3/ch/public/jan18/kumada_3ch_01a_0118.pdf.

[114] Bert Bergner, Eric DiBiaso, Chris Mandel, *Approach for Link Segment Transmission Parameter Definition*, TE Connectivity, Ed., Geneva, Switzerland. [Online]. Available: http://www.ieee802.org/3/ch/public/jan18/Bergner_DiBiaso_3ch_01b_0118.pdf.

[115] E. D. Bert Bergner, *Automotive Link Segment Analysis for NGAuto*, IEEE 802.3ch Multi-gig Automotive Ethernet PHY Task Force, Ed., Charlotte, NC, USA. [Online]. Available: http://www.ieee802.org/3/ch/public/sep17/DiBiaso_3ch_01a_0917.pdf.

[116] Natalie A. Wienckowski, *NGAUTO Proposed Cable Limits*, IEEE 802.3ch Multi-gig Automotive Ethernet PHY Task Force, Ed., Geneva, Switzerland. [Online]. Available: http://www.ieee802.org/3/ch/public/jan18/wienckowski_3ch_01a_0118.pdf.

[117] Ramin Farjadrad, *Channel Requirements for Optimum/Robust PHY Design 10GBASE-T1*, IEEE 802.3ch Multi-gig Automotive Ethernet PHY Task Force, Ed., Geneva, Switzerland. [Online]. Available: http://www.ieee802.org/3/ch/public/jan18/Farjad_3ch_01b_0118.pdf.

[118] Eric DiBiaso, Bert Bergner, Chris Mandel, *High Speed Channel Modeling and Analysis - Part 2*, IEEE 802.3ch Multi-gig Automotive Ethernet PHY Task Force, Ed., Pittsburgh, PA, USA. [Online]. Available: http://www.ieee802.org/3/ch/public/may18/DiBiaso_3ch_01_0518.pdf.

[119] Eric DiBiaso, *Insertion Loss Limit Analysis*, IEEE 802.3ch Multi-gig Automotive Ethernet PHY Task Force, Ed., San Diego, CA, USA. [Online]. Available: http://www.ieee802.org/3/ch/public/jul18/DiBiaso_3ch_01_0718.pdf.

[120] Ricky Vernickel, *Actual Cable Data update*, IEEE 802.3ch Multi-gig Automotive Ethernet PHY Task Force, Ed., Bangkok, Thailand. [Online]. Available: http://www.ieee802.org/3/ch/public/nov18/vernickel_3ch_01c_1118.pdf.

[121] Gerrit den Besten, Ricky Vernickel, Thomas Müller, and Josef Ohni, *Insertion Loss limit update proposal*, IEEE 802.3ch Multi-gig Automotive Ethernet PHY Task Force, Ed., Bangkok, Thailand. [Online]. Available: http://www.ieee802.org/3/ch/public/nov18/DenBesten_3ch_05_1118.pdf.

[122] Josef Ohni, *802.3ch channel performance at different temperatures*, IEEE 802.3ch Multi-gig Automotive Ethernet PHY Task Force, Ed., Pittsburgh, PA, USA. [Online]. Available: http://www.ieee802.org/3/ch/public/may18/ohni_3ch_01a_0518.pdf.

[123] B. Mund and C. Pfeiler, *Balunless measurement of coupling attenuation of screened balanced cables up to 2 GHz*, Anwenderforum Elektrische Kabel, Technische Akademie Esslingen, Ed., Esslingen, Germany. [Online]. Available: http://www.bmund.de/pdf-03/TAE%202014%20ac%20up%20to%202GHz%2020141003.pdf.

[124] Gerrit W. den Besten, *Coupling & shielding attenuation*, IEEE 802.3ch Multi-gig Automotive Ethernet PHY Task Force, Ed., Spokane, WA, USA. [Online]. Available: http://www.ieee802.org/3/ch/public/sep18/DenBesten_3ch_02b_0918.pdf.

[125] E. D. Bert Bergner, *SDP Screening & Coupling Attenuation for 802.3ch*, IEEE 802.3ch Multi-gig Automotive Ethernet PHY Task Force, Ed., Orlando, FL, USA. [Online]. Available: http://www.ieee802.org/3/ch/public/nov17/DiBiaso_Bergner_3ch_01_1117.pdf.

[126] Thomas Müller, *802.3ch coupling attenuation*, IEEE 802.3ch Multi-gig Automotive Ethernet PHY Task Force, Ed., Pittsburgh, PA, USA. [Online]. Available: http://www.ieee802.org/3/ch/public/may18/mueller_3ch_02a_0518.pdf.

[127] Josef Ohni, *Coupling Attenuation and IL Limit Proposal for 2.5 Gbit/s*, IEEE 802.3ch Multi-gig Automotive Ethernet PHY Task Force, Ed., Bangkok, Thailand. [Online]. Available: http://www.ieee802.org/3/ch/public/nov18/ohni_3ch_01a_1118.pdf.

[128] L. Halme and B. Mund, "EMC of Cables, Connectors and Components with Triaxial Test set-up", *Transfer*, vol. 62153, pp. 4–15, 2013. [Online]. Available: http://www.bmund.de/pdf-03/IWCS%20-%20Halme_Mund%20-%20EMC%20of%20Cables,%20Connectors.pdf.

[129] Thomas Müller, *802.3ch screening attenuation measurement results*, IEEE 802.3ch Multi-gig Automotive Ethernet PHY Task Force, Ed., Bangkok, Thailand. [Online]. Available: http://www.ieee802.org/3/ch/public/nov18/mueller_3ch_01a_1118.pdf.

[130] E. D. Bert Bergner, *Automotive Link Segment Analysis for NGAuto*, IEEE 802.3ch Multi-gig Automotive Ethernet PHY Task Force, Ed., Charlotte,

NC, USA. [Online]. Available: http://www.ieee802.org/3/ch/public/sep17/DiBiaso_3ch_01a_0917.pdf.

[131] Ali Javed and Mike Gardner, *Proposed Link Segment Configuration Test results*, IEEE 802.3ch Multi-gig Automotive Ethernet PHY Task Force, Ed., Charlotte, NC, USA. [Online]. Available: http://www.ieee802.org/3/ch/public/sep17/Javed_3ch_01_0917.pdf.

[132] Olaf Krieger, Christoph Wechsler, and Keld Lange, *Impact of used frequency spectrum on the automotive harness*, IEEE 802.3ch Multi-gig Automotive Ethernet PHY Task Force, Ed., Rosemont, IL, USA. [Online]. Available: http://www.ieee802.org/3/ch/public/mar18/krieger_3ch_02b_0318.pdf.

[133] Gerrit den Besten, Gitesh Bhagwat, Kambiz Vakilian, Mike Tu, *MDI Return Loss Consensus proposal*, IEEE 802.3ch Multi-gig Automotive Ethernet PHY Task Force, Ed., Vienna, Austria. [Online]. Available: http://www.ieee802.org/3/ch/public/jul19/DenBesten_3ch_03a_0719.pdf.

[134] Kambiz Vakilian, Kadir Dinc, German Feyh, Mike Tu, and Tom Souvignier, *MDI Return Loss Limit*, IEEE 802.3ch Multi-gig Automotive Ethernet PHY Task Force, Ed., Vienna, Austria. [Online]. Available: http://www.ieee802.org/3/ch/public/jul19/vakilian_3ch_01_0719.pdf.

[135] Natalie A. Wienckowski, *ECU Start-Up Requirements*, IEEE 802.3ch Multi-gig Automotive Ethernet PHY Task Force, Ed., New Orleans, LA, USA. [Online]. Available: http://www.ieee802.org/3/ch/public/may17/Wienckowski_3NGAUTO_01_0517.pdf.

[136] S. Carlson, *10G+ Automotive Ethernet Electrical PHYs - Call for Interest Consensus Meeting*, C. Mash, C. Wechsler, H. Zinner, O. Grau, N. Wienckowski, Ed., Vancouver, BC. [Online]. Available: http://grouper.ieee.org/groups/802/3/cfi/0319_1/CFI_01_0319.pdf.

[137] F. Nakamoto, T. Uchida, C. Miyazaki, N. Oka, and K. Misu, "A simplified model of a common mode choke coil for 3D field simulators", in *IEEE International Symposium on Electromagnetic Compatibility (EMC), 2012*, Piscataway, NJ: IEEE, 2012, pp. 617–622. DOI: 10.1109/ISEMC.2012.6351690.

[138] T. Hoshino, F. Amemiya, and N. Kuwabara, "Evaluation method of common-mode choke coil used for high speed telecommunications port", in *EMC 2005*, Piscataway, N.J: Institute of Electrical and Electronics Engineers, 2005, pp. 210–215. DOI: 10.1109/ISEMC.2005.1513502.

[139] V. Zwillich, W. Menzel, and H. Leier, "Worst case signal integrity analysis for in-vehicle data transmission via UTP cables", in *EMC Zurich 2007*, Piscataway, NJ: IEEE, 2007, pp. 159–162. DOI: 10.1109/EMCZUR.2007.4388220.

[140] M. Spägele *et al.*, "Radiated emission of automotive communication bus systems caused by mode-conversion of common-mode chokes and in-line-connectors", in *2013 International Symposium on Electromagnetic, Brugge, Belgium, 2013*, pp. 455–460.

[141] Z. Li, D. Pommerenke, and Y. Shimoshio, "Common-mode and differential-mode analysis of common-mode chokes", in *2003 IEEE Symposium on Electromagnetic Compatibility*, Piscataway, N.J: IEEE, 2003, pp. 384–387. DOI: 10.1109/ISEMC.2003.1236626.

[142] J.-L. Kotny, X. Margueron, and N. Idir, "High-Frequency Model of the Coupled Inductors Used in EMI Filters", *IEEE Transactions on Power Electronics*, vol. 27, no. 6, pp. 2805–2812, 2012. DOI: 10.1109/TPEL.2011.2175452.

[143] B. Razavi, *Design of analog CMOS integrated circuits*, Tata McGraw-Hill ed., ser. McGraw-Hill series in electrical and computer engineering. Circuits and systems. New Delhi and New York: Tata McGraw-Hill Pub. Co. Ltd, 2002, 2010.

[144] Life.augmented, *AN4511 Application note - Common mode filters*, 2016. [Online]. Available: https://www.st.com/content/ccc/resource/technical/document/application_note/d2/4d/6f/9d/bc/80/4d/97/DM00119609.pdf/files/DM00119609.pdf/jcr:content/translations/en.DM00119609.pdf.

[145] J.-K. Lee, W.-S. Kim, J. H. Kim, S. Lee, G. Cha, and S.-Y. Hahn, "Experimental result of transport current loss in bifilar winding solenoid type HTS coil", *IEEE Transactions on Appiled Superconductivity*, vol. 11, no. 1, pp. 2228–2231, 2001. DOI: 10.1109/77.920302.

[146] Q. Yu, T. W. Holmes, and K. Naishadham, "RF equivalent circuit modeling of ferrite-core inductors and characterization of core materials", *IEEE Transactions on Electromagnetic Compatibility*, vol. 44, no. 1, pp. 258–262, 2002. DOI: 10.1109/15.990733.

[147] M. Ai-Hamid, R. Vick, M. Krüger and T. Rinkleff, "Determination of equivalent circuit parameters of current compensated chokes and their use in filters with an application example", in *International Symposium on Electromagnetic Compatibility, Brugge, 2013*, pp. 1022–1027.

[148] Dr. Bernd Körber, *EMC Test Specification for BroadR-Reach Common Mode Chokes*, 2014. [Online]. Available: https://docplayer.net/65319200-Emc-test-specification-for-broadr-reach-common-mode-chokes.html.

[149] Bernd Körber, *100BASE-T1 EMC Test Specification for Common Mode Chokes*, Open Alliance, Ed. [Online]. Available: http://www.opensig.org/download/document/213/OA+100Base-T1_CMC+Test+Specification+v1.0_17.pdf.

[150] K. Matheus and T. Königseder, *Automotive Ethernet*. Cambridge: Cambridge University Press, 2015. DOI: 10.1017/CBO9781107414884. [Online]. Available: https://doi.org/10.1017/CBO9781107414884.

[151] W. Zimmermann and R. Schmidgall, *Bussysteme in der Fahrzeugtechnik: Protokolle, Standards und Softwarearchitektur*, 5., aktual. und erw. Aufl., ser. ATZ / MTZ-Fachbuch. Wiesbaden: Springer Vieweg, 2014. DOI: 10.1007/978-3-658-02419-2. [Online]. Available: http://gbv.eblib.com/patron/FullRecord.aspx?p=1783365.

[152] B. Körber *et al.*, "Ethernet für Kfz- Anwendungen – Randbedingungen und EMV- optimierte Lösungen", in *2013 International Symposium on Electromagnetic Compatibility*, 2013.

[153] D. Reynders and E. Wright, *Practical TCP/IP and Ethernet Networking for Industry*, 1. Aufl. s.l.: Elsevier professional, 2003. [Online]. Available: http://gbv.eblib.com/patron/FullRecord.aspx?p=288884.

[154] BROADCOM, *BroadR-Reach Physical Layer Transceiver Specification for Automotive App*, Broadcom Corporation, Ed., 2014. [Online]. Available: http://www.ieee802.org/3/1TPCESG/public/BroadR_Reach_Automotive_Spec_V3.0.pdf.

[155] "IEEE Approved Draft Standard for Ethernet Amendment 4: Physical Layer Specifications and Management Parameters for 1 Gb/s Operation over a Single Twisted Pair Copper Cable: IEEE P802.3bp/D3.4, April 2016 (Amendment of IEEE Std 802.3-2015 as amended by IEEE Std 802.3bw-2015, IEEE Std 802.3by-201X, and IEEE Std 802.3bq-201X)", *IEEE P802.3bp/D3.4, April 2016 (Amendment of IEEE Std 802.3-2015 as amended by IEEE Std 802.3bw-2015, IEEE Std 802.3by-201X, and IEEE Std 802.3bq-201X)*, pp. 1–220, 1 Jan. 2016.

[156] William Lo, Zhenyu Liu, Marvell, *Training & EEE Baseline Proposal*, IEEE 802.3bp - Interim Meeting - September 2014, Ed. [Online]. Available: http://www.ieee802.org/3/bp/public/sep14/Lo_3bp_01a_0914.pdf.

[157] Steve Carlson, *IEEE 802.3ch Multi-Gig Automotive Ethernet - PHY Task Force - Opening Report*, High Speed Design, Inc./Robert Bosch GmbH, Ed., Orlando, FL, USA. [Online]. Available: http://grouper.ieee.org/groups/802/3/minutes/nov17/1117_ch_open_report.pdf.

[158] S. Mortazavi, D. Schleicher, F. Schade, C. Gremzow, and F. Gerfers, "Toward Investigation of the Multi-Gig Data Transmission up to 5 Gbps in Vehicle and Corresponding EMC Interferences", in *2018 International Symposium on Electromagnetic Compatibility*, Piscataway, NJ: IEEE, 2018, pp. 60–65. DOI: 10.1109/EMCEurope.2018.8485142.

[159] G. d. Vendelin, A. M. Pavio, and U. L. Rohde, *Microwave circuit design using linear and nonlinear techniques*, 2. ed. Hoboken, NJ: Wiley, 2005. DOI: 10.1002/0471715832. [Online]. Available: http://search.ebscohost.com/login.aspx?direct=true&scope=site&db=nlebk&db=nlabk&AN=140460.

[160] S. Mortazavi, D. Schleicher, and F. Gerfers, "Characterization of common-mode choke for automotive ethernet networks enabling 100 Mbit/s", in *2017 International Symposium on Electromagnetic Compatibility - EMC Europe*, Piscataway, NJ: IEEE, 2017, pp. 1–6. DOI: 10.1109/EMCEurope.2017.8094720.

[161] NXP Semiconductors, *AN12088 - Application hints for TJA1100 Automotive Ethernet PHY*, NXP Semiconductors, Ed., 28.08.2017. [Online]. Available: https://www.nxp.com/docs/en/application-note/AN12088.pdf.

[162] M. Bargende, H.-C. Reuss, and J. Wiedemann, Eds., *15. Internationales Stuttgarter Symposium: Automobil- und Motorentechnik*, ser. Proceedings. Wiesbaden: Springer Vieweg, 2015. DOI: 10.1007/978-3-658-08844-6. [Online]. Available: http://dx.doi.org/10.1007/978-3-658-08844-6.

[163] IEEE 802.3 MULTI-GIG AUTOMOTIVE ETHERNET PHY - STUDY GROUP, *Adopted Objectives - Approved by 802.3 WG*, IEEE 802.3 MULTI-GIG AUTOMOTIVE ETHERNET PHY - STUDY GROUP, Ed., Vancouver, BC, Canada. [Online]. Available: http://www.ieee802.org/3/NGAUTO/0317_approved_objectives_3NGAUTO.pdf.

[164] S. Mortazavi, D. Schleicher, and F. Gerfers, "Characterization and verification of Gigabit ethernet-based bus systems in vehicles", in *2018 IEEE International Symposium on Electromagnetic Compatibility & 2018 IEEE Asia-Pacific Symposium on Electromagnetic Compatibility (EMC/APEMC)*, Piscataway, NJ: IEEE, 2018, pp. 428–433. DOI: 10.1109/ISEMC.2018.8393814.

[165] ——, "Modeling and Verification of Automotive Multi-Gig Ethernet Communication up to 2.5 Gbps and the Corresponding EMC Analysis", in *2018 IEEE Symposium on Electromagnetic Compatibility, Signal Integrity and Power Integrity (EMC, SI & PI)*, Piscataway, NJ: IEEE, 2018, pp. 329–334. DOI: 10.1109/EMCSI.2018.8495375.

[166] Ramin Farjadrad, *Channel Selection Tradeoffs for Automotive 2.5G/5.0G/10Gbps*, IEEE 802.3 Multi-Gig Automotive Ethernet PHY Task Force, Ed., Chicago. [Online]. Available: http://www.ieee802.org/3/ch/public/mar18/Farjadrad_3ch_01d_0318.pdf.

[167] S. Babenko, B.Bergner,A.Chini,M. Gardner,P. Gowravajhala,D. Ignjatovic, M. Jaenecke,A. Javed, M. Kaindl,B. Körber, B. Moffitt, T. Müller, H. Patel,N. Pischl,R. Pöhmerer, M. Rucks, M. Spägele, Y. Stricot, D. Wiesmayer, T. Wunderlich, S. Yoo, J.A. Yurtin, *Channel and Components Requirements for*

1000BASE-T1 Link Segment Type A, Open Alliance, Ed. [Online]. Available: http://opensig.org/download/document/235/TC9-Gbps-channel-and-components-2.0.pdf.

[168] Thomas Hähner, Bernhard Mund, Thomas Schmid, "History and recent trends of Triaxial test procedure", in *Proc. 67th IWCS Conference, Providence, RI, USA, Oct. 2018*. [Online]. Available: http://www.iwcs.org/66863-iwcs-1.4233397/t002-1.4234012/f0013-1.4234143/9-1-1.4234159.

[169] IEC, *Metallic communication cable test methods - Part 4 - 9: Electromagnetic compatibility (EMC) - Coupling attenuation of screened balanced cables, triaxial method*, May 2018.

[170] ——, *Metallic communication cable test methods: Electromagnetic compatibility (EMC) - Introduction to electromagnetic screening measurements*, Jan. 2014.

[171] O. Breitenbach, T. Hahner, and B. Mund, "Screening of cables in the MHz to GHz frequency range. Extended application of a simple measuring method", in *IEE Colloquium on Screening Effectiveness Measurements*, IEE, 6 May 1998, p. 7. DOI: 10.1049/ic:19980730.

[172] F. J. Furrer, *Fehlerkorrigierende Block-Codierung für die Datenübertragung*, ser. LHI36. Basel and s.l.: Birkhäuser Basel, 1981, vol. 36. DOI: 10.1007/978-3-0348-5818-2. [Online]. Available: http://dx.doi.org/10.1007/978-3-0348-5818-2.

[173] Open Alliance, *Channel and Components Requirements for 1000BASE-T1 Link Segment Type A (UTP)*, Open Alliance, Ed. [Online]. Available: http://www.opensig.org/download/document/235/TC9-Gbps-channel-and-components-2.0.pdf.

[174] Mike Jenkins and David Mahashin, *Eye Scan with MicroBlaze Processor MCS - XAPP743 (v1.0.1) - Application Note: 7 Series FPGAs*. [Online]. Available: https://www.xilinx.com/support/documentation/application_notes/xapp743-eye-scan-mb-mcs.pdf.

[175] M. Rahmani, R. Steffen, K. Tappayuthpijarn, E. Steinbach, and G. Giordano, "Performance analysis of different network topologies for in-vehicle audio and video communication", in *4th International Telecommunication Networking Workshop on QoS in Multiservice IP Networks, 2008*, Piscataway, NJ: IEEE, 2008, pp. 179–184. DOI: 10.1109/ITNEWS.2008.4488150.

[176] J. Kamieth, T. Steinbach, F. Korf, and T. C. Schmidt, "Design of TDMA-based in-car networks: Applying multiprocessor scheduling strategies on time-triggered switched ethernet communication", in *IEEE [International Conference on] Emerging Technologies and Factory Automation (ETFA),*

2014, Piscataway, NJ: IEEE, 2014, pp. 1–9. DOI: 10.1109/ETFA.2014.7005119.

[177] T. Steinbach, K. Muller, F. Korf, and R. Rollig, "Demo: Real-time Ethernet in-car backbones: First insights into an automotive prototype", in *2014 IEEE Vehicular Networking Conference (VNC)*, F. Dressler, Ed., Piscataway, NJ: IEEE, 2014, pp. 133–134. DOI: 10.1109/VNC.2014.7013331.

[178] R. Farjadrad, P. Langner, A. Razavi, G. Zimmerman, *FEC/Framing/Modulation for 10GBASE-T1 PHY*, Aquantia, Ed., USA, 2018. [Online]. Available: http://www.ieee802.org/3/ch/public/jul18/farjarad_3ch_01d_0718.pdf.

[179] S. Mortazavi, D. Schleicher, A. Stieler, A. Sinai, F. Gerfers, M. Hampe, "EMC Analysis of Shielded Twisted Pair and Shielded Parallel Pair Transmission Lines for Automotive Multi-Gig Ethernet", in *IEEE International Symposium on EMC, SI & PI, New Orleans, 2019*.

[180] C. M. Kozierok, C. Correa, R. B. Boatright, J. Quesnelle, and B. Metcalfe, *Automotive Ethernet: The definitive guide*, Edition 1.2. Madison Heights: Intrepid Control Systems, 2014.

[181] C. Gimeno Gasca, S. Celma Pueyo, and C. Aldea Chagoyen, *CMOS Continuous-Time Adaptive Equalizers for High-Speed Serial Links*, ser. Analog Circuits and Signal Processing. Cham and s.l.: Springer International Publishing, 2015. DOI: 10.1007/978-3-319-10563-5.

[182] T. Hubing, "Automotive EMC", in *IEEE International Symposium on Electromagnetic Compatibility, 2008*, Piscataway, NJ: IEEE, 2008, pp. 1–20. DOI: 10.1109/ISEMC.2008.4652192.

[183] ISO, *Road vehicles — Vehicle test methods for electrical disturbances from narrowband radiated electromagnetic energy — Part 1: General principles and terminology*, 2015. [Online]. Available: Available:https://www.iso.org/obp/ui/#iso:std:iso:11451:-1:ed-4:v1:en.

[184] ——, *Road vehicles — Component test methods for electrical disturbances from narrowband radiated electromagnetic energy — Part 1: General principles and terminology*, 2015. [Online]. Available: https://www.iso.org/obp/ui/#iso:std:iso:11452:-1:ed-4:v1:en.

[185] L. C. R. Farjadrad, *A Proposed Specification for RFI Ingress Limit in 802.3ch Automotive Links*, Aquantia, Ed., Spokane, 2018. [Online]. Available: http://www.ieee802.org/3/ch/public/sep18/farjarad_3ch_01b_0918.pdf.

[186] Texas Instruments, *Ethernet PHY Transceiver, Industrial, automotive, and consumer applications*, Texas Instruments, Ed., 2016. [Online]. Available: https://manualzz.com/doc/25857536/ethernet-phy-transceiver-reference-guide.

[187] P. Hank, S. Muller, O. Vermesan, and J. van den Keybus, "Automotive Ethernet: In-vehicle Networking and Smart Mobility", in *Design, Automation & Test in Europe Conference & Exhibition (DATE), 2013*, Piscataway, NJ: IEEE, 2013, pp. 1735–1739. DOI: 10.7873/DATE.2013.349.

[188] C. L. Justin Redd, *Spectral content of NRZ test patterns*, www.edn.com, Ed., San Jose, USA, 2004. [Online]. Available: https://m.eet.com/media/1134689/15451-447007.pdf.

[189] D. Watzenig and M. Horn, Eds., *Automated Driving: Safer and More Efficient Future Driving*. Cham and s.l.: Springer International Publishing, 2017. DOI: 10.1007/978-3-319-31895-0. [Online]. Available: http://dx.doi.org/10.1007/978-3-319-31895-0.

[190] R. Stahlmann, A. Festag, A. Tomatis, I. Radusch, and F. Fischer, Eds., *Starting European field tests for Car-2-X communication: the DRIVE C2X framework*, 2011. [Online]. Available: https://festag-net.de/wp-content/uploads/2019/11/its-wc2011_drivec2x_final_v2.pdf.

[191] M. Galvani, "History and future of driver assistance", *IEEE Instrumentation & Measurement Magazine*, vol. 22, no. 1, pp. 11–16, 2019. DOI: 10.1109/MIM.2019.8633345.

[192] M. Mody *et al.*, "High Performance Front Camera ADAS Applications on TI's TDA3X Platform", in *22nd IEEE International Conference on High Performance Computing*, Piscataway, NJ: IEEE, 2015, pp. 456–463. DOI: 10.1109/HiPC.2015.56.

[193] N. T. Nguyen *et al.*, Eds., *A Survey of ADAS Technologies for the Future Perspective of Sensor Fusion: Computational Collective Intelligence*, Springer International Publishing, 2016.

[194] Futurewei, Subsidiary of Huawei, *IEEE 802.3 Criteria for Standards Development (CSD)*. [Online]. Available: https://mentor.ieee.org/802-ec/dcn/17/ec-17-0069-00-ACSD-802-3ch.pdf.

[195] D. Derickson, *Digital communications test and measurement: High -speed physical layer characterization (paperback)*. Prentice Hall, 2012.

[196] G. S. Miljković, I. S. Stojković, and D. B. Denić, "Generation and application of pseudorandom binary sequences using virtual instrumentation,"" *Facta Universitatis, Series: Automatic Control and Robotics*, vol. 10, no. 1, pp. 51–58, 2011.

[197] Peter Wu, *Multi-level PAM Study for M-Gig Automotive PHYs-II*, IEEE 802.3ch Multi-gig Automotive Ethernet PHY Task Force, Ed., Pittsburgh, PA, USA. [Online]. Available: http://www.ieee802.org/3/ch/public/may18/wu_3ch_01a_0518.pdf.

[198] S. Frei, R. G. Jobava, and D. Topchishvili, "Complex approaches for the calculation of EMC problems of large systems", in *EMC 2004*, Piscataway, N.J: IEEE, 2004, pp. 826–831. DOI: 10.1109/ISEMC.2004.1349929.

[199] H. Chobanyan, I. Badzagua, T. Injgia, A. Gheonjian, and R. Jobava, "Application of hybrid MOM/MTL method to simulation of interaction between cable harness and antennas", in *International Seminar/Workshop on Direct and Inverse Problems of Electromagnetic and Acoustic Wave Theory, 2009*, Piscataway, NJ: IEEE, 2009, pp. 33–38. DOI: 10.1109/DIPED.2009.5307249.

[200] T. Kley, "Optimized single-braided cable shields", *IEEE Transactions on Electromagnetic Compatibility*, vol. 35, no. 1, pp. 1–9, 1993. DOI: 10.1109/15.249390.

[201] F. M. Tesche, M. v. Ianoz, and T. Karlsson, *EMC analysis methods and computational models*, ser. A Wiley-Interscience publication. New York: Wiley, 1997.

[202] S. Daijavad and B. J. Rubin, "Modeling common-mode radiation of 3D structures", *IEEE Transactions on Electromagnetic Compatibility*, vol. 34, no. 1, pp. 57–61, 1992. DOI: 10.1109/15.121668.

[203] EMCoS, *EMCoS Studio software*, 2018. [Online]. Available: https://www.emcos.com/?products=emcos-studio/release-highlights.

[204] F. G. Bogdanov *et al.*, "Validation of Hybrid MoM Scheme With Included Equivalent Glass Antenna Model for Handling Automotive EMC Problems", *IEEE Transactions on Electromagnetic Compatibility*, vol. 52, no. 1, pp. 164–172, 2010. DOI: 10.1109/TEMC.2009.2036003.

[205] F. Bogdanov *et al.*, "Computational techniques for automotive antenna simulations", in *New Trends and Developments in Automotive System Engineering*, IntechOpen, 2011.

[206] F. Bogdanov, L. Svanidze, A. Gheonjian, D. Eremyan, Z. Kutchadze, and R. Jobava, "Application of MoM-based Waveguide Port Approach to the Analysis of EM Coupling Problems Related to Microwave Antennas", in *12th European Conference on Antennas and Propagation (EuCAP 2018)*, Stevenage, UK: IET, 2018, 835 (5 pp.)–835 (5 pp.) DOI: 10.1049/cp.2018.1194.

[207] V. K. Singh and R. Kumar, "An optimized multichannel MAC scheme with dynamic control channel interval in dense VANET", *International Journal of Information Technology*, pp. 1–9,